FROM ISLAND ARC TO CRATON: TIMESCALES OF CRUSTAL FORMATION ALONG THE NEOPROTEROZOIC BI'R UMQ SUTURE ZONE, KINGDOM OF SAUDI ARABIA

BY

U.S. HARGROVE, R.J. STERN, W.R. GRIFFIN,
P.R. JOHNSON, AND M.G. ABDELSALAM

TECHNICAL REPORT
SGS-TR-2006-6

1427 H 2006 G

A Technical Report prepared by the
Saudi Geological Survey,
Jeddah, Kingdom of Saudi Arabia

The work on which this report is based was performed in support of Saudi Geological Survey Subproject 4.1.1.5.1.—*Research and Special Studies*. It has been edited and reviewed by staff of the Saudi Geological Survey. Product names used in this report are for descriptive purposes and in no way imply endorsement by SGS.

This report is a product of the Saudi Geological Survey; if the information herein is used in any form, either quoted or paraphrased, this report should be properly cited using the full serial number, the author's name(s), and the year of publication. The correct citation for this report is:

Hargrove, U.S., Stern, R.J., Griffin, W.R., Johnson, P.R., and Abdelsalam, M.G., 2006, From island arc to craton: timescales of crustal formation along the Neoproterozoic Bi'r Umq suture zone, Kingdom of Saudi Arabia: Saudi Geological Survey Technical Report SGS-TR-2006-6, 69 p., 4 tables, 32 figs.

In common with most reports produced by the Saudi Geological Survey, this report is available for sale to the public in hard copy format or on CD in PDF format. Please contact the SGS Publications Center at the address in Jeddah below for more information.

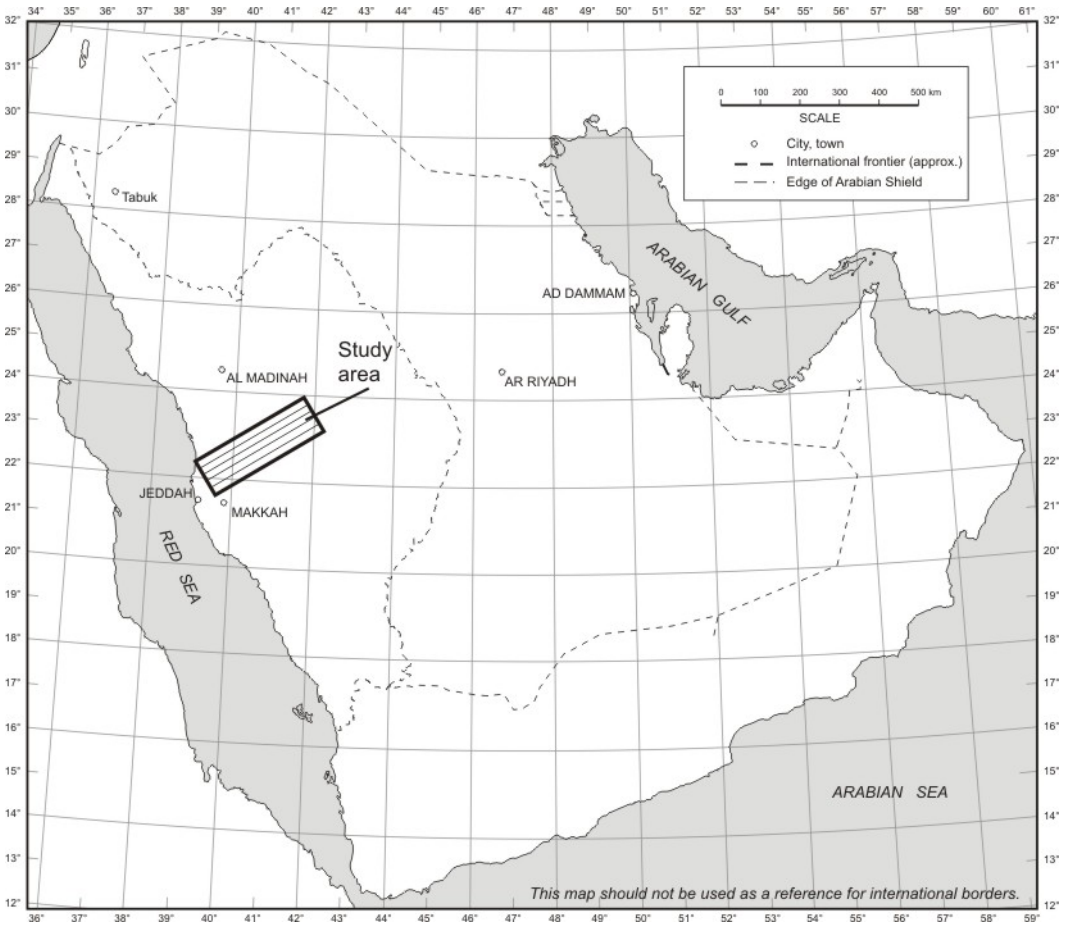

Index map of the Arabian Peninsula

For more information about the Saudi Geological Survey visit our website www.sgs.org.sa or write to or visit our headquarters in Jeddah or our office in Riyadh.

Saudi Geological Survey
Post Office Box 54141, Jeddah 21514
Tel. (966-2) 619-5000

Saudi Geological Survey-Riyadh Office
Post Office Box 6955, Riyadh 11452
Tel. (966-1) 476-5000

TABLE OF CONTENTS

FIGURES

TABLES

FROM ISLAND ARC TO CRATON: TIMESCALES OF CRUSTAL FORMATION ALONG THE NEOPROTEROZOIC BI'R UMQ SUTURE ZONE, KINGDOM OF SAUDI ARABIA

By

Ulysses S. Hargrove[a], Robert J. Stern[a], William R. Griffin[a], Peter R. Johnson[b], Mohamed G. Abdelsalam[a]

ABSTRACT

The Neoproterozoic Hijaz and Jeddah arc terranes that flank the Bi'r Umq suture zone (BUSZ) in western Saudi Arabia record some of the earliest magmatic and deformational events in the juvenile part of the Arabian-Nubian Shield (ANS). Detailed U-Pb ion microprobe (SHRIMP-RG) analyses were conducted on zircon from 31 plutonic and volcanic samples, the ages of which reveal a complex and protracted (820-520 Ma) tectono-magmatic history that is comparable to that of correlative units in eastern Sudan.

The results define four magmatic episodes (M1-M4) that record the transition of the ANS from discrete arcs to composite terranes to craton. The earliest igneous activity occurred simultaneously on both sides of the suture at ca. 825-800 Ma during M1, and possibly began as early as ca. 854 Ma. M1 was followed by a 15 Ma hiatus in magmatism that was accompanied by deformation, denudation, and exposure of the M1 units. Rifting of the arc terrane and emplacement of the Tharwah ophiolite, the age of which is tentatively reinterpreted to be 777 ± 17 Ma, may have occurred during this hiatus. Igneous activity resumed during the M2 magmatic episode (785-745 Ma), which represents the main crust-forming event, presumably above a subduction zone. M2 magmatism was contemporaneous with suture-related deformation, as recorded by ca. 785 and 750 Ma metatonalite plutons that exhibit structural evidence of syntectonic emplacement. Following the end of deformation and a nearly 50 Ma hiatus in magmatism along the BUSZ, magmatism was briefly reactivated during the M3 (700-633 Ma) episode and was associated with local extension. The final magmatic episode, M4 (598-566 Ma), as defined by previous studies, involved emplacement of numerous granitoids that are similar to postorogenic A-type igneous rocks present throughout the northern ANS and Saharan Africa. The origin of some of these has previously been attributed to anatexis of the lower continental crust as a result of orogenic crustal thickening, and they represent the cratonization of the ANS.

The results also provide new insights into the role of older continental material in construction of the ANS. Although the core of the shield where our samples originate is considered juvenile, with no crust older than ca. 870 Ma, some volcanic rocks and posttectonic granites from the BUSZ contain zircons that yield abundant early Neoproterozoic to Archean Pb-Pb ages; one of these (2840 Ma) is the oldest yet reported from the juvenile core of the Arabian Shield. Paleoproterozoic-Archean inherited zircon may be derived from basement of that age exposed in the southeastern ANS, but sources for abundant Mesoproterozoic inherited zircon do not occur anywhere in the shield. They could have been assimilated from terrigenous sediments that were shed from nearby passive margins, transported by glaciers, or subducted and then resurrected by partial melts of the subducted slab. Alternatively, they were assimilated from cryptic pre-Neoproterozoic crust that underlies the "juvenile" core of the ANS. Some zircon morphologies suggest a sedimentary (detrital) origin, whereas others are more consistent with in situ extraction of juvenile grains from older igneous basement. Inheritance in the Tharwah ophiolite supports the presence of older basement, as it is best explained by rifting of continental crust. The abundance of inherited zircon along the BUSZ greatly increases the known extent of the "contaminated" shield and suggests that previously unrecognized pre-Neoproterozoic crust played a significant, although cryptic, role in the evolution of the juvenile core of the ANS.

[a] *The University of Texas at Dallas, 2401 N. Floyd Rd. MS FO21, Richardson TX, USA*
[b] *Saudi Geological Survey, P.O. Box 54141, Jiddah 21514, Saudi Arabia*

من قوس جزيرة إلى رسيخة: الجداول الزّمنية للتكوّن القشري على طول نطاق درز بئر عمق التابع لحقب طلائع الأحياء الحديث في المملكة العربية السعودية

إعداد

يولسس.أس.هارجروف – روبرت جيه.ستيرن – ويليم آر.جريفن – بيتر آر.جونسون

و محمّد جي.عبد السّلام.

الخلاصة

يُسجّل إقليما الحجاز وجدّة القوسان التابعان لحقب طلائع الأحياء الحديث، اللّذان يحيطان بنطاق درز بئر عمق الواقع في الجزء الغربي من المملكة العربية السعودية، بعضاً من أوائل الأحداث الصّهارية والتشوّهية في الجزء الفتي من الدرع العربي النّوبي. تم القيام بتحاليل تفصيلية باستخدام المسبار الأيوني المصغّر "شرمب – آرجي" لتحديد اليورانيوم – الرصاص في الزركون من (٣١) عينة جوفية وبركانية أظهرت أعمارها (٥٢٠–٨٢٠ مليون سنة) تاريخاً حركياً صهارياً معقّداً وممتدّاً مشابهاً لتاريخ الوحدات المماثلة لها في شرق السّودان.

وحددت النتائج أربعة مراحل صهارية (م١ – م٤) تُسجّل تحوّل الدرع العربي النّوبي من أقواس متفرقة إلى أقاليم مركبّة ثم إلى رسيخة. وحدث أول نشاط ناري متزامناً على كِلا من جانبي الدرز حوالي ٨٢٥–٨٠٠ مليون سنة خلال المرحلة (م ١)، ويحتمل أن يكون ذلك النشاط قد بدأ في وقت أبكر حوالي ٨٥٤ مليون سنة. تلا المرحلة (م ١)، فترة زمنية تبلغ ١٥ مليون سنة توقّفت خلالها عملية النشاط الصّهاري وكانت مصحوبة بتشوّه وتعرية وانكشاف وحدات المرحلة (م ١). أما انفراج إقليم القوس وتبلور أوفيوليت ذروة، والذي أعيد تفسير عمرهما ليكون ٧٧٧± ١٧ مليون سنة بصورة غير أكيدة، يمكن أن يكونا قد حدثا خلال هذه الفسحة الزمنية. أستؤنف النشاط النّاري خلال المرحلة الصهارية (م ٢)(٧٨٥–٧٤٥ مليون سنة)، التي تمثّل الحادثة الأساسية لتكون القشرة، ويفترض أنها قد تمت فوق نطاق إنضواء.

تزامن النشاط الصهاري للمرحلة (م ٢) مع التشوّه المرتبط بالدرز، كما تم تسجيله بالتونواليت المتحوّل السحيق الذي يبلغ عمره حوالي ٧٨٥و ٧٥٠ مليون سنة والذي يظهر أدلة تركيبية عن التوضّع المتزامن البنائية. وبعد انتهاء التشوّه وانقضاء فسحة زمنية تبلغ حوالي ٥٠ مليون سنة من توقّف النشاط الصهاري على طول نطاق درز بئر عمق، أعيد تنشيط المرحلة الصّهارية (م ٣)(٧٠٠–٦٣٣ مليون سنة) وصاحبها تمدّد محلّي. أما المرحلة الصّهارية الأخيرة، (م ٤)(٥٩٨–٥٦٦ مليون سنة) كما تم تحديدها عن طريق الدراسات السّابقة، فقد اشتملت على توضّع العديد من أشباه الجرانيت المشابهة للصخور النّارية نوع–أ التالية للحركة التجبّلية المنتشرة في كافة أرجاء الجزء الشمالي من الدرع العربي النّوبي والصحراء الكبرى في أفريقيا. وقد نُسب أصل بعض هذه الصخور سابقاً إلى انصهار صخور القشرة القارية السفلية نتيجة التثخن القشري التجبّلي، وهي تمثّل تحوّل الدرع العربي النّوبي إلى رسيخة.

توفّر النتائج أيضاً نظرة عميقة جديدة إلى دور المواد القاريّة القديمة في بناء الدرع العربي النّوبي. على الرغم من أن لب الدرع الذي قمنا بجمع العينات منه يعتبر فتياً، مع عدم وجود قشرة يزيد عمرها عن حوالي ٨٧٠ مليون سنة، فإن بعض الصخور البركانية وصخور الجرانيت التالية للبنائية من نطاق درز بئر عمق تحتوي على زركون يعطي أعماراً كثيرة للرصاص/الرصاص تعود لحقب طلائع الأحياء الحديث الباكر إلى الدهر العتيق (الأركي)، وأحدها (٢٨٤٠ مليون سنة) هو أقدم عمر تم تسجيله حتى الآن من اللب الفتي للدرع العربي. وقد يكون الزركون الموروث العائد لحقب طلائع الأحياء القديم–الدهر العتيق مشتقّاً من قاعدة لها ذلك العمر متكشفة في الجزء الجنوبي الشرقي من الدرع العربي النّوبي، إلا أنه لا تتواجد أية مصادر لهذه الوفرة من الزركون الموروث العائد لحقب طلائع الأحياء المتوسط في أي جزء من الدرع العربي النّوبي. ومن الممكن أنها امتصت من رواسب قاريّة انفصلت من حواف سلبية (غير فعّالة) مجاورة قامت بنقلها مجلّدات، أو أنها انضوت ثم أعيدت عن طريق الذوبان الجزئي للوح المنضوي. وبالمقابل قد تكون تكوّنت عن طريق هضم وامتصاص قشرة خفية تابعة لحقب ما قبل طلائع الأحياء الحديث تقع تحت لب الدرع العربي النوبي الفتي. توحي بعض أشكال الزركون بأصل رسوبي (فتاتي)، بينما تنسجم أشكال أخرى مع الاستخلاص الموضعي للحبيبات الفتية من قاعدة ناريّة أقدم. يُرجّح التوارث في أوفيوليت ذروة وجود قاعدة أقدم، وأفضل توضيح لذلك هو انشقاق القشرة القاريّة.

إن وفرة تواجد الزركون الموروث على طول نطاق درز بئر عمق تعزّز المدى المعروف للدرع "الملوّث" وتوحي بأنّ القشرة التابعة لما قبل حقب طلائع الأحياء الحديث، الغير معروفة سابقاً، قد لعبت دوراً هامّاً، على الرغم من أنه خفي، في تطوّر اللب الفتي للدرع العربي النّوبي.

INTRODUCTION

The Arabian-Nubian shield (ANS) in northeast Africa and Arabia is an outstanding natural laboratory for studying the origin and evolution of juvenile crust, that is crust formed directly by partial melting of the mantle. The ANS is arguably the best-preserved and most widely exposed juvenile continental crust of Neoproterozoic age (1000 to 542 Ma, Gradstein and others, 2004) on the planet (Reymer and Schubert, 1984; Dixon and Golombek, 1988; Vervoort and Blichert-Toft, 1999; Patchett and Chase, 2002; Stern, 2002). It is preserved in roughly a dozen volcano-tectonic terranes that generally are regarded as having formed by subduction within and around a major ocean basin (Mozambique ocean of Dalziel, 1991). Terrane formation began at ca. 870 Ma and concluded at ca. 550 Ma when convergence between East and West Gondwana closed the Mozambique Ocean along the East African Orogen (EAO) (Stern, 1994). High-grade metamorphic terranes in the southern EAO, now exposed in the Mozambique belt in eastern and southern Africa, Madagascar (Ashwal and others, 1999; Collins and others, 2000; Muhongo and others, 2001), and Antarctica (Golynsky and Jacobs, 2001), record the evolution of the deep crust and upper mantle lithosphere in the most intense part of the collision zone. The northern part of the EAO, represented by the ANS, exposes higher levels of the orogen and records the tectonic and magmatic evolution of the upper crust prior to, during, and following terminal collision along the EAO (Stern, 1994). The compilation of Johnson and Woldehaimanot (2003) provides a more thorough overview of the ANS and its history.

The Bi'r Umq-Nakasib suture zone is a major Neoproterozoic structure that spans more than 600 km of the ANS from eastern Sudan to western Saudi Arabia (configured prior to Cenozoic rifting along the Red Sea). It is important for understanding the nature and timing of the earliest crust-forming events in the ANS, inasmuch as it records the onset of terrane accretion and juxtaposes two of the oldest juvenile arc terranes in the shield. Critical to developing a comprehensive model for the formation, deformation, and cratonization of the ANS is a foundation of abundant and reliable geochronometric ages. Much work was conducted in the 1980s using K-Ar, Rb-Sr, Sm-Nd, and conventional U-Pb dating techniques, which contributed significantly to our understanding of the Arabian Shield. However, the validity of much of the available geochronological control on major magmatic and tectonic events that affected the shield in Arabia is suspect, and the same may be true for northeast Africa. Darbyshire and others (1983) point out many problems inherent in the early dating campaigns in Arabia. Regarding the Rb-Sr technique, many of the existing ages are model ages rather than isochron ages, regression ages were commonly derived from only a few samples or were based on two-point 'isochrons', and characteristically low Rb-Sr ratios led to large errors on whole-rock isochron ages. Many K-Ar and model Rb-Sr isotopic systems were disturbed during Neoproterozoic or early Paleozoic magmatic and tectonic events, rendering them useful only for constraining the timing of those events (Darbyshire and others, 1983). Rb-Sr dating of felsic volcanic rocks has proved especially difficult (e.g. Kemp and others, 1980; e.g. Bokhari and Kramers, 1981; Calvez and Kemp, 1982), and in some cases resulted in large discrepancies between Rb-Sr ages and more robust ages determined by the U-Pb zircon method or relative ages derived from geological evidence (e.g. Calvez and Kemp, 1982).

For the most part, U-Pb zircon ages are superior for determining igneous crystallization ages compared to those obtained by Rb-Sr and K-Ar techniques, but even campaigns that employed this method encountered difficulties. The greatest problem facing conventional U-Pb zircon dating in the ANS is the issue of inheritance, that is the incorporation of zircon from older material into magmas. Inherited grains are commonly rounded, either due to mechanical abrasion of detrital grains or chemical dissolution by younger magma, and surrounded by overgrowths of juvenile zircon related to the host magmatic unit. Some studies have recognized the effect of inheritance on the ages they report, but unrecognized inheritance may have contributed to reduced resolution of many conventional multi-grain U-Pb zircon ages reported for the shield. For multi-grain studies, the obvious concern is the analysis of a heterogeneous population of grains from multiple original sources, whereas unrecognized cores are most problematic for the single grain method. In either case, the calculated age may be a geologically meaningless average of the ages of the older inherited and younger juvenile components that is weighted towards the component with the stronger isotopic signal or may include a geologically meaningless lower intercept of concordia by linear-regression through discordant grains. Many of the plutonic and volcanic samples analyzed during this study are rife with inherited zircon, some as old as Archean, which brings into question U-Pb ages from previous studies in which no inheritance was reported (e.g. Calvez and Kemp, 1982). Also of concern is that many conventional U-Pb ages from the shield are model ages. Cooper and others (1979) proposed that rifting along the Red Sea caused isotopic disturbance to many U-Pb systems, and as such recommended forcing the lower intercept of linear-regression lines through 15 ± 15 Ma on the concordia curve. This is known as the Tertiary lead-loss model, but its validity is contested. As noted by Pallister and others (1988b), "ion-microprobe studies are badly needed to evaluate lead-loss models in Shield rocks."

The present geochronologic study utilized the sensitive high-mass resolution ion microprobe with reverse geometry (SHRIMP-RG) specifically to overcome the limitations of other dating techniques. The reader is referred to Williams (1997) for the history of the SHRIMP ion microprobe and the advantages and disadvantages of the technique relative to conventional methods. Reported here are U-Pb ages determined by SHRIMP-RG ion microprobe analyses of single zircon crystals from Neoproterozoic ophiolitic, plutonic, and volcanic-sedimentary rocks of low metamorphic grade

along the Bi'r Umq suture zone in Saudi Arabia. These ages are coupled with geological information synthesized from fieldwork conducted as part of this study and from the literature observations to constrain the timing of some of the earliest magmatic and deformational events that generated and modified the juvenile crust along the Bi'r Umq suture zone. Sample locations are shown in Figure 3 and are listed in Table 1. Existing radiometric ages for the units are discussed and evaluated in the context of geological constraints and the new ages that are reported herein. Some units that were not dated as part of this study are also discussed because of their importance to understanding the overall history of the region.

Most of the Precambrian units along the BUSZ have not been formally named in accordance with internationally recognized guidelines for nomenclature (e.g., International Commission on Stratigraphy, North American Stratigraphic Code), although recommendations for formal names have been made for some units (Kemp and others, 1982a). Previous field studies were generally not of sufficient detail to warrant assignment of the plutonic units to formal lithodemic associations, nor were type sections described for the stratigraphic units. Accordingly, the names given to the units in the map areas are largely informal (e.g., Mahd group rather than Mahd Group). They are continued here, except where modification is warranted to conform to established guidelines and provide more information about the units. For example, the names of the Kamil suite and the Ramram complex are modified to the Kamil intrusive suite and Ramram intrusive complex in order to distinguish those recognizably igneous units from high-grade metamorphic complexes or structural complexes, and the name of the Qudayd suite is modified to the Qudayd meta-intrusive suite to reflect the original igneous character and significant deformational history of that unit.

ANALYTICAL METHODS

Bulk rock samples (<30 kg) were collected for geochronology during three field seasons in Saudi Arabia in 2001, 2003, and 2004 (hence sample prefixes SA01, SA03, and SA04). Samples were processed at the University of Texas at Dallas to extract zircon using standard crushing and mineral separation techniques. After separation, zircons from the least magnetic fractions were handpicked under a binocular microscope in distilled isopropyl alcohol to obtain the most transparent and most inclusion-free grains.

All analytical work was performed during two sessions in 2004 using the SHRIMP-RG ion microprobe, co-operated by the U.S. Geological Survey and Stanford University in the Stanford University Microanalysis Center (SUMAC). Zircon grains were mounted on glass slides in 1 x 6 μm rows using double-sided tape and cast in epoxy to form a disc 25 mm wide by 4 mm thick. The disc was ground and polished to a 1 μm finish to reveal quasi-equatorial sections through the grains. Digital images of the grains were captured via cathodoluminescence (CL) on a JEOL 5600LLV scanning electron microscope and via transmitted light on an optical microscope prior to and following analysis; image quality was enhanced using Photoshop®. Grain mounts were then washed with a saturated EDTA solution, thoroughly rinsed in distilled water, dried in a vacuum oven, and coated with gold.

Mounts typically sat in a loading chamber at high vacuum (10^{-7} torr) for several hours before being moved into the source chamber of the SHRIMP-RG. A primary O^{2-} ion beam varying in intensity from 4 to 6 nA was first rastered for 120 seconds over the analysis area to remove any surface contamination. The primary beam was then focused to generate secondary ions for an analysis time of 12 minutes and typically produced an ablation spot with a diameter of 20-40 μm and a depth of 1-2 μm. Nine peaks were measured sequentially for each spot and included $^{90}Zr_2{}^{16}O$, ^{204}Pb, background (0.050 amu above ^{204}Pb), ^{206}Pb, ^{207}Pb, 208Pb, ^{238}U, $^{232}Th^{16}O$, and $^{234}U^{16}O$. Autocentering on selected peaks and guide peaks for low or variable abundance peaks (i.e. $^{90}Zr_2{}^{16}O$ at 0.165 mass units below ^{204}Pb) was used to improve the reliability of locating peak centers. Measurements were made at a mass resolution of 6000-8000 (10% peak height), which eliminates isobaric interferences. Lead-isotope ratios were taken as measured after correction for background. Pb^+/U^+ ratios were calibrated against UO^+/U^+ and an overall normalization relating ion intensity to actual ratio was taken at the mean UO^+/U^+ and Pb^+/U^+ values.

Concentration data were calibrated against the R33 zircon standard (419 Ma quartz diorite of Braintree complex, Vermont, Black and others, 2004), which was analyzed four to five times at the start of each new mount and after a proximately every four unknown grains thereafter. Standard R33 was analyzed 218 times over the course of the analysis runs and produced an average $^{206}Pb/^{238}U$ age of 418 ± 4 Ma, with a standard deviation of ± 18 Ma. Table 2 shows the statistical results from the analyses of the R33 standard during ten different analytical sessions, some replicates, on six grain mounts. Data reduction followed the methods described by Williams (1997), and Ireland and Williams (2003) and was performed by J. Wooden at SUMAC using SQUID 1.02 software (Ludwig, 2001). Correction for common lead was performed by fitting a model age for the sample, based on the uncorrected data, to the lead evolution model of Stacey and Kramers (1975). Although this model is best suited for correction of common lead that is intrinsic to the grain, and not to surface contamination, the difference between this method and corrections based on modern lead ratios from Broken Hill, Australia, are probably minimal.

Analysis points were plotted and ages calculated by the first author using Isoplot/Ex 3.0 (Ludwig, 2000). Decay constants used for age calculation are as follows: ^{238}U = 1.55125 x 10-10; ^{235}U = 9.8485 x 10-10; ^{232}Th = 4.9475 x 10^{-10}. Statistical evaluations (e.g., chi-square tests) were not performed on the analytical results for individual samples because of the low number of points. Instead, analyses were selected based on geological information,

zircon morphology and cathodoluminescence, degree of concordancy, and visual discrimination between apparent populations of points on concordia diagrams to determine which were most likely to produce an appropriate and geologically meaningful age. Large clusters of data points on concordia diagrams were assumed to represent the juvenile component of the samples and outlying points to reflect either lead loss or inheritance of older zircon. Appearance of zircon in cathodoluminescence (CL) images was also used as a discriminant, where bright and dark areas were used respectively as proxies for low and high uranium content. For most samples, the final ages reported here are concordia ages (as defined by Ludwig, 1998) calculated from the maximum number of equivalent points (i.e. those analyses that are essentially indistinguishable in terms of their isotopic ratios and, therefore, concordia ages) from each sample, minus problematic analyses, as discussed in the text.

Brief hand-sample and petrographic descriptions as well as locations of the samples analyzed in this study are presented in Table 1. Analytical data acquired by SHRIMP-RG for all samples and apparent concordia ages are presented in Table 3. All analyses are plotted as two-sigma error ellipses on Tera-Wasserburg concordia diagrams (Tera and Wasserburg, 1972), and all MSWD values are measurements of scatter of the points relative to concordia (not to one another). Tera-Wasserburg plots are generally preferred over Wetherill plots (Wetherill, 1956) for microprobe studies for several reasons. First, they are plotted exactly as they are measured on the instrument, instead of deriving $^{235}U/^{207}Pb$ from the U isotopic constant. Second, the errors in measured $^{238}U/^{206}Pb$ are more weakly correlated with those of $^{207}Pb/^{206}Pb$ than of $^{235}U/^{207}Pb$. Third, lead loss from zircon is more easily distinguished from other forms of isotopic disturbance, as it tends to shift $^{238}U/^{206}Pb$ to higher values without affecting $^{207}Pb/^{206}Pb$, whereas isotopic disturbances (e.g., mixing, thermal resetting) affect $^{238}U/^{206}Pb$ as well as $^{207}Pb/^{206}Pb$ (Williams, 1998). Table 4 lists and presents a summary of our evaluations of all available radiometric ages for the BUSZ obtained during this study and reported by other authors, and Figure 4 shows the major plutonic and stratigraphic units discussed here in chronologic order according to the most robust ages available.

BI'R UMQ-NAKASIB SUTURE ZONE

The Bi'r Umq-Nakasib suture zone (BNSZ) is a major northeast-trending fold and thrust belt in the central ANS that marks the site of a paleosubduction zone and the collision of the Gebeit-Hijaz terrane in the north with the Haya-Jeddah terrane in the south (Fig. 1). Within the suture zone, the margins of the terranes consist of folded and tectonized ophiolitic nappes, allochthonous and para-autochthonous assemblages of volcanic, volcaniclastic, and epiclastic rocks, and voluminous plutonic rocks. Some of the plutons form

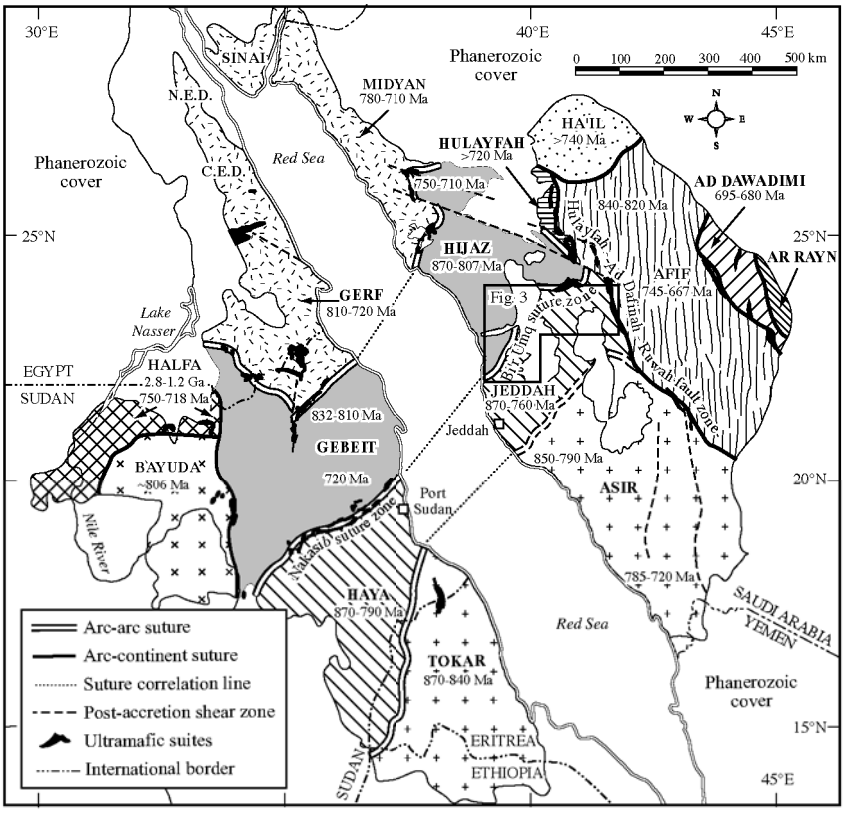

Figure 1. Map of the Arabian-Nubian Shield, modified from Johnson and Woldehaimanot (2003), showing the location and ages of crustal terranes, suture and mafic-ultramafic (ophiolite) suites. The location of figure 3 is outlined. N.E.D., Northern Eastern Desert; C.E.D.; Central Eastern Desert.

Table 1. Geochronological sample descriptions.

Unit name	Sample No.	Latitude Longitude	Lithology	Lithologic/petrographic description
Arj group, Jabal Azlam formation	SA03-259	23.82183° N 40.91045° E	Basaltic andesite	Clinopyroxene-plagioclase-phyric basaltic andesite; mesocratic, amygdaloidal, hiatal aphanitic-porphyritic, idiomorphic granular, recrystallized intersertal and locally pilotaxitic matrix. Euhedral to subhedral plagioclase, extensively altered calcic cores, fresh sodic rims; euhedral to subhedral pyroxene, pseudomorphed by chlorite + epidote. amygdules, silica + carbonate + chlorite filling, angular to smooth, irregular margins. Outcrop consists of in situ massive boulders, well indurated, mildly weathered.
Bari granodiorite	SA03-270	23.47695° N 40.92563° E	Granite	Biotite-hornblende granite; leucoratic, medium-grained, inequigranular, allotriomorphic to hypidiomorphic granular. 35% anhedral to subhedral plagioclase, minor marginal myrmekite, extensively altered calcic cores, less altered rims; 30% anhedral orthoclase, microperthitic, fresh; 25% anhedral quartz, strained; anhedral to suhbedral hornblende, mild alteration to chlorite, intergrown with Fe-Ti oxide; 10% anhedral biotite, minor alteration to chlorite; accessory Fe-Ti oxide, apatite, zircon. Massive, spheroidally weathered outcrops; numerous, 3-4 cm, subangular inclusions of melanocratic hornblende diorite with diffuse margins.
Bari hypabyssal rhyolite	SA03-269B	23.41537° N 40.81617° E	Rhyolite	Plagioclase-sanidine-phyric rhyolite; mesocratcic, hiatal porphyritic, completely spherulitic matrix. 15% euhedral to anhedral sanidine phenocrysts, microperthitic, commonly embayed, unaltered; 10% subhedral plagioclase phenocrysts, diffuse and annealed albite twins, minor Carlsbad twins, some small glomerocrysts, moderate alteration to sericite and epidote; 3% euhedral pyroxene, pseudomorphed by aggregates of fine-grained epidote and chlorite; 2% accessory subhedral to anhedral Fe-Ti oxide, fractured, partially altered to hematite. Outcrop is massive, minor fractures, no visible layering, rock is well indurated.
Dhukhr tonalite	SA03-269A	23.41537° N 40.81617° E	Metatonalite	Muscovite metatonalite; leucocratic, coarse-grained, inequigranular, allotriomorphic granular, phaneritic-porphyritic; incipient dynamic recrystallization. 60% subhedral to anhedral plagioclase, deformed twin lamellae, moderately altered cores, fresh rims, partial conversion to orthoclase, limited granophyre; 25% anhedral, heterogranoblastic quartz, strongly undulose extinction oriented inequigranular; 15% anhedral muscovite, kinked foliae, partly replaced by epidote. Minor inclusiosn of anhedral Fe-Ti oxide in other phases. Minor vein filled with carbonate + epidote. Numerous microfaults. Outcrops are weakly foliated, friable, and associated with abundant gruss.
Dhukhr tonalite	SA04-412	23.44497° N 41.39428° E	Quartz diorite	Hornblende quartz diorite; mesocratic, medium grained, inequigranular, allotriomorphic granular. Subhedral to anhedral plagioclase, locally subcumulate, patchy inversion to orthoclase, minor subgrains, minor granophyre; anhedral quartz, interstitial, moderate undulose extinction; anhedral intercumulate and subhedral cumulate hornblende, minor patchy alteration to chlorite + actinolite + quartz ± Fe-Ti oxide, minor symplectic quartz intergrowths. Outcrop is massive highly fractured, internally fresh.
Hufayriyah tonalite	SA03-271	23.50308° N 41.05682° E	Tonalite	Biotite-hornblende tonalite; mesocratic, inequigranular, medium grained, hypidiomorphic granular; minor microfaults. Anhedral plagioclase, deformed twin lamellae, moderate alteration; anhedral quartz, strongly undulose extinction; anhedral hornblende, minor alteration to chlorite, minor inclusions of Fe-Ti oxide; anhedral biotite, pseudomorphed by chlorite + epidote; accessory zircon and apatite. Outcrop is massive to weakly foliated (spaced cleavage).

Table 1 (continued).

Unit name	Sample No.	Latitude Longitude	Lithology	Lithologic/petrographic description
Hypabyssal intrusion, in Bi'rak group	SA04-366	22.70557° N 39.36603° E	Microgabbro	Micrograbbro; melanocratic, very fine-grained, relict orthocumulate texture. 80% subhedral cumulate plagioclase, compositional zoning with cores extensively altered to epidote, weakly altered rims; 20% anhedral augite, intercumulate, possibly ophitic, highly altered to epidote + calcite; minor calcite amygdules; subordinate cryptocrystalline material interstitial to plagioclase, partly repaced by epidote. Outcrop is green-sh grey, massive, and highly fractured. Unit may be thick lava flow or a hypabyssal intrusion.
Hypabyssal intrusion, in Bi'rak group	SA04-367	22.70503° N 39.36202° E	Microgabbro	Microgabbro; melanocratic, fine-grained, orthocumulate texture. 60% subhedral cumulate plagioclase, compositional zoning with cores extensively altered to epidote + calcite and less altered rims; 40% anhedral augite, intercumulate to subophitic, highly altered to epidote + calcite; minor calcite amygdule; subordinate cryptocrystalline material interstitial to plagioclase, partly repaced by epidote. Outcrop is massive, probably hypabyssal sill intruding thinly bedded and laminated volcaniclastic chert, sandstones, and siltstones.
Hypabyssal intrusion, in Dhukhr tonalite	SA03-268A	23.41562° N 40.81523° E	Dacite	Quartz-hornblende-plagioclase-phyric dacite; hiatal porphyritic texture, spherulitic and microlitic matrix. 20% subhedral to euhedral plagioclase phenocrysts, minor Carlsbad and abundant diffuse albite twins, cores highly altered to sericite and epidote, fresh rims; 5% subhedral to euhedral hornblende phenocrysts, minor simple twins, locally altered to chlorite + carbonate + Fe-Ti oxides, epidote coronae; 1% anhedral quartz phenocrysts, subrounded, minor embayments, commonly as cores to spherulites; trace orthoclase, fresh. Minor vein filled with epidote. Outcrop is massive, pinkish in color.
Kamil intrusive suite	SA01-110	22.25477° N 39.81663° E	Diorite	Hornblende diorite; mesocratic, medium grained, subequigranular, hypidiomorphic granular, orthocumulate. Subhedral plagioclase, subcumulate, rare granophyre, heavy alteration; postcumulate orthopyroxene(?), poikilitic, replaced by hornblende, chlorite + epidote + Fe-Ti oxide + carbonate; anhedral quartz, interstitial to postcumulate; accessory subhedral Fe-Ti oxides. Just east of Al Kamil town. Outcrop is massive, jointed, crossed by mafic dikes.
Kamil intrusive suite	SA04-318	22.41218° N 39.88825° E	Diorite	Hornblende diorite; mesocratic, coarse grained, weakly orthocumulate. Euhedral subcumulate to anhedral postcumulate plagioclae, moderate alteration; cumulate euhedral to postcumulate anhedral hornblende, partly replaced by chlorite + Fe-Ti oxide; postcumulate anhedral quartz, also subpoikilitic partly enclosing plagioclase; minor postcumulate anhedral orthoclase, highly altered. Outcrop massive, fractured, internally fresh.
Mahd group, Haf formation	SA03-158	23.42323° N 40.65807° E	Rhyolite	Plagioclase-phyric metarhyolite, possibly welded tuff; mesocrstic, hiatal porphyritic texture. Relict euhedral to subhedral plagioclase phenocrysts and some fargments, moderate alteration to sericite, epidote, muscovite; anhedral Fe-Ti oxides, finely disseminated in matrix; abundant spherulites, irregular shapes; small, irrgular patches of quartz, rutilated, caused by silicification; minor carbonate in matrix; minor obvious lithic fragments, angular to subrounded, likely more abundant. Outcrop is massive, well indurated, crossed by numerous fractures.

Table 1 (continued).

Unit name	Sample No.	Latitude Longitude	Lithology	Lithologic/petrographic description
Mahd group, Haf formation	SA03-174	23.50138° N 40.83773° E	Rhyolite	Quartz-feldspar-phyric rhyolite; mesocratic, hiatal porphyritic textureholocrystalline, matrix of microcrystalline quartz + plagioclase. 2% subhedral to anhedral plagioclase phenocrysts, albite twinning, fresh; 2% subhedral to euhedral K-feldspar phenocrysts (anorthoclase or sanidine), extensively altered; 1% anhedral quartz phenocrysts, embayments common; trace Fe-Ti oxidesdisseminated throughout matrix. Minor, irregularly shaped calcite amygdules. Outcrop reddish grey, shows well-developed flow lamination, minor angular lithic clasts <5 cm across.
Mahd group, Haf formation	SA03-215A	23.24232° N 40.55612° E	Basaltic andesite	Plagioclase-phyric basaltic andesite; melanocratic, seriate porphyritic texture, locally intergranular and variolitic. 40% subhedral to anhedral plagioclase phenocrysts, extensive alteration to epidote + sericite; 10% anhedral Fe-Ti oxide phenocrysts and as euhedral coronas around relict olivine cores; 1% anhedral augite interstitial to plagoioclase in matrix; trace relict olivine phenocrysts, marginal replacement by Fe-Ti oxides, also glomerocrystic ultramafic inclusion highly atered to talc, serpentinite, and minor carbonate. Matrix contains pilotaxitic plagioclase microlites and interstitial augite + Fe-Ti oxides, minor variolitic plagioclase, and epidote. Minor veins filled with epidote. Outcrop is massive, dark reddish grey, oxidation coronas around phenocrysts, minor calcite veins; outcrop contains several flow units.
Posttectonic intrusion, Missir megadike	SA01-88	22.30135° N 39.66717° E	Syenite	Biotite syenite; inequigranular, medium-grained, leucocratic. Subhedral plagioclase, cores moderately altered to sericite + epidote, fresh rims, minor Carlsbad twins; subhedral orthoclase, perthitic, moderately altered to sericite; anhedral quartz, weak undulatory extinction; anhedral biotite, partly pseudomorphed by chlorite and Fe-Ti oxides. Outcrop is massive, contains cm-scale angular mafic enclaves.
Posttectonic intrusion, Nukhu megadike	SA01-109A	22.27753° N 39.79393° E	Granite	Biotite granite; leucocratic, medium grained, equigranular, allortiomorphic granular. Subhedral plagioclase, moderate alteration; anhedral orthoclase, microperthitic, mild alteration; anhedral quartz, incipient undulatory extinction; 10% anhedral biotite, extensive repacement by chlorite Fe-Ti oxide; accessory apatite, titanite, Fe-Ti oxide. Outcrop is massive.
Post-tectonic intrusion, Hanak granite	SA04-373	22.77682° N 39.32427° E	Granite	Hornblende granite; leucocratic, medium grained, hiatal phaneritic-porphyritic and allotroimorphic granular. Subhedral, plagioclase phenocrysts (6 mm), extensive replacement by microcline, fine anhedral interstitial grains in matrix; medium grained anhedral microcline, phenocrysts are microperthitic with tartan twinning, minor alteration, also partly replacing plagioclase; anhedral quartz (2 mm), interstitial, pronounced undulatory extinction, some internal recrystallization, minor granoblastic texture; anhedral hornblende, phenocrysts (1 mm), glomerocrysts (3 mm), moderate replacement by Fe-Ti oxide + carbonate. Outcrop is highly wethered and jointed, weakly semi-schistose, contains rare cm-scale elongate mafic enclaves.

Table 1 (continued).

Unit name	Sample No.	Latitude Longitude	Lithology	Lithologic/petrographic description
Qudayd meta-intrusive suite, Khamrah gneiss	SA01-68	22.47097° N 39.48920° E	Metatonalite	Garnet-muscovite-biotite metatonalite; leucocratic, porphyroclastic semischistose to inequigranular tabular; no relict igneous textures. Anhedral plagioclase porphyroclasts, albite & pericline twins, augen with extensive marginal grain-size reduction, mild alteration; anhedral quartz porphyroclasts, augen with extensive marginal grain-size reduction, internal recrystallization, pronounced undulatory extinction; anhedral biotite, oriented, pre- to syntectonic, mild alteration to chlorite; anhedral muscovite, post-tectonic, radial aggregates; anhedral garnet porphyroblasts, poikiloblastic, subequant. Granoblastic polygonal matrix of plagioclase + quartz. Accessory apatite, metamict zircon. Outcrop is semischistose, m-scale (thickness) compositional layering, numerous m-scale (thickness) shear zones, several consanguinous mafic dikes, pegmatites, abundant melanocratic enclaves.
Qudayd meta-intrusive suite, Hadabah dike	SA01-122C	22.55590° N 39.60365° E	Metarhyolite	Muscovite-biotite-plagioclase-quartz-phyric metarhyolite; mesocratic, relict hiatal aphanitic-porphyritic. Relict plagioclase phenocrysts, extensive marginal grain-size reduction, some internal recrystallization, mild alteration; relict anhedral quartz phenocryts, deep embayments, extensive marginal grain-size reduction, pronounced undulatory extinction; anhedral biotite, porphyroclastic to porphyroblastic (pre- to syntectonic), elongate aggregates; anhedral muscovite, porphyroblastic, late syntectonic. Microgranoblastic polygonal matrix of plagioclase + quartz. Dike intruding Nida fm., internal foliation parallel to foliation in host, pinch-and-swell structure, inclusions of massive pegmatite from nearby Qudayd gneiss.
Qudayd meta-intrusive suite, Hadabah gneiss	SA01-123	22.55168° N 39.59023° E	Tonalite	Hornblende-biotite tonalite; leucocratic, hiatal porphyritic texture, granoblastic polysutured matrix. 40% medium-grained plagioclase porphyroclasts, simple and albite twins, slightly altered to sericite or partly replaced epidote; 40% very fine-grained quartz porphyroclasts, highly undulatory extinction, common internal subgrains, granoblastic polysutured margins; 15% fine-grained, allotriomorphic, pre-tectonic biotite, glomerocrystic clusters, commonly associated with hornblende; 5% allotriomorphic hornblende porphyrocalsts, fresh, glomerocrustic in places, commonly in clusters with biotite.
Raghiyah intrusive suite, Jabal Hadb ash Sharar	SA03-245A	23.79617° N 40.93932° E	Alkalic granite	Riebeckite granite; leucocratic, hiatal prophyritic texture. 30% fine-grained euhedral to subhedral plagioclase laths, interstitial to phenocrysts, fluidal texture surrounding phenocrysts, commonly glomerocrystic, radial in places, bent albite twinning; 25% anhedral quartz phenocrysts (eyes), rounded, undulatory extinction, common internal subgrains, poikilitically eclosing margin-parallel trains of plagioclase; 25% anhedral to subhedral microcline, microperthitic, tartan twinning, poikilitically enclosing and locally replacing plagioclase; 10% anhedral riebeckite phenocrysts, unaltered; 2% granular aggregates of anhedral titanite; euhedral, post-tectonic actinolite prisms. Outcrop is massive, contains abundant subangular, cm-scale, black lithic inclusions.
Raghiyah intrusive suite, Jabal Hadb ash Sharar	SA03-246	23.86893° N 40.96843° E	Quartz-microdiorite	Hornblende micro-quartz-diorite; leuco- to mesocratic, fine-grained, inequigranular texture. 57% anhedral to subhedral plagioclase, locally cumulate, compositional zonation with cores highly altered to sericite + calcite ± epidote and less altered rims; 20% anhedral quartz, interstitial to plagioclase; 15% anhedral to subhedral hornblende completely pseudomorphed by chlorite + actinolite + Fe-Ti oxide; 7% anhedral to subhedral Fe-Ti oxides interstitial to and/or partly replacing plagioclase; 1% amygdules partly filled with calcite, drusy quartz, and/or chlorite; abundant, microcrystalline needles of post-tectonic, euhedral actinolite. Low-standing outcrop, massive.

Table 1 (continued).

Unit name	Sample No.	Latitude Longitude	Lithology	Lithologic/petrographic description
Ramram intrusive complex	SA03-160	23.43348° N 40.66000° E	Granodiorite	Granophyric pyroxene granodiorite; mesocratic, fine grained, phaneritic-porphyritic and allotriomorphic granular. 50% anhedral to subhedral plagioclase (3 mm) phenocrysts, extensive alteration of calcic cores, less altered rims; 20% anhedral quartz (0.5 mm); 20% anhedral microcline (1 mm), fresh; 10% subhedral to anhedral inverted pigeonite (1 mm), partly to completely replaced by hornblende + anthophyllite ± chlorite; abundant interstitial granophyre; accessory apatite and Fe-Ti oxide. Outcrop is massive.
Ramram intrusive complex	SA03-267	23.45783° N 40.66605° E	Granite	Granophyric hornblende granite; leucocratic, fine grained, phaneritic-porphyritic and allotriomorphic to hypidiomorphic granular. 60% anhedral to subhedral plagioclase phenocrysts (2 mm), extensive alteration of calcic cores, less altered rims; 20% anhedral quartz (0.75 mm), interstitial; 10% anhedral orthoclase (0.75 mm); 5% subhedral hornblende (0.5mm), replacing original pyroxene(?), partly to completely replaced by chlorite ± epidte ± Fe-Ti oxides; abundant interstitial granophyre;accessory metamict zircon. Outcrop is massive, contains numerous melanocratic enclaves up to 5 cm.
Samran group, Amudan formation	SA01-94	22.37655° N 39.73742° E	Dacite	Hornblende-plagioclase-phyric dacite; mesocratic, hiatal aphanitic-porphyritic, hypidiomorphic granular; microcrystalline matrix of felsic minerals and Fe-Ti oxide. Subhedral plagioclase, glomerocrystic, highly altered; subhedral to anhedral hornblende pseudomorphed by chlorite + epidotes; rare rounded and embayed quartz. Minor <2 cm subangular lithic fragments. Outcrop is thickly bedded lava, deformed by broad open folds.
Samran group, Amudan formation	SA01-103	22.31832° N 39.76145° E	Andesite	Plagioclase-augite-phyric andesite; hiatal aphanitic-porhyritic, pilotaxitic matrix with disseminated Fe-Ti oxide. Subhedral to rounded anhedral plagioclase, shape-preferred orientation, some fragments, patchy alteration; euhedral to subhedral augite, moderate alteration to chlorite + epidotes + carbonate; minor quartz, rounded and embayed, unstrained; minor euhedral olivine xenocrysts, moderately serpentinized. 2.5 mm oblate circular inclusion of cumulate augite. Outcrop shows weak flow-banding and bedding-parallel rock cleavage.
Samran group, Amudan formation	SA03-278	22.30553° N 39.75987° E		Clinopyroxene-plagioclase-phyric andesite; hiatal porphyritic texture, intergranular matrix with finely disseminated Fe-Ti oxides. 20% coarse-grained, hypidiomorphic plagioclase phenocrysts, albite twinning, moderate alteration to sericite and epidote; 5% medium-grained, relict hypidiomorphic clinopyroxene (?), pseudomorphed by aggregates of epidote, reaction rims of Fe-Ti oxides; medium-grained, allotriomorphic quartz phenocrysts (or xenocrysts), commonly broken and/or embayed. Intergranular matrix composed of pilotaxitic plagioclase microlites, clinopyroxene, and Fe-Ti oxide.
Samran group, Shayban formation	SA01-74B	22.41577° N 39.55982° E	Rhyolite	Plagioclase-quartz-phyric rhyolite mesocratic, hiatal aphanitic-porphyritic; recrystallized matrix of microcrystalline quartz + plagioclase, fluidal texture defined by coarser stringers wrappng phenocrysts and accentuated by mild dynamic recrystallization. Subhedral plagioclase phenocrysts (1 mm) and glomerocrystic augen (4 mm), minor resorption, moderate alteration, minor marginal grain-size reduction; anhedral quartz phenocrysts (2 mm), glomerocrystic augen (15 mm), minor embayments, some fractured and attenuated fragments with intervening pressure shadows of quartz; minor anhedral chlorite after unknown mafic mineral. Outcrop massive to weakly foliated, spotted due to quartz augen, discontinuous mm-scale (width) quartz ribbons.

Table 1 (continued).

Unit name	Sample No.	Latitude Longitude	Lithology	Lithologic/petrographic description
Samran group, Shayban formation	SA01-84	22.43508° N 39.71533° E	Arkosic sandstone	Lithic arkose; coarse to very coarse grained, poorly sorted, very immature, grain suported, epiclastic. Minor orthomatrix of microcrystalline biotite aggregates, dominant pseudomatrix of diaggregated quartz + plagioclase + biotite. Anhedral quartz clasts (2.5 mm), angular, low sphericity; anhedral to subhedral plagioclase clasts (1.75 mm), moderately altered calcic cores, fresh sodic rims, preserved albite twins, angular to subangular, very low sphericity; anhedral orthoclase clasts (3 mm), angular, low sphericity; lithic fragments, subrounded to subangular, granitic, cherty (identical to holocrystalline matrix in felsic lava); subhedral Fe-Ti oxides, detrital, rare poikilotopic cement. Common pressure solution at contacts between labile framework grains. Outcrop is massive with no obvious sedimentary features; taken directly across wadi from margin of Kamil suite pluton.
Samran group, Shayban formation	SA03-279	22.45987° N 39.87938° E		No thin section.
Tharwah ophiolite complex	SA03-149	22.64050° N 39.39498° E	Metagabbro	Metagabbro; mesocratic, coarse grained, mesocumulate, hypidiomorphic granular. 60% subhedral augite (2.5 mm), cumulate, glomerocrysts (10 mm), partly replaced or pseudomorphed by anthophyllite + epidote + antigorite/lizardite; 40% relict plagioclase, postcumulate, partly oikocrystic, pseudomorphed by aggregates of micocrystalline brown epidote. Numerous veins filled with quartz + carbonate ± epidote. Outcrop shows rhythmic layering of mm- to cm-scale alternating pyroxene-rich and pyroxene-poor layers.

Table 2. Statistics for external standard R33 during ten separate analyses of six grain mounts.

Grain Mount	JW163	JW164a	JW164b	JW165	JW164 (cont'd)	JW165 (cont'd)	JW192	JW193	JW194
Weighted mean Pb^+/U^+:UO^+/U^+^1.6	.00850	.00476	.00511	.00499	.01050	.00481	.00270	.00495	.00481
2σ error of mean	0.62%	0.66%	0.61%	0.50%	0.81%	0.52%	0.57%	0.48%	0.37%
Calculated 2σ external spot-to-spot error	1.85%	0.00%	1.60%	1.53%	0.00%	0.00%	0.00%	0.00%	0.00%
MSWD	2.28	1.91	2.02	2.67	1.54	1.96	1.76	1.65	1.32
Number of analyses	18	8	16	18	6	5	12	15	16

the basement to the supracrustal units whereas others clearly intrude them. Stratigraphic, structural, and geochronologic characteristics of those units indicate that the BNSZ is an unequivocal suture (Johnson and others, 2002; Johnson and others, 2003). The broader zone of suture-related deformation is 5-65 km wide and, in a pre-Cenozoic configuration, extended >600 km from present-day eastern Sudan to western Saudi Arabia, making it one of the longest suture zone in the ANS. Available radiometric ages indicate that it is also the oldest, with suture-related deformation occurring in Sudan at ca. 780-740 Ma (Abdelsalam and Stern, 1993b; Abdelsalam, 1994; Wipfler, 1996; Stern and Abdelsalam, 1998; Johnson and others, 2003); suturing in Arabia is not well constrained. Cenozoic rifting along the Red Sea separated the suture into the Nakasib and Bi'r Umq segments in Sudan and Saudi Arabia, respectively, but the suture has the distinction of being one of the few basement features that have been convincingly correlated across the Red Sea (Camp, 1984; Nassief and others, 1984; Dixon and others, 1987; Shimron, 1990; Sultan and others, 1993; Johnson and others, 2002).

Nakasib suture zone in Sudan

The Nakasib suture zone in Sudan juxtaposes the Gebeit terrane to the north and the Haya terrane to the south (Fig. 1). It trends northeast, except in the central part where offset by the Oko shear zone (Abdelsalam, 1994). At its southwestern end the suture zone disappears beneath eolian sand of the Sahara desert and is truncated in the northeast by Cenozoic normal faults along the Red Sea coast.

Working primarily east of the Oko shear zone, Abdelsalam and Stern (1993a; 1993b) identified five thrust-bounded tectonostratigraphic groups within the Nakasib suture zone: (1) the Shalhout group of arc-related intermediate to felsic volcanic rocks, turbidites, and limestone; (2) mafic-ultramafic ophiolite assemblages with suprasubduction-zone geochemical signatures (Johnson and others, 2002); siliciclastic, marine sedimentary, and felsic volcanic rocks of the (3) Salatib and (4) Meritri groups; and (5) tholeiitic, rift-related mafic and subordinate felsic volcanic and epiclastic rocks of the Arba'at group, dated at ca. 790 Ma (Abdelsalam and Stern, 1993c).

Table 3. Analytical and calculated data from SHRIMP-RG analyses of zircon from the Bi'r Umq suture zone.

Sample	Grain & spot no.	Comm. ^{206}Pb (%)	U (ppm)	Th (ppm)	^{232}Th/ ^{238}U	^{207}Pb-corrected		^{204}Pb-corrected						^{204}Pb-corrected							
						^{206}Pb/ ^{238}U age	1s error (Ma)	^{207}Pb/ ^{206}Pb age	1s error (Ma)	Total ^{238}U/ ^{206}Pb	% error	Total ^{207}Pb/ ^{206}Pb	% error	^{238}U/ ^{206}Pb	% error	^{207}Pb/ ^{206}Pb	% error	^{207}Pb/ ^{235}U	% error	Error corr. coeff.*	Apparent concordia age
SA01-68	1.1	-0.23	48	14	0.31	796.4	13.2	777.9	62.7	7.62	1.7	0.06	3.0	7.61	1.7	0.0651	3.0	1.18	3.4	0.493	795±25
	2.1	0.23	113	47	0.43	666.0	9.1	558.3	89.9	9.17	1.4	0.06	2.4	9.22	1.4	0.0588	4.1	0.88	4.4	0.323	662±18
	3.1	0.75	52	14	0.29	764.7	13.1	896.5	72.7	7.88	1.7	0.07	3.1	7.90	1.7	0.0689	3.5	1.20	3.9	0.444	771±25
	4.1	0.36	99	35	0.37	773.4	10.5	888.8	43.6	7.82	1.4	0.07	2.1	7.81	1.4	0.0687	2.1	1.21	2.5	0.551	781±20
	5.1	0.59	50	14	0.28	774.5	13.0	830.6	72.2	7.79	1.7	0.07	2.9	7.82	1.7	0.0668	3.5	1.18	3.9	0.443	778±12
	6.1	0.88	37	9	0.24	765.1	14.6	851.1	92.6	7.87	1.9	0.07	3.6	7.91	2.0	0.0674	4.5	1.18	4.9	0.402	769±28
	7.1	0.87	114	30	0.27	694.9	9.5	845.2	61.4	8.71	1.4	0.07	2.7	8.74	1.4	0.0672	2.9	1.06	3.3	0.425	701±18
	8.1	1.92	95	27	0.29	668.6	9.5	986.3	72.1	8.97	1.4	0.08	2.3	9.04	1.4	0.0720	3.5	1.10	3.8	0.377	Discordant
	9.1	1.91	68	20	0.30	780.2	11.7	816.0	160.9	7.62	1.5	0.08	2.3	7.76	1.6	0.0663	7.7	1.18	7.9	0.204	781±24
	10.1	0.24	93	28	0.32	780.1	10.8	719.4	71.4	7.75	1.4	0.07	2.5	7.79	1.4	0.0633	3.4	1.12	3.7	0.390	777±21
	11.1	-0.06	109	35	0.33	788.9	10.3	791.8	42.6	7.69	1.3	0.06	2.0	7.68	1.3	0.0655	2.0	1.18	2.4	0.552	789±19
	12.1	0.23	122	43	0.36	781.9	9.9	800.7	45.4	7.74	1.3	0.07	1.8	7.75	1.3	0.0658	2.2	1.17	2.5	0.513	783±19
SA01-74B	1.1	0.09	200	88	0.46	769.6	8.5	770.5	36.5	7.88	1.1	0.07	1.6	7.89	1.1	0.0649	1.7	1.13	2.1	0.549	770±16
	2.1	0.30	142	66	0.48	698.6	8.7	758.2	43.2	8.71	1.3	0.07	2.0	8.72	1.3	0.0645	2.0	1.02	2.4	0.529	702±17
	3.1	0.01	262	173	0.68	1988.9	20.7	1979.2	10.6	2.77	1.0	0.12	0.6	2.77	1.0	0.1216	0.6	6.05	1.2	0.868	1982±19
	4.1	0.35	96	32	0.35	775.1	10.3	759.2	65.0	7.80	1.4	0.07	2.1	7.83	1.4	0.0645	3.1	1.14	3.4	0.407	774±20
	5.1	-0.04	215	116	0.56	720.7	8.1	776.7	32.7	8.46	1.2	0.06	1.6	8.44	1.2	0.0651	1.6	1.06	1.9	0.597	725±15
	6.1	2.19	944	37	0.04	1153.1	11.2	1483.9	19.3	4.99	1.0	0.10	0.6	5.02	1.0	0.0928	1.0	2.55	1.4	0.691	Discordant
	7.1	0.35	61	14	0.24	778.8	11.8	1018.3	53.1	7.76	1.5	0.07	2.6	7.71	1.5	0.0732	2.6	1.31	3.0	0.508	Discordant
	9.1	0.29	196	105	0.55	670.3	8.2	619.9	53.4	9.10	1.3	0.06	1.7	9.14	1.3	0.0605	2.5	0.91	2.8	0.453	688±16
SA01-84	1.1	0.94	130	116	0.92	633.6	4.3	727.3	124.4	9.59	0.7	0.07	1.5	9.65	0.8	0.0636	5.9	0.91	5.9	0.135	636±10
	2.1	0.57	27	12	0.48	765.5	9.7	882.6	75.7	7.89	1.3	0.07	3.6	7.89	1.3	0.0685	3.7	1.20	3.9	0.327	770±18
	3.1	0.12	54	25	0.48	806.9	7.1	899.1	53.7	7.49	0.9	0.07	1.9	7.47	0.9	0.0690	2.6	1.27	2.8	0.329	811±14
	3.2	0.38	88	59	0.70	921.5	6.2	724.9	115.3	6.48	0.7	0.07	1.3	6.56	0.8	0.0635	5.4	1.34	5.5	0.141	914±13
	4.1	-0.04	492	620	1.30	866.2	2.5	823.1	19.2	6.96	0.3	0.07	0.6	6.97	0.3	0.0665	0.9	1.32	1.0	0.303	864±5
	5.1	0.30	30	15	0.53	821.1	9.7	686.2	178.2	7.34	1.2	0.07	2.5	7.40	1.3	0.0624	8.3	1.16	8.5	0.158	817±20
	6.1	0.00	28	13	0.48	831.9	9.9	314.6	286.2	7.26	1.2	0.07	2.6	7.38	1.4	0.0527	12.6	0.98	12.7	0.112	817±22
	7.1	-0.13	26	9	0.38	818.7	10.2	1071.6	122.3	7.39	1.3	0.07	2.8	7.31	1.4	0.0751	6.1	1.42	6.2	0.218	828±21
	7.2	1.50	29	11	0.39	786.4	14.7	778.7	177.7	7.59	1.9	0.08	3.2	7.71	2.0	0.0651	8.5	1.16	8.7	0.227	786±29
	8.1	0.44	257	114	0.46	738.8	3.1	793.2	40.7	8.20	0.4	0.07	0.9	8.22	0.4	0.0656	1.9	1.10	2.0	0.220	741±6
	9.1	0.24	43	19	0.46	757.6	14.0	778.4	651.7	8.00	1.9	0.07	2.2	8.01	3.1	0.0651	31.0	1.12	31.1	0.099	758±44
	10.1	0.25	138	51	0.38	720.2	4.2	716.8	36.7	8.44	0.6	0.07	1.3	8.46	0.6	0.0633	1.7	1.03	1.8	0.324	770±8
	11.1	-0.07	155	104	0.69	837.2	4.3	816.5	23.2	7.22	0.5	0.07	1.1	7.22	0.5	0.0663	1.1	1.27	1.2	0.423	836±8
	12.1	1.07	649	274	0.44	710.5	2.0	791.8	38.2	8.49	0.3	0.07	0.6	8.56	0.3	0.0655	1.8	1.06	1.8	0.151	713±4
	13.1	-0.14	173	66	0.39	765.9	3.8	664.8	43.2	7.94	0.5	0.06	1.1	7.96	0.5	0.0617	2.0	1.07	2.1	0.247	762±7
	14.1	0.47	58	31	0.55	836.6	10.4	681.1	150.9	7.18	1.3	0.07	2.2	7.26	1.4	0.0622	7.1	1.18	7.2	0.188	831±21
	15.1	0.58	32	12	0.39	859.7	15.2	926.5	85.5	6.97	1.8	0.07	3.1	6.99	1.8	0.0699	4.2	1.38	4.5	0.399	863±29
	16.1	1.30	29	11	0.40	862.9	16.2	934.9	108.4	6.89	1.9	0.08	4.0	6.96	1.9	0.0702	5.3	1.39	5.6	0.340	866±31
	17.1	3.46	56	50	0.93	801.2	12.4	686.4	387.3	7.30	1.4	0.09	5.3	7.59	1.8	0.0624	18.1	1.13	18.2	0.098	798±27
	18.1	1.23	23	7	0.32	814.7	16.1	897.9	120.0	7.33	2.0	0.08	3.3	7.40	2.0	0.0690	5.8	1.29	6.2	0.331	818±31
	19.1	0.58	33	13	0.42	836.1	14.0	263.6	345.1	7.18	1.7	0.07	4.1	7.36	1.9	0.0515	15.0	0.97	15.1	0.123	819±29
	20.1	0.79	32	11	0.37	804.2	14.1	482.4	256.5	7.47	1.8	0.07	3.1	7.61	1.9	0.0568	11.6	1.03	11.8	0.163	794±29
	21.1	0.82	25	10	0.41	815.1	16.0	740.8	151.8	7.36	2.0	0.07	4.2	7.44	2.0	0.0640	7.2	1.19	7.5	0.272	812±31
	22.1	1.25	45	17	0.39	857.4	12.4	1248.6	81.4	6.94	1.5	0.08	2.5	6.91	1.5	0.0821	4.2	1.64	4.4	0.341	Discordant
	23.1	0.01	70	50	0.74	833.3	10.1	771.2	59.6	7.25	1.2	0.07	2.3	7.26	1.2	0.0649	2.8	1.23	3.1	0.402	830±19
	24.1	0.48	72	51	0.73	829.2	10.1	768.0	78.7	7.25	1.2	0.07	2.2	7.30	1.3	0.0648	3.7	1.22	3.9	0.320	826±19
SA01-88	1.1	5.80	736	792	1.11	476.2	5.4	586.9	258.6	12.29	0.9	0.10	0.7	13.00	1.0	0.0595	11.9	0.63	12.0	0.085	478±9
	2.1	0.62	146	129	0.91	697.2	7.9	740.6	64.5	8.70	1.2	0.07	2.4	8.74	1.2	0.0640	3.0	1.01	3.3	0.356	699±15
	3.1	2.93	374	269	0.74	559.5	5.9	667.4	145.2	10.71	1.0	0.08	1.5	10.99	1.1	0.0618	6.8	0.78	6.9	0.155	562±11
	4.1	0.43	167	103	0.64	709.6	7.9	726.1	42.6	8.56	1.1	0.07	1.6	8.59	1.1	0.0635	2.0	1.02	2.3	0.493	711±15
	5.1	1.45	109	79	0.75	600.8	8.6	469.8	200.7	10.09	1.4	0.07	2.3	10.28	1.5	0.0564	9.1	0.76	9.2	0.167	598±18
	6.1	0.85	136	58	0.44	646.7	8.8	801.9	78.8	9.40	1.4	0.07	3.0	9.42	1.4	0.0659	3.8	0.96	4.0	0.344	651±17
	7.1	1.04	92	51	0.57	681.8	10.1	599.7	150.3	8.87	1.5	0.07	2.4	8.99	1.6	0.0599	6.9	0.92	7.1	0.221	679±20
	8.1	0.96	306	194	0.66	554.7	6.6	737.2	62.0	11.02	1.2	0.07	1.9	11.06	1.2	0.0639	2.9	0.80	3.2	0.384	559±13
	9.1	1.65	179	85	0.49	533.9	7.6	897.4	62.7	11.39	1.4	0.07	2.4	11.43	1.4	0.0690	3.0	0.83	3.4	0.429	Discordant
	10.1	4.09	170	115	0.70	547.7	8.0	777.3	241.7	10.82	1.3	0.09	4.8	11.19	1.4	0.0651	11.5	0.80	11.6	0.122	552±15
	11.1	1.12	158	92	0.61	627.8	7.8	610.7	142.0	9.67	1.3	0.07	1.8	9.78	1.3	0.0602	6.6	0.85	6.7	0.198	627±16
	12.1	3.34	573	440	0.79	467.5	5.1	759.6	122.2	12.85	1.0	0.08	1.0	13.16	1.1	0.0645	5.8	0.68	5.9	0.181	472±10
	13.1	5.34	215	151	0.73	471.1	7.3	689.3	335.2	12.48	1.2	0.10	5.4	13.09	1.5	0.0624	15.7	0.66	15.8	0.092	475±13
	14.1	2.97	516	343	0.69	545.4	6.0	923.6	108.2	10.99	1.0	0.08	2.0	11.17	1.1	0.0698	5.3	0.86	5.4	0.204	553±12
	15.1	1.35	440	302	0.71	602.5	6.3	573.2	119.4	10.07	1.1	0.07	1.4	10.22	1.1	0.0592	5.5	0.80	5.6	0.198	602±13
	16.1	4.41	852	580	0.70	549.3	5.8	661.1	185.4	10.75	0.9	0.09	0.9	11.20	1.0	0.0616	8.7	0.76	8.7	0.115	551±11
	17.1	0.15	260	157	0.62	714.0	2.9	709.7	39.9	8.53	0.4	0.06	0.9	8.54	0.4	0.0630	1.9	1.02	1.9	0.225	714±6
	18.1	-0.07	140	157	1.16	835.0	5.0	897.4	40.4	7.24	0.6	0.07	1.2	7.21	0.6	0.0690	2.0	1.32	2.1	0.306	838±10
	19.1	7.47	1058	1801	1.76	398.3	4.0	747.3	239.8	14.52	0.2	0.12	0.5	15.51	0.4	0.0642	11.3	0.57	11.4	0.035	403±3
	20.1	-0.04	34	14	0.42	831.9	9.1	621.1	142.4	7.26	1.1	0.07	2.4	7.32	1.2	0.0605	6.6	1.14	6.7	0.178	825±19
	21.1	-0.38	43	14	0.34	887.0	8.6	816.6	46.7	6.81	1.0	0.07	2.1	6.80	1.0	0.0663	2.2	1.35	2.4	0.407	882±16
	22.1	-0.57	36	12	0.34	927.7	10.0	90.9	285.2	6.50	1.1	0.07	2.3	6.63	1.3	0.0478	12.0	0.99	12.1	0.104	Discordant

Table 3 (continued).

Sample	Grain & spot no.	Comm. ^{206}Pb (%)	U (ppm)	Th (ppm)	$^{232}Th/^{238}U$	^{207}Pb-corrected $^{206}Pb/^{238}U$ age (Ma)	^{207}Pb-corrected 1s error (Ma)	^{204}Pb-corrected $^{207}Pb/^{206}Pb$ age (Ma)	^{204}Pb-corrected 1s error (Ma)	^{204}Pb-corrected Total $^{238}U/^{206}Pb$	^{204}Pb-corrected % error	^{204}Pb-corrected Total $^{207}Pb/^{206}Pb$	^{204}Pb-corrected % error	^{204}Pb-corrected $^{238}U/^{206}Pb$	^{204}Pb-corrected % error	^{204}Pb-corrected $^{207}Pb/^{206}Pb$	^{204}Pb-corrected % error	^{204}Pb-corrected $^{207}Pb/^{235}U$	^{204}Pb-corrected % error	^{204}Pb-corrected Error corr. coeff.*	Apparent concordia age
SA01-94	1.1	0.11	72	21	0.30	737.6	8.9	742.1	69.0	8.24	1.2	0.06	3.2	8.25	1.2	0.0640	3.3	1.07	3.5	0.349	738±17
	2.1	0.21	69	19	0.29	750.4	9.0	693.6	59.4	8.08	1.2	0.07	1.8	8.12	1.2	0.0626	2.8	1.06	3.0	0.406	748±17
	3.1	-0.11	82	30	0.38	758.7	8.6	803.5	56.6	8.02	1.2	0.06	1.7	7.99	1.2	0.0659	2.7	1.14	2.9	0.397	761±17
	4.1	-0.13	106	54	0.53	765.1	8.2	734.1	31.5	7.95	1.1	0.06	1.5	7.94	1.1	0.0638	1.5	1.11	1.8	0.593	762±15
	5.1	0.05	149	70	0.49	750.0	7.3	768.5	26.1	8.10	1.0	0.06	1.2	8.10	1.0	0.0648	1.2	1.10	1.6	0.630	752±14
	6.1	0.23	118	36	0.32	741.1	7.6	765.1	33.0	8.19	1.0	0.07	1.4	8.20	1.0	0.0647	1.6	1.09	1.9	0.556	743±14
	7.1	-0.03	79	42	0.55	758.0	8.7	659.3	47.4	8.02	1.2	0.06	1.7	8.04	1.2	0.0616	2.2	1.06	2.5	0.470	752±16
	8.1	0.07	84	31	0.38	754.0	8.5	751.0	37.6	8.05	1.2	0.06	1.7	8.06	1.2	0.0643	1.8	1.10	2.1	0.547	754±16
	9.1	-0.02	126	55	0.45	754.6	7.6	752.7	27.9	8.05	1.0	0.06	1.3	8.05	1.0	0.0643	1.3	1.10	1.7	0.616	754±14
	10.1	0.40	167	66	0.41	728.4	7.0	783.4	37.2	8.33	1.0	0.07	1.1	8.34	1.0	0.0653	1.8	1.08	2.0	0.486	731±13
	11.1	0.02	64	25	0.41	769.8	9.5	863.3	39.5	7.88	1.3	0.07	1.9	7.86	1.3	0.0678	1.9	1.19	2.3	0.554	776±18
	12.1	0.04	115	47	0.42	755.0	7.8	736.2	35.6	8.04	1.1	0.06	1.4	8.05	1.1	0.0638	1.7	1.09	2.0	0.535	754±15
	13.1	0.11	153	42	0.28	762.3	7.4	795.9	25.0	7.96	1.0	0.07	1.2	7.96	1.0	0.0657	1.2	1.14	1.6	0.641	766±14
SA01-103	1.1	0.51	149	40	0.27	746.9	9.1	738.0	57.2	8.10	1.2	0.07	2.2	8.14	1.3	0.0639	2.7	1.08	3.0	0.420	746±17
	2.1	-0.09	125	34	0.28	750.6	9.5	662.7	51.2	8.11	1.3	0.06	2.2	8.12	1.3	0.0617	2.4	1.05	2.7	0.477	745±18
	3.1	0.05	287	97	0.35	745.9	8.1	712.5	35.2	8.15	1.1	0.06	1.5	8.16	1.1	0.0631	1.7	1.07	2.0	0.558	743±15
	4.1	0.41	147	55	0.39	748.6	9.2	796.0	52.5	8.09	1.3	0.07	2.0	8.11	1.3	0.0657	2.5	1.12	2.8	0.451	751±18
	5.1	0.27	277	121	0.45	680.0	8.7	660.4	51.1	8.96	1.3	0.06	1.5	8.99	1.3	0.0616	2.4	0.94	2.7	0.482	679±17
	6.1	0.42	173	74	0.45	716.6	8.3	601.4	90.2	8.47	1.2	0.07	1.6	8.54	1.2	0.0599	4.2	0.97	4.3	0.278	713±16
	7.1	0.11	175	85	0.50	748.5	8.7	756.4	36.8	8.11	1.2	0.07	1.6	8.12	1.2	0.0644	1.7	1.09	2.1	0.566	749±17
	8.1	0.23	88	51	0.61	762.5	10.5	734.6	72.6	7.95	1.4	0.07	2.2	7.97	1.4	0.0638	3.4	1.10	3.7	0.382	761±20
	9.1	0.01	123	68	0.57	760.6	9.3	841.9	61.0	7.98	1.3	0.06	1.8	7.96	1.3	0.0671	2.9	1.16	3.2	0.396	764±18
	10.1	0.02	339	128	0.39	749.7	7.8	761.3	24.2	8.11	1.1	0.06	1.1	8.10	1.1	0.0646	1.1	1.10	1.6	0.680	751±14
	11.1	0.27	174	51	0.30	762.2	8.6	810.9	32.5	7.95	1.2	0.07	1.5	7.95	1.2	0.0661	1.6	1.15	1.9	0.598	766±16
	12.1	0.07	291	135	0.48	755.1	7.9	716.7	42.7	8.04	1.1	0.07	1.2	8.06	1.1	0.0633	2.0	1.08	2.3	0.474	753±15
	13.1	-0.05	222	114	0.53	737.3	8.3	698.8	34.0	8.26	1.2	0.06	1.5	8.26	1.2	0.0627	1.6	1.05	2.0	0.585	734±16
	14.1	0.00	292	97	0.34	748.8	7.9	757.1	26.0	8.12	1.1	0.06	1.2	8.12	1.1	0.0645	1.2	1.10	1.6	0.660	750±15
	15.1	-0.09	251	111	0.46	754.3	8.2	710.2	30.9	8.06	1.1	0.06	1.4	8.07	1.1	0.0631	1.5	1.08	1.8	0.607	750±15
	16.1	0.14	241	104	0.45	759.3	8.2	805.1	27.0	7.99	1.1	0.07	1.3	7.99	1.1	0.0660	1.3	1.14	1.7	0.651	764±15
	17.1	0.05	176	64	0.38	745.1	8.8	772.2	35.5	8.16	1.2	0.06	1.7	8.15	1.2	0.0649	1.7	1.10	2.1	0.581	747±17
SA01-109A	1.1	0.13	233	140	0.62	715.2	7.9	760.7	30.1	8.51	1.1	0.06	1.4	8.51	1.1	0.0646	1.4	1.05	1.8	0.620	719±15
	2.1	0.17	119	66	0.57	701.3	9.2	622.2	87.4	8.69	1.3	0.06	2.2	8.73	1.4	0.0605	4.1	0.96	4.3	0.319	698±18
	3.1	0.20	454	318	0.72	682.8	7.0	744.4	24.0	8.93	1.1	0.06	1.1	8.93	1.1	0.0641	1.1	0.99	1.5	0.680	688±13
	4.1	0.30	129	58	0.46	705.3	8.9	707.0	58.1	8.62	1.3	0.07	1.9	8.65	1.3	0.0630	2.7	1.00	3.0	0.428	705±17
	5.1	0.33	139	97	0.72	689.1	8.7	715.2	49.8	8.83	1.3	0.07	2.0	8.86	1.3	0.0632	2.3	0.98	2.7	0.483	690±17
	6.1	0.24	160	80	0.52	708.8	8.4	697.6	45.6	8.58	1.2	0.06	1.7	8.61	1.2	0.0627	2.1	1.00	2.5	0.494	708±16
	7.1	0.53	133	98	0.76	680.9	8.6	710.0	60.8	8.93	1.3	0.07	2.0	8.97	1.3	0.0631	2.9	0.97	3.1	0.413	682±17
	8.1	1.30	740	560	0.78	455.3	5.0	673.0	50.1	13.49	1.1	0.07	1.0	13.57	1.1	0.0620	2.3	0.63	2.6	0.433	Discordant
	9.1	0.22	133	84	0.65	678.0	8.6	678.7	47.2	9.00	1.3	0.06	2.1	9.02	1.3	0.0621	2.2	0.95	2.6	0.507	678±17
	10.1	-0.08	282	207	0.76	737.1	7.8	662.7	35.8	8.26	1.1	0.06	1.2	8.28	1.1	0.0617	1.7	1.03	2.0	0.545	732±15
	11.1	0.14	204	95	0.48	710.8	8.2	761.2	33.5	8.57	1.2	0.06	1.6	8.56	1.2	0.0646	1.6	1.04	2.0	0.594	714±15
	12.1	-0.05	161	115	0.74	700.4	8.4	574.7	76.5	8.72	1.2	0.06	1.8	8.75	1.2	0.0592	3.5	0.93	3.7	0.334	696±16
	13.1	-0.07	105	58	0.57	695.8	9.6	704.9	49.7	8.78	1.4	0.06	2.4	8.77	1.4	0.0629	2.3	0.99	2.7	0.516	696±18
SA01-110	1.1	0.22	117	77	0.68	796.3	8.1	809.8	33.6	7.59	1.0	0.07	1.3	7.60	1.0	0.0661	1.6	1.20	1.9	0.547	797±15
	2.1	-0.05	83	43	0.53	823.7	9.2	766.0	40.2	7.34	1.1	0.07	1.6	7.35	1.1	0.0647	1.9	1.21	2.2	0.515	819±17
	3.1	0.09	72	19	0.28	799.4	9.2	834.4	36.3	7.57	1.2	0.07	1.7	7.56	1.2	0.0669	1.7	1.22	2.1	0.563	802±17
	4.1	-0.11	137	65	0.49	810.7	8.0	784.6	25.5	7.47	1.0	0.07	1.2	7.47	1.0	0.0653	1.2	1.21	1.6	0.643	808±15
	5.1	0.04	133	75	0.58	798.1	7.8	811.1	25.5	7.58	1.0	0.07	1.2	7.58	1.0	0.0661	1.2	1.20	1.6	0.639	799±15
	6.1	-0.02	93	52	0.58	812.7	8.8	812.0	30.7	7.44	1.1	0.07	1.5	7.44	1.1	0.0662	1.5	1.23	1.8	0.602	813±16
	7.1	0.01	69	25	0.38	806.6	9.5	779.4	38.8	7.50	1.2	0.07	1.7	7.51	1.2	0.0652	1.8	1.20	2.2	0.547	804±18
	8.1	0.44	93	51	0.57	803.8	8.6	821.3	47.7	7.50	1.1	0.07	1.4	7.53	1.1	0.0665	2.3	1.22	2.5	0.437	805±17
	9.1	0.43	142	59	0.43	783.2	7.6	830.9	43.8	7.71	1.0	0.07	1.4	7.73	1.0	0.0668	2.1	1.19	2.3	0.431	786±15
	10.1	0.07	113	71	0.65	802.4	8.2	770.3	32.8	7.54	1.1	0.07	1.3	7.55	1.1	0.0649	1.6	1.18	1.9	0.560	800±15
	11.1	0.24	118	70	0.61	784.6	7.9	761.2	44.1	7.71	1.0	0.07	1.3	7.73	1.0	0.0646	2.1	1.15	2.3	0.446	783±15
	12.1	0.11	91	48	0.55	816.6	8.9	782.2	35.8	7.40	1.1	0.07	1.5	7.41	1.1	0.0652	1.7	1.21	2.0	0.550	814±17
	13.1	0.41	70	38	0.56	770.5	8.9	745.8	64.8	7.84	1.2	0.07	1.7	7.88	1.2	0.0641	3.1	1.12	3.3	0.365	769±17
SA01-122C	1.1	0.10	118	24	0.21	744.7	7.5	777.1	28.0	8.16	1.0	0.06	1.3	8.16	1.0	0.0651	1.3	1.10	1.7	0.614	747±14
	2.1	-0.06	119	28	0.24	756.2	7.8	793.5	43.3	8.04	1.1	0.06	1.4	8.02	1.1	0.0656	2.1	1.13	2.3	0.458	758±15
	3.1	-0.02	596	40	0.07	760.2	6.1	742.7	13.7	7.99	0.8	0.06	0.6	7.99	0.8	0.0640	0.6	1.10	1.1	0.788	757±11
	4.1	0.48	240	59	0.26	736.8	6.5	760.9	34.5	8.22	0.9	0.07	0.9	8.25	0.9	0.0646	1.6	1.08	1.9	0.487	738±13
	5.1	-0.01	191	36	0.19	752.3	7.0	705.6	27.4	8.08	1.0	0.06	1.1	8.09	1.0	0.0629	1.3	1.07	1.6	0.599	748±13
	6.1	0.24	125	27	0.22	751.8	7.9	774.9	35.6	8.06	1.1	0.07	1.5	8.08	1.1	0.0650	1.7	1.11	2.0	0.536	753±15
	7.1	0.13	892	181	0.21	724.4	5.7	735.0	14.3	8.40	0.8	0.06	0.5	8.41	0.8	0.0638	0.7	1.05	1.1	0.771	726±10
	8.1	0.19	87	21	0.25	733.7	8.3	859.8	53.4	8.28	1.2	0.07	1.7	8.26	1.2	0.0677	2.6	1.13	2.8	0.414	739±16
	9.1	-0.01	150	37	0.26	758.6	7.6	763.4	27.2	8.01	1.0	0.06	1.3	8.01	1.0	0.0647	1.3	1.11	1.6	0.621	759±14

Table 3 (continued).

Sample	Grain & spot no.	Comm. ^{206}Pb (%)	U (ppm)	Th (ppm)	$^{232}Th/^{238}U$	^{207}Pb-corrected $^{206}Pb/^{238}U$ age (Ma)	^{207}Pb-corrected 1s error (Ma)	^{204}Pb-corrected $^{207}Pb/^{206}Pb$ age (Ma)	^{204}Pb-corrected 1s error (Ma)	^{204}Pb-corrected Total $^{238}U/^{206}Pb$	^{204}Pb-corrected % error	^{204}Pb-corrected Total $^{207}Pb/^{206}Pb$	^{204}Pb-corrected % error	^{204}Pb-corrected $^{238}U/^{206}Pb$	^{204}Pb-corrected % error	^{204}Pb-corrected $^{207}Pb/^{206}Pb$	^{204}Pb-corrected % error	^{204}Pb-corrected $^{207}Pb/^{235}U$	^{204}Pb-corrected % error	^{204}Pb-corrected Error corr. coeff.*	Apparent concordia age
	10.1	-0.04	252	67	0.28	747.7	6.7	740.4	20.8	8.13	0.9	0.06	1.0	8.13	0.9	0.0640	1.0	1.08	1.3	0.684	747±12
	11.1	0.06	276	96	0.36	745.5	6.6	780.3	23.3	8.15	0.9	0.06	0.9	8.15	0.9	0.0652	1.1	1.10	1.4	0.635	749±12
	12.1	0.16	341	102	0.31	724.2	6.2	725.0	25.0	8.40	0.9	0.06	1.0	8.41	0.9	0.0635	1.2	1.04	1.5	0.598	724±6
	13.1	1.08	296	124	0.43	739.3	6.7	761.5	82.9	8.14	0.9	0.07	2.1	8.22	0.9	0.0646	3.9	1.08	4.0	0.230	740±13
	14.1	0.57	319	97	0.32	659.2	5.8	749.2	35.1	9.23	0.9	0.07	0.9	9.26	0.9	0.0642	1.7	0.96	1.9	0.481	663±11
SA01-123	1.1	0.14	191	51	0.28	760.6	5.3	798.8	27.6	7.97	0.7	0.07	1.3	7.97	0.7	0.0658	1.3	1.14	1.5	0.474	763±10
	2.1	0.17	216	95	0.46	772.9	5.3	705.9	36.7	7.84	0.7	0.07	1.3	7.87	0.7	0.0629	1.7	1.10	1.9	0.374	770±10
	3.1	0.30	126	34	0.28	733.5	6.7	715.9	58.1	8.27	0.9	0.07	1.8	8.30	0.9	0.0632	2.7	1.05	2.9	0.325	733±13
	4.1	-0.04	378	138	0.38	786.5	3.9	733.5	24.2	7.71	0.5	0.07	0.9	7.72	0.5	0.0638	1.1	1.14	1.3	0.403	784±7
	5.1	0.02	220	58	0.27	799.3	5.6	745.8	32.2	7.57	0.7	0.07	1.4	7.59	0.7	0.0641	1.5	1.16	1.7	0.426	796±11
	6.1	0.27	209	56	0.28	747.2	5.3	734.3	61.0	8.12	0.7	0.07	1.4	8.14	0.7	0.0638	2.9	1.08	3.0	0.251	747±11
	7.1	2.54	249	49	0.20	737.6	5.8	688.3	153.5	8.04	0.7	0.08	1.5	8.26	0.8	0.0624	7.2	1.04	7.2	0.115	736±12
	8.1	0.18	179	52	0.30	756.5	5.7	723.8	39.5	8.02	0.8	0.07	1.4	8.04	0.8	0.0635	1.9	1.09	2.0	0.384	755±11
	9.1	0.40	154	46	0.31	745.6	6.2	761.4	44.3	8.12	0.8	0.07	1.6	8.15	0.8	0.0646	2.1	1.09	2.3	0.374	746±12
	10.1	0.60	177	37	0.21	714.0	5.4	585.1	80.1	8.49	0.8	0.07	1.4	8.58	0.8	0.0595	3.7	0.96	3.8	0.209	710±11
	11.1	0.40	220	75	0.35	757.5	5.3	671.0	69.8	7.99	0.7	0.07	1.3	8.04	0.7	0.0619	3.3	1.06	3.3	0.221	755±11
	12.1	0.19	197	71	0.37	758.4	5.4	762.9	36.4	7.99	0.7	0.07	1.3	8.01	0.7	0.0646	1.7	1.11	1.9	0.388	759±10
	13.1	0.03	172	52	0.31	753.3	6.0	681.1	56.1	8.07	0.8	0.06	1.5	8.09	0.8	0.0622	2.6	1.06	2.8	0.302	751±12
	14.1	0.34	202	56	0.29	770.7	8.1	700.3	62.0	7.85	1.1	0.07	1.4	7.89	1.1	0.0628	2.9	1.10	3.1	0.351	768±16
	15.1	0.57	241	79	0.34	744.6	7.6	613.7	78.9	8.12	1.0	0.07	1.2	8.21	1.1	0.0603	3.7	1.01	3.8	0.280	740±15
	16.1	0.57	248	88	0.37	744.3	7.8	708.9	61.0	8.12	1.1	0.07	1.3	8.18	1.1	0.0630	2.9	1.06	3.1	0.352	743±15
	17.1	0.77	161	55	0.36	743.7	8.4	762.6	70.2	8.11	1.2	0.07	1.5	8.17	1.2	0.0646	3.3	1.09	3.5	0.333	744±16
SA03-149	1.1	4.57	548	391	0.74	719.5	8.3	642.2	233.6	8.08	1.0	0.10	2.1	8.49	1.1	0.0611	10.9	0.99	10.9	0.100	718±15
	2.1	0.53	57	21	0.37	779.3	12.6	743.6	93.0	7.74	1.7	0.07	2.8	7.79	1.7	0.0641	4.4	1.13	4.7	0.355	778±24
	3.1	0.23	190	90	0.49	673.1	8.1	676.9	41.7	9.06	1.2	0.06	1.8	9.09	1.2	0.0621	2.0	0.94	2.3	0.532	673±15
	4.1	0.28	59	23	0.40	783.1	11.9	531.7	226.6	7.72	1.5	0.07	4.7	7.81	1.6	0.0581	10.3	1.02	10.5	0.156	776±24
	5.1	0.51	229	218	0.98	1020.8	5.2	1119.5	18.5	5.80	0.5	0.08	0.7	5.80	0.5	0.0769	0.9	1.83	1.1	0.494	Discordant
	6.1	0.61	194	115	0.61	991.9	5.3	1086.6	29.2	5.97	0.5	0.08	1.2	5.99	0.5	0.0757	1.5	1.74	1.6	0.347	998±10
	7.1	0.20	77	44	0.58	1103.4	9.4	1129.8	56.5	5.35	0.9	0.08	1.2	5.35	0.9	0.0773	2.8	1.99	3.0	0.305	1105±18
	8.1	0.28	503	243	0.50	1058.7	3.7	1117.3	11.3	5.59	0.4	0.08	0.5	5.59	0.4	0.0768	0.6	1.90	0.7	0.533	Discordant
	9.1	-0.25	46	21	0.47	1137.4	12.5	1029.4	102.5	5.20	1.1	0.08	1.6	5.21	1.2	0.0736	5.1	1.95	5.2	0.231	1131±25
SA03-158	1.1	0.24	230	140	0.63	723.7	4.0	829.8	30.2	8.40	0.6	0.07	1.0	8.38	0.6	0.0667	1.4	1.10	1.6	0.366	728±8
	2.1	-0.04	53	20	0.39	769.8	8.6	476.7	180.4	7.89	1.1	0.06	2.0	7.96	1.3	0.0566	8.2	0.98	8.3	0.153	761±18
	3.1	0.06	49	17	0.36	783.5	9.0	611.9	111.7	7.73	1.2	0.07	2.0	7.78	1.2	0.0602	5.2	1.07	5.3	0.229	778±18
	4.1	-0.14	264	179	0.70	810.0	4.2	716.4	31.9	7.48	0.5	0.06	0.9	7.49	0.5	0.0632	1.5	1.16	1.6	0.340	806±8
	5.1	0.14	62	20	0.33	767.6	8.3	702.6	110.3	7.90	1.1	0.07	1.9	7.93	1.2	0.0628	5.2	1.09	5.3	0.218	766±17
	6.1	0.15	169	83	0.51	730.2	4.5	748.1	55.1	8.32	0.6	0.06	1.1	8.33	0.7	0.0642	2.6	1.06	2.7	0.242	731±9
	7.1	-0.12	225	150	0.69	777.7	4.2	762.7	24.3	7.81	0.5	0.06	1.1	7.80	0.5	0.0646	1.2	1.14	1.3	0.430	777±8
	8.1	0.06	162	67	0.42	784.9	5.5	692.1	68.7	7.72	0.7	0.07	1.2	7.75	0.8	0.0625	3.2	1.11	3.3	0.227	782±11
	9.1	-0.11	54	21	0.40	825.6	10.0	694.2	99.4	7.33	1.2	0.07	2.9	7.35	1.3	0.0626	4.7	1.17	4.8	0.261	820±19
	10.1	0.09	58	20	0.36	793.4	9.0	361.4	110.5	7.63	1.2	0.07	2.0	7.74	1.2	0.0538	4.9	0.96	5.0	0.235	Discordant
	11.1	0.51	105	60	0.60	772.1	7.6	780.2	80.6	7.82	1.0	0.07	1.7	7.86	1.0	0.0652	3.8	1.14	4.0	0.261	772±15
	12.1	-0.15	180	124	0.71	810.8	5.2	680.2	53.4	7.47	0.7	0.06	1.2	7.50	0.7	0.0622	2.5	1.14	2.6	0.262	806±10
	13.1	0.20	105	52	0.51	743.4	6.0	773.7	40.4	8.16	0.8	0.07	1.4	8.17	0.8	0.0650	1.9	1.10	2.1	0.396	745±12
	14.1	-0.11	51	21	0.42	818.9	9.8	916.0	106.9	7.39	1.2	0.07	2.1	7.35	1.3	0.0696	5.2	1.30	5.4	0.240	822±20
	14.2	-0.48	99	32	0.34	870.5	7.6	481.0	106.1	6.95	0.9	0.06	1.5	7.01	0.9	0.0567	4.8	1.12	4.9	0.191	Discordant
	15.1	0.05	57	24	0.43	811.3	9.0	801.4	105.3	7.45	1.1	0.07	2.0	7.46	1.2	0.0658	5.0	1.22	5.2	0.232	811±18
	16.1	0.13	114	55	0.50	783.1	6.1	786.4	36.4	7.73	0.8	0.07	1.4	7.74	0.8	0.0654	1.7	1.16	1.9	0.417	783±12
	17.1	0.04	104	43	0.43	806.4	6.9	720.6	89.7	7.50	0.9	0.07	1.5	7.53	0.9	0.0634	4.2	1.16	4.3	0.214	803±14
	18.1	-0.18	128	59	0.47	819.5	6.2	810.5	35.4	7.39	0.8	0.06	1.3	7.38	0.8	0.0661	1.7	1.24	1.9	0.417	819±12
SA03-160	1.1	0.41	224	197	0.91	752.9	8.1	788.2	38.9	8.04	1.1	0.07	1.2	8.06	1.1	0.0654	1.9	1.12	2.2	0.514	755±16
	2.1	0.02	792	1197	1.56	772.3	6.7	759.7	18.7	7.86	0.9	0.07	0.7	7.86	0.9	0.0646	0.9	1.13	1.3	0.712	771±12
	3.1	0.21	385	411	1.10	763.4	6.9	731.9	31.8	7.94	0.9	0.07	0.9	7.96	0.9	0.0637	1.5	1.10	1.8	0.529	761±13
	4.1	0.28	215	194	0.93	778.0	8.1	770.2	40.0	7.77	1.1	0.07	1.3	7.80	1.1	0.0649	1.9	1.15	2.2	0.492	778±15
	5.1	3.03	360	316	0.91	782.6	8.2	531.2	267.5	7.51	1.0	0.09	3.1	7.81	1.1	0.0580	12.2	1.02	12.3	0.092	776±16
	6.1	0.28	232	193	0.86	745.8	7.4	767.5	33.9	8.13	1.0	0.07	1.2	8.15	1.0	0.0648	1.6	1.10	1.9	0.535	747±14
	7.1	0.13	245	183	0.77	781.0	7.9	802.3	26.6	7.75	1.0	0.07	1.2	7.76	1.0	0.0659	1.3	1.17	1.6	0.633	783±15
	8.1	0.36	413	354	0.88	768.5	7.8	810.6	32.1	7.87	1.0	0.07	0.9	7.89	1.1	0.0661	1.5	1.16	1.9	0.565	772±15
	9.1	0.15	754	715	0.98	777.7	6.6	784.1	17.6	7.79	0.9	0.07	0.7	7.80	0.9	0.0653	0.8	1.15	1.2	0.724	779±12
	10.1	0.70	220	188	0.88	752.2	8.1	890.2	65.3	8.02	1.1	0.07	1.8	8.04	1.1	0.0687	3.2	1.18	3.4	0.334	757±16
	11.1	0.67	238	236	1.02	726.5	8.8	750.8	77.9	8.33	1.2	0.07	2.6	8.38	1.2	0.0643	3.7	1.06	3.9	0.317	727±17
	12.1	0.20	251	225	0.93	775.8	7.9	762.0	37.2	7.80	1.0	0.07	1.2	7.82	1.0	0.0646	1.8	1.14	2.1	0.510	775±15

Table 3 (continued).

Sample	Grain & spot no.	Comm. ^{206}Pb (%)	U (ppm)	Th (ppm)	$^{232}Th/^{238}U$	^{207}Pb-corrected		^{204}Pb-corrected						^{204}Pb-corrected							Apparent concordia age
						$^{206}Pb/^{238}U$ age (Ma)	1s error (Ma)	$^{207}Pb/^{206}Pb$ age (Ma)	1s error (Ma)	Total $^{238}U/^{206}Pb$	% error	Total $^{207}Pb/^{206}Pb$	% error	$^{238}U/^{206}Pb$	% error	$^{207}Pb/^{206}Pb$	% error	$^{207}Pb/^{235}U$	% error	Error corr. coeff.*	
SA03-174	1.1	4.81	828	1259	1.57	860.6	9.6	1606.1	30.4	6.66	1.0	0.11	0.5	6.74	1.0	0.0990	1.6	2.03	1.9	0.517	Discordant
	2.1	0.66	57	29	0.52	1015.4	15.2	1227.0	55.6	5.82	1.5	0.08	2.2	5.80	1.6	0.0812	2.8	1.93	3.2	0.480	Discordant
	3.1	0.61	54	38	0.72	1123.2	17.3	1223.8	46.8	5.22	1.6	0.08	2.2	5.23	1.6	0.0811	2.4	2.14	2.9	0.554	1137±31
	4.1	0.26	755	466	0.64	953.1	9.1	1001.8	15.1	6.26	1.0	0.07	0.7	6.26	1.0	0.0726	0.7	1.60	1.2	0.798	966±15
	5.1	0.03	572	213	0.38	289.3	3.2	314.8	36.7	21.78	1.1	0.05	1.6	21.77	1.1	0.0527	1.6	0.33	2.0	0.571	290±6
	6.1	-0.36	128	89	0.72	1001.9	11.9	884.7	37.7	5.97	1.2	0.07	1.6	5.98	1.2	0.0685	1.8	1.58	2.2	0.558	993±21
	7.1	-0.17	473	259	0.57	1178.7	11.4	1144.2	13.7	4.99	1.0	0.08	0.7	4.99	1.0	0.0779	0.7	2.15	1.2	0.824	1164±17
	8.1	0.81	173	78	0.46	191.3	3.5	117.8	128.4	32.93	1.8	0.06	3.3	33.26	1.8	0.0484	5.4	0.20	5.7	0.317	191±7
	9.1	-0.01	318	79	0.26	618.5	6.5	577.8	33.1	9.93	1.1	0.06	1.3	9.94	1.1	0.0593	1.5	0.82	1.9	0.580	616±13
	10.1	0.28	669	474	0.73	430.8	4.3	455.1	30.3	14.43	1.0	0.06	1.1	14.46	1.0	0.0561	1.4	0.53	1.7	0.601	432±9
	11.1	0.22	122	55	0.46	521.2	7.2	621.5	55.0	11.85	1.4	0.06	2.6	11.84	1.4	0.0605	2.5	0.70	2.9	0.483	524±14
	12.1	0.89	83	44	0.55	453.8	7.1	764.9	64.5	13.59	1.6	0.06	3.1	13.56	1.6	0.0647	3.1	0.66	3.4	0.459	Discordant
	13.1	1.83	341	135	0.41	262.6	3.2	673.6	73.7	23.62	1.2	0.07	1.9	23.74	1.2	0.0620	3.4	0.36	3.7	0.332	Discordant
	14.1	0.01	172	132	0.79	413.4	5.4	447.7	54.3	15.10	1.3	0.06	2.5	15.08	1.3	0.0559	2.4	0.51	2.8	0.475	414±11
	15.1	0.36	115	66	0.59	1554.2	18.7	1616.7	29.0	3.65	1.2	0.10	1.2	3.65	1.2	0.0996	1.6	3.76	2.0	0.624	1574±30
	16.1	0.22	215	96	0.46	409.6	5.0	357.5	86.5	15.21	1.2	0.06	2.1	15.27	1.2	0.0537	3.8	0.48	4.0	0.309	409±10
	17.1	0.45	156	171	1.13	1581.9	17.5	1649.0	17.3	3.58	1.1	0.10	0.9	3.58	1.1	0.1013	0.9	3.90	1.5	0.772	1615±24
	18.1	0.43	251	3	0.01	1032.8	11.0	1120.8	22.8	5.73	1.1	0.08	1.1	5.73	1.1	0.0770	1.1	1.85	1.6	0.693	Discordant
	19.1	2.93	795	431	0.56	946.2	9.8	1462.5	20.6	6.14	1.0	0.10	0.6	6.16	1.0	0.0918	1.1	2.05	1.5	0.680	Discordant
	20.1	0.47	1429	40	0.03	380.7	3.7	469.8	39.4	16.36	1.0	0.06	1.5	16.39	1.0	0.0564	1.8	0.47	2.0	0.487	382±100
SA03-215A	1.1	0.92	517	220	0.44	235.5	2.2	169.7	115.4	26.63	0.9	0.06	2.0	26.92	0.9	0.0495	4.9	0.25	5.0	0.186	235±4
	2.1	0.12	321	29	0.09	1167.2	9.8	1179.7	13.0	5.03	0.9	0.08	0.6	5.04	0.9	0.0793	0.7	2.17	1.1	0.798	1172±15
	3.1	0.75	394	194	0.51	1366.1	11.3	1409.8	19.6	4.20	0.8	0.09	0.5	4.23	0.9	0.0893	1.0	2.91	1.3	0.639	1378±19
	4.1	0.52	83	86	1.07	1921.7	21.4	1978.9	26.7	2.86	1.1	0.12	1.5	2.87	1.1	0.1215	1.5	5.85	1.9	0.594	1945±31
	5.1	0.14	250	121	0.50	644.3	5.9	626.2	36.2	9.50	0.9	0.06	1.1	9.52	0.9	0.0606	1.7	0.88	1.9	0.488	643±11
	6.1	0.13	284	219	0.80	99.0	1.2	-96.5	146.7	64.53	1.2	0.05	3.1	64.91	1.2	0.0443	6.0	0.09	6.1	0.204	99±2
	7.1	4.64	448	246	0.57	1101.5	13.0	1355.2	98.6	5.12	1.1	0.12	1.2	5.30	1.1	0.0868	5.1	2.26	5.2	0.211	1116±23
	8.1	0.10	471	55	0.12	1117.3	9.0	1101.1	15.2	5.28	0.8	0.08	0.5	5.29	0.8	0.0762	0.8	1.99	1.1	0.741	1113±15
	9.1	0.34	220	211	0.99	1660.2	14.5	1705.4	10.4	3.39	0.9	0.10	0.5	3.39	0.9	0.1045	0.6	4.24	1.1	0.846	1689±17
	10.1	0.18	67	98	1.50	2708.9	34.5	2723.6	10.3	1.91	1.1	0.19	0.6	1.91	1.1	0.1879	0.6	13.55	1.3	0.872	2722±20
	11.1	0.30	223	60	0.28	1855.1	16.4	1892.8	8.9	2.99	0.9	0.12	0.5	2.99	0.9	0.1158	0.5	5.34	1.0	0.876	1883±16
	12.1	-0.12	116	92	0.81	1365.0	13.8	1321.4	19.2	4.25	1.0	0.09	0.9	4.25	1.0	0.0853	1.0	2.77	1.4	0.725	1349±21
	13.1	0.07	424	209	0.51	461.5	4.0	403.2	25.8	13.46	0.9	0.06	1.0	13.50	0.9	0.0548	1.2	0.56	1.5	0.606	459±8
	14.1	0.25	348	169	0.50	1678.0	14.0	1710.1	8.1	3.36	0.9	0.11	0.4	3.36	0.9	0.1048	0.4	4.30	1.0	0.890	1701±14
SA03-245A	1.1	0.42	72	31	0.44	736.1	10.7	874.5	55.9	8.23	1.5	0.07	2.7	8.22	1.5	0.0682	2.7	1.14	3.1	0.480	743±20
	2.1	0.56	126	59	0.48	1046.2	13.0	1179.6	39.9	5.64	1.3	0.08	2.0	5.64	1.3	0.0793	2.0	1.94	2.4	0.533	1061±24
	3.1	0.28	370	226	0.63	1257.9	12.7	1244.0	26.2	4.63	1.0	0.08	0.8	4.64	1.0	0.0819	1.3	2.43	1.7	0.617	1255±22
SA03-246	1.1	0.51	91	49	0.56	621.1	8.9	507.6	104.7	9.84	1.4	0.06	2.9	9.92	1.5	0.0574	4.8	0.80	5.0	0.294	618±17
	2.1	0.30	160	61	0.39	1102.2	12.5	1131.9	28.6	5.35	1.2	0.08	1.3	5.36	1.2	0.0774	1.4	1.99	1.9	0.631	1108±22
	3.1	2.41	397	270	0.70	1206.0	12.4	1428.4	48.3	4.74	1.0	0.10	1.1	4.80	1.0	0.0901	2.5	2.59	2.7	0.379	Discordant
	4.1	0.15	175	64	0.38	752.6	8.9	686.6	43.2	8.06	1.2	0.07	1.7	8.09	1.2	0.0624	2.0	1.06	2.4	0.513	748±17
	5.1	0.05	82	68	0.86	1030.3	13.7	972.7	53.0	5.77	1.4	0.07	1.9	5.78	1.4	0.0715	2.6	1.71	2.9	0.469	1024±25
	6.1	-0.12	94	25	0.27	1032.9	13.4	1020.0	36.8	5.76	1.3	0.07	1.8	5.76	1.3	0.0732	1.8	1.75	2.3	0.593	1021±31
SA03-259	1.1	1.77	121	72	0.61	2569.1	28.1	2710.2	8.5	2.01	1.0	0.19	0.5	2.01	1.0	0.1863	0.5	12.80	1.1	0.885	Discordant
	2.1	0.11	138	78	0.59	1060.0	10.3	1083.3	20.8	5.59	1.0	0.08	1.0	5.59	1.0	0.0756	1.0	1.86	1.4	0.696	1065±18
	3.1	0.11	207	130	0.65	1473.3	13.1	1492.8	12.0	3.89	0.9	0.09	0.6	3.89	0.9	0.0932	0.6	3.30	1.1	0.823	1484±17
SA03-267	1.1	0.62	73	37	0.53	755.9	11.1	788.6	65.3	7.99	1.5	0.07	2.5	8.03	1.5	0.0654	3.1	1.12	3.5	0.434	769±21
	2.1	0.19	117	54	0.47	736.7	9.6	809.0	44.1	8.24	1.3	0.07	2.1	8.24	1.3	0.0661	2.1	1.11	2.5	0.537	746±20
	3.1	0.78	76	34	0.46	728.0	11.0	804.3	66.4	8.30	1.5	0.07	2.6	8.34	1.5	0.0659	3.2	1.09	3.5	0.438	747±53
	4.1	0.14	66	26	0.40	761.2	13.1	427.1	156.9	7.97	1.8	0.07	2.9	8.07	1.8	0.0554	7.0	0.95	7.3	0.248	736±22
	5.1	0.37	73	35	0.50	761.1	11.2	885.9	50.8	7.95	1.5	0.07	2.5	7.94	1.5	0.0686	2.5	1.19	2.9	0.521	732±21
	6.1	0.57	61	29	0.50	760.3	11.7	748.7	105.4	7.94	1.6	0.07	2.6	7.99	1.6	0.0642	5.0	1.11	5.2	0.306	727±26
	7.1	28.11	84	34	0.41	726.0	37.2	1376.9	1021.0	6.03	1.6	0.29	3.4	8.14	3.8	0.0877	53.1	1.49	53.2	0.071	730±20
	8.1	1.35	65	17	0.28	681.7	10.7	774.2	142.4	8.84	1.6	0.07	2.7	8.93	1.7	0.0650	6.8	1.00	7.0	0.237	684±21
	9.1	0.15	75	37	0.51	750.3	10.7	661.9	66.1	8.09	1.5	0.07	2.4	8.13	1.5	0.0616	3.1	1.05	3.4	0.430	746±20
	10.1	2.50	76	34	0.46	720.4	10.6	1010.1	93.6	8.25	1.5	0.08	2.3	8.36	1.5	0.0729	4.6	1.20	4.9	0.307	760±21
	11.1	0.60	40	14	0.35	731.9	13.3	602.4	129.8	8.27	1.8	0.07	3.4	8.36	1.9	0.0600	6.0	0.99	6.3	0.298	760±23
	12.1	0.41	60	24	0.41	733.9	11.4	781.0	67.9	8.26	1.6	0.07	2.8	8.28	1.6	0.0652	3.2	1.09	3.6	0.442	758±21
	13.1	0.22	68	24	0.36	768.6	10.7	523.3	141.4	7.88	1.4	0.07	2.3	7.96	1.5	0.0578	6.4	1.00	6.6	0.224	749±25
SA03-268A	1.1	0.80	166	154	0.96	2661.2	11.7	2721.8	6.1	1.94	0.4	0.19	0.4	1.94	0.4	0.1877	0.4	13.32	0.5	0.714	Discordant
	2.1	-0.01	52	16	0.31	1201.7	9.8	1091.9	84.3	4.88	0.8	0.08	2.9	4.91	0.8	0.0759	4.2	2.13	4.3	0.195	1195±18
	3.1	0.25	182	142	0.81	830.3	3.9	886.7	21.4	7.26	0.5	0.07	1.0	7.26	0.5	0.0686	1.0	1.30	1.1	0.419	834±7
	4.1	-0.27	237	68	0.29	1209.1	5.9	1136.1	16.4	4.86	0.5	0.08	0.7	4.86	0.5	0.0776	0.8	2.20	1.0	0.525	Discordant
	5.1	1.36	150	109	0.75	799.9	4.3	765.1	92.1	7.47	0.5	0.08	1.0	7.58	0.6	0.0647	4.4	1.18	4.4	0.133	799±9

Table 3 (continued).

Sample	Grain & spot no.	Comm. ^{206}Pb (%)	U (ppm)	Th (ppm)	$^{232}Th/^{238}U$	^{207}Pb-corrected $^{206}Pb/^{238}U$ age	^{207}Pb-corrected 1s error (Ma)	^{204}Pb-corrected $^{207}Pb/^{206}Pb$ age	^{204}Pb-corrected 1s error (Ma)	^{204}Pb-corrected Total $^{238}U/^{206}Pb$	^{204}Pb-corrected % error	^{204}Pb-corrected Total $^{207}Pb/^{206}Pb$	^{204}Pb-corrected % error	^{204}Pb-corrected $^{238}U/^{206}Pb$	^{204}Pb-corrected % error	^{204}Pb-corrected $^{207}Pb/^{206}Pb$	^{204}Pb-corrected % error	^{204}Pb-corrected $^{207}Pb/^{235}U$	^{204}Pb-corrected % error	^{204}Pb-corrected Error corr. coeff.*	Apparent concordia age
	6.1	-0.20	217	166	0.79	830.9	3.6	742.7	25.7	7.28	0.4	0.07	0.9	7.29	0.4	0.0640	1.2	1.21	1.3	0.342	Discordant
	7.1	0.34	326	523	1.66	1169.1	3.6	1160.4	24.4	5.01	0.3	0.08	0.6	5.03	0.3	0.0785	1.2	2.15	1.3	0.255	1168±7
SA03-269A	3.1	2.50	21	5	0.23	818.2	18.0	937.8	211.3	7.20	2.2	0.09	4.2	7.35	2.3	0.0703	10.3	1.32	10.6	0.220	823±36
	4.1	1.00	21	2	0.09	802.8	18.7	646.4	190.8	7.46	2.4	0.07	4.2	7.58	2.4	0.0612	8.9	1.11	9.2	0.263	797±36
	5.1	0.60	66	8	0.13	805.1	12.0	524.5	170.4	7.47	1.5	0.07	2.3	7.59	1.6	0.0579	7.8	1.05	7.9	0.200	795±24
SA03-269B	1.1	0.41	149	74	0.52	770.2	8.3	812.3	40.1	7.85	1.1	0.07	1.4	7.87	1.1	0.0662	1.9	1.16	2.2	0.501	800±17
	2.1	0.51	112	41	0.38	792.8	9.4	888.8	58.8	7.60	1.2	0.07	1.7	7.61	1.2	0.0687	2.8	1.24	3.1	0.398	788±17
	3.1	0.34	152	73	0.49	768.5	8.5	788.0	45.0	7.87	1.1	0.07	1.6	7.89	1.1	0.0654	2.1	1.14	2.4	0.468	781±19
	4.1	0.17	130	55	0.43	763.6	8.7	795.9	35.2	7.94	1.2	0.07	1.6	7.94	1.2	0.0657	1.7	1.14	2.0	0.571	773±16
	5.1	0.70	97	31	0.33	779.1	9.8	817.0	51.0	7.73	1.3	0.07	1.8	7.77	1.3	0.0663	2.4	1.18	2.8	0.466	770±16
	6.1	0.09	155	66	0.44	797.5	8.9	837.9	39.0	7.59	1.1	0.07	1.9	7.58	1.1	0.0670	1.9	1.22	2.2	0.522	766±16
	7.1	0.37	135	54	0.42	785.5	9.2	821.6	36.8	7.69	1.2	0.07	1.6	7.71	1.2	0.0665	1.8	1.19	2.1	0.562	762±17
	8.1	0.78	172	93	0.56	757.2	8.6	860.1	55.0	7.96	1.2	0.07	1.8	7.99	1.2	0.0677	2.6	1.17	2.9	0.402	755±16
	9.1	0.86	118	44	0.38	748.8	9.6	884.6	51.8	8.05	1.3	0.07	1.8	8.08	1.3	0.0685	2.5	1.17	2.8	0.464	756±18
	10.1	0.27	161	71	0.46	754.1	8.3	773.8	42.6	8.04	1.1	0.07	1.5	8.05	1.1	0.0650	2.0	1.11	2.3	0.490	797±18
SA03-270	1.1	0.18	382	351	0.95	777.4	7.2	813.8	20.5	7.79	1.0	0.07	1.0	7.79	1.0	0.0662	1.0	1.17	1.4	0.696	782±13
	2.1	0.02	357	313	0.91	784.0	7.3	747.5	26.0	7.73	1.0	0.07	1.0	7.74	1.0	0.0642	1.2	1.14	1.6	0.615	780±14
	3.1	0.50	113	43	0.39	779.5	9.3	761.4	55.1	7.74	1.2	0.07	1.7	7.79	1.2	0.0646	2.6	1.14	2.9	0.427	778±18
	4.1	0.62	150	55	0.38	746.2	8.5	835.2	50.3	8.10	1.2	0.07	1.6	8.12	1.2	0.0669	2.4	1.14	2.7	0.438	750±16
	5.1	0.27	178	77	0.45	802.2	8.7	669.5	56.3	7.53	1.1	0.07	1.4	7.58	1.1	0.0619	2.6	1.12	2.9	0.392	795±17
	6.1	0.57	88	31	0.36	786.3	10.2	719.5	97.5	7.66	1.3	0.07	1.9	7.73	1.4	0.0633	4.6	1.13	4.8	0.285	784±20
	7.1	0.34	217	99	0.47	768.6	7.6	765.4	49.4	7.87	1.0	0.07	1.8	7.90	1.0	0.0647	2.3	1.13	2.6	0.398	768±15
	8.1	0.94	89	49	0.57	759.2	9.8	704.4	111.6	7.93	1.3	0.07	1.9	8.02	1.4	0.0629	5.2	1.08	5.4	0.251	757±19
	9.1	0.27	228	118	0.53	769.2	7.8	691.3	55.5	7.87	1.0	0.07	1.4	7.91	1.0	0.0625	2.6	1.09	2.8	0.373	765±15
	10.1	0.34	249	134	0.56	772.0	7.6	754.2	44.6	7.83	1.0	0.07	1.3	7.87	1.0	0.0644	2.1	1.13	2.3	0.435	771±15
	11.1	0.34	157	63	0.42	778.8	8.4	774.9	48.5	7.76	1.1	0.07	1.4	7.79	1.1	0.0650	2.3	1.15	2.6	0.435	779±16
	12.1	0.34	213	82	0.40	779.6	7.9	780.7	40.4	7.75	1.0	0.07	1.2	7.78	1.0	0.0652	1.9	1.16	2.2	0.477	780±15
	13.1	0.42	181	73	0.42	779.6	8.3	831.6	34.5	7.75	1.1	0.07	1.4	7.76	1.1	0.0668	1.7	1.19	2.0	0.550	783±16
SA03-271	1.1	1.40	47	19	0.43	781.1	12.2	884.3	98.7	7.65	1.6	0.08	3.5	7.73	1.6	0.0685	4.8	1.22	5.0	0.314	785±23
	2.1	1.35	64	32	0.51	779.8	10.8	523.8	268.6	7.67	1.4	0.08	2.7	7.85	1.6	0.0578	12.2	1.02	12.3	0.129	773±23
	3.1	0.47	101	31	0.31	785.5	9.9	757.7	81.3	7.68	1.3	0.07	1.8	7.73	1.3	0.0645	3.9	1.15	4.1	0.323	784±19
	4.1	0.46	99	41	0.43	800.9	10.4	789.3	61.0	7.52	1.3	0.07	1.9	7.56	1.3	0.0655	2.9	1.19	3.2	0.417	800±20
	5.1	0.40	98	46	0.48	747.5	10.2	661.9	101.9	8.10	1.4	0.07	2.2	8.16	1.4	0.0616	4.8	1.04	5.0	0.288	744±20
	6.1	0.81	88	43	0.50	780.9	10.1	640.6	134.2	7.70	1.3	0.07	2.9	7.80	1.4	0.0610	6.2	1.08	6.4	0.213	776±20
	7.1	0.64	97	31	0.33	782.0	9.8	773.1	89.8	7.70	1.3	0.07	2.3	7.76	1.3	0.0650	4.3	1.15	4.5	0.293	782±19
	8.1	0.39	119	51	0.44	792.9	9.5	681.0	77.8	7.61	1.2	0.07	1.7	7.67	1.2	0.0622	3.6	1.12	3.8	0.322	788±18
	9.1	0.74	80	39	0.50	789.3	10.8	657.7	101.8	7.62	1.4	0.07	2.4	7.71	1.4	0.0615	4.7	1.10	5.0	0.287	784±21
	10.1	5.39	102	43	0.44	763.7	18.4	632.7	794.5	7.52	1.2	0.11	14.6	7.99	2.0	0.0608	36.9	1.05	37.0	0.055	760±29
	11.1	0.41	93	43	0.48	790.1	9.9	704.2	63.0	7.64	1.3	0.07	1.8	7.69	1.3	0.0629	3.0	1.13	3.2	0.399	785±19
	12.1	0.72	95	25	0.28	773.8	10.1	894.8	46.8	7.78	1.3	0.07	1.9	7.80	1.3	0.0689	2.3	1.22	2.6	0.506	781±19
SA03-277	1.1	0.11	175	62	0.36	1069.8	11.8	1075.8	25.7	5.53	1.1	0.08	1.2	5.54	1.1	0.0753	1.3	1.87	1.7	0.666	1071±21
	2.1	0.33	308	243	0.81	243.8	3.1	184.2	107.3	25.86	1.3	0.05	2.4	25.99	1.3	0.0498	4.6	0.26	4.8	0.267	243±6
SA03-278	1.1	2.03	102	41	0.42	754.3	9.7	660.1	175.7	7.89	1.3	0.08	2.2	8.08	1.4	0.0616	8.2	1.05	8.3	0.165	752±19
	2.1	1.89	80	30	0.39	731.7	10.7	905.5	117.7	8.16	1.5	0.08	2.2	8.26	1.5	0.0692	5.7	1.15	5.9	0.259	737±21
	3.1	1.70	121	62	0.53	734.6	9.7	807.1	120.5	8.14	1.3	0.08	2.2	8.26	1.4	0.0660	5.8	1.10	5.9	0.234	737±19
	4.1	1.52	139	70	0.52	756.0	9.7	722.6	160.2	7.91	1.3	0.08	3.2	8.05	1.4	0.0634	7.6	1.09	7.7	0.176	755±19
	5.1	1.36	80	33	0.43	857.5	21.2	633.1	218.8	6.93	2.5	0.08	2.5	7.09	2.6	0.0608	10.2	1.18	10.5	0.250	848±41
	6.1	1.31	164	65	0.41	732.3	9.4	787.7	99.6	8.20	1.3	0.07	2.5	8.29	1.3	0.0654	4.7	1.09	4.9	0.267	734±18
	7.1	2.53	119	61	0.53	699.7	9.9	902.5	162.2	8.50	1.4	0.08	2.1	8.65	1.5	0.0691	7.9	1.10	8.0	0.191	705±20
	8.1	1.66	86	37	0.45	729.8	10.4	758.4	135.9	8.20	1.4	0.08	2.1	8.33	1.5	0.0645	6.4	1.07	6.6	0.226	731±21
	9.1	1.07	135	59	0.45	743.7	9.1	698.1	116.2	8.09	1.2	0.07	1.7	8.19	1.3	0.0627	5.5	1.06	5.6	0.231	742±18
	10.1	0.80	129	52	0.42	646.8	9.0	734.4	91.5	9.40	1.4	0.07	2.3	9.45	1.4	0.0638	4.3	0.93	4.6	0.316	649±18
	11.1	1.58	105	54	0.53	766.8	10.1	424.0	272.4	7.79	1.3	0.08	2.8	8.01	1.5	0.0553	12.2	0.95	12.3	0.121	758±21
	12.1	1.27	75	30	0.42	768.0	11.0	842.9	124.2	7.80	1.4	0.08	3.6	7.88	1.5	0.0672	6.0	1.17	6.1	0.239	770±21
	13.1	1.22	74	31	0.43	750.0	11.3	585.7	241.5	8.01	1.5	0.07	4.1	8.15	1.6	0.0595	11.1	1.01	11.2	0.147	745±23
	14.1	1.39	125	55	0.45	674.9	8.8	901.5	71.7	8.93	1.3	0.07	1.9	8.98	1.3	0.0691	3.5	1.06	3.7	0.359	682±17
SA03-279	1.1	0.72	163	87	0.55	736.3	7.5	671.1	85.8	8.21	1.0	0.07	1.3	8.28	1.1	0.0619	4.0	1.03	4.2	0.258	734±15
	1.2	0.38	134	74	0.57	774.8	5.3	741.8	60.5	7.81	0.7	0.07	1.2	7.84	0.7	0.0640	2.9	1.13	3.0	0.247	774±11
	2.1	0.29	50	25	0.52	659.6	6.8	831.7	78.9	9.19	1.0	0.07	1.9	9.22	1.1	0.0668	3.8	1.00	3.9	0.274	664±14
	2.2	0.26	90	49	0.57	783.9	9.3	741.3	60.5	7.71	1.2	0.07	1.7	7.75	1.2	0.0640	2.9	1.14	3.1	0.394	782±18
	3.1	0.19	120	37	0.32	791.6	8.7	847.1	31.6	7.64	1.1	0.07	1.5	7.64	1.1	0.0673	1.5	1.22	1.9	0.597	796±16
	3.2	1.07	217	52	0.25	872.9	4.8	736.8	72.2	6.86	0.6	0.07	1.0	6.93	0.6	0.0639	3.4	1.27	3.5	0.172	868±10

Table 3 (continued).

Sample	Grain & spot no.	Comm. ^{206}Pb (%)	U (ppm)	Th (ppm)	$^{232}Th/^{238}U$	^{207}Pb-corrected $^{206}Pb/^{238}U$ age (Ma)	^{207}Pb-corrected 1s error (Ma)	^{204}Pb-corrected $^{207}Pb/^{206}Pb$ age (Ma)	^{204}Pb-corrected 1s error (Ma)	^{204}Pb-corrected Total $^{238}U/^{206}Pb$	^{204}Pb-corrected % error	^{204}Pb-corrected Total $^{207}Pb/^{206}Pb$	^{204}Pb-corrected % error	^{204}Pb-corrected $^{238}U/^{206}Pb$	^{204}Pb-corrected % error	^{204}Pb-corrected $^{207}Pb/^{206}Pb$	^{204}Pb-corrected % error	^{204}Pb-corrected $^{207}Pb/^{235}U$	^{204}Pb-corrected % error	^{204}Pb-corrected Error corr. coeff.*	Apparent concordia age
	4.1	0.05	462	447	1.00	771.4	6.6	741.0	22.8	7.86	0.9	0.07	0.8	7.88	0.9	0.0640	1.1	1.12	1.4	0.634	768±12
	5.1	0.15	111	63	0.59	807.6	9.4	788.3	42.2	7.48	1.2	0.07	1.7	7.50	1.2	0.0654	2.0	1.20	2.3	0.510	806±18
	6.1	0.16	189	89	0.48	768.4	7.7	769.9	31.1	7.89	1.0	0.07	1.3	7.90	1.0	0.0649	1.5	1.13	1.8	0.573	769±15
	6.2	0.91	117	45	0.40	771.4	5.8	660.0	80.3	7.83	0.8	0.07	1.4	7.90	0.8	0.0616	3.7	1.08	3.8	0.208	768±12
	7.1	0.83	270	204	0.78	739.1	3.4	611.5	58.6	8.20	0.5	0.07	0.8	8.27	0.5	0.0602	2.7	1.00	2.8	0.180	735±7
	7.2	0.34	304	255	0.87	765.9	6.9	758.8	36.0	7.90	0.9	0.07	1.0	7.93	0.9	0.0645	1.7	1.12	1.9	0.481	765±13
	8.1	0.11	290	248	0.88	763.3	4.5	837.8	42.1	7.92	0.6	0.07	1.9	7.93	0.6	0.0670	2.0	1.16	2.1	0.279	766±9
	8.2	0.18	246	186	0.78	836.1	8.0	853.8	25.1	7.21	1.0	0.07	1.1	7.22	1.0	0.0675	1.2	1.29	1.6	0.630	838±15
	9.1	3.67	478	227	0.49	781.1	7.7	897.4	178.5	7.48	0.9	0.10	2.2	7.73	1.0	0.0690	8.7	1.23	8.7	0.117	785±15
	9.2	1.58	471	243	0.53	771.0	3.2	795.4	66.3	7.74	0.4	0.08	0.6	7.86	0.4	0.0657	3.2	1.15	3.2	0.123	772±6
	10.1	0.72	98	61	0.65	797.9	6.5	679.3	41.6	7.57	0.8	0.07	1.4	7.62	0.8	0.0622	1.9	1.12	2.1	0.394	791±12
	10.2	0.11	142	80	0.58	811.7	8.7	782.4	41.4	7.44	1.1	0.07	1.4	7.46	1.1	0.0652	2.0	1.21	2.3	0.488	810±16
	11.1	13.80	106	68	0.67	788.6	18.6	501.8	1257.7	6.69	0.9	0.17	5.4	7.76	3.4	0.0573	57.1	1.02	57.2	0.059	781±50
	11.2	0.11	51	27	0.55	752.5	8.1	835.3	58.7	8.04	1.1	0.07	1.9	8.05	1.1	0.0669	2.8	1.15	3.0	0.366	756±16
	12.1	4.83	64	35	0.56	776.7	10.1	719.4	326.8	7.45	1.0	0.10	4.4	7.83	1.3	0.0633	15.4	1.12	15.5	0.087	775±20
SA04-318	1.1	0.32	56	23	0.43	722.6	7.8	439.5	124.2	8.40	1.1	0.07	2.0	8.51	1.1	0.0557	5.6	0.90	5.7	0.201	714±16
	1.2	0.48	86	27	0.33	754.9	6.8	916.1	38.1	8.01	0.9	0.07	1.5	8.00	0.9	0.0696	1.9	1.20	2.1	0.445	Discordant
	2.1	0.23	118	36	0.32	749.4	5.5	816.2	27.4	8.09	0.8	0.07	1.3	8.09	0.8	0.0663	1.3	1.13	1.5	0.498	753±11
	3.1	0.19	113	49	0.45	776.0	5.9	752.0	59.2	7.80	0.8	0.07	1.4	7.82	0.8	0.0643	2.8	1.13	2.9	0.273	775±12
	4.1	-0.02	213	138	0.67	801.5	4.6	663.4	59.1	7.55	0.6	0.07	1.0	7.59	0.6	0.0617	2.8	1.12	2.8	0.217	797±9
	5.1	0.35	390	102	0.27	871.3	4.1	746.0	61.1	6.89	0.5	0.07	0.9	6.94	0.5	0.0641	2.9	1.27	2.9	0.173	867±8
	6.1	-0.24	176	80	0.47	822.4	5.4	709.8	47.9	7.37	0.7	0.06	1.2	7.38	0.7	0.0630	2.3	1.18	2.4	0.290	818±10
	7.1	0.06	165	79	0.50	783.1	5.0	801.8	26.4	7.74	0.7	0.07	1.1	7.74	0.7	0.0659	1.3	1.17	1.4	0.464	784±10
	8.1	0.10	201	89	0.46	777.0	4.6	690.4	65.5	7.80	0.6	0.07	1.1	7.83	0.6	0.0625	3.1	1.10	3.1	0.205	774±9
	9.1	1.59	151	63	0.43	717.3	5.0	768.3	91.8	8.36	0.7	0.08	1.2	8.48	0.7	0.0648	4.4	1.05	4.4	0.167	719±10
	10.1	-0.17	121	56	0.48	778.4	5.7	670.9	53.9	7.80	0.7	0.06	1.3	7.82	0.8	0.0619	2.5	1.09	2.6	0.288	774±11
	11.1	-0.78	220	100	0.47	1030.5	6.1	787.3	42.5	5.81	0.6	0.07	1.1	5.83	0.6	0.0654	2.0	1.55	2.1	0.289	Discordant
	12.1	0.28	117	41	0.37	718.0	5.4	675.4	70.4	8.46	0.8	0.07	1.3	8.50	0.8	0.0620	3.3	1.01	3.4	0.235	717±11
	13.1	0.20	49	22	0.46	774.7	8.9	721.3	146.9	7.82	1.2	0.07	2.0	7.85	1.3	0.0634	6.9	1.11	7.0	0.181	773±19
	14.1	0.19	136	52	0.40	765.9	5.4	757.8	65.2	7.91	0.7	0.07	1.3	7.93	0.8	0.0645	3.1	1.12	3.2	0.237	766±11
	15.1	-0.13	144	64	0.46	797.3	5.3	634.0	71.1	7.61	0.7	0.06	1.2	7.64	0.7	0.0609	3.3	1.10	3.4	0.212	792±11
	16.1	-0.19	243	171	0.73	845.8	4.8	753.0	33.0	7.15	0.6	0.07	1.0	7.16	0.6	0.0643	1.6	1.24	1.7	0.351	841±9
	17.1	0.19	170	79	0.48	756.9	5.2	727.7	64.8	8.01	0.7	0.07	1.2	8.04	0.7	0.0636	3.1	1.09	3.1	0.233	756±10
SA04-366	1.1	0.21	89	45	0.52	761.7	8.4	621.8	60.8	7.96	1.1	0.07	1.7	8.01	1.1	0.0605	2.8	1.04	3.0	0.374	Discordant
	2.1	-0.05	84	29	0.35	794.6	9.1	803.2	37.1	7.63	1.2	0.07	1.7	7.62	1.2	0.0659	1.8	1.19	2.1	0.554	871±28
	3.1	0.06	60	25	0.43	841.9	11.5	1046.0	87.3	7.16	1.4	0.07	2.0	7.11	1.4	0.0742	4.3	1.44	4.6	0.317	851±23
	4.1	0.02	43	22	0.52	873.9	13.7	793.5	164.3	6.89	1.6	0.07	2.3	6.91	1.7	0.0656	7.8	1.31	8.0	0.214	836±23
	5.1	0.05	142	62	0.45	808.3	7.0	799.3	37.3	7.48	0.9	0.07	1.3	7.49	0.9	0.0658	1.8	1.21	2.0	0.447	838±19
	6.1	-0.25	102	44	0.45	870.4	9.8	928.7	64.3	6.94	1.2	0.07	1.6	6.90	1.2	0.0700	3.1	1.40	3.3	0.353	817±16
	7.1	-0.58	72	26	0.37	962.2	11.6	584.1	74.4	6.25	1.2	0.07	2.0	6.30	1.2	0.0595	3.4	1.30	3.6	0.342	808±13
	8.1	0.02	91	30	0.34	839.5	9.6	812.8	67.4	7.19	1.2	0.07	1.6	7.20	1.2	0.0662	3.2	1.27	3.4	0.348	795±17
	9.1	-0.30	57	20	0.36	840.4	12.1	791.1	50.6	7.20	1.5	0.06	2.1	7.20	1.5	0.0655	2.4	1.26	2.8	0.524	755±16
	10.1	0.01	108	49	0.47	820.5	8.4	762.0	55.7	7.37	1.1	0.07	1.5	7.38	1.1	0.0646	2.6	1.21	2.8	0.373	1394±20
	11.1	-0.17	120	66	0.56	1405.6	13.3	1374.0	18.3	4.11	1.0	0.09	1.0	4.11	1.0	0.0876	1.0	2.94	1.4	0.715	Discordant
	12.1	-4.78	222	197	0.92	3150.1	36.5	2838.9	5.4	1.66	0.7	0.20	0.3	1.66	0.7	0.2016	0.3	16.71	0.7	0.894	Discordant
SA04-367	1.1	0.52	142	49	0.36	1416.6	11.6	1524.3	17.7	4.05	0.8	0.09	0.8	4.04	0.8	0.0948	0.9	3.23	1.3	0.667	Discordant
	2.1	0.44	35	19	0.56	778.3	13.7	552.2	236.4	7.76	1.8	0.07	2.6	7.85	1.9	0.0586	10.8	1.03	11.0	0.176	871±29
	3.1	0.30	40	21	0.54	858.6	14.4	1158.5	125.0	7.00	1.7	0.07	2.4	6.93	1.8	0.0785	6.3	1.56	6.6	0.275	828±25
	4.1	0.17	138	23	0.17	1038.2	8.9	1034.9	35.8	5.71	0.9	0.08	1.1	5.72	0.9	0.0738	1.8	1.78	2.0	0.449	830±28
	4.2	0.05	365	151	0.43	1022.1	7.8	959.3	39.8	5.82	0.8	0.07	1.0	5.84	0.8	0.0711	1.9	1.68	2.1	0.377	Discordant
	5.1	0.02	246	57	0.24	360.7	2.7	293.3	45.4	17.37	0.8	0.05	1.6	17.41	0.8	0.0522	2.0	0.41	2.1	0.359	820±30
	6.1	0.28	72	35	0.49	1560.8	17.0	1533.6	33.2	3.64	1.1	0.10	1.1	3.66	1.1	0.0953	1.8	3.59	2.1	0.537	799±23
	7.1	-0.06	186	82	0.46	950.2	7.1	908.1	32.2	6.30	0.8	0.07	1.0	6.31	0.8	0.0693	1.6	1.52	1.7	0.443	771±28
	8.1	-0.62	127	67	0.55	1285.9	12.1	1156.0	71.8	4.56	1.0	0.08	1.1	4.56	1.0	0.0784	3.6	2.37	3.8	0.270	416±7
	9.1	-0.51	340	114	0.35	1981.4	10.8	1911.7	7.7	2.79	0.5	0.12	0.4	2.79	0.5	0.1171	0.4	5.78	0.7	0.786	360±5
	10.1	0.15	111	35	0.32	1109.9	11.7	1111.5	32.5	5.31	1.1	0.08	1.2	5.32	1.1	0.0766	1.6	1.99	2.0	0.559	Discordant
	11.1	-0.07	44	14	0.33	845.3	12.7	349.6	213.7	7.14	1.5	0.07	2.3	7.26	1.6	0.0535	9.5	1.02	9.6	0.170	1554±28
	13.1	0.01	745	45	0.06	418.7	3.3	249.5	88.1	14.90	0.8	0.06	1.6	14.97	0.8	0.0512	3.8	0.47	3.9	0.210	1275±23
	14.1	0.35	285	163	0.59	1727.0	9.7	1780.7	8.5	3.24	0.6	0.11	0.5	3.24	0.6	0.1089	0.5	4.63	0.7	0.773	1110±21
	15.1	0.05	597	211	0.37	1022.5	5.7	1024.9	14.6	5.82	0.6	0.07	0.6	5.82	0.6	0.0734	0.7	1.74	0.9	0.624	1038±17
	16.1	0.12	47	25	0.54	821.2	13.9	1015.2	102.8	7.35	1.7	0.07	2.5	7.30	1.8	0.0730	5.1	1.38	5.4	0.332	1023±10
	17.1	-0.25	47	35	0.76	828.0	16.2	728.2	71.2	7.31	2.0	0.06	2.9	7.32	2.0	0.0636	3.4	1.20	3.9	0.513	1017±15
	18.1	0.07	46	28	0.64	796.0	12.2	843.7	59.8	7.60	1.6	0.07	2.3	7.59	1.6	0.0672	2.9	1.22	3.3	0.480	947±13

Table 3 (continued).

Sample	Grain & spot no.	Comm. ^{206}Pb (%)	U (ppm)	Th (ppm)	$^{232}Th/^{238}U$	^{207}Pb-corrected $^{206}Pb/^{238}U$ age (Ma)	^{207}Pb-corrected 1s error (Ma)	^{204}Pb-corrected $^{207}Pb/^{206}Pb$ age (Ma)	^{204}Pb-corrected 1s error (Ma)	^{204}Pb-corrected Total $^{238}U/^{206}Pb$	^{204}Pb-corrected % error	^{204}Pb-corrected Total $^{207}Pb/^{206}Pb$	^{204}Pb-corrected % error	^{204}Pb-corrected $^{238}U/^{206}Pb$	^{204}Pb-corrected % error	^{204}Pb-corrected $^{207}Pb/^{206}Pb$	^{204}Pb-corrected % error	^{204}Pb-corrected $^{207}Pb/^{235}U$	^{204}Pb-corrected % error	^{204}Pb-corrected Error corr. coeff.*	Apparent concordia age
SA04-373	1.1	0.16	139	69	0.52	562.2	5.3	626.9	35.6	10.96	1.0	0.06	1.7	10.95	1.0	0.0607	1.6	0.76	1.9	0.500	564±10
	2.1	0.16	124	66	0.55	574.7	5.7	337.6	158.0	10.71	1.0	0.06	2.0	10.80	1.1	0.0532	7.0	0.68	7.1	0.154	570±12
	3.1	0.06	127	61	0.50	595.6	5.6	704.2	61.3	10.33	1.0	0.06	1.7	10.29	1.0	0.0629	2.9	0.84	3.0	0.320	598±11
	4.1	0.01	131	72	0.57	589.4	5.5	633.0	46.9	10.44	1.0	0.06	1.6	10.43	1.0	0.0608	2.2	0.80	2.4	0.403	591±11
	5.1	0.12	115	63	0.56	572.4	5.7	746.7	84.3	10.76	1.0	0.06	1.8	10.70	1.1	0.0642	4.0	0.83	4.1	0.255	576±12
	6.1	0.32	134	75	0.58	574.4	5.2	581.3	67.5	10.69	0.9	0.06	1.6	10.73	0.9	0.0594	3.1	0.76	3.2	0.287	575±10
	7.1	-0.06	163	82	0.52	612.7	5.1	641.4	44.3	10.03	0.9	0.06	1.4	10.02	0.9	0.0611	2.1	0.84	2.2	0.386	614±10
	8.1	-0.14	126	53	0.43	602.8	5.7	500.9	51.0	10.22	1.0	0.06	1.7	10.24	1.0	0.0572	2.3	0.77	2.5	0.389	599±11
	9.1	-0.12	119	56	0.49	598.8	6.0	501.6	72.2	10.29	1.0	0.06	1.8	10.31	1.0	0.0573	3.3	0.77	3.4	0.301	596±12
	10.1	-0.07	131	67	0.53	608.8	5.8	501.4	83.4	10.10	1.0	0.06	1.6	10.13	1.0	0.0573	3.8	0.78	3.9	0.257	606±12
	11.1	-0.08	152	83	0.56	624.0	5.5	542.4	53.8	9.85	0.9	0.06	1.5	9.87	0.9	0.0583	2.5	0.82	2.6	0.345	621±11
	12.1	0.09	248	159	0.66	581.2	4.1	624.7	26.8	10.59	0.7	0.06	1.2	10.58	0.7	0.0606	1.2	0.79	1.4	0.497	583±8
	13.1	0.26	119	58	0.50	601.8	6.0	665.0	55.8	10.19	1.0	0.06	1.7	10.20	1.0	0.0617	2.6	0.83	2.8	0.366	604±12
	14.1	0.13	110	55	0.51	609.5	6.3	643.7	195.9	10.07	1.1	0.06	1.8	10.07	1.3	0.0611	9.1	0.84	9.2	0.136	610±15
	14.2	0.02	149	82	0.57	611.5	5.5	610.7	59.7	10.05	0.9	0.06	2.0	10.05	0.9	0.0602	2.8	0.83	2.9	0.316	612±11
	15.1	0.08	148	79	0.55	628.5	5.6	609.6	57.3	9.76	0.9	0.06	1.5	9.77	0.9	0.0602	2.6	0.85	2.8	0.331	628±11
	15.2	0.24	76	34	0.46	616.0	8.2	332.9	117.0	9.95	1.4	0.06	2.2	10.06	1.4	0.0531	5.2	0.73	5.3	0.258	608±16
	16.1	0.27	112	56	0.51	590.8	6.2	519.8	88.3	10.39	1.1	0.06	1.7	10.44	1.1	0.0577	4.0	0.76	4.2	0.263	589±12
SA04-412	1.1	-0.04	52	37	0.74	806.0	11.5	849.3	51.2	7.51	1.5	0.07	2.5	7.50	1.5	0.0674	2.5	1.24	2.9	0.509	809±22
	2.1	0.40	62	23	0.38	758.0	10.1	939.9	58.0	7.98	1.4	0.07	2.0	7.96	1.4	0.0704	2.8	1.22	3.1	0.436	Discordant
	3.1	-0.05	45	22	0.50	832.1	12.5	830.9	49.3	7.26	1.5	0.07	2.3	7.26	1.5	0.0668	2.4	1.27	2.8	0.547	832±23
	3.2	0.18	45	20	0.45	843.1	13.5	902.8	47.4	7.14	1.6	0.07	2.3	7.14	1.7	0.0691	2.3	1.34	2.8	0.583	849±25
	4.1	-0.04	48	21	0.45	847.5	12.6	354.4	205.9	7.12	1.5	0.07	2.2	7.24	1.6	0.0536	9.1	1.02	9.3	0.175	Discordant
	5.1	0.84	38	21	0.56	794.8	13.0	640.0	83.3	7.56	1.7	0.07	2.4	7.66	1.7	0.0610	3.9	1.10	4.2	0.398	786±25
	6.1	0.26	39	20	0.53	832.3	13.6	968.8	83.8	7.24	1.7	0.07	2.4	7.22	1.7	0.0714	4.1	1.36	4.4	0.383	839±27
	7.1	0.42	53	23	0.46	802.9	11.0	534.3	171.1	7.51	1.4	0.07	2.0	7.61	1.5	0.0581	7.8	1.05	8.0	0.187	794±22
	8.1	0.05	48	28	0.59	869.0	13.0	937.2	56.9	6.93	1.5	0.07	2.2	6.91	1.5	0.0703	2.8	1.40	3.2	0.487	874±25
	9.1	0.06	100	49	0.51	801.6	8.1	834.3	33.5	7.55	1.0	0.07	1.5	7.54	1.0	0.0669	1.6	1.22	1.9	0.543	804±15
	10.1	0.20	58	42	0.75	849.4	11.1	874.7	92.5	7.09	1.3	0.07	1.9	7.09	1.4	0.0682	4.5	1.33	4.7	0.296	851±22
	10.2	0.33	42	19	0.46	818.4	12.6	851.7	135.8	7.36	1.6	0.07	2.3	7.38	1.7	0.0674	6.5	1.26	6.7	0.246	820±25
	11.1	-0.23	54	43	0.82	868.3	12.6	637.8	113.3	6.95	1.5	0.07	2.1	6.99	1.5	0.0610	5.3	1.20	5.5	0.279	857±24
	11.2	0.08	74	25	0.35	832.1	10.5	844.8	64.3	7.25	1.3	0.07	1.8	7.25	1.3	0.0672	3.1	1.28	3.4	0.392	833±20
	12.1	0.00	44	29	0.69	844.9	13.3	406.1	165.3	7.14	1.6	0.07	2.2	7.25	1.7	0.0548	7.4	1.04	7.6	0.220	Discordant
	13.1	0.14	70	26	0.39	841.0	10.6	601.7	113.6	7.17	1.3	0.07	1.8	7.24	1.3	0.0599	5.2	1.14	5.4	0.246	831±21
	14.1	-0.01	49	19	0.40	817.0	12.3	799.8	135.4	7.40	1.6	0.07	2.2	7.41	1.6	0.0658	6.5	1.22	6.7	0.244	816±25
	15.1	-0.15	37	16	0.44	860.6	14.3	386.1	256.2	7.01	1.7	0.07	3.5	7.11	1.8	0.0544	11.4	1.05	11.6	0.158	844±29
	16.1	0.26	83	26	0.32	796.6	9.0	700.0	102.2	7.58	1.2	0.07	1.7	7.63	1.2	0.0628	4.8	1.13	4.9	0.243	793±18
	16.2	0.02	46	31	0.69	796.3	12.0	862.7	58.5	7.60	1.5	0.07	2.3	7.59	1.6	0.0678	2.8	1.23	3.2	0.483	800±23

* Error correlation coefficient between $^{207}Pb/^{235}U$ and $^{206}Pb/^{238}U$.

Deformation along the Nakasib suture occurred between ca. 780 and 740 Ma and emplaced the volcanosedimentary and ophiolitic nappes along subhorizontal thrusts, followed by folding of northeast-trending structures about northeast-trending upright axes (Abdelsalam and Stern, 1993a; Abdelsalam and Stern, 1993b). Subsequent deformation along the Oko shear zone generated north-trending upright folds, and northwest-trending shear zones transposed the northeasterly structures of the Nakasib suture, which was offset ca. 10 km (Abdelsalam, 1994). This last event occurred sometime between 700 and 560 Ma and was associated with convergence along the EAO (Abdelsalam, 1994).

Controversy has arisen from research on the Nakasib suture, where arc plutonic terranes, suprasubduction-zone type ophiolitic nappes, and volcanosedimentary sequences exposed within the suture zone have been interpreted to record (1) a single episode of arc generation above a south-dipping subduction zone, consumption of a large ocean basin, and accretion of arc terranes (Abdel-Rahman, 1993; Schandelmeier and others, 1994; Wipfler, 1996; Johnson and others, 2002) and (2) a complete Wilson cycle (although on a smaller than typical scale) that involved rifting of a pre-existing arc terrane, subsequent seafloor spreading in a back-arc basin, north-dipping subduction of the back-arc oceanic crust, and reassembly of the arc terrane (Abdelsalam and Stern, 1993a; Abdelsalam and Stern, 1993b; Abdelsalam, 1994; Stern and Abdelsalam, 1998). Resolution of this controversy may hinge upon studies of correlative rocks along the Bi'r Umq suture zone in Saudi Arabia and the recognition of lithological, structural, and geochemical trends relevant to the competing models.

Bi'r Umq Suture Zone in Saudi Arabia

The Bi'r Umq suture zone (BUSZ) in Saudi Arabia juxtaposes the Hijaz terrane to the north and the Jeddah terrane to the south (Figs. 1, 2); the majority of the units discussed herein lie within the deformed northern half of the Jeddah terrane. The BUSZ is truncated at the southwestern end by steep normal faults along the Red Sea and at the northeastern end by younger suture-

Table 4. All radiometric age data for the study areas.

Unit name - Lithology	U-Pb zircon SHRIMP-RG (this study)	U-Pb zircon Conventional	Rb-Sr	Sm-Nd	K-Ar	Evaluation	Sources
Arj group			651 ± 40 w			Rejected: too young, geological conflict	
Bari granodiorite	**776 ± 6**					Crystallization age	This study
	~771					Crystallization age	
Bi'r Umq ophiolite - post-pbduction keratophyre		764 ± 3				Single-point upper intercept model age	Pallister and others (1988)
- post-pbduction keratophyre		782 ± 5				Single-point upper intercept model age	Pallister and others (1988)
- trondhjemite				828 ± 47 m		Crystallization age	Dunlop and others (1986)
- basalt			831 ± 47 w			Crystallization age	Dunlop and others (1986)
- diorite		**838 ± 10**				Crystallization age	Pallister and others (1988)
Dhukhr tonalite			774 ± 101 w			Rejected: high error, geological conflict	Fleck and Hadley (1985)
	803 ± 17					Minimum crystallization age	This study
		811 ± 4				Crystallization age	Stoeser & Stacey (1988)
	813±10					Crystallization age	This study
		816 ± 4				Crystallization age	Calvez & Kemp (1982)
			665 m			Rejected: too young, geological conflict	Aldrich (1978)
Furayh group			633 ± 15 w				
			663 ± 44 w				
Ghamr group			748 ± 22 w			Minimum age	Calvez & Kemp (1982)
					555 ± 15	Rejected: too young	
Hufayriyah tonalite			692 ± 15 m			Rejected: too young	Brown and others (1978)
		760 ± 10				Minimum crystallization age	Calvez & Kemp (1982)
	785 ± 6					Crystallization age	This study
Hypabyssal intrusion - in Bi'rak group	812 ± 23					Crystallization age	
- in Bi'rak group	854 ± 15					Validity unknown	
Kamil suite			709 ± 164 w			Rejected: too young, high errors	Fleck (1985)
					760	Validity unknown	
			769 ± 39 w			Crystallization age	Fleck (1985)
			763 ± 159 w			Provisional age, but high errors	Fleck and others. (1979)
	772 ± 6					Crystallization age	This study
					800	Validity unknown	
	802 ± 5					Crystallization age	This study
			~825 m		~800 m	Maximum crystallization age	Aldrich and others (1978)
			965 m			Rejected: too old	
Mahd group - Haf formation			572 ± 35 w			Rejected: too young	Brown and others (1978)
			726 ± 21 w			Rejected: too young	Huckerby (1984)
			726 ± 33 w			Rejected: too young	Calvez & Kemp (1982)

Table 4 (continued).

Unit name - Lithology	U-Pb zircon SHRIMP-RG (this study)	U-Pb zircon Conventional	Rb-Sr	Sm-Nd	K-Ar	Evaluation	Sources
			772 ± 36 w			Crystallization age	Huckerby (1984)
	777 ± 5					Crystallization age	This study
Post-tectonic rocks - Umm Gerad syenogranite			580 ± 9 w			Crystallization age	Al-Shanti & Abdel-Monem (1982)
- Hanak granite	**596 ± 10**					Crystallization age	This study
- Subh suite			687 ± 18 w			Crystallization age	(Clark and Duyverman, 1983)
- Subh suite		696				Maximum crystallization age	Aleinikoff and Stoeser (1988)
- Nukhu granite dike	**699 ± 7**					Crystallization age	This study
Qudayd suite - Khamrah gneiss					585 ± 12	Rejected: too young	G. Brown in Gettings and Stoeser (1
- Hadabah dike	**747 ± 5**					Crystallization age	This study
- Hadabah gneiss	**751 ± 5**					Crystallization age	This study
- Khamrah gneiss	**782 ± 7**					Crystallization age	This study
Rabigh suite			800 ± 75 w			Rejected: high errors	Al Shanti and others (1984)
		807 ± 8				Provisional age	C. Hedge, in Al-Shanti and Abdel-Monem (1982), Camp (1986)
			945 ± 28			Rejected: too old	
Raghiyah suite			520 ± 15 m			Provisionally rejected: too young	Brown and others(1978)
			566 ± 30 w			Crystallization age	Brown and others (1978)
			567 ± 86 w			Crystallization age	Fleck and Hadley (1985)
			573 ± 22 w			Crystallization age	Calvez & Kemp (1982)
			575 ± 28 w			Crystallization age	Calvez & Kemp (1982)
			584 ± 26 w			Crystallization age	Calvez & Kemp (1982)
			590 ± 10 w			Crystallization age	Brown and others (1978)
			~598 w			Crystallization age	Fleck and Hadley (1985)
Ramram complex			741 ± 92 w			Provisional minimum age: high errors	Huckerby (1984)
	749 ± 10					Crystallization age	This study
			758 ± 35 w			Crystallization age	Huckerby (1984)
			764 ± 14 w			Crystallization age	Huckerby (1984)
		769 ± 5				Maximum crystallization age	Calvez & Kemp (1982)
	769 ± 6					Maximum crystallization age	This study
Samran group - Amudan formation	**746 ± 6**					Crystallization age	This study
	752 ± 4					Crystallization age	This study
	753 ± 6					Crystallization age	This study
Samran group - Shayban formation	**771 ± 1**					Crystallization age	This study
	777 ± 28					Crystallization age	This study
- arkose	**825 ± 7**					Age of basement protolith	This study
Samran group - Nida formation					585 ± 12	Rejected: too young	Brown and othes (1978)
Tharwah ophiolite complex - diorite	777 ± 17					Minimum crystallization age	This study
- diorite		**870 ± 11**				Maximum crystallization age	Pallister and others (1988)

Most robust ages shown in bold. Data sources given in text. m = mineral; w= whole-rock

related structures of the Hulayfah-Ad Dafinah-Ruwah fault zone (Figs. 1-3) (Johnson and Kattan, 2001). The central part of the Bi'r Umq suture zone is obscured by Quaternary alluvium and Cenozoic flood basalts beneath Harrat Rahat, which separates the suture into the Tharwah segment in the southwest and the Bi'r Umq segment in the northeast (Fig. 2). The two segments are believed to be continuous, based on common lithologic and structural characteristics and the continuity of aeromagnetic trends beneath the flood basalts (Johnson and others, 2002). The aeromagnetic trends also show the change in orientation of structures along the BUSZ from mainly northeast in the Tharwah segment to more or less east-west in the Bi'r Umq segment, which suggests that the suture zone forms a syntaxis beneath Harrat Rahat.

The oldest rocks in the BUSZ occur along the northern margin of the Jeddah terrane, where 811-816 Ma old foliated tonalite in the Dhukhr and Furayhah batholiths forms the basement of the Bi'r Umq segment (Fig. 3B) (Calvez and Kemp, 1982; Stoeser and Stacey, 1988). The basement is overlain by folded and sheared volcano-sedimentary rocks of the Mahd and Ghamr groups, dated at ca. 770 Ma and ca. 750 Ma, respectively (Calvez and Kemp, 1982). Similarly deformed volcanosedimentary rocks of the Samran group (Fig. 3A), which Johnson (1998) considered to be para-autochthonous, occur at the same stratigraphic level in the Tharwah segment, but older basement has not been recognized there. The Samran and Mahd groups, which are tentatively

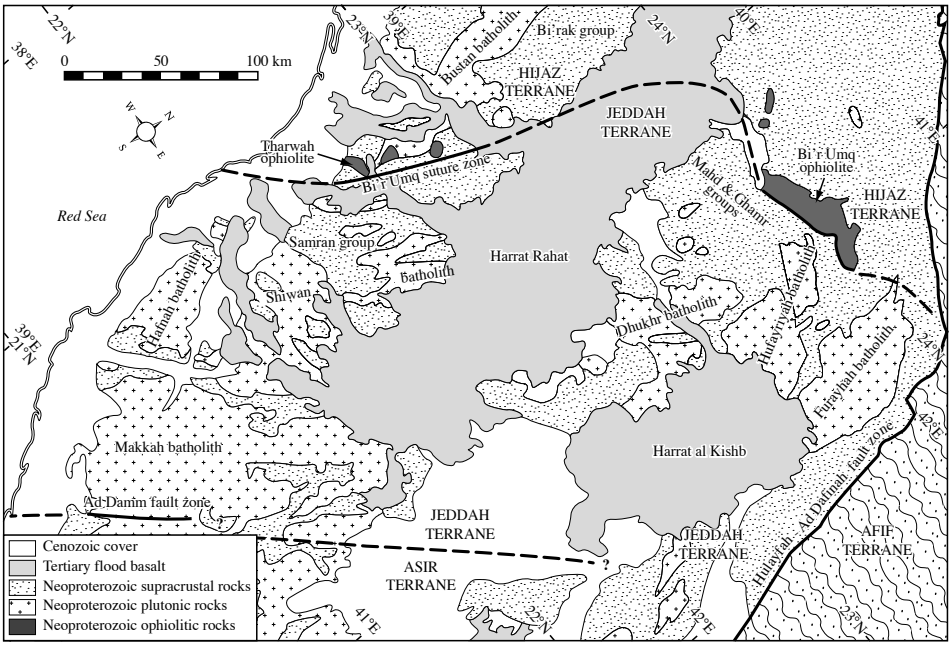

Figure 2. Geologic map of the Jeddah terrane, modified after Brown and others (1989), showing the distribution of Neoproterozoic plutonic rocks in the greater Jeddah batholith, associated supracrustal rocks, and major ophiolite complexes. The Jeddah terrane is bounded to the north by the Bi'r Umq suture zone, to the east by the Hulayfah-Ad Dafinah-Ruwah fault zone, to the south by the Ad Damm fault zone, and to the west by the Red Sea rift.

The Bi'r Umq suture zone and the margins of the Jeddah and Hijaz terranes affected by suture-related deformation mostly lie within the Rabigh (Ramsay, 1986b), Umm al Bi'rak (Camp, 1986b), and Mahd adh Dhahab (Kemp and others, 1982b) 1:250,000-scale quadrangle map areas. The Rabigh quadrangle was also mapped in more detail at a scale of 1:100,000 (Gilboy and Skiba, 1978a, 1978b, 1978c, 1978d). A number of more detailed investigations were conducted over subsets of the map areas, generally for the purposes of mineral exploration for the Saudi Arabian Deputy Ministry for Mineral Resources (Al-Shanti, 1970; Kana'an, 1970; Liddicoat, 1971; Alabouvette and others, 1972; Abu Rashid, 1973; Jourde, 1976; Ono, 1976a, 1976b; Kana'an, 1977; Fujii and Okumi, 1978; Fujii and others, 1978; Ozawa, 1978; Hopwood, 1979; Kana'an and Liddicoat, 1979). The following descriptions are based on the published literature, geological survey reports, correlated with the Arba'at group and Ariab series in the Nakasib suture zone, are respectively intruded by ca. 770-760 Ma old, locally sheared, arc-related plutons of the Shiwan and Hufayriyah batholiths. Syntectonic tonalite of the Qudayd suite also intrudes the Samran group, but geologically meaningful ages for the suite have not been previously obtained.

In the Tharwah segment, volcanic-sedimentary rocks north of the suture belong to the Bi'rak group (Fig. 3A), but stratigraphic or structural equivalents of these are not exposed in the Bi'r Umq segment. The Bi'rak group is intruded by ca. 807 Ma arc-related plutons of the Rabigh suite (Al-Shanti and others, 1984; C. Hedge, cited as pers. comm. in Camp, 1986a). The main exposures of the Tharwah ophiolite, dated at ca. 870 Ma (Pallister and others, 1988b), are surrounded by the Bi'rak group and lie entirely within the Hijaz terrane, except for a small nappe exposed in the Jeddah terrane

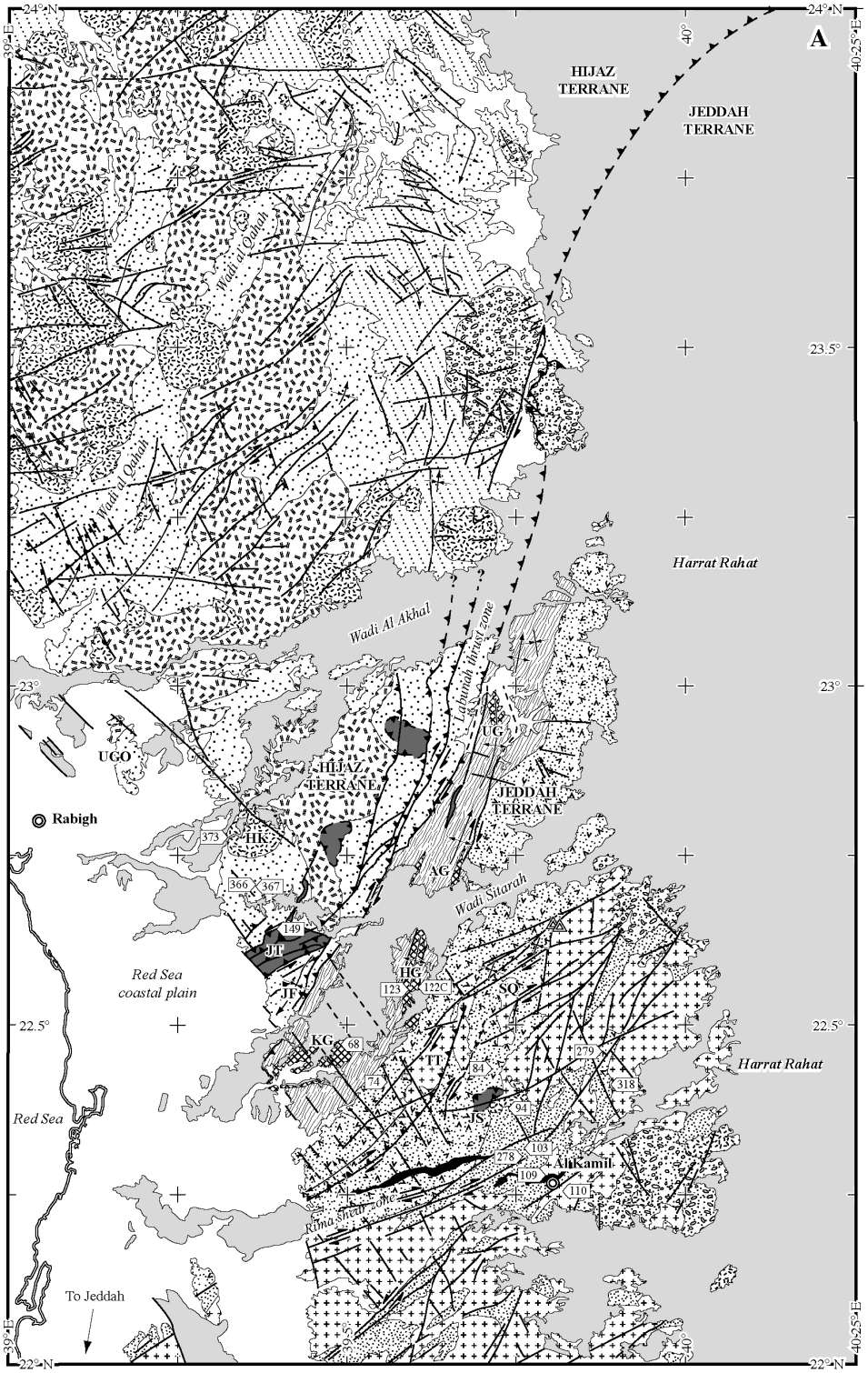

Figure 3. Geologic map of the (A) Tharwah and (B) Bi'r Umq segments of the Bi'r Umq suture zone in the western Arabian Shield. The locations of geochronological samples obtained during this study are indicated. AG, Asad gneiss; HG, Hadab gneiss; JF, Jabal Farasan; JH, Jabal Hammah; JHD, Jabal Hbad ad Dayahin; JHS, Jabal Habd ash Sharar; JJ, Jabal Jural; JR, Jabal Ramram; JS, Jaww serpentinite; JT, Jabal Tharwah; KG, Khamrah gneiss; SQ, Shagiyah quartz-diorite; TT, Thufir trondhjemite; UG, Ukaz gneiss; UGO, Umm Gerad outlier. Maps are modified from Kemp and others (1982b), Camp (1986b), Roobol (1989), and Johnson (1998).

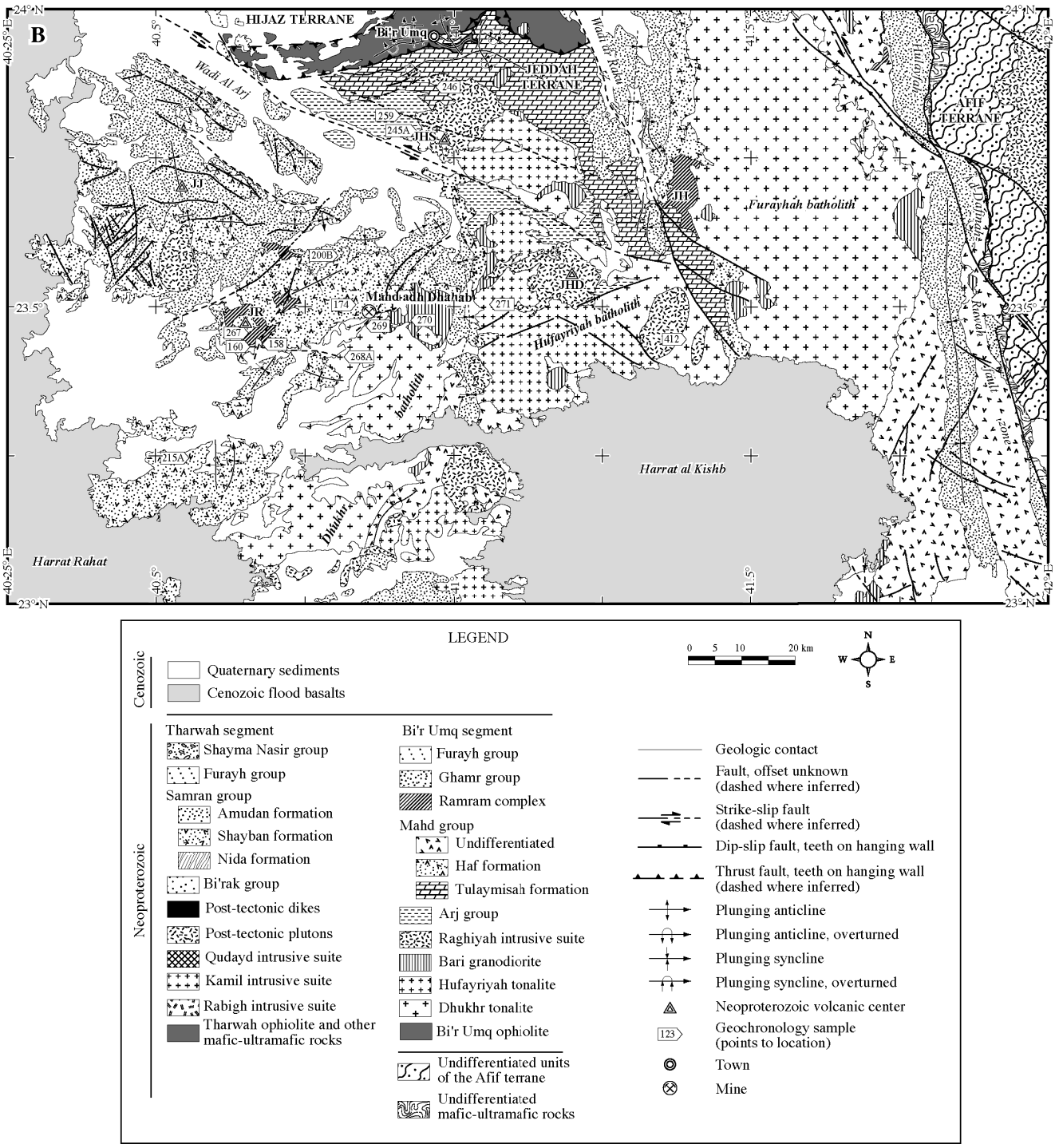

Figure 3 (continued).

far to the southeast of the main ophiolite occurrences. The Bi'r Umq ophiolite (Fig. 3B), dated at ca. 840-830 Ma (Pallister and others, 1988b), was thrust directly onto the Jeddah terrane over parts of the Mahd group. Both ophiolites are bounded by high angle reverse faults and define structures that are either synforms (Al-Rehaili and Warden, 1980) or flower structures (Johnson and others, 2002).

Late syntectonic to posttectonic, volcanosedimentary deposits of the ca. 663-633 Ma Furayh group (Aldrich and others, 1978) north of the suture overlie the Bi'rak group and Rabigh suite in the Tharwah segment and the Bi'r Umq ophiolite in the Bi'r Umq segment. The youngest stratigraphic unit is the posttectonic Shayma Nasir group (Fig. 3A), which unconformably overlies deformed units to the north and south of the Tharwah segment. The suture zone was also punctuated between ca. 700 to 520 Ma by small, undeformed, largely alkaline to peralkaline granitic and monzogranitic intrusions and related volcanic rocks (Brown and others, 1978; Al-Shanti and Abdel-Monem, 1982; Calvez and Kemp, 1982; Clark and Duyverman, 1983; Fleck, 1985; Aleinikoff and Stoeser, 1988). This was the last major magmatic episode to affect the shield until Cenozoic

rifting to form the Red Sea.

In the Tharwah segment (Fig. 3A), the main structural elements are the Labunah thrust zone along the axis of the suture and the Samran fold-thrust belt to the southeast. Johnson (1998) identified two (D1, D2) phases of progressive, suture-related, brittle-ductile deformation and a later (D3) phase of extensional brittle deformation. The D1 phase generated northeast-trending structures including moderately dipping thrust faults and dextral shear zones in the Labunah thrust zone, upright tight to isoclinal folds in the Samran group, and vertical foliation in the plutonic rocks south of the suture. Subsequent D2 folding rotated the thrusts to near vertical and produced younger upright folds and subvertical shear zones with variably dextral to sinistral and reverse-to-normal senses of motion. The structural evidence indicates northwest-southeast-directed oblique dextral shortening that was accompanied by greenschist-facies metamorphism. A late (D3) phase of brittle deformation was associated with extension along east-west-trending shear zones (Johnson, 1998).

In the Bi'r Umq segment (Fig. 3B), a similar history of progressive polyphase deformation was documented, but is less well constrained. Early (D1) deformation involved south-vergent thrusting along the Bi'r Umq fault on the southern edge of the Bi'r Umq ophiolite. Motion on the fault changed to dextral and sinistral strike slip during later (D2) deformation (Johnson and others, 2002). The northeast and northwest orientations of large-scale folds in the Mahd group just south of the ophiolite are parallel to the Bi'r Umq fault and are consistent with an origin during D1 thrusting. North-trending folds in the Mahd and Ghamr groups and large-scale warping about north-trending axes of earlier east-west-trending structures, including the Bi'r Umq thrust fault and the ophiolite itself, are evidence of even later east-west-directed shortening, probably associated with sinistral transpression-related suturing with the Afif terrane to the east along the Hulayfah-Ad Dafinah-Ruwah fault zone (Johnson and Kattan, 2001) (Fig. 3B) or due to terminal collision between East and West Gondwana. That later suturing event may also have caused westward translation of the Furayhah batholith, motion along the strike-slip faults in Wadi al Arj and Wadi Ar Raku, and northwest-directed expulsion of the intervening block containing the Bi'r Umq ophiolite. Johnson and others (2002), however, associated motion along the Arj fault with the post-accretionary Najd fault system.

Deformation along the BUSZ was accompanied by greenschist-facies metamorphism with an increase in metamorphic grade towards the bounding thrusts. In most places, however, original volcanic, sedimentary, and plutonic textures are well preserved. Notable exceptions are where amphibolite-facies assemblages developed within dynamothermal aureoles surrounding intrusive bodies or where shearing has obliterated original features.

GEOCHRONOLOGY OF PLUTONIC AND HYPABYSSAL INTRUSIONS

The names of the plutonic units discussed here are numerous, and it is easy for a reader unfamiliar with the region to become lost in the nomenclature. To assist the reader, Figure 2 provides a regional-scale view of the Jeddah terrane that shows the most prominent geographic features and the general distribution of plutonic (lithodemic), supracrustal (lithostratigraphic), and ophiolitic rocks. For the most part, our results indicate that the Neoproterozoic plutonic assemblage underlying the Jeddah terrane (Fig. 2) is composed of nested pre-, syn-, and posttectonic intrusions that range in size from dikes to batholiths and that were emplaced episodically over a protracted period (ca. 820-520 Ma). The older, arc-related plutonic tract is inferred to be continuous, being interrupted only by shear zones and by major lithospheric boundaries along the BUSZ to the north, the Ad Damm fault zone to the south, the Hulayfah-Ad Dafinah fault zone to the east, and the Red Sea to the west. The intrusive rocks are concealed over significant areas by broadly coeval Neoproterozoic supracrustal rocks and by Cenozoic cover. The batholiths shown in Figure 2 represent the largest continuous exposures of intrusive basement and occupy large domal structures, which are flanked by synforms that contain the supracrustal rocks. The present-day shapes of these features are the result of suture-related and younger deformation. The batholiths, therefore, represent multiple intrusive events and are composites of plutons and smaller intrusions that may belong to more than one lithodemic unit. Some confusion may arise from the informal nomenclature, which includes the shared names of batholiths and lithodemic units with smaller areal extents. For example, the Hufayriyah batholith in the eastern part of the Jeddah terrane is underlain by plutons of the Hufayriyah tonalite and also by plutons of the Dhukhr tonalite, Bari granodiorite, and Raghiyah intrusive suite.

The following outlines the lithodemic nomenclature for the study area. Plutonic rocks south of the suture comprise the Kamil and Qudayd intrusive suites in the west (Figs. 2, 3A) and the Dhukhr and Hufayriyah tonalite assemblages, Bari granodiorite, and Ramram intrusive complex in the east (Figs. 2, 3B). The Rabigh intrusive suite is the main plutonic representative north of the suture in the west, but equivalent rocks are not exposed in the study area east of Harrat Rahat. Numerous posttectonic plutons, such as those of the Raghiyah intrusive suite and the Subh suite, and hypabyssal intrusions occur throughout the study area (Fig. 2). Plutonic rocks associated with the ophiolitic complexes are discussed separately from the other plutonic rocks. The intrusive units are discussed below in order from oldest to youngest.

Dhukhr tonalite

The Dhukhr tonalite (Kemp and others, 1982a) has three major occurrences south of the Bi'r Umq segment of the BUSZ: the entire northeast-trending Dhukhr batholith, significant areas in the northern and central parts of the Hufayriyah batholith, and the majority of the Furayhah batholith (Fig. 3B). The Dhukhr and Furayhah batholiths consist of coarse-grained, locally porphyritic, biotite-hornblende tonalite showing alignment of elongate minerals; subordinate lithologies include coarse-grained biotite-hornblende granodiorite, fine-grained hornblende diorite and associated minor hornblendite, and minor gabbro (Kemp and others, 1982a). Several major northwest-trending dike-like bodies of coarse-grained, (garnet)-biotite-hornblende-muscovite trondhjemite that intrude the long axis of the Furayhah batholith were mapped by Kemp an others (1982b) as Hufayriyah tonalite. Based on the geographic location, lithologic associations, and intrusive relationships of these bodies, however, the recommendations of Kemp and others (1982a) are followed here and those bodies are included with the Dhukhr tonalite.

The inferred Dhukhr rocks along the eastern side of the Hufayriyah batholith are hornblende-biotite-muscovite trondhjemite (Kemp and others, 1982a). The easternmost part of the Hufayriyah batholith where it is intruded by two elliptical posttectonic plutons of the Raghiyah intrusive suite was originally mapped as Hufayriyah tonalite (Kemp and others, 1982b), but is reinterpreted here as part of the Dhukhr tonalite for the following reasons. (1) Outcrops of the Hufayriyah tonalite almost everywhere show clear intrusive relationships with thermally metamorphosed rocks of the Mahd group, as supported by previously reported age information (1982), but diamictite in the lowermost Tulaymisah formation on the east side of the Hufayriyah batholith contains tonalite clasts and dips to the east away from the margin of the batholith, which suggests that this part of the batholith was emplaced, uplifted, and exposed prior to deposition of the Mahd group. (2) Reconstruction prior to sinistral faulting along the Wadi al Arj fault would juxtapose the easternmost part of the Hufayriyah batholith with known exposures of Dhukhr tonalite north of the fault, suggesting that Dhukhr tonalite originally continued into the eastern part of the batholith. (3) Outcrops in the eastern Hufayriyah batholith more closely resemble typical Dhukhr tonalite than Hufayriyah tonalite in terms of degree of weathering and extent of deformation. (4) The age calculated for one of the samples (SA04-412), discussed below, from the eastern Hufayriyah batholith is much older than ages determined here and by Calvez and Kemp (1982) for the Hufayriyah tonalite, but is identical to that of previously published ages for typical Dhukhr tonalite (Calvez and Kemp, 1982). The contact between the Dhukhr and Hufayriyah tonalite assemblages in the eastern Hufayriyah batholith is tentatively shown in Figure 3B as lying along a northwest-trending fault, but more detailed fieldwork and mapping are needed to more accurately locate the contact.

Outcrops of the Dhukhr plutonic rocks typically have a stronger foliation and are more deeply weathered than other plutonic assemblages along the BUSZ. These features, the fact that the Dhukhr batholith is unconformably overlain by the less-deformed Mahd group, and clasts of Dhukhr tonalite within a basal conglomerate in the Mahd group, suggest that the plutonic basement represented by the Dhukhr tonalite was affected by deformation, uplift, and denudation prior to deposition of the supracrustal rocks.

Aldrich (1978) reported a Rb-Sr mineral isochron age of 665 Ma for the Dhukhr tonalite, but this does not agree with observed geological relationships and almost certainly has undergone thermal resetting of the isotopic system. An Rb-Sr whole-rock isochron age of 774 ± 101 (7 points, MSWD = 0.07), reported by Fleck and Hadley (1982) for Dhukhr tonalite in the Furayhah batholith, has such large errors that it is not useful as a crystallization age. The mean of that age, if taken as an approximate crystallization age, is more consistent with that of the Bari granodiorite, dated herein at 778.5 ± 4.7 Ma. Part of the Bari granodiorite assemblage intrudes the Dhukhr tonalite only 2 km away from where Fleck and Hadley (1982) obtained their samples. Calvez and Kemp (1982) reported a conventional U-Pb zircon age of 816 ± 4 Ma for the Dhukhr tonalite in the Dhukhr batholith. That age has a lower intercept age of 133 ± 30 Ma, which those authors interpret as geologically meaningless. The quality of the age could not be evaluated because neither the individual analytical errors nor the MSWD were reported. Nevertheless, the age is very similar to the conventional U-Pb zircon age of 811 ± 4 Ma reported by Stoeser and Stacey (1988) for the Dhukhr tonalite in the Furayhah batholith, and the two ages have been used by others to identify the Dhukhr tonalite as the oldest plutonic unit along the BUSZ.

Two ages were obtained for the Dhukhr tonalite, and age information was obtained on zircon from a hypabyssal dacite intruding the Dhukhr batholith. Sample SA04-412 (Tables 1, 3) is from hornblende quartz-diorite in the eastern Hufayriyah batholith, ca. 55 km east of Mahd adh Dhahab (Fig. 3B). Twenty analyses were conducted on 16 zircon grains, and data points for the analyses are plotted on the concordia diagram in Figure 5A. Two-sigma error ellipses for all but three of the analyses are concordant. Ages range from ca. 785 to 875 Ma and together do not allow the calculation of a concordia age. Discordant points were omitted from all calculations, as were a pair of points (3.1 and 3.2, Tables 1, 2) from the rim and center of a grain, the calculated ages of which are within error of each other but with a reverse relationship (with respect to the means). An age spectrum of the breadth seen in Figure 5A is most likely due either to inheritance involving only slightly older crust or to isotopic disturbance, such as lead loss, or a combination of the two processes. Loss of lead is not obvious from the distribution of points in Figure 5A or on a standard Wetherill plot, nor is it evident from CL imagery or thin section. Lead loss is therefore ruled out as a significant contribution to the complexity of this

sample.

Inheritance of older zircon is supported by the morphologies and internal architecture of the analyzed grains as revealed by CL images and ages (Fig. 5B). The zircon grains from sample SA04-412 can be divided into two end-member classes. Class 1 consists of the youngest grains, which also are the most euhedral, show pyramidal terminations, and exhibit igneous compositional and minor sector zoning. Very similar ages determined from the tip (793 ± 18 Ma, spot 16.1) and center (800 ± 23 Ma, spot 16.2) of one of the Class 1 grains coupled with the lack of obvious internal grain boundaries suggest that Class 1 grains do not contain inherited cores and are entirely juvenile. Class 2 grains typically exhibit obvious boundaries between anhedral, high-U cores and thin, euhedral, low-U epitaxial overgrowths. The core of a Class 2 grain yielded the oldest age (874 ± 25 Ma, spot 8.1) from the sample, and Class 2 grains show the largest age differences (ca. 20-25 Ma) between rims and cores. For example, spots 11.1 (core) and 11.2 (rim) produced ages of 857 ± 24 Ma and 833 ± 20, respectively, and spots 10.1 (core) and 10.2 (rim) yielded ages of 851 ± 22 Ma and 820 ± 25, respectively.

The six youngest points, two of which (16.1 and 16.2, Tables 1, 2) are from the core and rim of the same grain, define a vertical array with very similar $^{238}U/^{206}Pb$ ages. Data for these six points yield a concordia age of 799 ± 8.2 (MSWD = 0.17). However, as there is no obvious reason for limiting the points arbitrarily, additional points were added until a concordia age could no longer be obtained. Data for the ten youngest points that fit this criterion yield a concordia age of 813 ± 10 Ma (MSWD = 0.4), which agree with ages of 811 ± 4 Ma (Stoeser and Stacey, 1988) and 816 ± 3 Ma (Calvez and Kemp, 1982) for Dhukhr tonalite in the Furayhah and Dhukhr batholiths, respectively. The oldest points included in this group are from the rims of grains 10 and 11, discussed above, suggesting that the oldest out of the ten youngest ages are still from juvenile zircon. The ca. 812 Ma age is the best estimate of the crystallization age for this part of the Dhukhr tonalite.

Data for the four oldest grains from sample SA04-412 yield a concordia age of 858 ± 12 Ma (MSWD = 0.116), which may reflect the average age of inherited zircon in the sample. Convincing radiometric ages for crust of similar age have been reported for the Tharwah and Bi'r Umq ophiolite complexes (Pallister and others, 1988b) and for the Erkowit pluton south of the Nakasib suture in Sudan, although a similar age for microgabbro intruding the Bi'rak group (Figs. 3A, 4, Table 4) north of the suture is reported in a later section. It is therefore unlikely that the zircons producing this age are juvenile with respect to the Dhukhr tonalite, and those grains, if not more, are almost certainly xenocrystic.

Sample SA03-269A (Tables 1, 3) is a leucocratic muscovite metatonalite from the Dhukhr batholith ca. 3 km south of Mahd adh Dhahab mine (Fig. 3A). The sample produced abundant apatite and other accessory minerals but scant zircon, which is reflected in the low whole-rock concentration of Zr (33 ppm, Hargrove, 2006). Data points for the three grains analyzed are plotted on the concordia diagram in Figure 5C. The ca. 823 Ma apparent age of the oldest zircon is similar to the 816 Ma age reported by Calvez and Kemp (1982), but the other two grains yield younger apparent ages of ca. 797-795 Ma, which may reflect lead loss at that time. Together, all three grains yield a concordia age of 803 ± 17 Ma (MSWD = 2.2). The low number of points and high scatter make this a poor constraint on the crystallization age of the sample, but it is similar to other ages for the Dhukhr tonalite reported here and by Calvez and Kemp (1982) and Stoeser and Stacey (1988). The ca. 803 Ma age is therefore interpreted as a minimum crystallization age for the Dhukhr tonalite in the northern Dhukhr batholith, although the possibility that it reflects lead loss at ca. 800 Ma is acknowledged.

Sample SA03-268A (Tables 1, 3) is from leucocratic, quartz-hornblende-plagioclase-phyric spherulitic dacite intruding the Dhukhr tonalite ca. 9 km south-southwest of Mahd adh Dhahab (Fig. 3B). It is unclear whether the intrusion is related to the Dhukhr tonalite association or if it is younger. The hypabyssal character and lack of a strong deformational fabric typically associated with the Dhukhr tonalite suggest that it is a subvolcanic intrusion, possibly related to the nearby Mahd group or associated intrusive bodies. Seven zircon grains were analyzed and the results are plotted as two-sigma error ellipses on the concordia diagram in Figure 5D. The analyses range in age from ca. 800 Ma to >2700 Ma. No concordia age could be calculated for this sample, but three of the data points plot on or just off concordia in an age range consistent with their being juvenile grains from the intrusion itself, if it is related to the Dhukhr tonalite. Alternatively, if the dacite is significantly younger than the Dhukhr tonalite, then all of the zircon grains were inherited from Dhukhr tonalite or older rocks. Four data points are from obviously inherited grains, three of which are Mesoproterozoic in age and one of which is Archean.

Rabigh intrusive suite

Mafic to felsic plutonic rocks of the Rabigh intrusive suite occur north of the Tharwah segment of the BUSZ. The suite is divided into the Hajar, Bustan, and Shufayyah intrusive complexes (Fig. 3A). They are described below from south to north away from the suture. Only the Hajar complex was visited during this study, but no ages were determined for any part of the Rabigh suite.

The Hajar intrusive complex is a composite tonalite-quartz diorite batholith intruding the Bi'rak group close to the Tharwah ophiolite. Parts of the complex were mapped by Gilboy and Skiba (1978a), and were described by Abu Rashid (1973), Kana'an (1970; 1977), and Skiba and Gilboy (1975). The Hajar complex is dominated by biotite-hornblende tonalite that is gradational into quartz diorite at the margins of the batholith. The rocks are medium-grained, leucocratic, and show hypidiomorphic granular texture with euhedral plagioclase, quartz, minor

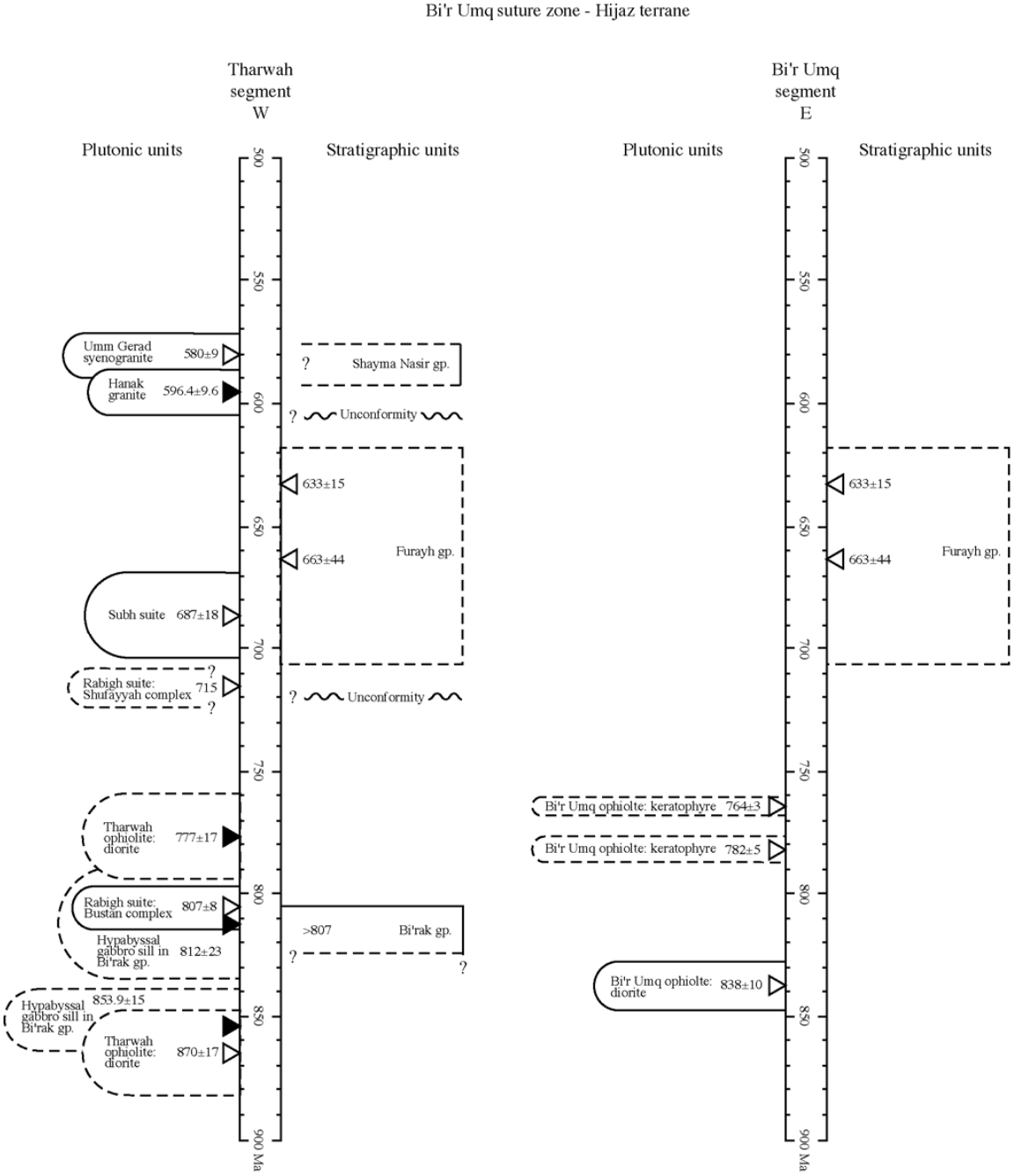

Figure 4. Major plutonic and stratigraphic units along the Bi'r Umq suture zone in the (A) Hijaz and (B) Jeddah terranes shown in chronologic order from oldest (bottom) to youngest (top), based on the most robust radiometric ages obtained during this study (black triangles) and reported by other authors (white triangles), cited in the text. The central columns are timescales in millions of years before present. Stratigraphic units (rectangles) are shown to the right of the timescales and plutonic units (capsules) are shown to the left. Vertical dimensions of objects representing plutonic and stratigraphic units reflect actual maxima and minima for available age constraints (including errors) on the units. The positions of unconformities with question marks do not correspond to a specific time. Dashed lines represent approximate, inferred, or unknown age limits.

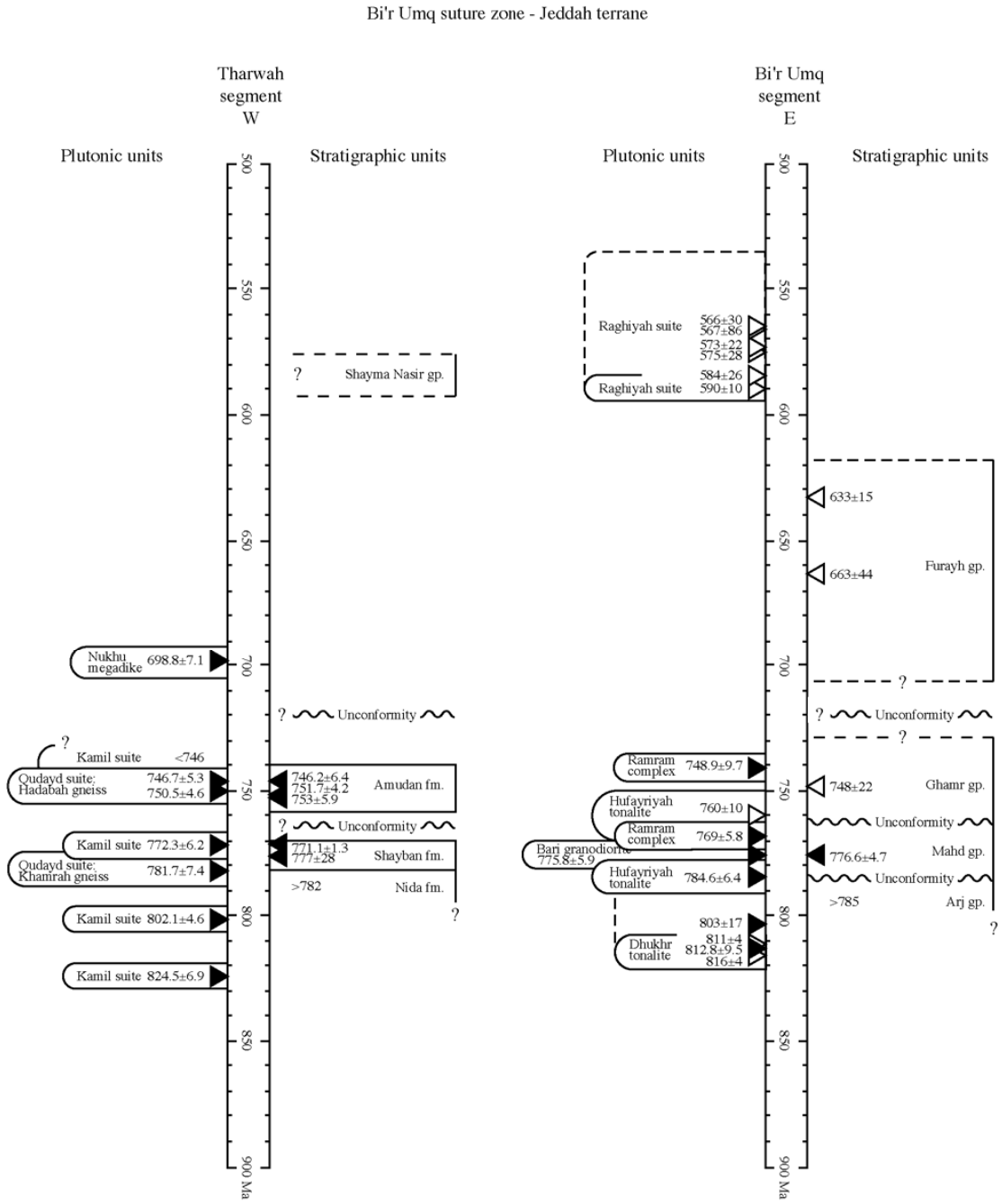

Figure 4 (continued).

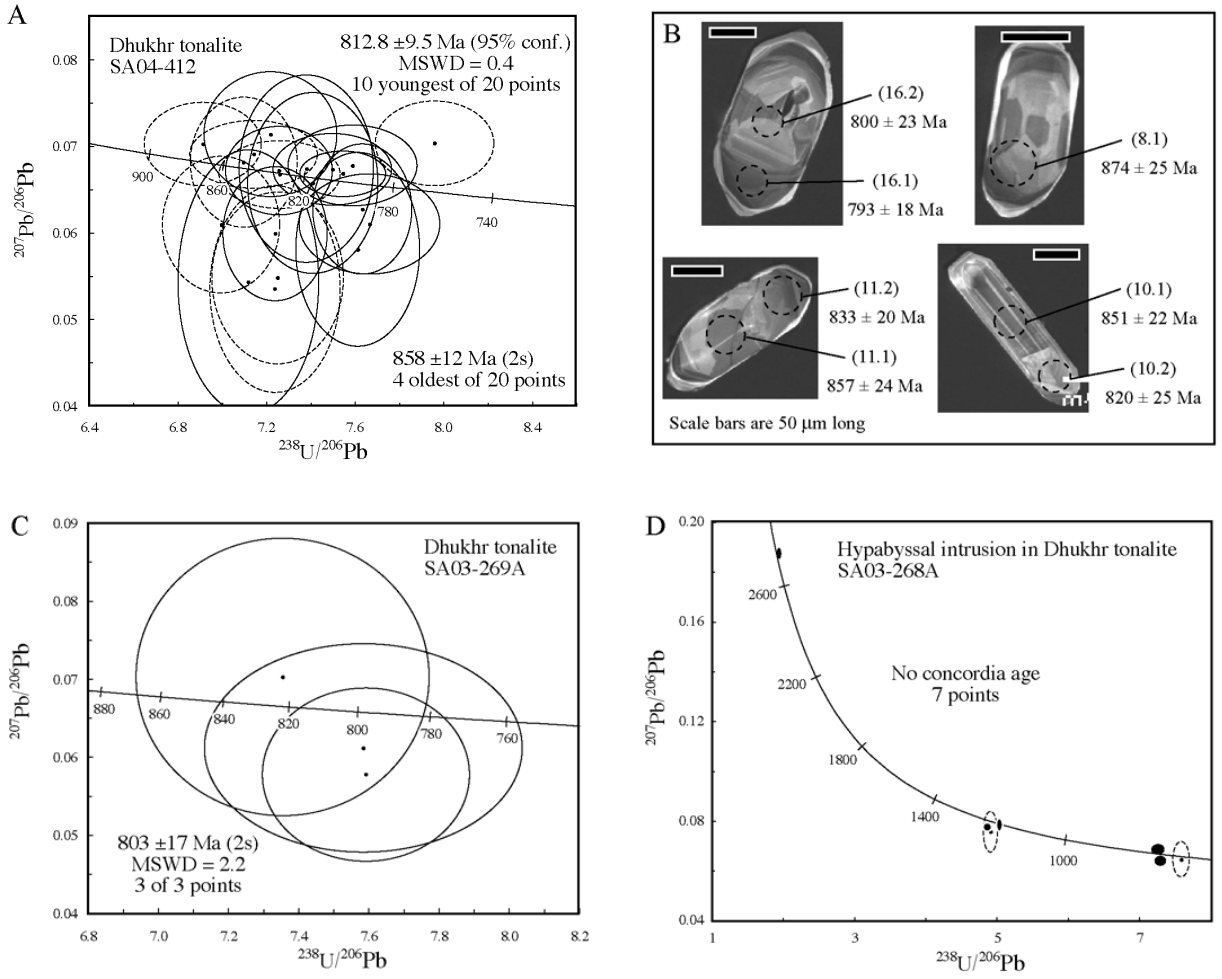

Figure 5. (A) Tera-Wasserburg concordia diagram for sample SA04-412 of the Dhukhr tonalite. (B) Cathodoluminscence images of zircon from sample SA04-412, mapped as Hufayriyah tonalite by Kemp and others (1982b). Labels indicate grain and analysis spot numbers (in parentheses) corresponding to apparent ages from Table 3. Dashed circles represent dimensions of larger rastered areas; analyses spots are ca. one-third smaller. All scale bars are 50 µm long (C) Tera-Wasserburg concordia diagrams for sample SA03-269A of the Dhukhr tonalite and (D) sample SA03-268A from a hypabyssal dacite intrusion cutting the Dhukhr tonalite. Sample information is given in Table 1 and analytical data in Table 3. Data points are shown with 2σ error ellipse; dashed ellipses were excluded from age calculations; and some ellipses are for better visibility.

K-feldspar, hornblende, biotite, and rare clinopyroxene (Ramsay, 1986a). A penetrative foliation occurs throughout the batholith and becomes more intense in the marginal quartz diorite, where it is oriented parallel to the contact and continues into the metamorphic aureole developed in the host Bi'rak group. Locally abundant xenoliths range in size from cm-scale up to hundreds of meters across, show reaction rims, and are generally rounded, but mafic enclaves in the marginal quartz diorite are elongate parallel to the foliation and contacts (Ramsay, 1986a).

Plutonic rocks of the Bustan intrusive complex intrude the Bi'rak group southeast of Wadi al Qahah (Fig. 3A). Parts of the Bustan complex have been mapped by Al-Shanti (1970), Gilboy and Skiba (1978a), Camp (1986b), and Ramsay (1986b). The complex comprises plutons of tonalite, granodiorite, diorite, gabbro, and monzonite, the largest of which is a north-trending bimodal batholith composed of hornblende tonalite to trondhjemite and subordinate gabbro displaying hypidiomporphic-granular to inequigranular texture (Camp, 1986b). Contact metamorphic aureoles are locally developed within the host Bi'rak group, and the plutonic rocks are typically unfoliated, although the southernmost units become progressively cataclastized and sheared near intrusive contacts (Ramsay, 1986a). Xenoliths are common in the Bustan intrusive complex.

Tonalite from the main part of the Bustan complex was dated by C. Hedge (cited as pers. comm. in Camp, 1986a) and yielded a conventional U-Pb zircon age of 807 ± 8 Ma, which is consistent with an Rb-Sr whole-rock isochron age of 800 ± 75 Ma (Al-Shanti and others, 1984) obtained from tonalite exposed in the Umm Gerad erosional outlier (UG in Fig. 3A). Al-Shanti and others (1983) reported an Rb-Sr isochron age of 945 ± 28 Ma (6 points, MSWD = 2.0) for the same tonalite, but this age is suspect.

The Shufayyah intrusive complex is a large composite pluton that intrudes the Bi'rak group northwest of Wadi al Qahah (Fig. 3A) and consists of gabbro, diorite, quartzdiorite, and monzodiorite that show hypidiomorphic-granular to inequigranular texture. C. Hedge (cited as pers. comm. in Camp, 1986a) obtained a conventional U-Pb zircon age of 715 Ma (errors and MSWD not reported) for gabbro of the Shufayyah complex. The validity of that age cannot be determined from the available information.

Kamil intrusive suite

The Kamil intrusive suite (Fig. 3A) occurs along the southern flank of the Tharwah segment of the BUSZ and extends nearly 90 km south of the area in Figure 3A, where it is considered to be a younger component of the Makkah batholith (Moore and Al-Rehaili, 1989a; Moore and Al-Rehaili, 1989b). Within the study area in Figure 3A, the suite was mapped by Rexworthy (1972), Kana'an (1970; 1977) and Gilboy and Skiba (1978b; 1978d), and was described in detail by Skiba and Gilboy (1975) and comprises the Thufir trondhjemite (TT in Fig. 3A), the Shagiyah quartz diorite, and the Shiwan intrusive complex, plus numerous small intrusions. The Shiwan intrusive complex, which underlies the Shiwan batholith, is predominantly leucocratic to mesocratic, coarse-grained and locally porphyritic hornblende tonalite that exhibits hypidiomorphic-granular and subordinate hiatal porphyritic texture. Outcrops typically exhibit a weak tectonic fabric, except within the Rima shear zone (Fig. 3A) where the rocks exhibit lit-par-lit texture with schistose to gneissic metatonalite structurally interleaved on the cm- to m-scale with metavolcanic-sedimentary deposits of the Shayban formation (Fig. 6A). Melanocratic enclaves are common in the Shiwan complex and are identical to the host rock in terms of modal mineralogy and trace-element concentrations (Hargrove, 2006), but have a higher content of mafic minerals. The enclaves commonly are irregularly shaped and have diffuse to crenulate margins, but where a tectonic foliation is developed in the host the enclaves are more angular and highly attenuated parallel to the foliation (Fig. 6B). Contact relationships between individual Shiwan intrusions are complex and commonly gradational, but up to five distinct lithologies with sharp contacts were locally distinguished at outcrop scale. Contacts with the Samran group are generally sharp and nearly vertical, but can be convolute with apophyses of tonalite that enclose xenoliths and large septa of the country rock. Contact metamorphism in the Samran group is limited to development of contact-parallel planar fabrics and silicification or alteration to granofels or hornfels (Skiba and Gilboy, 1975; Roobol, 1989).

The Shagiyah quartz diorite (SQ in Fig. 3A) intrudes the Shayban formation northwest of the Shiwan complex and is composed of massive, medium-grained diorite exhibiting hypidiomorphic granular texture. It is indistinguishable from the Shiwan complex in terms of modal mineralogy (Ramsay, 1986a) and chemical data from a single analysis reported by Rexworthy (1972). The Thufir trondhjemite (TT in Fig. 3A) intrudes the Shayban formation (Samran group) to the west of the Shagiyah intrusion and consists of leucocratic, medium- to coarse-grained trondhjemite, subordinate tonalite, and minor diorite (Skiba and Gilboy, 1975; Ziab, 1982; N. Jackson, pers. comm., as cited in Ramsay, 1986a).

Fleck (1985) reported a three-point Rb-Sr whole-rock isochron age of 769 ± 39 Ma (MSWD = 0.84) for tonalite intruding older plutons of the Shiwan intrusive complex ca. 4 km south of the area in Figure 3A. The large error is probably due to the limited number of points, but the low scatter suggests the age is meaningful, as supported by a very similar U-Pb zircon SHRIMP-RG age reported below. Other parts of the Kamil intrusive suite have yielded Rb-Sr whole-rock isochron ages of 763 ± 159 Ma (Fleck and others, 1979) and 709 ± 164 Ma (Fleck, 1985). However, those ages are not in agreement with observed field relations between the units dated (Ju'uranah complex of Moore and Al-Rehaili, 1989b) and are not useful as crystallization ages because of the large errors. Pegmatite intruding the Kamil suite (Ju'uranah complex of Moore and Al-Rehaili, 1989b) to the south of Figure 3A yielded a K-Ar age of ca. 800 Ma for muscovite and a Rb-Sr mineral isochron age of ca. 825 Ma, and trondhjemite from another part of the same complex yielded a K-Ar age of ca. 760 Ma for biotite and a Rb-Sr mineral isochron age of ca. 965 Ma (Aldrich and others, 1978). The ca. 825, 800, and 760 Ma ages are consistent with published ages and ages determined here for parts of the Kamil suite and may be viable crystallization ages, although the K-Ar age should be treated with caution. The 965 Ma age is similar to the ca. 945 Ma age reported by Al-Shanti and others (1983) for the Bustan intrusive complex north of the BUSZ, but

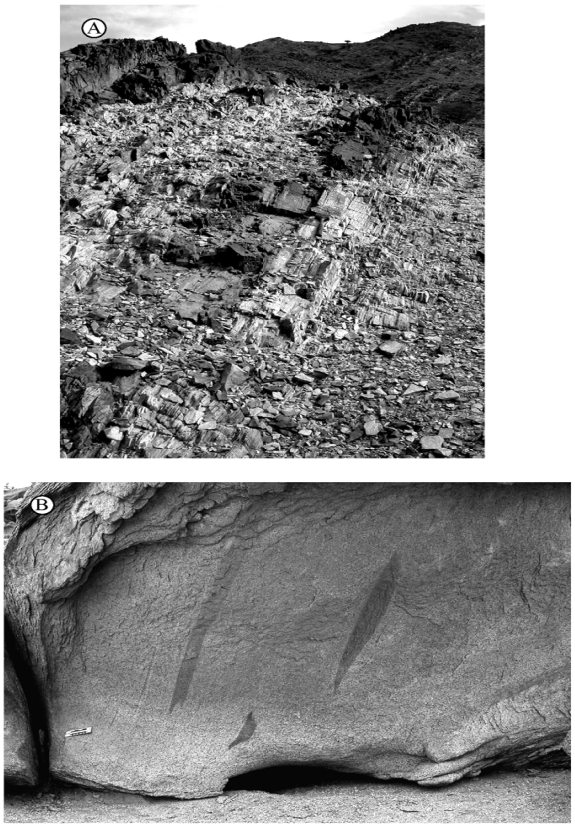

Figure 6. Photographs of outcrops of the Kamil intrusive suite. (A) Lit-par-lit texture in the Rima shear zone, where layers of schistose to gneissic metatonalite of the Shiwan intrusive complex are structurally interleaved on the cm- to m-scale with metavolcanic-sedimentary deposits of the Shayban formation. Width of image at bottom is ca 3 m. View looking east. (B) elongate, angular melanocratic enclaves in more leucocratic tonalite of the Shiwan intrusive complex. Enclaves are attenuated parallel to the tectonic foliation in the tonalite. Scale card at lower left is 16.5 cm long.

the meaning of these ages is unclear. No other crust of similar age has been identified in the area of the BUSZ, but the ages have been cited as evidence for the onset of terrane formation at that time. It is possible that the minerals that yielded those ages experienced rubidium loss soon after emplacement, leading to erroneously high ages. Therefore the recommendation is made that they be discounted and that reference to them as crust-forming ages be discontinued.

Two samples from different parts of the Shiwan intrusive complex were dated during this study. Sample SA04-318 (Tables 1, 3) is from a body of hornblende diorite in the Shiwan intrusive complex approximately 19 km northeast of Al Kamil (Fig. 3A). The U-Pb isotopic systematics for this sample are complex. Seventeen grains were analyzed, and two-sigma error ellipses are plotted on the concordia diagram in Figure 7A. Ellipses for eleven of the data points form a loose cluster about concordia. At least two of those appear to belong to a conspicuous array of points that trend away from the cluster to much lower $^{238}U/^{206}Pb$ at the same $^{207}Pb/^{206}Pb$, probably reflecting inheritance of slightly older zircon that may have experienced recent lead loss. One point (11.1, Table 3) shows apparent reverse discordance. A geological explanation for reverse discordance in this sample is unlikely, because no high-grade metamorphic event capable of inducing U-loss is recorded along the BNSZ and because the sample does not exhibit mineral assemblages consistent with metamorphic conditions above the lower greenschist facies. For the same reason, the possibility that some zircon may have undergone internal redistribution of Pb, which increased the Pb/U ratios at the analysis sites and led to calculation of erroneously high ages (c.f. Williams and others, 1984) can also be eliminated. Analysis point 11.1 is therefore omitted as aberrant and the other points inferred to reflect inheritance (± lead loss) are also omitted.

Three data points plot to the right of the main cluster at higher $^{238}U/^{206}Pb$ and appear to have experienced recent loss of lead. Two of the nine remaining data points, both of which plot at the upper right of the cluster and one of which is highly discordant, were not equivalent to the remainder of the points in the main group and prevented calculation of a concordia age. Upon eliminating the problematic data points discussed above, the remaining cluster of seven points yielded a concordia age of 772 ± 6 Ma (MSWD = 0.58), which is interpreted as the most reasonable estimate for the crystallization age of the hornblende diorite. That age is within error of the ca. 769 Ma Rb-Sr age reported by Fleck (1985) for the Shiwan complex south of the area in Figure 3A, suggesting that much of the Shiwan batholith was emplaced at that time. It is also within error of the ca. 770 Ma ages for the Shayban formation, reported in a later section, and is consistent with field evidence that the complex intrudes the Shayban formation, which may be the volcanic equivalent of part of the Shiwan intrusive complex.

Sample SA01-110 (Tables 1, 3) is hornblende diorite from the Shiwan complex just southeast of Al Kamil (Fig. 3A). Zircon grains from the sample generally exhibit igneous characteristics, including prismatic morphologies with pyramidal terminations and well-developed oscillatory zoning in CL images. The grains range in size from 100 to 380 µm and most are fragments of much coarser grains. Analyses for thirteen grains cluster tightly about concordia in Figure 7B and yield a concordia age of 800 ± 6 (MSWD = 0.24). The error ellipse for the point with the highest $^{238}U/^{206}Pb$ does not overlap many of the ellipses, and the zircon corresponding to this point may have experienced minor lead loss. However, omitting this point does not significantly affect the calculated age or improve the errors, thus the 800 ± 6 Ma age is interpreted as the age of igneous crystallization of the diorite.

Evidence for ca. 825 Ma plutonic basement beneath the Samran group, discussed in a later section, the ca. 800 Ma age reported here for sample SA01-110 from the Shiwan complex, the 772 Ma age reported here for sample SA03-318 from the Shiwan complex, and the ca. 770 Ma Rb-Sr age reported by Fleck (1985) for the Shiwan complex south of Figure 3A all suggest that what is mapped as the Shiwan intrusive complex is actually a composite of multiple intrusive phases emplaced over a protracted period from ca. 825 to 770 Ma. Such a protracted intrusive history is similar to the Dhukhr and

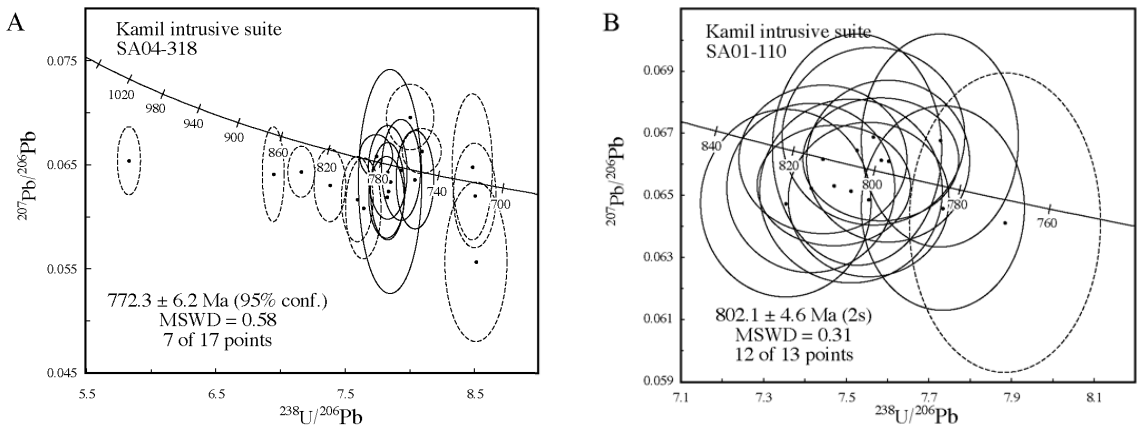

Figure 7. Tera-Wasserburg concordia diagrams for sample (A) SA04-318 of granodiorite and (B) SA0-110 of diorite from the Shiwan intrusive complex, Kamil suite. Sample information is given in Table 1 and analytical data in Table 3. Data points are shown with 2σ error ellipses and dashed ellipses were excluded from age calculations.

Hufayriyah tonalite assemblages and suggests that parts of the Kamil intrusive suite should be reassigned to new units based on their ages, but more detailed fieldwork and geochronology will be needed to delimit the extents of such units.

Hufayriyah tonalite

Rocks assigned by Kemp and others (1982a; 1982b) to the Hufayriyah tonalite underlie the bulk of the Hufayriyah batholith, exposed to the north and southwest of Harrat Kishb, and occur within several minor stocks at the northern end of the Dhukhr batholith (Fig. 3B). Major dike-like bodies of trondhjemite in the Furayhah batholith and in the eastern part of the Hufayriyah batholith were assigned by Kemp and others (1982b) to the Hufayriyah tonalite association, but are reinterpreted here as part of the Dhukhr tonalite, as discussed previously.

The Hufayriyah tonalite association consists of coarse-grained, leucocratic to mesocratic, commonly porphyritic (biotite)-hornblende tonalite and quartz-diorite, subordinate coarse-grained biotite-muscovite trondhjemite, and minor olivine-hornblende gabbro and pyroxenite (Conraux, 1966; Kemp and others, 1982a). Primary igneous fabrics are common where plagioclase shows a shape-preferred orientation, and hornblende quartz-diorite locally exhibits orthocumulate texture. Outcrops of the Hufayriyah association typically exhibit a poorly developed tectonic foliation. In many places, the tonalite clearly intrudes the Tulaymisah formation and undifferentiated parts of the Mahd group, which exhibit discontinuous contact metamorphic aureoles (Kemp and others, 1982a; Kemp and others, 1982b). The Hufayriyah tonalite is intruded in places by the Bari granodiorite and the Raghiyah intrusive suite (Kemp and others, 1982a; Kemp and others, 1982b).

Brown and others (1978) reported a three-point Rb-Sr mineral isochron age of 692 ± 15 Ma (Table 3) for granite in the Hufayriyah pluton, which is much younger than the SHRIMP-RG age reported below and the conventional U-Pb zircon age of 760 ± 10 Ma (4 points, MSWD not reported) obtained by Calvez and Kemp (1982) for tonalite at the northern end of the Hufayriyah batholith (Fig. 3B). The sample of Brown and others (1978) comes from granite in a part of the Hufayriyah tonalite intruded by abundant dikes related to the posttectonic Raghiyah intrusive suite, which has been dated between 598 and 520 Ma. It is therefore likely either that the Rb-Sr isotopic systematics of the sample were disturbed by intrusion of the younger Raghiyah granites or, because granite is not part of the typical the Hufayriyah assemblahge, that the granite dated by Brown and others (1978) is actually part of the Raghiyah intrusive suite. In either case, such a young crystallization age for the Hufayriyah tonalite should be rejected.

One sample of Hufayriyah tonalite in the Hufayriyah batholith was dated during this study. Sample SA03-271 (Tables 1, 3) is a biotite-hornblende tonalite ca. 20 km east of Mahd adh Dhahab (Fig. 3B). The U-Pb systematics of zircon from this sample are simple. Twelve zircon grains were analyzed, and data points are plotted on the concordia diagram in Figure 8. The points form a fairly tight group with concordant error ellipses. If all twelve points are included in the calculation, a concordia age of 781 ± 8 Ma (MSWD = 0.33) is obtained. The point with the highest $^{238}U/^{206}Pb$ may have experienced some lead loss, but excluding it from the calculation, and/or the point with the high error in $^{207}Pb/^{206}Pb$, does not significantly alter the age of the sample. Therefore, the 781 ± 8 Ma age is interpreted as the crystallization age of the tonalite. This age is ca. 20 Ma older than the conventional U-Pb zircon age of 760 ± 10 Ma determined by Calvez and Kemp (1982) for Hufayriyah tonalite in the northern part of the Hufayriyah batholith and suggests that the Hufayriyah tonalite assemblage was intruded during at least two distinct pulses at ca. 780 Ma and again at 760 Ma. However, it is acknowledged that these ages are within 3 Ma of each other when taking the errors into account.

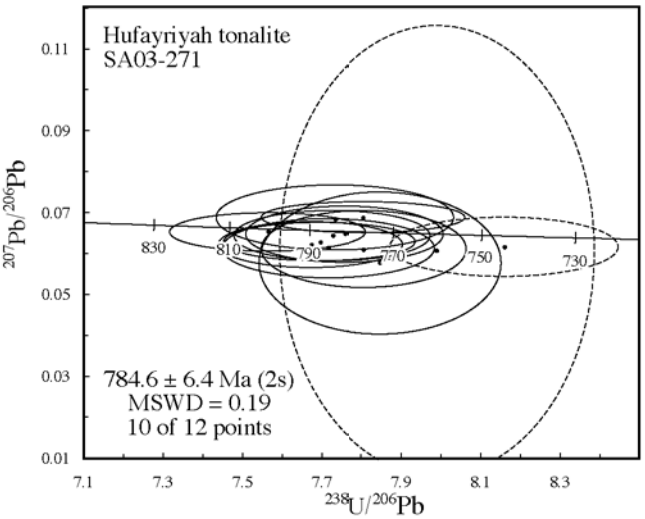

Figure 8. Tera-Wasserburg concordia diagram for sample SA03-271 of tonalite from the Hufayriyah tonalite association. Sample information is given in Table 1 and analytical data in Table 3. Data points are shown with 2σ error ellipses and dashed ellipses were excluded from age calculations.

Qudayd metaintrusive suite

Outcrops of the Qudayd metaintrusive suite occur in four domes of variably deformed tonalitic orthogneiss enclosed by the Nida formation (Samran group) that are shown in Figure 3A as the Khamrah (KG), Hadabah (HG), Asad (AG), and Ukaz (UG) gneisses. The domes are elongated along the axis of a major northeast-trending antiform that parallels the Labunah thrusts. Parts of the suite were mapped by Nebert (1969), Kana'an (1970; 1977), Rexworthy (1972), and Gilboy and Skiba (1978a; 1978b; 1978c), and were described in detail by Skiba and Gilboy (1975). The outcrop patterns of the Qudayd intrusions in Figure 3A are the same as those shown by Ramsay (1986b), except for the Asad gneiss (AG) immediately north of Wadi Sitarah. There, Gilboy and Skiba (1978b) ma ped a major northeast-trending antiform, the eastern limb of which is underlain by Qudayd metatonalite (as shown in Fig. 3A). The core and western limb of the antiform are

underlain by quartzofeldspathic gneiss and amphibole-rich schist, which Ramsay (1986b) included as part of the Asad gneiss and which are reinterpreted as part of the Nida formation, based on several lines of evidence. First, quartzofeldspathic gneiss and amphibole-rich schist are common in the Nida formation close to Qudayd intrusions. Second, these lithologies are more consistent with derivation from lavas, volcaniclastic rock, or even epiclastic rock than from a tonalitic intrusion (Fig. 9A, B), which was acknowledged by Gilboy and Skiba (1978b). Third, on the more detailed map of Gilboy and Skiba (1978b) the non-tonalitic units display a complex fold interference pattern that can only be explained if the protolith was originally a thin, concordant, sheet-like intrusion into the Nida formation and if both the intrusion and host experienced multiple episodes of isoclinal folding. Such complex geometry is not consistent with other exposures of the Qudayd metatonalite, but is consistent with structures observed within the Nida formation.

show a shape-preferred orientation, elongate mafic-rich schlieren, and a weak mesoscopic compositional layering defined by variations in content of mafic minerals. Outcrops are commonly crossed by shear zones up to 1 m wide and oriented subparallel to the regional foliation and show evidence of intense grain-size reduction in a protomylonitic fabric. Mafic enclaves are not as common in Qudayd intrusions as in other plutonic units, but where they occur they are rounded to subangular.

Qudayd intrusions are surrounded by well-developed dynamothermal aureoles in which volcaniclastic deposits of the Nida formation show a marked increase in strain and metamorphic grade. Contacts with the host Nida formation vary from sharp and nearly vertical to transitional over several meters. In the latter case, a lit-par-lit texture is characterized by apophyses of metatonalite up to 1 m wide that are structurally interleaved with metamorphosed volcaniclastic deposits of the host. The apophyses partly enclose large septa of the Nida formation (Fig. 10A), and large elongate

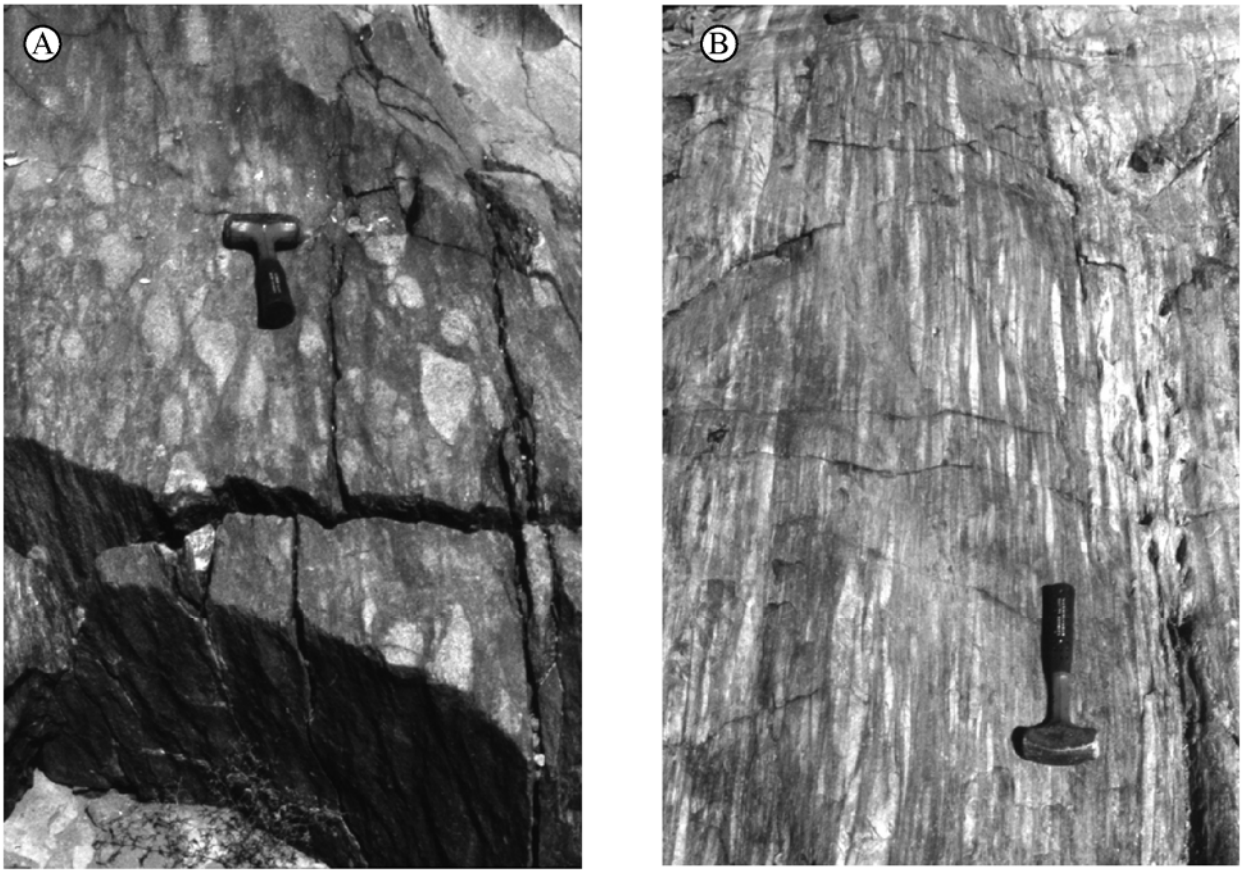

Figure 9. Photographs of outcrops of the Nida formation, Samran group, which serves as before and after views with respect to deformation along the Bi'r Umq suture zone. (A) Before – moderately deformed, angular lithic clasts in volcaniclastic breccias near the contact with the Shayban formation ca. 500 m east of the Hadabah gneiss. (B) after – highly flattened and attenuated lithic clasts define lenticular banding in paragneiss ca. 150 m west of the Asad gneiss. Outcrop is representative of a large area previously mapped by Ramsay (1986b) as Asad gneiss, part of the Qudayd intrusive suite, but reinterpreted here as part of the Nida formation.

Much of the Qudayd suite consists of foliated, leucocratic to locally melanocratic (garnet)-hornblende-muscovite-biotite metatonalite showing variably schistose porphyroclastic, augen gneissic, and relict hypidiomorphic granular textures. In less-deformed parts of the metatonalite, original igneous foliation is defined by euhedral, coarse-grained plagioclase phenocrysts that

islands of mafic hornfels near the core of the Hadabah gneiss dome were interpreted by Ramsay (1986a) as roof pendants of precursory andesitic country rock.

Many deformed plutonic units in the Arabian Shield are referred to in the literature as syntectonic, implying that the intrusions were emplaced at the same time as

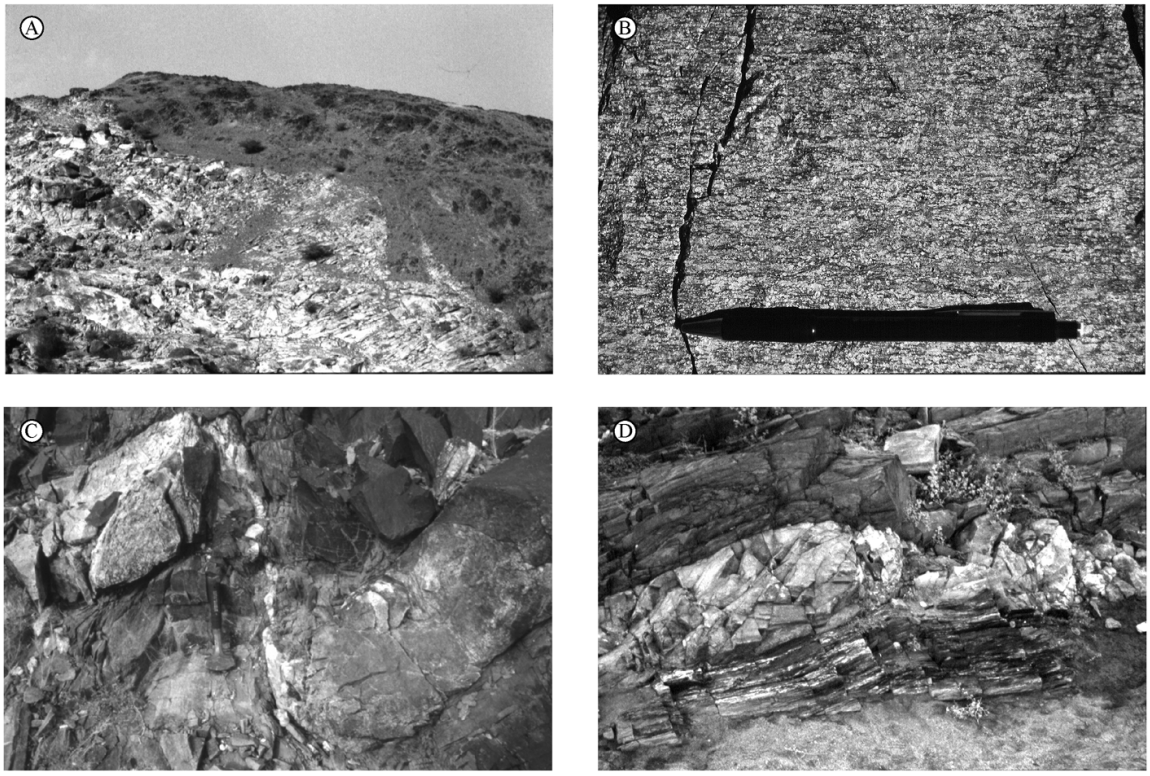

Figure 10. Photographs of outcrops of the Hadabah gneiss, Qudayd intrusive suite. (A) Intrusive contact between metatonalite (light) and dominantly greenschist-facies phyllite and schist of the Nida formation (dark). Note large septum of Nida phyllite at right partly enclosed by apophysis of metatonalite. Field of view is ca. 100 m across at bottom. View looking northeast approximately parallel to trend of foliation in Nida formation. (B) Ultramylonitic metatonalite on western side of Hadabah gneiss. Pencil for scale and is oriented parallel to foliation in outcrop. (C) Deformed dike of pegmatitic Qudayd tonalite (light) of the Hadabah gneiss intruding Nida phyllite (dark) on eastern side of Hadabah gneiss. Dike shows right-lateral offset parallel to foliation in host Nida formation. View looking northeast. Hammer in center for scale. (D) Deformed dike of Qudayd metarhyolite (SA01-122C), dated here at 746.7± 5.3 Ma, intruding Nida phyllite on eastern side of Hadabah gneiss. Dike shows pinch-and-swell texture. View looking east. Hammer in center for scale.

regional deformation. They show characteristics of solid-state deformation, which could just as easily be interpreted as evidence for pretectonic intrusion. Few "syntectonic" intrusions, if any, in the Arabian Shield have been scrutinized for evidence that they were actually deformed at or near the solidus temperature, which is the best evidence for syntectonic (sensu stricto) emplacement. Presented below are four lines of evidence, which indicate that the tonalitic protolith to the Hadabah gneiss was emplaced into the Labunah thrust zone during active deformation and was deformed while still close to the solidus temperature of the tonalite (cf. Paterson and others, 1989).

(1) In less deformed parts of the metatonalite, a strictly igneous foliation is parallel to the tectonic foliation within the orthogneiss and along its margins in the Nida formation. The igneous foliation is partly defined by large plagioclase phenocrysts orientated parallel to the tectonic foliation and by biotite-hornblende-rich schlieren that have diffuse, wispy margins and are elongate parallel to the tectonic fabric in the metatonalite. In many places, the original igneous foliation is difficult to distinguish from the structural overprint, which is defined by porphyroclasts (augen) of feldspar and quartz wrapped by discontinuous lenticular bands of biotite ± hornblende. Recognition of igneous versus metamorphic foliation is discussed more thoroughly in Paterson and others (1989). Small patches of non-foliated amphibolite and coarse-grained hornblende diorite occur in the cores of some schlieren, suggesting that residual heat (above the solidus temperature) was available after the schlieren formed. The schlieren, not including neocrystalline cores, appear similar to those in plutons that have not undergone solid-state deformation and their morphologies are interpreteded to be largely due to supersolidus flow and subsequent recrystallization.

(2) Near the contact with the Nida formation on the western side of the Hadabah gneiss, where more detailed work was conducted, Nida phyllites are transitional over tens of meters into banded amphibole-plagioclase gneiss with a protomylonitic fabric, and the metatonalite is transitional over a few meters into orthomylonite containing amphibolite facies assemblages of garnet + hornblende + quartz + plagioclase. The mylonitic metatonalite (Fig. 10B) exhibits a diffuse gneissic banding defined by syntectonic hornblende aggregates and veinlets of quartz showing granoblastic-polygonal texture that drape plagioclase porphyroclasts and garnet porphyroblasts. Kinematic indicators in the

mylonitic metatonalite, including sigmoidal tails on felsic porphyroclasts and a well-developed mineral (feldspar + quartz) stretching lineation, reveal a subhorizontal right-lateral sense of shear. Independent evidence for this shear regime is abundant in the Nida formation and includes shear banding that develops into an S-C fabric, en-echelon offset of boudins from dismembered quartz veins, subvertically plunging isoclinal folds, and a well-defined subhorizontal mineral-stretching lineation (locally L-S tectonite).

(3) On the eastern side of the Hadabah gneiss, late-stage unmetamorphosed dikes of pegmatitic muscovite tonalite, up to several meters wide, extend from the margin of the Hadabah gneiss into the Nida formation. Close to the Hadabah gneiss the dikes cut directly across the main fabric in the Nida formation, including protomylonitic quartzofeldspathic gneiss at the contact, but contain a variably strong to faint fabric oriented parallel to that in the host Nida schists. Several meters to tens of meters farther from the contact the dikes show right-lateral offset (Fig. 10C) and are transposed into the foliation in the Nida phyllites. Transposed limbs of the dikes show pinch-and-swell structure that progresses laterally to boudinage, and boudins are highly rotated and enclosed by anastomosing foliae of Nida phyllite.

(4) Zones of coarse-grained, unfoliated hornblende diorite and hornblendite intrude the western, more deformed margin of the metatonalite and parts of the host Nida formation. These zones and the dikes provide evidence for high heat flux after the most intense mylonitic deformation ceased.

The above features are interpreted herein as indications that the tonalite protolith to the Hadabah gneiss intruded into an active dextral shear zone within the Nida formation and was deformed while at or very near the solidus temperature. High-temperature metamorphic assemblages in the mylonitic rocks suggest that the shear zone was broader and more active during the initial stages of intrusion. Later, after the bulk of the tonalite was emplaced, the heat flux into the Nida formation decreased such that late-stage pegmatitic dikes were only mildly deformed at greenschist-facies conditions and only along discrete cm- to m-thick shear zones in the Nida formation away from the main intrusive contact. Such characteristics suggest that the shear zone was lubricated by the tonalitic magma, facilitating initially high-temperature ductile deformation along the margins of the tonalite and subsequent lower-temperature, less ductile deformation after most of the tonalite cooled below the solidus temperature.

The most compelling evidence for syntectonic intrusion of the Hadabah gneiss is found along contacts with the Nida formation, but contacts between the Nida formation and the Khamrah gneiss are obscured by Tertiary basalt, making it difficult to determine if that body is also syntectonic. Based on similar outcrop features of the Khamrah and Hadabah gneisses, however, the inference is made that both bodies underwent similar episodes of high-temperature deformation.

A robust crystallization age for the Hadabah gneiss would constrain the timing of deformation along the Labunah thrust zone. The only existing radiometric age for the Qudayd intrusive suite is a K-Ar date of 585 ± 12 Ma (Table 3) for the Khamrah gneiss (G. Brown in Gettings and Stoeser, 1981), which corresponds to late thermal resetting.

Three samples from the Qudayd metaintrusive suite were analyzed during this study, one from the Khamrah gneiss, one from the Hadabah gneiss, and one from a late-stage dike emanating from the Hadabah gneiss. Sample SA01-68 (Tables 1, 3) is from a penetratively deformed, garnet-bearing augen metatonalite in the Khamrah gneiss (KG in Fig. 3A). The exposure from which this sample was taken displays an igneous foliation, which is defined by abundant elongated and parallel melanocratic enclaves and alternating leucosomes and mesosomes that are up to 3 m thick and laterally continuous for tens of meters. The igneous fabric is overprinted by a tectonic fabric defined at hand-sample scale by discontinuous foliae of igneous biotite that partly drape abundant augen of feldspar ± quartz and subordinate garnet porphyroblasts. The outcrop is crossed by numerous, laterally continuous shear zones that are up to one meter wide and parallel to the main deformational fabric. In thin section, the sample shows evidence of strain, including pronounced undulatory extinction in quartz and grain-size reduction at the boundaries of quartz and plagioclase porphyroclasts. Metamorphic mineralogy is restricted to the greenschist-facies assemblage of garnet + muscovite + biotite + quartz + plagioclase.

On the concordia diagram in Figure 11A, data points for nine of the twelve grains analyzed from sample SA01-68 form a tight group that intersects concordia at ca. 780 Ma. Three other data points with higher $^{238}U/^{206}Pb$ plot to the right of the group, which is interpreted to reflect lead loss. The main group of points yields a concordia age of 782 ± 7 Ma (MSWD = 3.3). The high MSWD reflects the higher $^{207}Pb/^{206}Pb$ of some points in the group, but the low range in $^{238}U/^{206}Pb$ indicates that the quality of the age is still high, and the 782 ± 7 Ma age is taken as the igneous crystallization of the tonalite protolith to the orthogneiss. Thus, the Khamrah gneiss is similar in age to the part of the Hufayriyah tonalite dated here at ca. 780 Ma.

Sample SA01-123 (Tables 1, 3) is from biotite metatonalite in the Hadabah gneiss (HG in Fig. 3A). In outcrop, a magmatic foliation is defined by plagioclase euhedra exhibiting flow-alignment, locally abundant enclaves of thinly banded, melanocratic amphibolite gneiss that are elongate and oriented parallel to one another, and diffuse biotite-rich schlieren that are elongate parallel to the plagioclase euhedra and the enclaves. The magmatic foliation is subparallel to a strong tectonic fabric defined by aggregates of biotite that drape plagioclase euhedra and elongate aggregates of recrystallized quartz. On the concordia diagram in

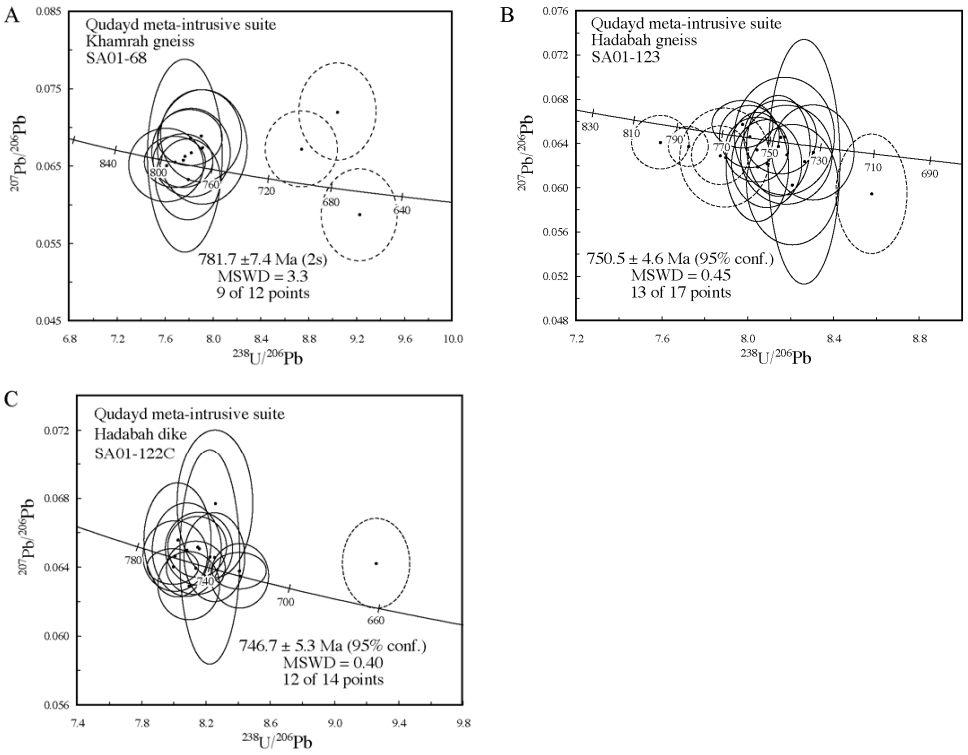

Figure 11. Tera-Wasserburg concordia diagrams for the Qudayd meta-intrusive suite. (A) Sample SA01-68 of metatonalite from the Khamrah gneiss. (B) Sample SA01-123 of tonalite from the Hadabah gneiss. (C) Sample SA01-122C of a dike extending from the Hadabah gneiss into the Nida formation. Sample information is given in Table 1 and analytical data in Table 3. Data points are shown with 2σ error ellipses and dashed ellipses were excluded from age calculations.

Figure 11B, error ellipses for thirteen of the seventeen analyzed grains cluster about concordia at ca. 750 Ma. Three points plotting to the left of the group are significantly older than, and appear to be unrelated to, the group (i.e. they appear to be inherited grains), and one point plotting to the right of the group is interpreted to have experienced recent lead loss. Upon elimination of those four points, a concordia age of 751 ± 5 Ma (MSWD = 0.45) is obtained, which is interpreted as the age of igneous crystallization of the tonalite protolith to the orthogneiss.

Sample 01-122C (Tables 1, 3) is from a deformed metarhyolite dike (Fig. 10D) extending from the eastern margin of the Hadabah gneiss into Nida greenschist (Fig. 3A). The connection between the dike at the sample locality and the main body of metatonalite several tens of meters away is covered, but the trend of the dike suggests that it is an apophysis of the pluton. On the concordia diagram in Figure 11C, the error ellipses for all data points are concordant, and most plot in a tight group. One data point lies far to the right of the group, most likely due to recent lead loss, and is omitted from the age calculation. Two other points lie just on the right edge of the group and together they prevent calculation of a concordia age, although this is not obvious on Figure 11C; elimination of either point produces an identical concordia age. In order to calculate an age using the maximum number of equivalent points, the point (12) with the highest $^{238}U/^{206}Pb$ was eliminated. Doing so yields a concordia age of 747 ± 5 Ma (MSWD = 0.4), which is interpreted as the age of crystallization of the dike and which is indistinguishable from the age of 751 ± 5 Ma for the main Hadabah gneiss obtained from sample SA01-123. The ages reported for the Hadabah gneiss and related dike are identical to SHRIMP-RG ages reported in a later section for the Amudan formation, which may be the extrusive equivalent of the Hadabah gneiss.

The new ages for the Qudayd metaintrusive suite, which is interpreted as a series of truly syntectonic plutons, are the first direct age constraints on the timing of deformation along the BUSZ. The disparity between them suggests that shearing along the Labunah thrust zone occurred either during two discrete episodes at ca. 780 and 750 Ma or during a single prolonged event. In either case, the ages support the interpretation by Stern and Abdelsalam (Abdelsalam and Stern, 1993a; Abdelsalam and Stern, 1993b; Abdelsalam, 1994; Stern and Abdelsalam, 1998) that deformation along the Nakasib suture zone in Sudan occurred sometime in the interval 780-740 Ma.

Bari granodiorite

Stocks and small plutons of Bari granodiorite (Kemp and others, 1982a; Kemp and others, 1982b) are widespread in the Bi'r Umq area (Fig. 3B). They were described in part by Radain (1978) and Kemp and others (1982a), and consist of variably leucocratic to mesocratic biotite-hornblende granodiorite, tonalite, trondhjemite and

minor granite. Intrusive relationships between the Bari and Hufayriyah associations are commonly unclear, but at least two Bari stocks appear to intrude the Hufayriyah tonalite (Kemp and others, 1982a; Kemp and others, 1982b). Massive, spherulitic rhyolite porphyry (SA03-269B), which occurs near the contact with the Dhukhr tonalite and was dated herein at ca. 771 Ma, may be a chilled-margin facies of the Bari granodiorite, as suggested by the common occurrence of granitic pegmatite dikes intruding Dhukhr dioritic rocks near contacts with the Bari granodiorite. Contacts with the Mahd group are generally sharp and clearly intrusive, and in places show the effects of contact metamorphism. Radiometric ages have not been previously reported for the Bari granodiorite, but geochronological data are reported here for one Bari intrusion.

Sample SA03-270 (Tables 1, 3) is from massive biotite-hornblende granite located ca. 7 km east-southeast of Mahd adh Dhahab (Fig. 3B). Analyses of thirteen zircon grains are plotted on the concordia diagram in Figure 12A. Error ellipses for all of the points are concordant and the majority form a tight group at ca. 770 Ma. Together, the thirteen points yield a concordia age of 776 ± 6 Ma (MSWD = 0.022). Three of the points are apparent outliers from the group; one is barely concordant and lies to the lower left of the group, and the other two lie at the right edge of the group and may have experienced recent lead loss. After omitting these three points from the calculation, the remaining ten points yield a concordia age of 770.0 ± 4.9 Ma (MSWD = 0.09). This second age is not an obvious improvement over the first and actually results in a slightly higher MSWD. Therefore, the first age of 776 ± 6 Ma, calculated using all thirteen data points, is taken as the igneous age of the sample. That age is within error of the ages reported in later sections for the Mahd group and the Ramram intrusive complex, which suggests that the Bari granodiorite may be the plutonic equivalent of those units. It is also within error of the ca. 780 Ma ages of Hufayriyah tonalite and the Qudayd metaintrusive suite (Khamrah gneiss).

Sample SA03-269B is from a hypabyssal intrusion of spherulitic, plagioclase-quartz-phyric rhyolite that penetrates the 803 ± 17 Ma Dhukhr tonalite (SA03-269A). Data for ten zircons are plotted on the concordia diagram in Figure 12B and scatter along concordia between ca. 800 and 760 Ma. Although the error ellipses for all points are concordant, they do not yield a concordia age. The oldest zircons from this sample were probably inherited from the Dhukhr tonalite. In CL images, no obvious differences are observed between the grains, and only one inherited "core" is visible, although this was not analyzed. Eliminating either of the two oldest points produces the same result, a concordia age of 772 ± 9 Ma (MSWD = 9.0), and eliminating both points yields an age of 769 ± 6 (MSWD = 8.0). Eliminating only those points with the highest error in $^{207}Pb/^{206}Pb$, including the oldest points, markedly decreases the scatter and increases the age to 776 ± 9 (MSWD = 4.0). Further eliminating all but the four most equivalent and concordant points greatly reduces the amount of scatter, but yields a minimum age of 766 ± 8 (MSWD = 1.8).

Determining the crystallization age of the rhyolite depends upon the criteria used to exclude data from the calculation. The best approximation for the crystallization age of the rhyolite most likely is close to the mean of the calculated ages (minus the oldest "inherited" zircons), which is ca. 771 ± 9 Ma (MSWD ~2.9). This is identical to the age of the Bari granodiorite from sample SA03-270 above, and to ages reported later in the text and by other authors (Calvez and Kemp, 1982) for the Mahd group and the Ramram complex. The inferred age and hypabyssal nature of the rhyolite suggest that it is not part of the Dhukhr tonalite, which it intrudes. It is inferred from the similarity in age and the proximity of the sample to the margin of a Bari granodiorite pluton that the hypabyssal rhyolite is a chilled margin facies of the Bari pluton.

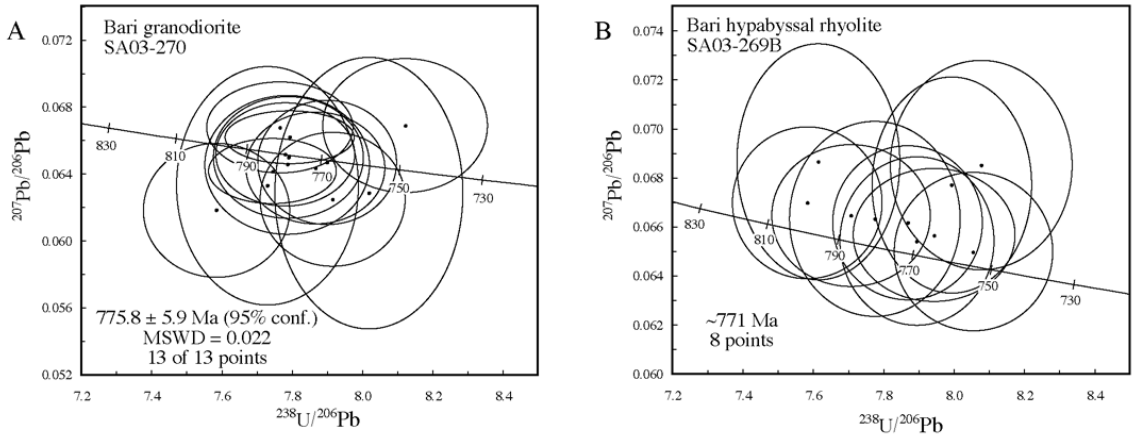

Figure 12. Tera-Wasserburg concordia diagrams for (A) sample SA03-270 of granite and (B) sample SA03-269B for rhyolite from the Bari granodiorite association. Sample information is given in Table 1 and analytical data in Table 3. Data points are shown with 2σ error ellipses.

RAMRAM INTRUSIVE COMPLEX

Subvolcanic rocks of the Ramram intrusive complex (Ramram complex of Dottin, 1975; Kemp and others, 1982a; Kemp and others, 1982b) were mapped in two main places in the Bi'r Umq area, at and near Jabal Ramram northwest of the Dhukhr batholith and at

Jabal Hammah at the western margin of the Furayhah batholith. Near Jabal Hammah (JH in Fig. 3B), the Ramram complex intrudes the Mahd group and the Furayhah batholith and comprises layered gabbro up to 2 km thick that is transitional upwards into granophyric granite and sheets of porphyritic rhyolite (Kemp and others, 1982a).

A similar lithologic association makes up part of the remnant stratovolcano and caldera at Jabal Ramram (JR in Fig. 3B) and has been described by Lefevre (1969), Dottin (1975), Kemp and others (1982a), Afifi (1983), and Roobol and White (1985). The structure of the volcano and the relationships of its constituent units are beautifully preserved and are only mildly deformed, and an excellent aerial photograph of the volcano is shown in Roobol and White (1985). The edifice is ca. 20 km in diameter and is constructed of lava flows and volcaniclastic rocks of the Mahd group with outward centripetal dips. Those deposits are intruded by felsic ring dikes that define the margins of an 8-km-wide caldera (Afifi, 1983; Roobol and White, 1985). The ring dikes consist of variably granophyric granodiorite and granite containing hornblende and inverted pigeonite. Intrusions of augite-phyric gabbro, diorite, and anorthosite occur at the eastern and western margins of the ring dikes, and gabbroic to dioritic sills intrude the Haf formation several kilometers north of Jabal Ramram (Dottin, 1975; Kemp and others, 1982a; Kemp and others, 1982b). The caldera is filled with melanocratic, felsic, welded pyroclastic-flow deposits, which dip radially inward near contacts with the ring dikes and are horizontal at the center of the caldera. They exhibit subvertical columnar jointing and well-developed eutaxitic texture and contain abundant xenoliths of granophyre from the ring dikes that increase in size and number toward the caldera walls. Calvez and Kemp (1982) reported that the rhyolite in places is gradational with the granite in the ring dikes. Observed geological relationships indicate that the Ramram complex is the intrusive equivalent of the Mahd group, and the caldera at Jabal Ramram was the main eruptive center for the abundant Mahd pyroclastic-flow deposits, as suggested by Calvez and Kemp (1982).

Huckerby (1984) reported three Rb-Sr whole-rock isochron ages for the Ramram intrusive complex of 741 ± 92 Ma (4 points, MSWD = 1.2), 758 ± 35 Ma (4 points, MSWD = 2.3), and 764 ± 14 (8 points, MSWD = 1.4) (Table 3). The youngest of these ages has such a large error that it is not useful, but the oldest is within error of the U-Pb zircon age of 769 ± 5 Ma reported by Calvez and Kemp (1982) for granophyre in the ring dike (Table 3).

New ages were obtained for two parts of the Jabal Ramram ring dike. Sample SA03-160 (Tables 1, 2) is from granophyric pyroxene granodiorite at the southern outer margin of the ring dike at Jabal Ramram (JR in Fig. 3B). On the concordia diagram in Figure 13A the data ellipses for twelve zircon analyses plot in a fairly tight group. Two data points, whose respective error ellipses lie to the right and upper-right of the group, prevented calculation of a concordia age. The point to the right of the group probably experienced recent lead loss and was omitted from the age calculations. The remaining eleven points yield a concordia age of 769 ± 6 Ma (MSWD = 0.70), which is interpreted as the crystallization age of the granodiorite. This age is within error of the 764 ± 14 Ma Rb-Sr age reported by Huckerby (1984) and is indistinguishable from the 769 ± 5 Ma U-Pb age reported by Calvez and Kemp (1982) for granophyre in the northeastern part of the ring dike.

Sample SA03-267 (Tables 1, 3) is from granophyric hornblende granite close to the inner margin of the Jabal Ramram ring dike and the contact with the caldera-fill ignimbrites (Fig. 3B). On the concordia diagram in Figure 13B, most of the points plot within a tight group about concordia. The discordant point that plots to the upper right of the group was omitted. The point with the highest $^{238}U/^{206}Pb$ prevents the calculation of an age, presumably plots to the right of the group because of lead loss, and also was omitted. An age of 749 ± 9 Ma (MSWD = 0.83) is obtained from the remaining eleven points and is interpreted as the intrusion age of the granite. This age is significantly younger than the ca. 765-770 Ma U-Pb zircon ages reported here and by Calvez and Kemp (1982) for the ring dike.

It should be noted that the group of points from sample SA03-267 (Fig. 13B) could also be viewed as comprising two distinct populations with overlapping error ellipses, one which produces a concordia age of 757.6 ± 9 Ma (MSWD = 0.045) and the other which yields an age of 735 ± 11 Ma (MSWD = 2.7). This interpretation might otherwise seem unnecessary, especially considering the statistical quality of the 749 ± 9 Ma age, were it not for a Rb-Sr isochron age of 726 ± 33 Ma reported by Calvez and Kemp (1982) for the caldera-fill ignimbrites. Calvez and Kemp (1982) dismissed that age on the grounds that it was unrealistically young due to Sr contamination, but it is very similar to the age of the younger group above. It is probable that the age of the young group and the young Rb-Sr age rejected by Calvez and Kemp (1982) reflect partial disturbances of the respective isotopic systems. If so, then the younger points should be omitted from the age calculation, and the igneous age of the sample would be best represented by the 758 ± 9 Ma age for the older zircon group. In either case, the age of the inner granite is at least 11 Ma younger than the age of the granodiorite at the outer margin of the Ramram ring dike. Because of the high level of intrusion for this body, a protracted period of cooling from the outside to the inside of the dike can be ruled out. The most likely explanation for the disparity in age is that the Ramram ring dike is actually a complex of two phases, an older ca. 770-Ma granodiorite phase toward the outer margin and a younger granite phase that intruded the granodiorite sometime between 758 and 749 Ma, depending on which age is accepted. The contact between two such intrusive phases is not obvious in the field and locating it would require more detailed fieldwork. The younger age of 749 Ma is preferred because it is derived from a

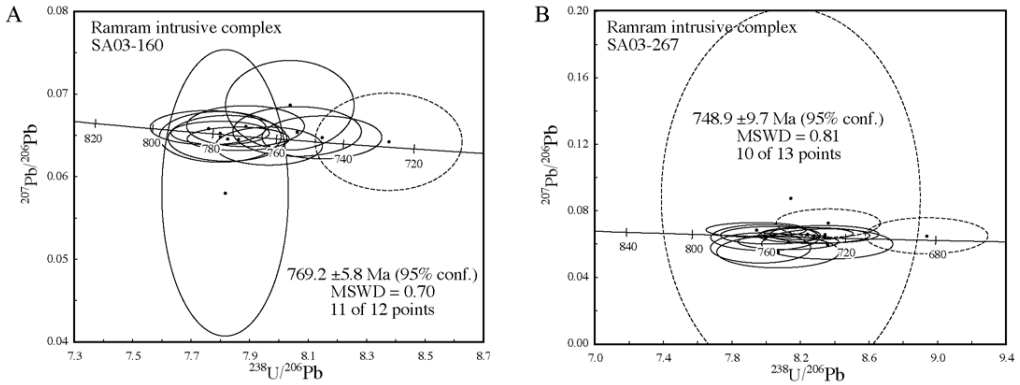

Figure 13. Tera-Wasserburg concordia diagrams for samples (A) SA03-160 of granodiorite and (B) SA03-267 of granite from the Ramram intrusive complex. Sample information is given in Table 1 and analytical data in Table 3. Data points are shown with 2σ error ellipses and dashed ellipses were excluded from age calculations.

greater number of analyses and is indistinguishable from the 748 ± 22 Ma age (1982) for the Ghamr group, the source of which has not previously been identified.

Posttectonic intrusions

Miscellaneous posttectonic intrusions

Deformed volcanic and plutonic units in the Tharwah and Bi'r Umq areas are intruded by younger undeformed bodies of various size and composition. A pluton of syenogranite intrudes the Bustan complex (Rabigh intrusive suite) at the northern end of the Umm Gerad erosional outlier (UG in Figure 3A). An Rb-Sr whole-rock isochron age of 580 ± 9 Ma for the syenogranite (Al-Shanti and Abdel-Monem, 1982) is the only previously reported constraint on the timing of posttectonic magmatism along the Tharwah segment of the BUSZ.

A pair of east-west-trending, posttectonic megadikes intrudes the Samran group (Fig. 3A). One consists of monzogranite and minor gabbro (Nukhu granite of Ramsay, 1986a) and the other of a cogenetic suite of olivine syenite, syenograbbro, and gabbro (Skiba and Gilboy, 1975). Although the dikes are contorted in plan view, they contain no internal fabric and truncate all regional Precambrian stratigraphic and structural trends. Orientation of the dikes parallel to the Rima shear zone and their discordancy with northeast-oriented regional stratigraphic and structural trends suggest that the dikes intruded along east-northeast-trending fractures (Skiba and Gilboy, 1975) that probably formed during the D3 extensional event of Johnson (1998) in the Samran fold-thrust belt. The orientation and lithologies of the dikes suggest that they are cogenetic, which is confirmed by geochronologic data reported here.

Sample SA01-109A (Tables 1, 3) is a biotite granite from the east-west-trending megadike (Nukhu granite of Ramsay, 1986a) located just north of Al Kamil (Fig. 3A). Thirteen zircons were analyzed, and error ellipses for the data points are plotted on the concordia diagram in Figure 14A. One data point plotting far to the right of the main group is interpreted as having experienced lead loss and was omitted. Another point that plots slightly to the left of the main group prevents the calculation of an age, may be inherited, and also was omitted. Ellipses for the remaining eleven data points form a loose cluster about concordia, and the data for these points yield a concordia age of 699 ± 7 Ma (MSWD = 4.3). Scatter of the points relative to concordia is high, but the age is a reasonable approximation for crystallization of the dike. Based on geologic evidence that the dike is posttectonic, the ca. 700 Ma age provides an important lower limit on the timing of regional deformation along the BUSZ. It also precludes the possibility mentioned by Ramsay (1986a) that the dike is post-Precambrian or even Tertiary in age.

Sample SA01-88 is a biotite syenite from the megadike (Missir dike of Ramsay, 1986a) to the west of Al Kamil (Fig. 3A). Error ellipses for the 22 analyzed points show considerable scatter on the concordia diagram in Figure 14B and range in apparent age from ca. 400 to 900 Ma. Eighteen points define an array with an upper intercept of concordia at ca. 700 Ma. If these data are interpreted to reflect varying degrees of lead loss from approximately 700 Ma old zircons, then the upper intercept age provides additional support for the ca. 698 Ma age from the Nukhu dike dated by sample SA01-109A. The four points in Figure 14B with the oldest apparent ages would best be interpreted as inherited from older basement.

Sample SA03-373 (Tables 1, 3) comes from a semicircular body of hornblende granite ca. 13 km north of the Tharwah ophiolite (Fig. 3A). The intrusion, which here is informally called the Hanak granite after nearby Wadi al Hanak, was originally mapped as part of the Hajar complex of the Rabigh intrusive suite (Gilboy and Skiba, 1978a; Ramsay, 1986b) and underlies the village of Al Hajar, after which the complex was named. Ramsay (1986a) noted that a smaller intrusion, which is included in Figure 3A as part of the Hanak granite, is distinct in satellite imagery, and suggested that it is younger than the Rabigh suite and possibly posttectonic, which is confirmed by the new age reported below. The outline of the Hanak granite is significantly larger in Figure 3A than that shown by Ramsay (1986a) in order to cover both the intrusion to which he referred and the area from which sample SA03-373 was obtained. Data from eighteen zircon grains show significant scatter on the concordia diagram in Figure 14C, spanning an interval

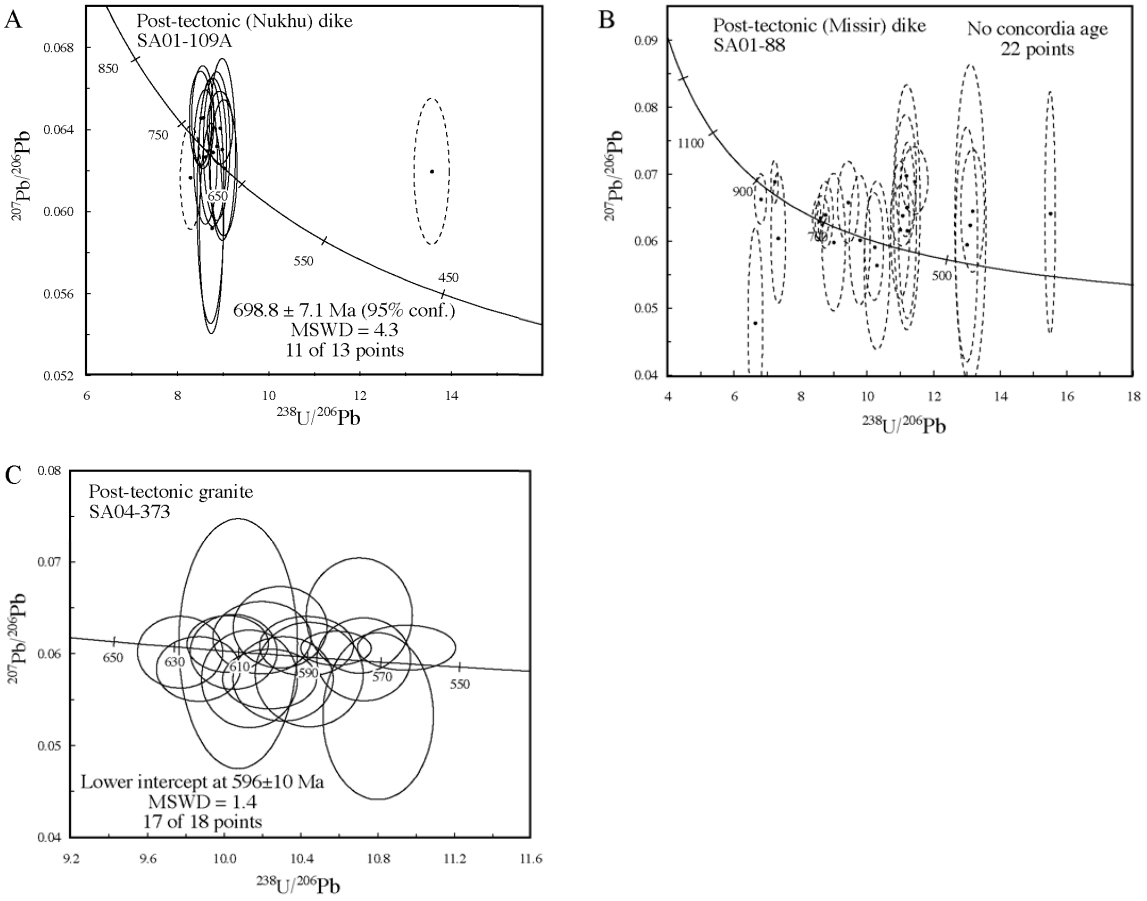

Figure 14. Tera-Wasserburg concordia diagrams for samples (A) SA01-109A of granite from the Nukhu posttectonic megadike, (B) SA01-88 of syenite from the Missir posttectonic megadike, and (C) SA04-373 of granite from a posttectonic pluton intruding the Rabigh intrusive suite and the Bi'rak group. Sample information is given in Table 1 and analytical data in Table 3. Data points are shown with 2σ error ellipses and dashed ellipses were excluded from age calculations

of nearly 65 Ma. The scatter prevents the calculation of a concordia-intercept age and gives no obvious visible indication for exclusion of points due to inheritance or lead loss. A Model 2 fit of the data produces a lower intercept (mean) age of 596 ± 10 Ma (no upper intercept), which is nearly identical to several Rb-Sr isochron ages for the Raghiyah intrusive suite, discussed below, to which this intrusion may be genetically related. It should be stressed that this number is merely the average for points ranging from ca. 630 to 565 Ma, and is not intended to date the igneous crystallization of the granite. Moreover, a Model 2 fit weighs the data points equally and ignores data point errors, such that the error on the calculated age is commonly unreliable. The age does, however, provide information on the timing of posttectonic granitic magmatism north of the BUSZ.

Raghiyah intrusive suite

In the Bi'r Umq area (Fig. 3B), Kemp and others (1982a) assigned most of the posttectonic rocks to the Raghiyah suite, which has been recognized on both sides of the Hulayfah-Ad Dafinah-Ruwah fault zone and thus post-dates suturing against the Afif terrane to the east. The Raghiyah intrusive suite may also be related to similar intrusions north of the Tharwah segment, including the granite dated here by sample SA04-373. The Raghiyah intrusions are generally semicircular to elliptical in plan view, are discordant with steep, sharp contacts against older plutonic and volcanic units, and typically show a close association of different intrusive phases with characteristic, in places bimodal, lithologies. The most widespread lithology is (hornblende)-biotite monzogranite and associated riebeckite leucogranite. The Raghiyah intrusions are peralkaline, and Radain and others (1981) suggested that the parental magmas of the peralkaline rocks formed by partial melting of the lower crust as a result of thrust-related overthickening (Kemp and others, 1982a).

The intrusions at Jabal Habd ash Sharar and Jabal Habd ad Dayahin (JHS and JHD in Fig. 3B) were interpreted as ring dikes associated with cauldron subsidence or caldera collapse (Kemp and others, 1982a; Roobol and White, 1985). Riebeckite granite from the ring dike complexes yielded Rb-Sr isochron ages of 590 ± 10 Ma (Brown and others, 1978) and 584 ± 26 Ma (Calvez and Kemp, 1982). A large crescent-shaped body of biotite-hornblende granodiorite and quartz-monzodiorite, which intrudes the Hufayriyah batholith and the Mahd group between Jabal Habd ash Sharar and the Bi'r Umq ophiolite, yielded an Rb-Sr whole-rock isochron age of 573 ± 22 Ma (Calvez and Kemp, 1982).

Poorly exposed intrusions of granite and monzogranite with elliptical outlines and northerly elongation occur

in several locations in the Bi'r Umq area. Calvez and Kemp (1982) obtained an Rb-Sr errorchron age of 575 ± 28 Ma (6 points, MSWD = 5.85) for north-northwest-elongated granite intruding the Mahd and Ghamr groups northwest of Jabal Ramram; a younger Rb-Sr mineral isochron age of 520 ± 15 Ma (number of points and MSWD not reported, Brown and others, 1978) for biotite from the same granite, may have been reset. Rapakivi granite and a smaller body of fluorite-bearing granite, both elongated north-northeast, intrude the eastern margin of the Hufayriyah batholith. The rapakivi granite yielded Rb-Sr whole-rock isochron ages of 567 ± 86 Ma (3 points, MSWD = 0.01, Fleck and Hadley, 1982) and 566 ± 30 Ma (errors and MSWD not reported, Brown and others, 1978). The fluorite-bearing granite yielded Rb-Sr model ages of 602 Ma and 594 Ma (mean of 598 Ma) (Fleck and Hadley, 1982).

Exposures of monzogranite west of Harrat Kishb and just east of the Hulayfah-Ad Dafinah-Ruwah fault zone (Fig. 3B) are associated with mafic-ultramafic cumulates. The eastern occurrence is a 2700-m-thick layered succession of two-pyroxene gabbro, (plagioclase)-olivine pyroxenite, peridotite, and clinopyroxene troctolite (Kemp and others, 1982a). The relationship between the granitic and mafic-ultramafic rocks is unclear. Contacts between them were not observed during this study and are not discussed by Kemp and others (1982a). Those authors only noted a markedly close spatial relationship between the two lithotypes at the western exposure, but on the map of Kemp and others (1982b) the gabbros appear to be spatially more closely associated with the Hufayriyah tonalite, which they intrude, than with the granitic rocks. Following Kemp and others (1982a), however, the mafic-ultramafic rocks are here included as part of the Raghiyah intrusive suite.

Several bodies of syenite, monzonite, and monzogranite (Camp, 1986b; 1986a) intrude the Bi'rak, Furayh, and Shayma Nasir groups and the Rabigh intrusive suite north of the Tharwah segment of the BUSZ. An older phase includes aegerine granite (Camp, 1986b; 1986a), from which Aleinikoff and Stoeser (1988) attempted to obtain a U-Pb zircon age. Only an estimate for a maximum age of 696 Ma could be derived, but this is within error of the 698.8 ± 7.1 Ma age reported here for the Nukhu granite megadike intruding the Shayban formation and Kamil suite. Other parts of the Subh suite yielded a single-point Rb-Sr model age of 659 ± 7 Ma (C. Hedge, cited as pers. comm. in Aleinikoff and Stoeser, 1988) and an Rb-Sr whole-rock isochron age of 687 ± 18 Ma (Clark and Duyverman, 1983). A younger group of plutons (Camp, 1986b; Camp, 1986a) with elliptical outlines intrudes the Subh suite and is therefore younger than 687 Ma and possibly younger than ca. 660 Ma. The locations, compositions, apparent ages, and morphologies of the Suwaylih and Khuls suite intrusions suggest that they are related to the Raghiyah intrusive suite, but radiometric ages are needed to confirm the correlation.

Zircon grains from two samples of the Raghiyah intrusive suite were analyzed during this study, but crystallization ages could not be determined for either sample. Sample SA03-245A (Tables 1, 3) comes from riebeckite granite at the western margin of the Habd ash Sharar intrusion (JHS in Fig. 3A), which was dated at ca. 590 Ma (Brown and others, 1978; Calvez and Kemp, 1982). The sample yielded sparse zircon despite very high Zr concentration (1800 ppm, Hargrove, 2006). Only three zircons were probed, and error ellipses for the data points are plotted on the concordia diagram in Figure 15A. They range in age from ca. 745 to 1255 Ma and are interpreted to represent zircon grains inherited from middle Neoproterozoic and Mesoproterozoic crust.

Sample SA03-246 is from hornblende granodiorite at the southern margin of the arcuate intrusion north of Jabal Habd ash Sharar (JHS in Fig. 3B). This sample produced more zircon than sample SA03-245A, despite a much lower Zr concentration (200 ppm, unpublished data). Such a situation may be due to the effects of alkali concentrations on Zr saturation in alkaline and peralkaline magmas (Aleinikoff and Stoeser, 1988). Error ellipses for six zircon grains are shown on the concordia diagram in Figure 15B, where the data scatter widely from ca. 620 Ma to about 1430 Ma. It is unclear if the two youngest grains are inherited, but the older grains from this sample, as well as from the previous sample, are interpreted to reflect the presence of Mesoproterozoic crust with which the parental melts to the Raghiyah suite interacted.

GEOCHRONOLOGY OF SUPRACRUSTAL SEQUENCES

Neoproterozoic stratigraphic units south of the BUSZ include the Samran and Shayma Nasir groups in the Tharwah segment (Fig. 3A) and the Arj, Mahd, and Ghamr groups in the Bi'r Umq segment (Fig. 3B). North of the suture, the stratigraphic units consist of the Bi'rak and Furayh groups and part of the Shayma Nasir group. The units are discussed here in order of decreasing age and higher stratigraphic level.

Bi'rak group

Volcanic, volcaniclastic, and epiclastic rocks exposed along the BUSZ were originally assigned to the Samran group (Skiba and Gilboy, 1975; Gilboy and Skiba, 1978a, 1978c, 1978b, 1978d), but Ramsay (1986a) reassigned the rocks north of the suture to the Bi'rak Group (Fig. 3A) and provisionally classified them as the oldest stratigraphic unit along the suture. The Bi'rak group consists of mafic to felsic lavas and volcaniclastic rocks, associated epiclastic rocks, marble, and chert that are variably schistose and generally metamorphosed in the greenschist facies (Camp, 1986a; Ramsay, 1986a). Ramsay (1986b; 1986a) and Camp (1986b; 1986a) divided the Bi'rak group into the Labunah, Suri, and Qahah formations, but the Milhah formation is herein also included in the group. The formations are not distinguished in Figure 3A, but are discussed here from

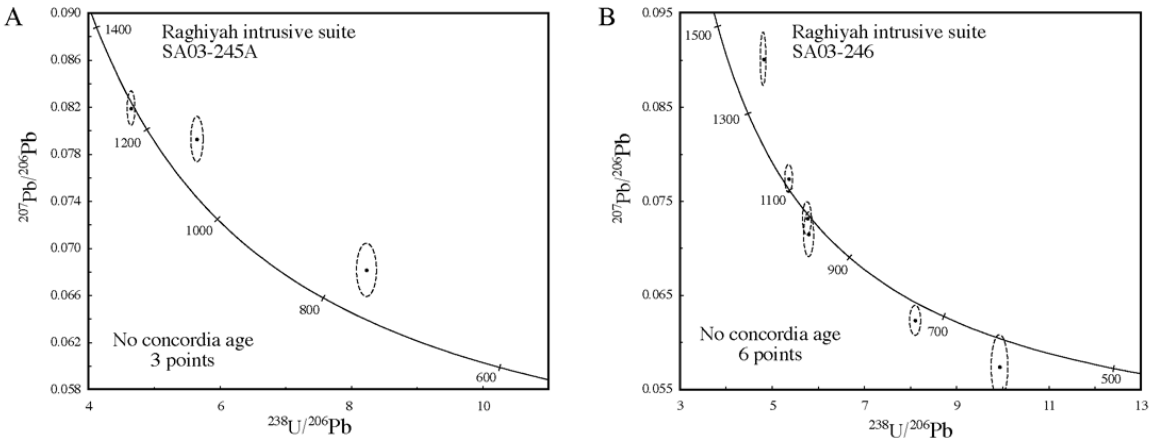

Figure 15. Tera-Wasserburg concordia diagrams for samples (A) SA03-245A of alkalic granite and (B) SA03-246 of quartz-diorite from the Raghiyah intrusive suite. Sample information is given in Table 1 and analytical data in Table 3. Data points are shown with dashed 2σ error ellipses.

southeast to northwest in order of increasing stratigraphic level and decreasing age. None of the formations have been dated, but the Labunah and Suri formations are intruded by 807 Ma tonalite of the Rabigh intrusive suite and the Milhah formation is intruded by 715 Ma gabbro of the Rabigh suite (C. Hedge, cited as pers. comm. in Al-Shanti and Abdel-Monem, 1982; C. Hedge, cited as pers. comm. in Camp, 1986a).

The Labunah formation occurs in a northeasterly trending belt within and northwest of the Labunah thrust zone. The formation is in thrust contact with the Nida formation of the Samran group to the southeast (Camp, 1986a; Ramsay, 1986a; Johnson, 1998; Johnson and others, 2002) and underlies the Qahah formation to the west (Camp, 1986a). The Labunah formation is considered to be equivalent to the Suri formation, based on lithologic similarities and the fact that both are in contact with the Qahah formation, although the apparent juxtaposition (Camp, 1986a) of the Labunah and Qahah formations does not indicate the relative stratigraphic positions of the two. The Labunah formation consists of dominantly basaltic to andesitic and less abundant felsic lava, volcaniclastic rocks, and tuff, and subordinate fine-grained siliciclastic rocks, marble, and chert (Camp, 1986a; Ramsay, 1986a, and references therein). Most of the deposits are deformed into tight to isoclinal folds, which are most conspicuous in interbedded chert and marble layers (Fig. 16A). The results of thrusting along the Labunah thrust zone are especially visible in the southern face of Jabal Farasan (Fig. 16B), where marble and chert of the Labunah formation are telescoped over presumably younger phyllites of the Nida formation in the Samran group. The dominant facies of the Labunah formation is that of a marine setting. The greater proportion of marble in the Labunah formation and its more seaward position relative to the remaining Bi'rak group to the northwest supports the suggestion by Camp (1986a) that the Labunah formation represents a more distal facies of the Suri formation.

The Suri formation is >5000 m thick and consists primarily of massive lavas of predominantly basalt and basaltic andesite and subordinate dacite, abundant pillow lavas, and sheeted mafic dikes; the upper portion of the succession contains rare hyaloclastite, volcaniclastic and epiclastic sandstone, and marble (Camp, 1986a). The formation changes from a lower, deep-oceanic facies characterized by mafic to felsic volcanic rocks and subordinate volcaniclastic debris to an upper, shallower-marine facies characterized by more abundant intermediate tuffaceous and volcaniclastic rocks and subordinate volcanic rocks. Camp (1986a) interpreted this facies change to reflect a transition from an immature island arc or rift setting to a more mature

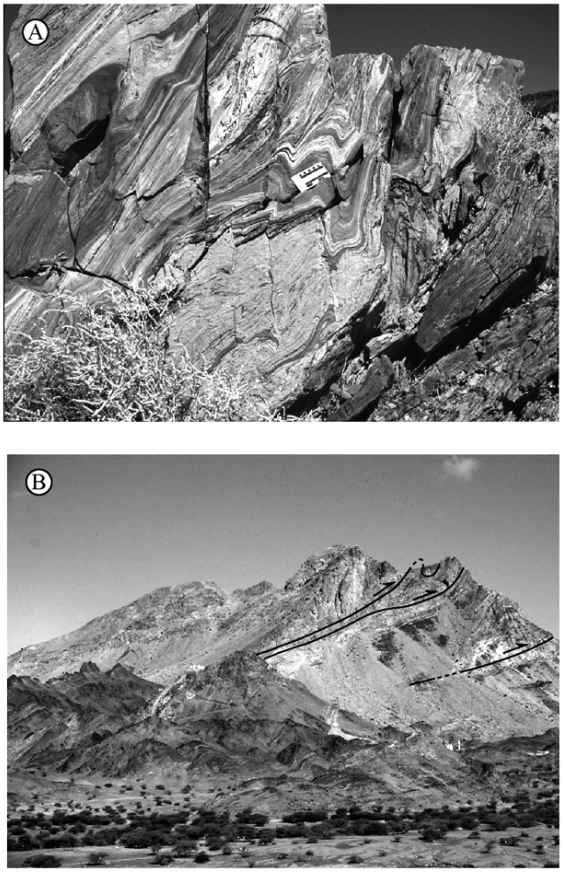

Figure 16. Photographs of outcrops of the Labunah formation. (A) Banded calcite marble (top) is interleaved with massive dolomite marble (bottom center) and laminated chert (bottom right). (B) View of Jabal Farasan looking northwest, showing marble (light) and greenschist (dark) of the Labunah formation and the location and sense of shear of major fault surfaces in the Labunah thrust zone, based on interpretation of Nebert (1969).

system.

The Qahah formation is exposed in the area between Suri and Labunah formations. The lower contact with the Suri formation is commonly marked by monomict conglomerate or breccia, finer grained clastic rocks derived from the underlying Suri formation, and possible turbidite (Camp, 1986a; Ramsay, 1986a). The rest of the formation consists of coarse-grained siliceous epiclastic rocks, shale, less abundant marl and limestone passing upwards into basaltic to andesitic and subordinate dacitic to rhyolitic lava and volcaniclastic rocks. The Qahah formation was interpreted as a primitive island-arc assemblage (Ramsay, 1986a). Camp (1986a) interpreted the basal units of the Qahah formation to reflect uplift and erosion of the Suri formation and deposition into an arc- or rift-related marine basin. The lower contacts of the Qahah formation represent a major shift in depositional setting from one of subaqueous and largely basaltic volcanism in the underlying Suri and Labunah formations to one dominated by clastic deposition with only subordinate volcanism (Camp, 1986a).

The Milhah formation overlies the Qahah formation, with locally recognizable unconformity, in a minor northeast-trending belt along the western side of Wadi al Qahah. A basal polymict conglomerate is overlain by a 1500-m-thick sequence dominated by basalt to andesite lava and tuff and containing subordinate volcanic-lithic arenite, shale, and conglomerate; subvolcanic rhyolite intrusions also occur (Camp, 1986a). Camp (1986b) originally mapped the Milhah formation separate from the Bi'rak group. He indicated that the Milhah formation is difficult to distinguish from parts of the Furayh group and suggested that the two are continuous, but that is inconsistent with the 663-633 Ma ages for the Furayh group and the fact that the Milhah formation must be older than 715 Ma gabbro of the Rabigh suite (Aldrich and others, 1978) that intrudes it. Although that age for the Rabigh suite is likely too young, the Milhah formation is tentatively assigned here to the Bi'rak group on the basis that both the Bi'rak group and Milhah formation are older than the Rabigh suite, whereas the Furayh group is clearly younger, as discussed in a later section.

Although most of the geochronology samples from this study are from the southern flank of the BUSZ, samples SA04-366 and SA04-367 are from microgabbro sills intruding the Qahah formation on the northern flank of the suture ca. 37 km east-southeast of Rabigh (Fig. 3A). The results of analyses of 12 zircon grains from sample SA04-366 are plotted on the concordia diagram in Figure 17A. The data range in apparent age from ca. 755 Ma to >2800 Ma, with the majority of the ellipses forming a loose group at ca. 840-880 Ma. Among the points in the group, the point with the lowest $^{238}U/^{206}Pb$ is discordant and the point with the highest $^{238}U/^{206}Pb$ appears to have experienced lead loss. Both points were eliminated from the age calculations. The remaining eight points do not yield a concordia age. The three oldest points (4.1-6.1) all show larger errors in $^{207}Pb/^{206}Pb$ than the other five and may constitute a separate population, possibly inherited from older crust. The remaining five points yield a concordia age of 854 ± 15 Ma (MSWD = 0.000). The very low MSWD points to the highly correlated nature of the analyses. The age is not very robust, but it is consistent with the Bi'rak group being older than the ca. 807 Ma tonalite of the Rabigh suite that intrudes it (C. Hedge, cited as pers. comm. in Al-Shanti and Abdel-Monem, 1982; C. Hedge, cited as pers. comm. in Camp, 1986a). If the age for the gabbroic sill is taken as a best estimate for the crystallization age, then the Bi'rak group is older than 854 Ma.

Sample SA04-367 comes from a separate, but probably related microgabbro sill only a few hundred meters from the site of the preceding sample. Results of the analyses of 18 zircons are plotted on the concordia diagram in Figure 17B. The data range in apparent age from 360 Ma to 1915 Ma, but five of the analyses form a tight group that yields a concordia age of 812 ± 23 Ma (MSWD = 0.36), which is taken as the crystallization age of the gabbro. That age is also consistent with the Bi'rak group being older than the ca. 807 Ma tonalite of the Rabigh suite that intrudes it (C. Hedge, cited as pers. comm. in Al-Shanti and Abdel-Monem, 1982; C. Hedge, cited as pers. comm. in Camp, 1986a), but

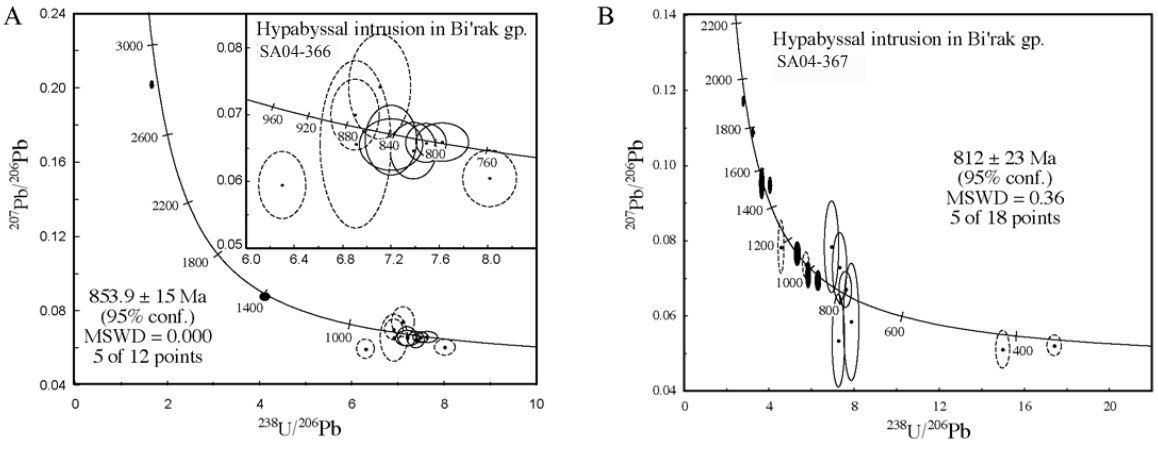

Figure 17. Tera-Wasserburg concordia diagrams for samples (A) SA04-366 and (B) SA04-367 of hypabyssal gabbroic sills intruding the Qahah formation, Bi'rak group. Sample information is given in Table 1 and analytical data in Table 3. Data points are shown with 2σ error ellipses, dashed ellipses were excluded from age calculations, and some ellipses are filled for better visibility.

is substantially younger than the inferred age of the previous sample. It is unclear if the data from either sample actually represents the age of the Bi'rak group, but the ages do indicate widespread inheritance of significantly older zircon.

Arj group

The Arj group (Fig. 3B) is the lowermost stratigraphic unit in the Bi'r Umq segment of the BUSZ and is probably the oldest unit on the south side of the suture. The Arj group was studied by Jourde (1976), Alabouvette and others (1972), and Kemp and others (1982a; 1982b), who divided the group into the Sumayir, Sayid, and Jabal Azlam formations. The Sumayir formation occurs north of the BUSZ and corresponds to the Bi'r Umq ophiolite. The Sayid and Jabal Azlam formations occur to the south of the suture and constitute what is referred to hereafter as the Arj group. Because of limited occurrences, the Sayid and Jabal Azlam formations are not differentiated in Figure 3B. Johnson and others (2002; 2003) combined these rocks with the Mahd group, but the distinction of Kemp and others (1982a) between the groups is herein retained for the following reasons: (1) wherever the two groups occur together the contact is an angular unconformity; (2) although both are folded, the Arj group was deformed prior to development of the erosional surface onto which the Tulaymisah formation of the Mahd group was deposited; and (3) the abundance of volcanic clasts in the breccia at the base of the Mahd group indicates that an older volcanic sequence was present in the area prior to deposition of the Mahd group. The provenance of the volcanic clasts is not known, but the Arj group is a likely source.

The Arj group, as redefined here, occupies a discontinuous, arcuate belt along the margins of the Hufayriyah batholith in the northern part of the Bi'r Umq area (Fig. 3B), and most of it occurs on the southern limb of a major east-west-trending syncline in the footwall of the Bi'r Umq thrust. The thickness of the group cannot be determined, because the base is not exposed and because of intense deformation near the suture (Kemp and others, 1982a). The angular unconformity between the Arj group and overlying Mahd group and the more intense folding in the Arj group suggest that the Arj group was deformed and uplifted, possibly at the same time as the Dhukhr tonalite, prior to deposition of the Mahd group. The older Sayid formation contains basaltic to andesitic lava and tuff, laminated felsic crystal-vitric tuff, pyroclastic and volcaniclastic quartz-keratophyre, and chert, limestone, sandstone, and conglomerate (Kemp and others, 1982a). The top of the Sayid formation is conformable with the overlying Jabal Azlam formation, which is up to 7000 m of basaltic to andesitic volcaniclastic and intrusive breccia, massive intrusive andesite, coarse- to fine-grained sandstone, and siltstone, and conglomerate containing clasts of contemporaneous volcanic rocks including quartz-keratophyre. Sedimentary rocks increase in proportion upward and eastward (Kemp and others, 1982a). Kemp and others (1982a) interpreted the Arj group as having formed in an intracratonic rift.

The only previously reported age for the Arj group, as defined here, is an Rb-Sr whole-rock isochron age of 651 ± 40 Ma (Brown and others, 1978). Such a young age is contrary to geological evidence that the Arj group is the oldest stratigraphic unit in the Bi'r Umq area and is therefore rejected as an eruption age. The Arj group is at least 781 Ma old, as it is intruded and contact-metamorphosed by the Hufayriyah tonalite dated during this study at 780.6 ± 7.6 Ma. A single sample from the Arj group was collected for geochronology during this study. Sample SA03-259 is from basaltic andesite ca. 9 km northwest of Jabal Habd ash Sharar (JHS in Fig. 3B). It has a very low Zr concentration (10 ppm, unpublished data) and produced only three zircon crystals. Error ellipses for three data points are plotted on the concordia diagram in Figure 18. No concordia age was obtained, because all three grains are clearly inherited, two from a Mesoproterozoic source and one from an Archean source.

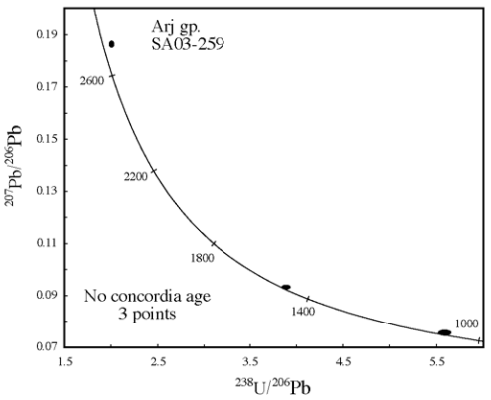

Figure 18. Tera-Wasserburg concordia diagram for sample SA03-259 of basaltic andesite from the Jabal Azlam formation, Arj group. Sample information is given in Table 1 and analytical data in Table 3. Data points are shown as filled 2σ error ellipses for better visibility.

Samran group

Volcanic, volcaniclastic, and epiclastic rocks of the Samran group occur within the northeast-trending Samran fold-thrust belt on the southern flank of the BUSZ. Within the area of Figure 3A, the Samran group is divided into the Nida, Shayban, and Amudan formations, which are discussed from north to south in order of decreasing age and higher stratigraphic level (Gilboy and Skiba, 1978a, 1978c, 1978b, 1978d; Ramsay, 1986b, 1986a). The age of the Samran group is poorly constrained. The group is intruded by several plutons of the Kamil intrusive suite. Fleck (1985) obtained an Rb-Sr isochron age of 769 ± 39 Ma from tonalite of the Kamil intrusive suite just south of the Tharwah area. This does not constrain the age of the Samran group, however, because the tonalite dated by Fleck (1985) intruded other parts of the Kamil suite and is nowhere in contact with rocks of the Samran group.

Nida formation

The Nida Formation (Fig. 3A) is the structurally and stratigraphically lowest unit of the Samran group and was mapped by Kana'an (1970; 1977), Liddicoat (1971), Nebert (1969), (Gilboy and Skiba, 1978a, 1978c, 1978b, 1978d), and Ramsay (1986a). It is exposed within a large antiform parallel to the Labunah thrusts and to the trend of the Qudayd meta-intrusive suite. On the northern limb of the antiform the formation is intruded by plutonic rocks of the Qudayd meta-intrusive suite, and the top of the formation is truncated by the Labunah thrust (Ramsay, 1986a). On the southern limb, the top of the Nida formation is conformably overlain by, and is transitional into, the Shayban formation. Because of its structural complexity, the thickness of the Nida formation has not been determined (Camp, 1986a; Ramsay, 1986a).

The Nida formation has a basaltic to andesitic bulk composition (Skiba and Gilboy, 1975) and generally is the most deformed and has the highest metamorphic grade in the Samran group. The highest grade occurs adjacent to plutons of the Qudayd meta-intrusive suite, where amphibolite-facies mineral assemblages are developed, and quartz-garnet-plagioclase-hornblende (amphibolite) schist and gneiss interlayered on the cm- to m-scale with well-foliated quartzofeldspathic schist and gneiss (Fig. 19). In places, these are interlayered lit-par-lit with horizons of deformed quartzofeldspathic orthogneiss derived from the Qudayd intrusions. Away from the pluton margins, metamorphic grade decreases, and the Nida formation consists of dark green, variably foliated, quartz-plagioclase-amphibole-chlorite schist (greenschist). At greater distances from the Qudayd plutons, where metamorphic grade is lowest, the dominant lithology changes to porphyroclastic and lithoclastic quartzofeldspathic schist and finally to weakly schistose volcanic and volcaniclastic rocks, which generally consist of basalt to basaltic-andesite lava, mafic lapilli-ash tuff and tuff breccia (Fig. 9A), volcaniclastic debris-flow deposits, and minor micaceous quartzite and marble. Roobol (1989) interpreted parts of the Nida formation as a distal facies of the Shayban formation.

The Nida formation is intruded by the 782 Ma Khamrah gneiss of the Qudayd suite, which provides a minimum age for the formation. A K-Ar date of 585 ± 12 Ma reported by Brown and others (1978) for hornblende from mafic schist in the formation is almost certainly a cooling age, as it is unrealistically younger than the U-Pb zircon age of the Khamrah gneiss reported above, and is inconsistent with all observed geological relationships between the Nida formation and other units.

Shayban formation

The Shayban formation (Fig. 3A) conformably overlies the Nida formation. The contact is transitional, but on a large scale the Shayban formation is distinguished from the Nida formation by a change in lithology, lower metamorphic grade, and greater preservation of original depositional and lithological features. Like the Nida formation below, the Shayban formation is highly deformed as it lies well within the Samran fold-thrust belt. A thickness of up to 20 km is possible for the Shayban formation, but this does not allow for repetition by faulting or folding (Ramsay, 1986a). Because of potentially economic metal and massive sulfide deposits, parts of the Shayban formation have been mapped and described in detail (Nebert, 1969; Kana'an, 1970; Liddicoat, 1971; Rexworthy, 1972; Ono, 1976a, 1976b; Kana'an, 1977; Fujii and Okumi, 1978; Fujii and others, 1978; Gilboy and Skiba, 1978a, 1978b, 1978c, 1978d; Ozawa, 1978; Kana'an and Liddicoat, 1979; Ziab, 1982; Al-Muallem, 1983).

North of Wadi Sitarah (Fig. 3A) the Shayban formation consists of andesitic to felsic volcaniclastic rocks, felsic lava, lithic arenite and conglomerate containing much more abundant plutonic clasts than elsewhere in the formation (Ramsay, 1986a). South of Wadi Sitarah the formation consists of lithologies that Roobol (1989) mapped as the remnants of two superimposed, fault-dismembered stratovolcanoes. He interpreted green, chlorite-rich, phyllitic to schistose metatuff and volcaniclastic metasandstone as a distal volcanic facies, lava flows and pyroclastic, submarine volcaniclastic, and epiclastic deposits as a proximal facies, and lava domes, near-vent pyroclastic deposits, and intrusive rocks as a central vent facies. Roobol (1989) also interpreted the Nida formation to be at least partly equivalent to the

Figure 19. Photograph of outcrop of the Nida formation on east side of Hadabah gneiss. Amphibolite-facies quartz-garnet-plagioclase-hornblende schist and gneiss (dark) are interlayered on the cm- to m-scale with well-foliated quartzofeldspathic schist and gneiss (light). View looking northeast. Scale card in center is 16.5 cm long.

distal facies of the Shayban volcanoes. The Shayban formation probably represents the remains of a number of closely spaced, possibly coalescent, volcanic edifices developed in a young oceanic arc or rift system. These volcanic centers may correlate with the Ramram caldera, ca. 125 km to the northeast. Much, though not all, of the Shayban formation exhibits characteristics consistent with a submarine depositional environment, including green colors, the presence of hyaloclastite (Fig. 20A) and pillow lava (Fig. 20B), abundant water-stratified volcaniclastic and epiclastic rocks, and marble.

Three samples from the Shayban formation were analyzed during this study. Sample SA01-74B (Tables 1, 2) comes from massive to weakly foliated plagioclase-quartz-phyric rhyolite lava southwest of the Thufir trondhjemite (TT in Fig. 3A). Despite its felsic chemistry, the sample yielded very little zircon, and error ellipses for the eight grains that were analyzed scatter widely on the concordia diagram in Figure 21A. The two points that plot on the left side of the diagram are clearly inherited from Mesoproterozoic to Paleoproterozoic sources, but the source of the inheritance is unknown. The six remaining points form two groups. One group consists of three points that form a nearly vertical array and have very similar $^{238}U/^{206}Pb$ despite the strong discordancy of one point. The other group comprises three points that form a more horizontal array and plot to the right of the first group, most likely due to lead loss. The three points from the first (vertical) group yield a concordia age of 777 ± 28 Ma (MSWD = 2.8). The low number of points and the large scatter make this a very poor constraint on the age of the Shayban formation. However, considering the lack of any other age information for this unit, an extrusion age of ca. 775 Ma is tentatively assigned for the Shayban formation. That age is within error of the ages reported herein for the Haf formation (Mahd group), Ramram intrusive complex, and the Bari granodiorite, and offers the first radiometric evidence that the Samran and Mahd groups are correlative.

Sample SA03-279 (Tables 1, 3) is from ca. 24 km north-northeast of Al Kamil (Fig. 3A). A total of 21 analyses were conducted on 12 zircon grains from this sample, and the results are plotted as ellipses on the concordia diagram in Figure 21B. The data plot along concordia between ca. 870 Ma and 660 Ma, with the greatest concentration of points at 800-760 Ma and several obvious outliers. The sample is somewhat problematic, because six grains (1-3, 7, 8, 10) yielded younger ages from their cores than from their rims. The cause of this inverse age relationship is unknown. One explanation is that radiation damaged cores were inherited by the host magma, which precipitated new zircon overgrowths, and subsequent lead loss affected only the metamict cores. For example, analysis spots 2.1 and 2.2 are from a core-rim pair. Spot 2.2 (rim) plots within the main group, but spot 2.1 (core) plots far to the right with the highest $^{238}U/^{206}Pb$ for all the grains and has clearly experienced recent lead loss. Radiation damaged cores should have higher U concentrations than juvenile overgrowths, but for many of the problematic grains the reverse is seen in Table 3. In CL images, some of the problematic grains show U-rich cores surrounded by generally U-poor overgrowths, whereas others show the opposite, and still others show no obvious cores and only continuous compositional zoning from center to edge.

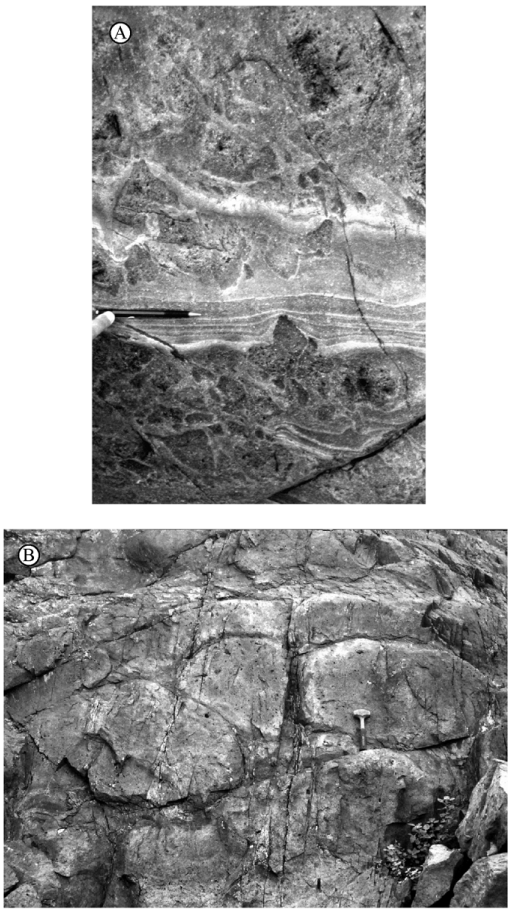

Figure 20. Photographs of outcrops of the Shayban formation, Samran group, between the northern tips of the Shagiyah quartz diorite and Thufir trondhjemite bodies (SQ and TT in Fig. 3A). (A) Hyaloclastite containing angular, ash- to block-sized juvenile volcanic fragments interlayered with water-stratified, laminated ash-fall tuff. Pencil for scale. (B) Vesicular basaltic-andesite pillow lava. Hammer for scale.

In order to calculate a potentially meaningful age, all analyses from cores of problematic grains were eliminated. Also eliminated were the single discordant point that plots to the lower left of the group, the point with the conspicuously high error in $^{207}Pb/^{206}Pb$ compared to other analyses, two points that plot just to the right of the group and appear to have experienced recent lead loss, and the four points plotting to the left of the main group that appear to be inherited. The remaining 10 points produce a concordia age of 771 ± 4 Ma (MSWD = 1.3), which is a reasonable estimate for the extrusion age of the lava. This age is within error of the age reported above for the Shayban formation, as well as for the Mahd-Ramram-Bari association, and the significance of this is discussed in a later section. The area where this sample was taken was previously mapped as part of the Amudan formation (Gilboy and Skiba, 1978d; Ramsay, 1986b). Based on the similarity in the age for this sample and for sample SA01-74B

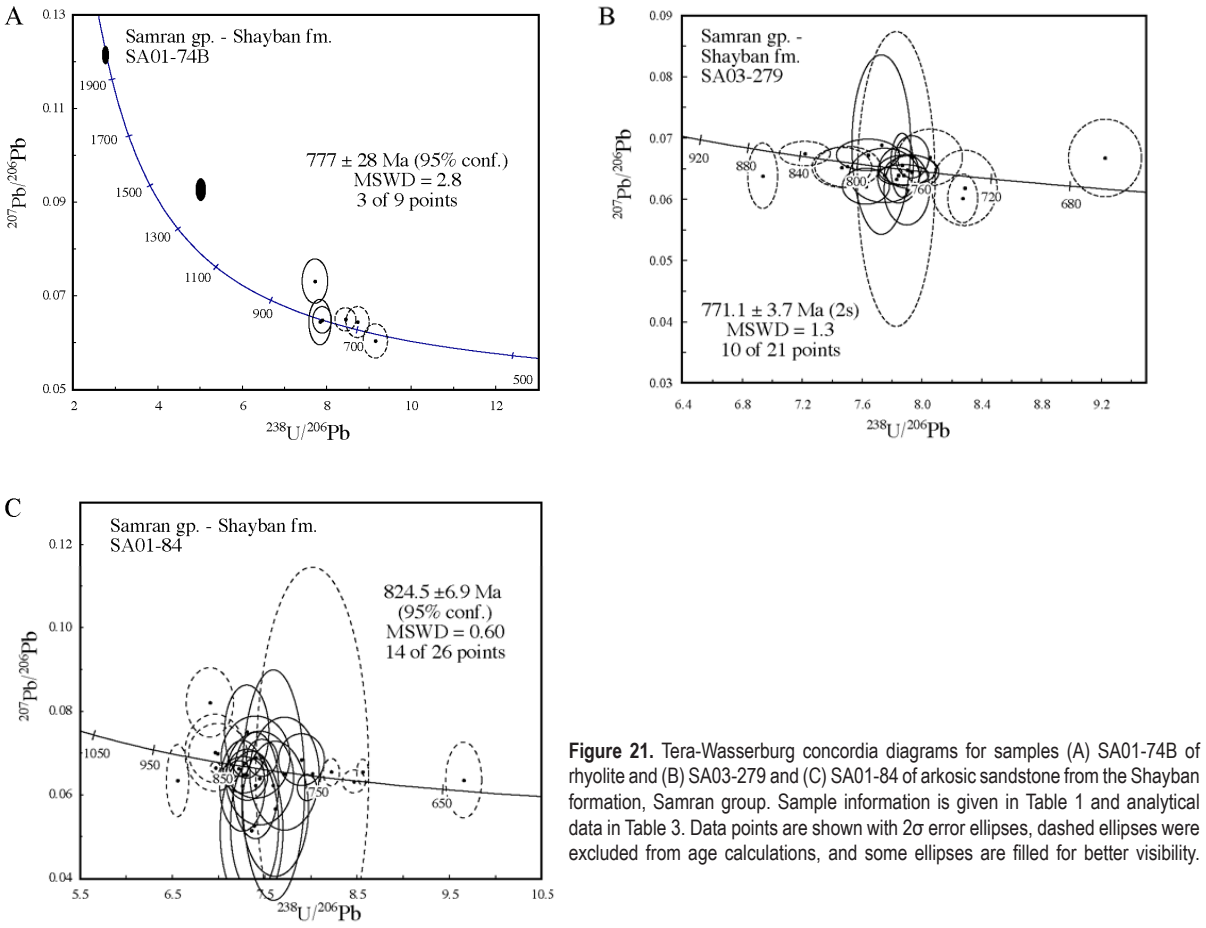

Figure 21. Tera-Wasserburg concordia diagrams for samples (A) SA01-74B of rhyolite and (B) SA03-279 and (C) SA01-84 of arkosic sandstone from the Shayban formation, Samran group. Sample information is given in Table 1 and analytical data in Table 3. Data points are shown with 2σ error ellipses, dashed ellipses were excluded from age calculations, and some ellipses are filled for better visibility.

and based on the large discrepancy between the age for this sample and the other Amudan samples, discussed below, this sample is here reinterpreted as part of the Shayban formation. The extent of Shayban deposits in the area of sample SA03-279 is unknown, so the contact between the Shayban and the Amudan formations there is tentatively placed along a northwest-trending fault, as shown in Figure 3A.

Indirect evidence for plutonic basement older than dated parts of the Kamil intrusive suite is provided by analyses of zircon grains from massive sandstone in the Shayban formation interbedded with rhyolitic to andesitic lavas and tuffaceous rocks. Sample SA01-84 (Tables 1, 2) is from a very immature lithic arkose located ca. 20 km northwest of Al Kamil (Fig. 3A). The sample contains angular lithic and crystal fragments, mostly plagioclase and quartz, derived from a proximal plutonic source. On the concordia diagram in Figure 21C, ellipses for twenty-six data points scatter widely along concordia. A relatively tight group plotting at ca. 820 Ma is defined by 14 of the 26 points. Seven points plot along concordia to the right of the group, which isattributed to lead loss. Five points plot to the left of the group and most likely represent xenocrystic zircon grains inherited by the plutonic protolith to the sandstone. Such an interpretation is supported by analyses of a grain that was probed twice, which produced ages of 914 ± 13 Ma (core, spot 3.2) and 811 ± 14 Ma (rim, spot 3.1). The fact that the majority of the points form a tight group suggests that they represent zircon grains derived from the same plutonic source. Together, the 14 tightly grouped data points yield a concordia age of 825 ± 7 Ma (MSWD = 0.60), which is interpreted as the igneous crystallization age of the plutonic protolith to the arkose. The nearest exposed Kamil pluton is tonalite of the Shiwan complex, which Roobol (1989) interpreted as intrusive into the Shayban formation and, therefore, cannot be the source of the zircon in sample SA01-84. The provenance of the zircon is unknown, but it is probably an older part of the Kamil suite; the Rabigh suite north of the suture is too young (807 Ma) and too distant to be a likely source. The large difference between the age of this sample and the ages of lavas from the Shayban formation implies that a major nonconformity occurs in the Tharwah area between the Samran group and part of the Kamil intrusive suite, similar to the nonconformity between the Mahd group and Dhukhr tonalite in the Bi'r Umq area.

Two other samples from the Shayban formation did not yield enough zircon to provide further information on the age of the Shayban formation. However, a late Mesoproterozoic $^{207}Pb/^{206}Pb$ model age of 1071 ± 2 Ma (Table 3) for a zircon grain from one of those samples (SA03-277), which is located just north of the Shagiyah intrusion ca. 27 km from sample SA01-74B, indicates that inheritance is endemic to the Shayban formation.

Amudan formation

The Amudan formation is at least structurally, if not stratigraphically, concordant on the underlying Shayban

formation (Ramsay, 1986a). Close to the contact, the Shayban and Amudan formations are equally deformed, but farther southeast the Amudan becomes progressively less deformed. Ramsay (1986a) noted that the base of the Amudan formation rests without angular discordance on top of the Shayban formation, but he was unable to determine if the contact was a major disconformity or if the Amudan deposits are the less deformed, more subaerial, upper parts of the Shayban succession. During a detailed structural traverse, the contact was observed to be a transitional zone up to 200-m-thick and consisting of a fold-repeated sequence of vertically dipping and alternating horizons of laminated felsic tuff and plagioclase-phyric lava, each <2 m thick. The basal conglomerate and arenite described by Ramsay (1986a) as marking the contact with the Shayban formation were not observed by the present authors, despite repeated attempts to locate them. The top of the Amudan formation was intruded by, or is in fault contact with, plutonic rocks of the Kamil intrusive suite. The estimated thickness of at least 8 km does not allow for folding and faulting (Ramsay, 1986a).

Lavas in the Amudan formation range from basaltic andesite to rhyolite, but are dominated by intermediate compositions. Excellent examples of welded, partly rheomorphic lapilli-ash-flow tuff with well-preserved eutaxitic texture are also present (Fig. 22A). Epiclastic rocks make up a significant portion of the Amudan formation and include water-stratified tuffaceous siltstone or chert, normally graded pebble conglomerate, laminated sandstone and siltstone, and polymict cobble-boulder conglomerate and breccia. A conspicuous polymict conglomerate (Fig. 22B) of unknown thickness occurring mid-level in the formation contains abundant rounded cobbles and boulders of plutonic, volcanic, and epiclastic rock and is interpreted herein as an alluvial fan deposit. Reddish outcrops, volcanic rocks, a general lack of pillow lava, notable amounts of welded pyroclastic-flow deposits, very little marble, and abundant coarse-grained epiclastic rocks with common plutonic clasts are characteristic and suggest that the Amudan formation was deposited in a largely subaerial environment on the flanks of emergent volcanic edifices in a maturing arc or rift environment.

Three samples from the Amudan formation were analyzed during this study. Sample SA01-94 (Tables 1, 2) is from thickly bedded hornblende-plagioclase-phyric dacite lava ca. 15 km northwest of Al Kamil (Fig. 3A). Thirteen zircons were analyzed, and error ellipses for all points fall in a tight cluster about concordia in Figure 23A. The data yield a concordia age of 753 ± 6 Ma (MSWD = 0.95), which is taken as the age of extrusion of the dacite.

Sample SA01-103 (Tables 1, 3) is from flow-banded plagioclase-augite-phyric andesite lava ca. 7 km northwest of Al Kamil (Fig. 3A). Data points for 15 of the 17 grains analyzed from this sample cluster tightly about concordia in Figure 23B. Two younger grains appear to have experienced recent lead loss and were omitted from the age calculation. The remaining 15 data points yielded a concordia age of 752 ± 4 Ma (MSWD = 0.016), which is identical to the age for sample SA01-94 and is also interpreted as the extrusion age of the lava.

Sample SA03-278 (Tables 1, 3) comes from clinopyroxene-plagioclase-phyric andesite ca. 6 km

Figure 22. Photographs of outcrops of the Amudan formation, Samran group. (A) Highly compacted, welded, and flow-banded, lapilli-ash-flow lithic-crystal-vitric tuff showing well-preserved eutaxitic texture, in which highly flattened and silicified pumice lapilli (light) are enclosed by a devitrified glassy matrix (dark). Pencil for scale is oriented parallel to flow banding. (B) Polymict cobble-boulder conglomerate. Clasts are typically rounded and consist of granite, diorite, rhyolite, laminated ash tuff or siltstone, and crystal tuff, among others. Hammer for scale.

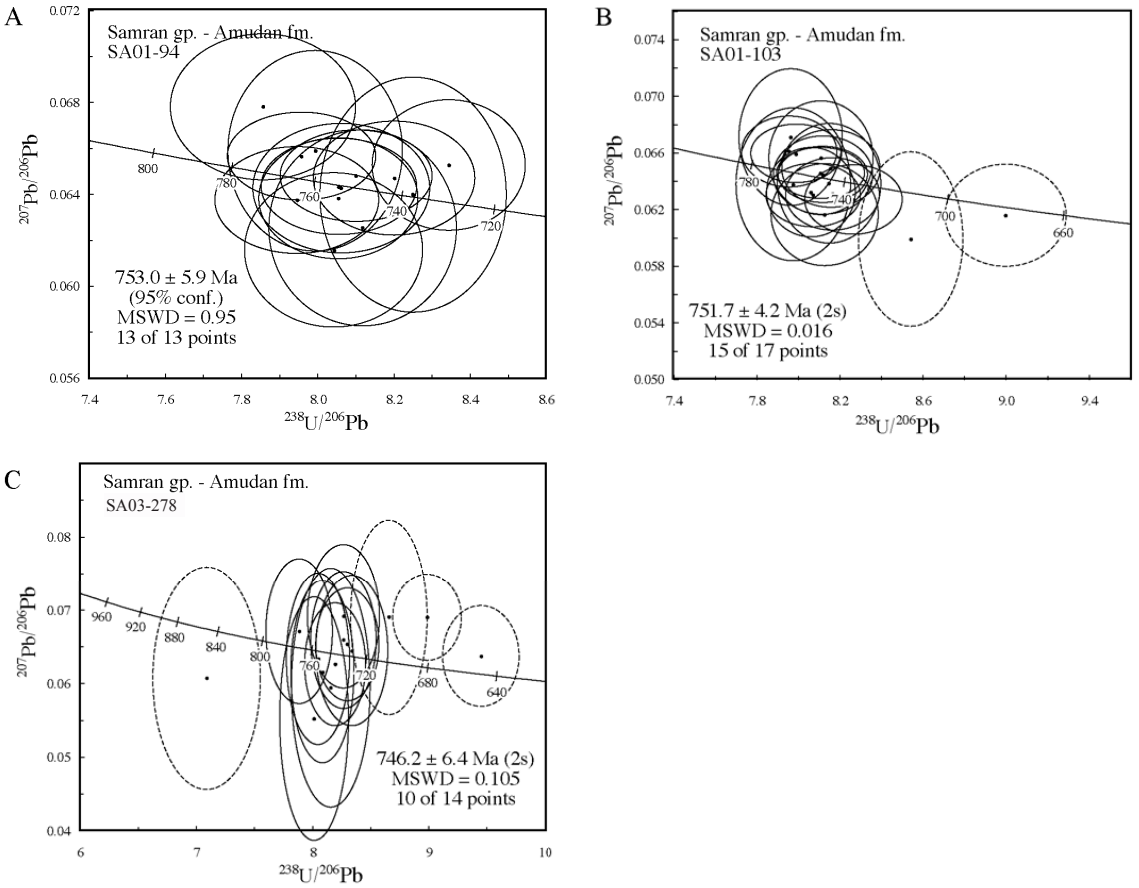

Figure 23. Tera-Wasserburg concordia diagrams for samples (A) SA01-94 of dacite, (B) SA01-103 of andesite and (C) SA03-278 of andesite from the Amudan formation, Samran group. Sample information is given in Table 1 and analytical data in Table 3. Data points are shown with 2σ error ellipses and dashed ellipses were excluded from age calculations.

northwest of Al Kamil (Fig. 3A). Data points for the 14 zircon grains analyzed are plotted on the concordia diagram in Figure 23C. Error ellipses for ten of the data points cluster in a tight group about concordia at ca. 750 Ma. One grain that plots to the left of the group appears to be inherited and three others that plot to the right of the group are interpreted to have sustained recent lead loss. Data for the ten remaining points yield a concordia age of 746 ± 6 Ma (MSWD = 0.105), which is interpreted as the extrusion age of the lava and is within error of the ages from the two previous Amudan samples.

The fact that the Amudan and Shayban deposits show such distinct lithological and age differences suggests that the Amudan formation records a significant shift to a largely subaerial environment from the more submarine environment in which the Shayban formation was deposited. Moreover, the 777-771 Ma ages for the Shayban formation and the much younger 753-746 Ma ages for the Amudan formation confirm that the two formations are separated by a major disconformity and are not part of the same volcanic sequence. The ages for the Amudan formation are indistinguishable from those obtained here for the Hadabah gneiss (751 ± 5 Ma) and related dike (747 ± 5 Ma) of the Qudayd metaintrusive suite. The two units are nowhere in contact, but the similarity in ages suggests that the Hadabah gneiss is the plutonic equivalent of the Amudan formation. The Amudan ages are also within error of the 760 ± 10 Ma age reported by Calvez and Kemp (1982) for the younger part of the Hufayriyah tonalite and the 749 ± 10 Ma age reported here for the younger part of the Ramram intrusive complex.

Mahd group

The Mahd group (Fig. 3B) occurs at the same structural and stratigraphic level as the Samran group on the southern flank of the BUSZ, but is much less deformed, and much of the sequence in the south is horizontal. The two groups generally are considered equivalent, but a lack of adequate radiometric age information on the Samran group has precluded definitive correlation. The Mahd group contains several economically important metal and massive sulfide deposits and has been mapped and described by a number of workers (e.g. Goldsmith and Kouther, 1971; Worl, 1978; Kemp and others, 1982a; Kemp and others, 1982b; Afifi, 1989; Johnson and others, 2002). Kemp and others (1982a) divided the Mahd group into the Tulaymisah and Haf formations, which they considered to be stratigraphically equivalent. However, the two formations have distinct lithologies, and the geographic positions of the Tulaymisah and Haf formations relative to the suture are similar to the Nida and Shayban formations in the Samran group. The Mahd group is therefore discussed in terms of the apparent stratigraphic position, as determined by equivalent rocks

in the Tharwah area, with the lower part of the group represented by the Tulaymisah formation in the north and the upper part by the Haf formation farther south.

Tulaymisah formation

The Tulaymisah formation occurs at the core of an east-west-trending syncline immediately south of the Bi'r Umq ophiolite, from which is it separated by a major thrust fault, and in a belt between the Hufayriyah and Furayhah batholiths at the southern end of Wadi ar Raku (Fig. 3B). The largely volcaniclastic and epiclastic Tulaymisah deposits rest unconformably on Dhukhr tonalite in the Furayhah and Hufayriyah batholiths and on folded beds of the Arj group. The lower parts of the formation in the south typically consist of matrix-supported conglomerate and epiclastic breccia, coarse-grained tuffaceous, arkosic, siliceous, and lithic sandstone, volcanic breccia, andesitic to felsic volcanic rocks, and minor limestone (Kemp and others, 1982a). Coarse-grained sedimentary rocks commonly contain plutonic detritus and clasts of contemporaneous volcanic rock. Towards the north and east, and upwards in the section, the Tulaymisah rocks change from the more proximal deposits just mentioned to more distal deposits. They include laminated and/or cross-stratified and normally graded turbidite sandstone, siltstone, and mudstone, limestone, tuff, volcanic breccia, and pillow lava (Kemp and others, 1982a).

The characteristics displayed by the Tulaymisah formation suggest that it was deposited on the flank of a submarine volcano. The volcanic edifice and its plutonic basement underwent episodic erosion and occasional subaerial exposure during deposition of the formation. Chlorite-rich crystal tuff is similar to deposits in the Nida formation at the base of the Samran group (Fig. 3A). The Tulaymisah formation has not been dated by radiometric means, but is younger than the 812 Ma Dhukhr tonalite in the eastern Hufayriyah batholith that it nonconformably overlies and is older than the 760 Ma (Calvez and Kemp, 1982) Hufayriyah tonalite that intruded and contact-metamorphosed the formation.

Haf formation

The Haf formation rests nonconformably on the Dhukhr tonalite and at its base is a polymict, variably grain- and matrix-supported diamictite (Fig. 24A) that contains clasts of sedimentary, volcanic, and plutonic rocks, including the underlying Dhukhr tonalite. The diamictite is discontinuously preserved and is typically <2 m thick. The deposit may be a tillite. The rest of the formation consists of a rhyolitic volcanic and sedimentary lower member and basaltic to rhyolitic volcanic upper member. Both members of the Haf formation show a progression similar to that in the Tulaymisah formation and the Samran group, from more proximal deposits in the south to more distal deposits in the north, but the change is subtle. In the south, the lower member consists of reddish, variably welded, rhyolitic pyroclastic-flow deposits, sandstones, and mud-cracked mudstones, consistent with near-shore or subaerial deposition. Farther north, rhyolitic tuff, basaltic lavas, conglomerate, sandstone, and limestone all display features more consistent with subaqueous deposition. Likewise, the upper member progresses from subaerial mafic lavas, silicic tuff, sandstone and breccia in the south to more subaqueous basaltic to rhyolitic volcanic breccia, epiclastic breccia and conglomerate, and sandstone in the north. Variably welded, locally rheomorphic, rhyolitic lapilli-ash-flow deposits (Fig. 24B) are volumetrically important components of the Haf formation, and their deposition is probably related to caldera formation at Jabal Ramram. They are also host to Au-bearing, stratabound, massive sulfide deposits at the Mahd adh Dhahab mine (Fig. 3B), and their economic importance has led to a number of radiometric dates for the Haf formation.

Calvez and Kemp (1982) reported an Rb-Sr whole-rock isochron age of 772 ± 28 Ma (7 points, MSWD = 3.94) for Haf rhyolite on the northwest flank of the Furayhah batholith, which is identical to the 772 ± 36 Ma age (8 points, MSWD = 0.2) reported by Huckerby (1984) for amphibolite ca. 10 km west of the mine. Those two ages agree with the conventional, multi-grain U-Pb zircon age of 769 ± 5 Ma reported by Calvez and Kemp (1982) for granophyre in the Ramram complex, which is generally cited as the igneous age for the Mahd group. Younger Rb-Sr whole-rock isochron ages of 726 ± 21 Ma (4 points, MSWD = 0.5) and 726 ± 33 Ma (9 points, MSWD = 1.03) were reported for the Haf formation by Huckerby (1984) and Calvez and Kemp (1982), respectively. Calvez and Kemp (1982) rejected their 726 Ma age as being too young. The probability that the Rb-Sr systematics of at least some of the samples have not remained closed since extrusion cannot be ignored based on the known tectonic, magmatic, and hydrothermal events that have affected the area since deposition of the Mahd group. Brown and others (1978) reported a two-point Rb-Sr whole-rock tie-line age of 572 ± 35 Ma for porphyritic felsite just west of the mine. This age is unrealistically young, does not agree with observed geologic relationships, and is most likely thermally reset.

Three samples from the Haf formation were analyzed during this study, but only one yielded a reliable concordia age. Sample SA03-158 (Tables 1, 3) is from plagioclase-phyric rhyolitic welded tuff on 3the southern flank of the Ramram stratovolcano (JR in Fig. 3B). Data from 19 zircon grains analyzed are plotted on the concordia diagram in Figure 25A. One grain was analyzed in two spots, in an apparent core (spot 14.1) and on the rim (spot 14.2). Three of the data points were discordant, including that for spot 14.2, and were omitted from all calculations. The remaining points appear to define three discrete groups. Data for the oldest group of seven points yield a concordia age of 810 ± 7 Ma (MSWD = 10.4). The scatter is very high, but the age is interpreted here to reflect the average age of the basement through which the rhyolite erupted and is similar to ages for the Dhukhr tonalite reported here and by other authors.

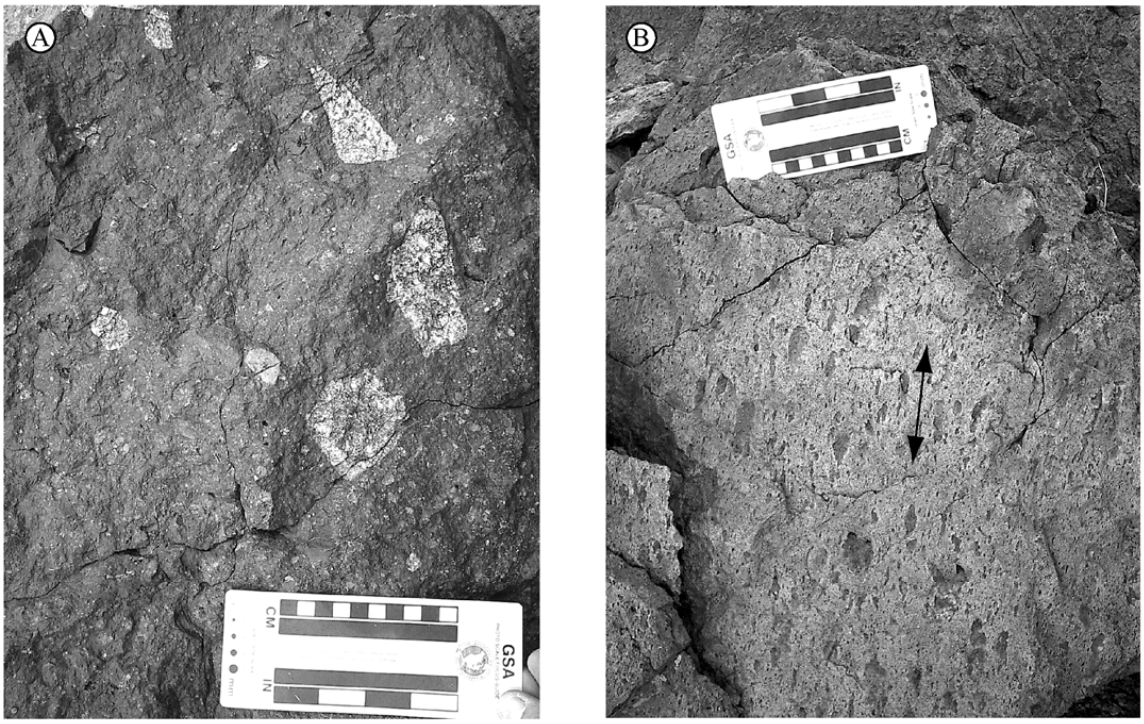

Figure 24. Photograph of outcrop of the Haf formation, Mahd group. (A) Diamictite at the base of the Haf formation, where it unconformably overlies the Dhukhr tonalite on the west side of the Dhukhr batholith. Clasts are angular and consist of granodiorite, rhyolite, green felsite, flow-banded aphyric lava, and laminated tuff or siltstone, among others. Coarse-grained clasts up to 50 cm across are supported by a finer-grained matrix of pebble and sand-sized clasts. Clasts of underlying tonalite are more abundant close to the contact. (B) Welded lapilli-ash-flow crystal-vitric-tuff. View is perpendicular to bedding. Pumice lapilli (dark) are elongated on bedding surface in direction of flow, indicated by the arrows. Parallel to bedding, the rock exhibits eutaxitic texture.

A concordia age of 777 ± 5 Ma (MSWD = 1.6) was obtained for the middle group of seven data points and is interpreted as the age of extrusion of the rhyolite. That age is indistinguishable from the 769 Ma U-Pb zircon ages reported here and by Calvez and Kemp (1982) for the Ramram ring dike, providing a direct age relationship between the Ramram intrusive complex and the Mahd group, and is also identical to the 776 Ma age reported here for the Bari granodiorite. Therefore, the Bari granodiorite, Ramram intrusive complex, and Haf formation are proposed to represent the plutonic, subvolcanic, and extrusive components of the same magmatic system.

The youngest group of three points (after removal of a third, discordant point) in Figure 25A yields a poorly defined concordia age of 736 ±7 Ma (MSWD = 0.75), which probably reflects partial lead loss. That age is similar to the Rb-Sr age of 726 ± 33 Ma for the Ramram caldera-fill rhyolites, which Calvez and Kemp (1982) discounted as too young, and is identical to the 735 ± 11 Ma age for the 'young array' from Ramram granite sample SA03-267. If zircon from samples so closely associated in space did not show such similarities in age, they would otherwise be discounted as having experienced recent lead loss. However, the similarities warrant mention of the possibility that the isotopic composition of some of the zircon was disturbed at ca. 730 Ma, either thermally or through lead loss as a result of weathering, producing the young ages. The combined data for points in the middle and youngest groups from sample SA03-158 do not yield a concordia age, as would be expected if they all experienced the same disturbance at the same time. Most likely, the younger zircon population has simply experienced a mild degree of recent lead loss due to exposure and their ages are not geologically significant.

Sample SA03-174 (Tables 1, 3) is from rhyolite lava ca. 3 km northwest of Mahd adh Dhahab. Error ellipses for the data are plotted on the concordia diagram in Figure 25B and show a wide range in apparent age from ca. 290 Ma to >1600 Ma. Significant discordance of many data points and some very young (Paleozoic) apparent ages are most easily explained by severe lead loss.

Sample SA03-215A is from basaltic andesite lava ca. 45 km southwest of Mahd adh Dhahab. As shown by the concordia diagram in Figure 25C, error ellipses for most of the 14 analyses from this sample are concordant, and only one point appears to have experienced lead loss. Point 6.1, which has an apparent age of 99 Ma, is not shown in Figure 25C. The remaining points show a range in apparent age from 235 Ma to ca. 2700 Ma. No concordia age could be determined, and the Paleozoic ages are again most likely due to severe lead loss. Samples SA03-174 and SA03-215A, as well as sample SA03-268A from hypabyssal dacite, which intrudes the Dhukhr tonalite and is inferred to be related to the Mahd group, contain the oldest (Archean) inherited grains south of the BUSZ and indicate that severe lead loss and inheritance are common features in zircon from the Mahd group.

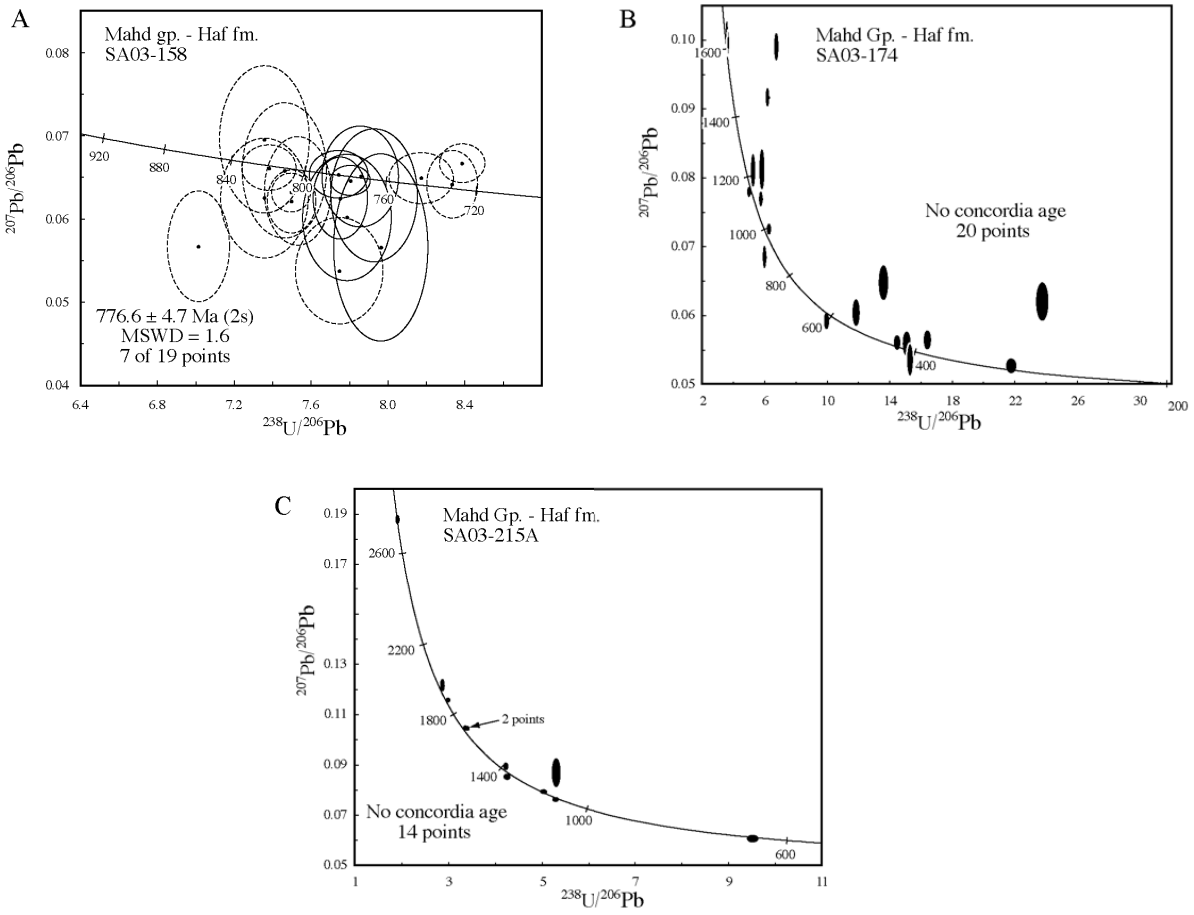

Figure 25. Tera-Wasserburg concordia diagrams for samples (A) SA03-158 of rhyolite, (B) SA03-174 of rhyolite, and (C) SA03-215A of basaltic-andesite from the Haf formation, Mahd group. Sample information is given in Table 1 and analytical data in Table 3. Data points are shown with 2σ error ellipses, dashed ellipses were excluded from age calculations, and some ellipses are filled for better visibility.

GHAMR GROUP

The youngest stratigraphic unit south of the BUSZ in the Bi'r Umq area is the Ghamr group, which Kemp (1980) divided into the Kharzah and Gharmati formations, but these are not differentiated in Figure 3B. The Ghamr group is generally less deformed than the Arj and Mahd groups, despite its proximity to the suture, and in many places is horizontal.

The Kharzah formation at the base of the Ghamr group overlies the Mahd group across a striking angular unconformity and elsewhere lies directly upon plutonic basement in the Dhukhr, Hufayriyah, and Furayh batholiths. It is up to 4 km thick and consists of the following: a basal member of breccia, conglomerate, sandstone, and rhyolitic ash-flow tuff; a weakly bedded middle member of volcanic boulder breccia, matrix-supported conglomerate, fine-grained tuffaceous rocks, andesitic lava, and locally significant carbonate; and an upper member of coarse-grained, laminated sandstone and dessicated mudstone, basalt to basaltic-andesite lava flows, pillow lava, and hydroclastic breccia, and epiclastic breccia and conglomerate (Kemp and others, 1982a). Clasts within the epiclastic deposits (Fig. 26) are typically derived from contemporaneous volcanic deposits and/or from underlying plutonic basement. The Kharzah formation is characterized by abrupt facies changes, internal angular unconformities, and extreme variations in thickness, and Kemp and others (1982a) interpreted the Kharzah formation as deposited in a near-shore submarine to largely subaerial environment associated with a major volcanic edifice.

Figure 26. Photograph of out-of-place, locally derived boulder from polymictic breccia in the Kharzah formation, Ghamr group. Clasts are angular and include abundant flow-banded and folded rhyolite.

The Gharmati formation unconformably overlies the Kharzah formation and, where that is absent, the Mahd group. The Gharmati formation is up to 2 km thick and consists of a lower member containing basal breccia and conglomerate, silicic tuffs, fine-grained volcaniclastic sediments, and local limestone and an upper sandstone member of pebble to boulder conglomerate, laminated coarse-grained sandstone, and mudstone. Clasts within the conglomerates are of sedimentary, volcanic, and plutonic origin (Kemp and others, 1982a), and quartz-keratophyric clasts may be derived from the Arj group. Kemp and others (1982a) report that mixtitic tuffaceous beds in the lower member locally contain rounded, striated clasts of plutonic rock; it is unclear if the striations are glacial in origin.

The Ghamr group is penetrated by abundant hypabyssal intrusions, mostly similar in composition to Ghamr group volcanic rocks (Kemp and others, 1982a). Kemp and others (1982a) interpreted the close spatial association of the intrusions with pillow lavas and greater thicknesses of eastward-thinning pyroclastic deposits of the Kharzah formation to indicate a major volcanic center near Jabal Juraf (JJ in Fig. 3B).

Several samples were taken from the Ghamr group for dating during this study, but were not processed to extract zircon. Calvez and Kemp (1982) obtained an Rb-Sr whole-rock isochron age of 748 ± 22 Ma (5 points, MSWD = 0.98) from one of the subvolcanic intrusions, a thick tabular body of microgranite (subvolcanic rhyolite in Kemp and others, 1982b) intruding conformably into the Kharzah formation on the northwestern flank of the Furayhah batholith. Biotite from the same subvolcanic intrusion yielded an Rb-Sr model age of 555 ± 15 Ma (Brown and others, 1978), but this date has clearly been affected by resetting. The 748 Ma age is similar to the 749 ± 10 Ma age reported here for part of the Ramram complex, suggesting that the Ghamr group may also have a link to volcanic activity at the Jabal Ramram caldera, and is also similar to the 753-746 Ma ages reported here for the Amudan formation, which may be the along-strike equivalent of the Ghamr group in the Bi'r Umq segment of the BUSZ. The unconformities that separate the Ghamr group from the Mahd group and the Amudan formation from the Shayban formation indicate that uplift, rotation, and denudation occurred throughout the region between ca. 770 and 750 Ma.

Furayh group

The Furayh group, first named by Delfour (1981) in the area northeast of Figure 2B, unconformably overlies the Bi'rak group and the Rabigh suite north of the Tharwah segment of the suture. In the area shown in Figure 3A, the group consists only of the Qidirah formation, which is at least 3500 m thick (Pellaton, 1981; Camp, 1986b). The Qidirah formation comprises a basal sequence of conglomerate, sandstone, and tuff, overlain by mafic to intermediate volcanic rocks with rare pillows, dacitic to rhyolitic pyroclastic-flow and fall deposits with local columnar jointing, polymict conglomerate with rare plutonic clasts, immature coarse-grained epiclastic rocks, shale, and rare limestone. The lithological characteristics of the Qidirah formation were interpreted by Camp (1986b) to reflect a high-energy depositional environment associated with emergent volcanism, erosion, and redeposition in proximal marine and subaerial basins.

Rb-Sr whole-rock isochron ages were obtained for two members of the Qidirah formation. The lower member yielded an age of 633 ± 15 Ma (Aldrich and others, 1978) and the upper member yielded an age of 663 ± 44 Ma (C. Hedge, cited as pers. comm. in Camp, 1986a). The relative ages do not agree with the geologic relationship between the two units, but together may constitute a reasonable age range for the group.

Shayma Nasir group

Mildly metamorphosed and weakly deformed volcanic, volcaniclastic, and epiclastic rocks of the Shayma Nasir group were assigned by early workers (Skiba and Gilboy, 1975; Gilboy and Skiba, 1978a, 1978b, 1978c, 1978d) to the Fatimah (Murdamah) group of epeirogenic basinal deposits in the central Jeddah terrane (Camp, 1984). The Shayma Nasir group was deposited in three basins in the Tharwah area that were developed unconformably on the Furayh group north of the suture and the Samran group and plutonic rocks of the Kamil intrusive suite south of the suture. Equivalent rocks are not observed east of Harrat Rahat (Fig. 3). The Shayma Nasir group is divided into the Rayyan, Talhah, and Uaibikh formations, which correspond to the three basins they occupy, and all exhibit similar characteristics. Outcrops of the Shayma Nasir group were only briefly visited during this study, and the following description is distilled from the compilation of Ramsay (1986a). The top of the group has been removed by erosion and thus any estimate of thickness is a minimum. The base of the group is commonly marked by unmetamorphosed polymictic conglomerate containing rounded clasts derived from the underlying plutonic and volcanic rocks. North of the suture the Rayyan formation contains homogeneous deltaic deposits of arkosic sandstone, siltstone, shale, and minor pebble conglomerate (Camp, 1986a). The Talhah and Uaibikh formations to the south of the suture contain mafic to felsic lava flows, tuff and welded tuff, agglomerate, and arkosic sandstone (Ramsay, 1986a). Radiometric ages are not available for the Shayma Nasir group, but it is younger than the 663-633 Ma Furayh group (Brown and others, 1978) on which it is deposited.

OPHIOLITE COMPLEXES

Mafic and ultramafic assemblages of the Tharwah and Bi'r Umq complexes along the northern flank of the BUSZ have been interpreted as ophiolites, the presence of which is partly responsible for the recognition of the BUSZ as a major crustal boundary between the Hijaz and Jeddah terranes. Compared to other igneous units along the

BUSZ the ophiolites are poorly preserved, having been subjected to greenschist-facies metamorphism, variable conversion to serpentinite and listwaenite, folding and faulting associated with obduction, and dismemberment by later transcurrent faulting. However, in places, the original igneous and sedimentary features are preserved. The ophiolites are only briefly described here, but for fuller accounts of the lithologic and structural characteristics the reader is referred to the citations listed in the following paragraphs, notably Nassief and others (1984), Johnson and others (2004), Pallister and others (1988b), and Ramsay (1986a).

Tharwah ophiolite complex

The Tharwah ophiolite complex near Jabal Tharwah (JT in Fig. 3A) is one of the best-exposed and most complete ophiolite sequences in the ANS and has been the subject of many studies (Nebert, 1969; Gilboy and Skiba, 1978a; Nassief, 1981; Nassief and others, 1984; Ramsay, 1986a, 1986b; Pallister and others, 1988a; Johnson, 1998; Johnson and others, 2002; Dilek and Ahmed, 2003; Johnson and others, 2004; Stern and others, 2004). Ramsay (1986a) assigned the Tharwah complex and several other occurrences of mafic and ultramafic rocks to the Thamarah suite, but their relationship is not clear. Included among these are two heavily altered and metamorphosed gabbroic bodies (Ash Sha'af and Nasir gabbros of Ramsay, 1986a) along strike to the northeast of the Tharwah complex. Very little is known about them and they were not visited during this study. Ramsay (1986a) indicated that in places faulted contacts are clear, but commonly the highly altered metagabbro in the Ash Sha'af and Nasir bodies is indistinguishable from mafic volcanic rock in the enclosing Bi'rak group, making a correlation of the gabbros to the Tharwah complex tentative at best. A small outlier of serpentinite, gabbro, listwaenite, diabase, marble, and quartzite (Jaww serpentinite of Ramsay, 1986a) occupies a minor synform in thrust fault contact with the Samran group and Kamil intrusive suite south of the Tharwah segment of the suture. Ramsay (1986b; 1986a) assigned the outlier to the Thamarah suite, although some of the rock types strongly resemble parts of the Bi'rak group. Johnson (1998) suggested that the outlier is related to the Tharwah ophiolite and occupies a nappe that is rooted in the Labunah thrust zone and displaced ca. 40 km to the south.

The Tharwah complex underlies an east-west-trending synform in thrust contact with the Bi'rak group. The ophiolitic character is evident in a mantle sequence of harzburgite and dunite, a lower crustal sequence of layered gabbro, pyroxenite, peridotite, and dunite, an upper crustal sequence of tonalite, trondhjemite, diorite/gabbro, and sheeted dikes, and a supracrustal sequence of basalt lava flows and pillows, chert, metapelite, and mélange (Nassief and others, 1984). Chromite compositions from Tharwah peridotite are transitional between suprasubduction-zone and mid-ocean ridge environments (Nassief and others, 1984; Dilek and Ahmed, 2003), which suggests the ophiolite could be part of an island-arc built on mid-ocean ridge lithosphere (Dick and Bullen, 1984).

Pallister and others (1988b) dated three zircon fractions from gabbro of the Tharwah ophiolite complex. A single coarse-grained fraction yielded a nearly concordant U-Pb model age of 870 ± 11 Ma. Two other fractions were highly discordant and yielded $^{207}Pb/^{206}Pb$ (Tertiary Pb loss) model ages of ca. 1250 Ma. Pallister and others (1988b) attributed the older ages to assimilation of zircon from older basement material. The assumption is supported by lead isotopic data from gabbroic feldspar separates, which straddle the orogene curve on a plot of $^{207}Pb/204Pb$ vs. $^{206}Pb/204Pb$, whereas data from other ophiolites of the ANS have lead isotopic compositions closer to average mantle or MORB (Pallister and others, 1988b). The presence of inherited zircon grains in the gabbro means that an 870 Ma crystallization age is suspect and may be an average from Mesoproterozoic and younger (<870 Ma) zircon grains. This age is especially important because it is the oldest reported from any ophiolite in the ANS.

Attempts were made to date gabbro in the Tharwah complex, but were only partly successful. Sample SA03-149 (Tables 1, 3) is combined from two samples collected within meters of each other from the same body of moderately altered, coarse-grained, layered meta-leucogabbro in the northern part of the Tharwah ophiolite complex (Fig. 27), only a few hundred meters from where Pallister and others (1988b) collected their sample. Nine zircon grains were analyzed, and error ellipses for the data are plotted on the concordia diagram in Figure 28, as are data from Pallister and others (1988b). The data points from sample SA03-149 form two arrays corresponding to the two samples, the horizontal trends of which suggest lead loss. The most concordant of the zircons in the older array yields a concordia age of ca. 1130 Ma, which probably reflects the age of inheritance. The lower array can be resolved into two points that are nearly identical and yield a concordia age of 777± 17 Ma (MSWD = 0.68) and two younger points that appear to have experienced lead loss. This two-point concordia age is weak, but if it approximates the igneous age for the metagabbro, then it casts further doubt on the 870 ± 11 Ma age obtained by Pallister and others (1988b) for metagabbro at nearly the same location. Our data do not support an emplacement age of 870 Ma for the Tharwah ophiolite.

Bi'r Umq ophiolite complex

The Bi'r Umq ophiolite complex occurs at the northern edge of the area in Figure 3B and is separated from the Mahd group to the south by the Bi'r Umq thrust. The rocks of the Bi'r Umq ophiolite, originally assigned by Ramsay (1986a) to the Sumayir formation of the Arj group, are generally recognized as separate from the other Arj group formations, as discussed previously. The Bi'r Umq ophiolite is not as well preserved or as complete as the Tharwah complex, but contains most

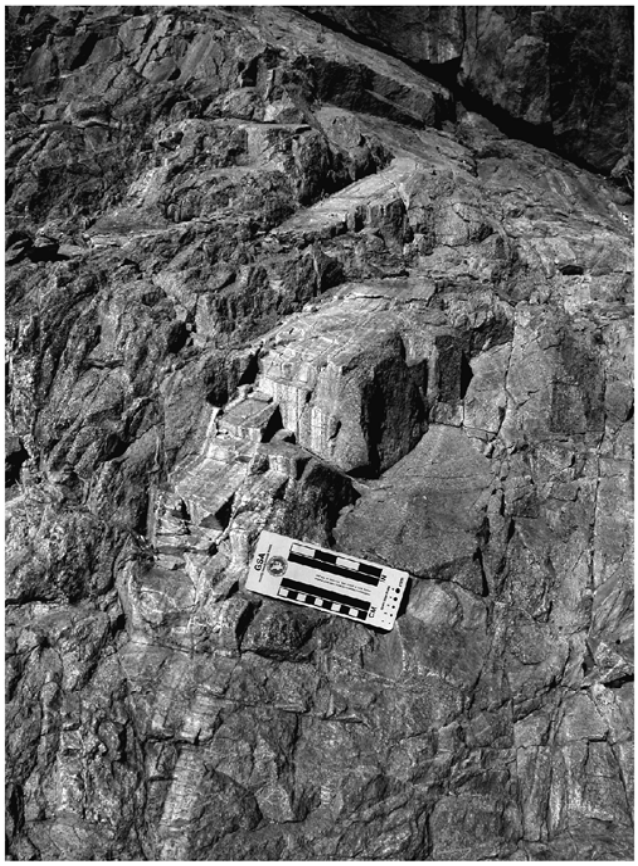

Figure 27. Photograph of outcrop of fine- to coarse-grained, rhythmically layered gabbro (SA03-149) in the Tharwah ophiolite complex, dated here at 777 ± 17 Ma.

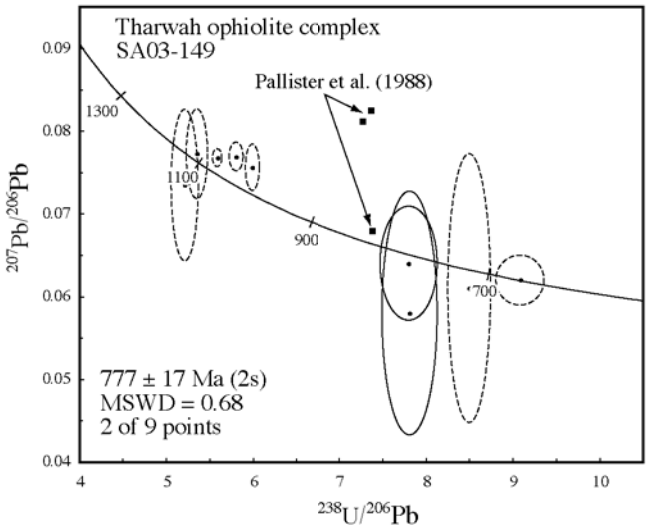

Figure 28. Tera-Wasserburg concordia diagram for sample SA03-149 of layered gabbro from the Tharwah ophiolite complex. Sample information is given in Table 1 and analytical data in Table 3. Data points are shown with 2σ error ellipses and dashed ellipses were excluded from age calculations.

of the ophiolitic sequence, including: (1) a minor mantle section of variably serpentinized and carbonated cumulate dunite and harzburgite; (2) a lower crustal section of gabbro, diorite, and trondhjemite; and (3) a dominant supracrustal section of basaltic lava flows, pillow lava, breccia, and tuff, felsic tuff, limestone, chert, and mélange (Hopwood, 1979; Al-Rehaili, 1980; Al-Rehaili and Warden, 1980; Alsac and others, 1982; Kemp and others, 1982a; Le Metour and others, 1982; Pallister and others, 1988b). Mafic and ultramafic rocks constitute a minor part of the assemblage concentrated near the Bi'r Umq fault, and a sheeted dike complex is absent. Chromite compositions from the peridotite are alpine-type (island-arc), supporting the interpretation by Le Metour and others (1982) that the ophiolite formed in a back-arc setting.

The Bi'r Umq ophiolite was not dated during this study. Dunlop and others (1986) reported an Rb-Sr whole-rock isochron age of 831 ± 47 Ma (3 points, MWSD = 0.04) for basalt and an Sm-Nd mineral isochron age of 828 ± 47 Ma (5 points, MSWD = 0.61) for trondhjemite from the Bi'r Umq ophiolite. Both of those ages agree with the U-Pb model age of 838 ± 10 Ma (3 points, MSWD = 3.3) obtained by Pallister and others (1988b) for hornblende diorite close to the Bi'r Umq thrust. There is debate, however, over whether the diorite is native to the ophiolite (Al-Rehaili, 1980) or is part of the allochthonous Jeddah terrane to the south of the Bi'r Umq thrust (Le Metour and others, 1982). Two zircon fractions from a single sample of undeformed quartz keratophyre that intruded along the Bi'r Umq thrust yielded upper concordia-intercept (Tertiary Pb loss) model ages of 764 ± 3 Ma and 782 ± 5 Ma (Le Metour and others, 1982; Pallister and others, 1988b). Le Metour and others (1982) interpreted the keratophyre as having intruded after obduction of the Bi'r Umq ophiolite. In agreement with this interpretation, the inference by Pallister and others (1988b) that the ages for the diorite and keratophyre loosely constrain motion on the Bi'r Umq thrust to sometime between ca. 760 Ma and 840 Ma is hereby followed.

DISCUSSION AND CONCLUSIONS

Evolution of the BUSZ and the Ophiolite Problem

A controversy arose from research in Sudan regarding the tectonic evolution of the Nakasib suture zone, the along-strike equivalent of the BUSZ. Tectonostratigraphic units along the Nakasib suture have been variously interpreted to record (1) a single episode of subduction and arc accretion (Abdel-Rahman, 1993; Schandelmeier and others, 1994; Wipfler, 1996) and (2) a complete Wilson cycle (Abdelsalam and Stern, 1993a; Abdelsalam and Stern, 1993b; Abdelsalam, 1994; Stern and Abdelsalam, 1998). In the Wilson cycle model, rifting of the continuous Haya-Gebeit arc terrane, development of a passive margin, and subsequent seafloor spreading that separated the Haya and Gebeit terranes all preceded resumption of arc magmatism and eventual suturing; the Arba'at group was interpreted as a passive margin sequence (Abdelsalam and Stern, 1993a; Abdelsalam and Stern, 1993b; Abdelsalam, 1994; Stern and Abdelsalam, 1998). In contrast, the arc accretion model requires that

the Haya and Gebeit terranes are unrelated (precluding rifting), and that the Ariab group volcanic rocks in Sudan, along-strike equivalents farther west of the Arba'at group, record the complete progression of a maturing arc system rather than a rifting event (Abdel-Rahman, 1993; Schandelmeier and others, 1994; Wipfler, 1996).

The validity of these models hinges upon constraining the ages of the major lithotectonic units along the suture and the tectonic environment(s) in which they formed. For example, Stern and Abdelsalam (1998) interpreted lavas of the Arba'at group as break-up tholeiites, the 790 ± 2 Ma U-Pb zircon age of which marks the onset of their proposed rifting event. The much greater age of the Ariab group, constrained by a single-zircon Pb-evaporation age of 888 ± 4 Ma for a coeval hypabyssal stock (Deschamps and others, 2004), negates previously inferred correlations with the Arba'at group and allows for the possibility that both interpretations for the tectonic origins of those units are correct (i.e. the Arba'at group is a passive margin sequence recording a rifting event, and the Ariab group is an older volcanic arc sequence recording subduction of a back-arc basin). This controversy also applies to rocks along the BUSZ in Arabia. Roughly equivalent rocks of the Arj, Mahd, and Samran groups have been variously interpreted as arc- and rift-related (Kemp and others, 1982a; Roobol and others, 1982; Roobol and others, 1983; Camp, 1986a; Roobol, 1989; Johnson and others, 2002; Johnson and others, 2003).

The relative ages of the ophiolite suites and the flanking terranes are also of primary concern to the controversy. The argument for rifting of a continuous arc terrane is supported if the ophiolites are younger than or of similar age to the oldest rocks in the flanking terranes, but is precluded if the ophiolites are significantly older. No age information exists for the ophiolites along the Nakasib suture zone in Sudan, but correlative ophiolites along the BUSZ in Arabia have conventional U-Pb zircon model ages of 870 ± 11 Ma and 838 ± 10 Ma (Pallister and others, 1988b). A $^{207}Pb/^{206}Pb$ evaporation age of 870 ± 5 Ma (Kröner and others, 1991) for trondhjemite from the Erkowit pluton, interpreted as an arc-related composite intrusion to the south of the Nakasib suture, is identical to the 870 ± 11 Ma age for gabbro in the Tharwah ophiolite complex. Such a close association in space and time of arc magmatism and seafloor spreading argues for back-arc rifting of a continuous terrane, but is not conclusive. The two-point concordia age of 777 ± 17 Ma reported here for metagabbro from the Tharwah ophiolite complex is far from robust, but it brings into question the 870 ± 11 Ma age obtained by Pallister and others (1988b) and suggests that the ophiolite is younger than the flanking terranes. The above argument is admittedly simplistic, perhaps too much so, but it does help to illustrate the need for much more detailed geochronology, and perhaps mapping, in order to finalize the relationship between the ophiolites and the flanking terranes.

Precambrian zircon grains have been recovered from continental type rocks and even mid-ocean ridge type gabbros in several locations along the Mid-Atlantic Ridge (White and McKenzie, 1989; Bonatti and others, 1996, and references therein; Pilot and others, 1998), and the sources of the zircon grains were attributed to slivers of continental crust that were entrained in the ridge during rifting. The presence of inherited zircon in the Tharwah ophiolite is also a support for rifting along the BUSZ, because ophiolite-related magmas are generated by seafloor spreading and could only incorporate material from preexisting crustal material if the ophiolite formed during rifting of an arc or continent. Recall that zircon grains from one of our samples and from that of Pallister and others (1988b) yielded Mesoproterozoic ages of ca. 1130 and 1250 Ma, respectively. These two independent studies demonstrate that the Tharwah ophiolite assimilated older basement material during its formation. Similarly, trondhjemite associated with an ophiolite complex (Urd group) between the Ad Dawadimi and Ar Rayn terranes (Fig. 1) contains zircon grains dated at 2000 Ma (Calvez and others, 1983), suggesting that inheritance in ophiolites of the ANS may be widespread. The conventional multi-grain U-Pb zircon age of 870 Ma obtained by Pallister and others (1988b) for the Tharwah ophiolite could be interpreted as an average age between a Mesoproterozoic or older inherited component and a Neoproterozoic (ca. 777 Ma) juvenile component. The ca. 838 Ma age for gabbro in the Bi'r Umq ophiolite (Dunlop and others, 1986; Pallister and others, 1988b) argues against such an interpretation, as do the 782-764 Ma ages for post-obduction keratophyre intruding the Bi'r Umq ophiolite. However, the ophiolite ages are model ages from conventional multi-grain analyses and the relationship between the diorite and the Bi'r Umq ophiolite is, again, contentious. An important lesson is that dating ophiolites in the ANS requires intragrain-domain analyses using the ion microprobe in order to fully address the problem of pervasive inheritance and to avoid the pitfalls of composite ages determined using more conventional techniques.

The arguments both for and against rifting of the terranes flanking the Bi'r Umq-Nakasib suture zone are problematic. In particular, the discrepancy in zircon ages for the Tharwah ophiolite gabbros, coupled with the debate over whether gabbro in the Bi'r Umq ophiolite is allochthonous or is part of the autochthonous Jeddah terrane, underscore the need for more detailed geochronological studies of the ophiolites on both sides of the Red Sea. The documented problem of inheritance requires that future dating of the ophiolites be conducted on single zircon grains, preferably using the ion microprobe, in order to discriminate between juvenile and inherited zircon. In the absence of more conclusive evidence, the available data from the ophiolites and flanking terranes are interpreted as more supportive of the Wilson cycle (rift) model than the simple arc-accretion model.

Timing of Deformation Along the BUSZ

Deformation along the Bi'r Umq-Nakasib suture zone

was previously bracketed between ca. 780 and 760 Ma by radiometric ages for the youngest deformed (i.e. pre- or syntectonic) and oldest undeformed (i.e. posttectonic) plutonic and supracrustal units along the Nakasib suture zone in Sudan (Stern and Abdelsalam, 1998). The ages of diorite and post-obduction keratophyre in the Bi'r Umq ophiolite (Pallister and others, 1988b) also loosely constrain the timing of deformation in the Bi'r Umq segment of the BUSZ, but the relation of the diorite to the ophiolite sequence is debated. Deformed metatonalitic plutons of the Qudayd metaintrusive suite provide the first direct evidence for the timing of deformation along the BUSZ, as they were deformed at or near the solidus temperature, indicating that the tonalitic protoliths to the Qudayd gneisses intruded an active shear zone. The new zircon ages of 751 ± 5 Ma for the Hadabah gneiss and 747 ± 5 Ma for a related late-stage dike provide a very tight constraint on the timing of late-stage subhorizontal dextral shear along the Labunah thrust zone and folding in the Samran fold belt (D2 event of Johnson, 1998), and the age of 782 ± 7 Ma for the Khamrah gneiss may constrain the timing of earlier thrusting along the BUSZ (D1 event of Johnson, 1998). These ages support the conclusions of Stern and Abdelsalam (1998) that deformation along the Nakasib suture zone occurred between 780 and 750 Ma and locally lasted until 740 Ma. One outstanding problem is whether D1 and D2 were discrete events or were part of the same progressive episode of deformation.

Crustal Evolution Along the BUSZ

The ANS is an unparalleled natural laboratory for studying the processes of crustal evolution during the Neoproterozoic. It has the thickness (~40 km) of true continental crust (Gettings and others, 1986; Badri, 1991; Al-Damegh and others, 2005) and a P-wave velocity structure typical of post-Archean continental crust (Durrheim and Mooney, 1991). Samples of the deep crust and mantle lithosphere have been brought up in several places by alkali basalts of Tertiary age and are mineralogically like those expected for continental lithosphere formed in the Neoproterozoic (Henjes-Kunst and others, 1990; McGuire and Stern, 1993). The ANS formed by processes indistinguishable from that of modern plate tectonics, as shown by the fact that it contains numerous ophiolites (Stern and others, 2004) that help define identifiable sutures separating well-defined tectonostratigraphic terranes (Stoeser and Camp, 1985; Johnson and Woldehaimanot, 2003). Because the BUSZ is the oldest suture and juxtaposes the two oldest juvenile terranes of Neoproterozoic age in the ANS, it is the earliest record of how and when continental crust in the ANS was formed, assembled, and cratonized. The new U-Pb zircon ages reported herein, coupled with existing radiometric ages for units along the BUSZ, provide one of the most complete geochronologic frameworks for any part of the ANS. These data are presented in Figs. 29 and 30 and are interpreted to define roughly four magmatic episodes, referred to here as M1-M4, which contributed to the formation of continental crust in the terranes flanking the BUSZ. In this section, the nature and timing of plutonic and deformational events that shaped the crust along the flanks of the BUSZ are discussed in relation to four identified magmatic episodes; the ophiolite complexes are not included as part of these episodes.

The earliest crust-forming event, M1, identified during this study is defined by ages clustering between ca. 825 and 800 Ma (Figs. 29, 30). The upper age limit on M1 (825 ± 7 Ma) comes from immature arkosic sandstone in the Shayban formation, which is interpreted to be derived from a local plutonic source, possibly an unrecognized older part of the Kamil intrusive suites. The age for hypabyssal microgabbro (854 ± 15 Ma) intruding the Bi'rak group north of the suture zone could extend the timeframe of M1, but it is a tenuous crystallization age. Additional M1 magmatic events included emplacement of the Dhukhr tonalite (816-803 Ma) in the Dhukhr and Furayhah batholiths, deposition of the Bi'rak group (812 Ma), intrusion of the Rabigh suite (807-800 Ma), and intrusions of part of the Kamil suite (800 Ma). Deposition of the Arj group (undated),

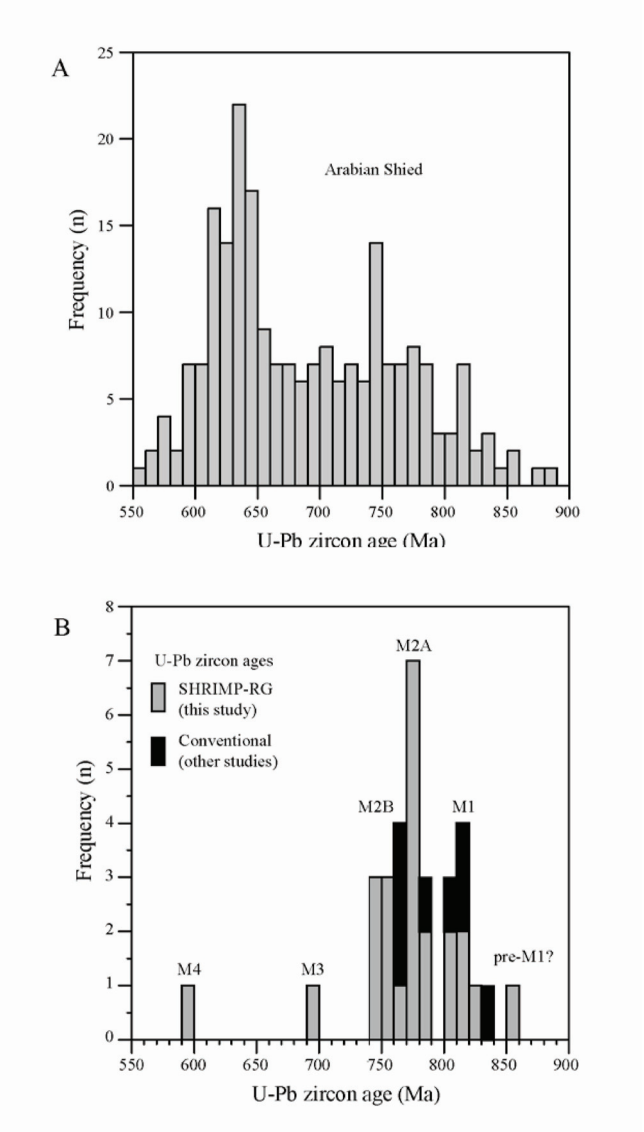

Figure 29. Histogram of all U-Pb concordia (crystallization) ages for units dated during this study, showing magmatic episodes inferred from concordant ages.

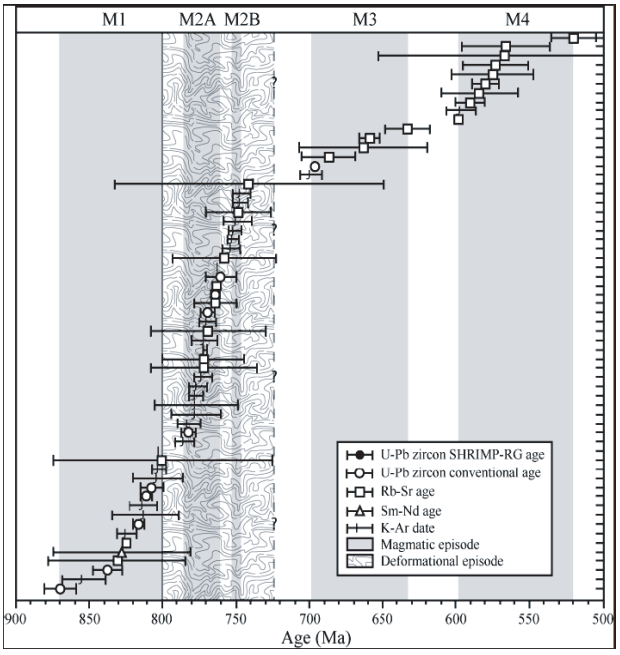

Figure 30. Diagram showing distribution of radiometric ages obtained for plutonic and volcanic units along the Bi'r Umq suture zone. Ages that are rejected as crystallization ages are not included. Data sources are cited in the text.

which was deformed along with the Dhukhr batholith prior to the emplacement of M2-related units (see section 2.3.2), and deposition of the Nida formation (undated), which was laid down prior to intrusion of the 780 Ma Khamrah gneiss of the Qudayd suite, may have been associated with M1 or early M2 magmatism. Concurrent magmatism during M1 on both sides of the BUSZ supports the model of Abdelsalam and Stern (1993) that the Gebeit-Hijaz and Haya-Jeddah terranes were part of the same arc terrane that rifted and was reassembled along the trend of the BUSZ, but could also be the result of magmatism along two roughly parallel subduction zones, one beneath the Jeddah terrane and the other beneath the Hijaz terrane.

Ages for M1 magmatism in Saudi Arabia are similar to the $^{207}Pb/^{206}Pb$ zircon evaporation ages of several major plutonic bodies along the Nakasib suture zone in Sudan. The oldest is an age of 870 ± 5 Ma (Kröner and others, 1991) for the Erkowit pluton south of the Nakasib suture. A younger age of 852 ± 13 Ma for part of the Erkowit pluton (Kröner and others, 1991) may correlate with subvolcanic intrusions in the Bi'rak group, which herein is tentatively assigned an age of ca. 854 Ma. The ages of 810 ± 12 Ma and 812 ± 18 Ma (Schandelmeier and others, 1994) for the Adaiamet and Jabal Tala granodiorites, respectively, on the south side of the Nakasib suture are identical to the 816-811 Ma ages of the Dhukhr tonalite (Calvez and Kemp, 1982). Overall, the data for M1 (and pre-M1) argue for the generation of an extensive plutonic (Haya-Jeddah) terrane beginning at ca. 870 Ma and lasting until ca. 800 Ma.

The presence of 850 Ma and older crust south of the Nakasib suture in the Haya terrane in Sudan suggests that crust of similar (pre-M1) age may also exist south of the BUSZ beneath the Jeddah terrane. This is supported by the ca. 854 Ma age for subvolcanic intrusions in the Bi'rak group and the 800-1000 Ma apparent ages of more than three-dozen zircons dated during this study that predate the calculated ages of their host rocks.

Episode M1 was apparently followed by a hiatus in magmatism represented by a gap in the data in Figs. 29 and 30 between ca. 800 and 785 Ma. The gap could merely represent a sampling bias, but the general continuity of the rest of the M1-M2 age spectrum in Figs. 29 and 30 argues against this. Deformation, exposure, and denudation of the Dhukhr tonalite and the Arj group, part of the Kamil intrusive suite, and possibly the Nida formation in the Samran group, and development of major unconformities occurred sometime during the magmatic hiatus between M1 and M2 and could be attributed to the onset of collision or possibly to earlier rift-related extension. It can be argued that rifting of the combined Haya-Jeddah-Gebeit-Hijaz terrane occurred during the magmatic hiatus and is recorded by the 790 Ma Arba'at group (Stern and Abdelsalam, 1998) and possibly by generation of the Tharwah ophiolite, if the 777 ± 17 Ma age reported here for gabbro in the Tharwah complex is a crystallization age. Rifting may even have caused the hiatus. A Cenozoic analogue for such a model may be found in the Izu-Bonin-Mariana (IBM) arc system, where rifting of the arc to form the Shikoku and Parece Vela back-arc basins at 25-17 Ma was associated with a disruption, although not a complete absence, of arc magmatism, which resumed when seafloor spreading began in the back-arc (Taylor, 1992; Kobayashi and others, 1995; Lee and others, 1995; Stern and others, 2003).

Intrusion of the Khamrah gneiss at 780 Ma marked the reinitiation of igneous activity in what is inferred from Figs. 29 and 30 as the second magmatic episode, M2 (785-745 Ma). Geologic units representing M2 provide the greatest number of analyses in this study and include the first large volumes of volcanic material to be produced, or at least preserved, south of the BUSZ. The distribution of points in Figs. 29 and 30 suggests that M2 may be divided into two smaller episodes, M2A (785-770 Ma) and M2B (755-745 Ma), based on a gap in the U-Pb zircon data at 770-755 Ma; only a K-Ar date for the Kamil suite and an Rb-Sr age with large errors for the Ramram complex lie within the U-Pb data gap. Episode M2A in the Bi'r Umq area involved the emplacement of the Hufayriyah tonalite (780-760 Ma), the Bari granodiorite (776 Ma) and the subvolcanic Ramram intrusive complex (769 Ma), as well as deposition of their volcanic equivalents in the Mahd group (777-772 Ma). In the Tharwah area, M2A magmatism produced much of the Kamil intrusive suite (772-769 Ma) and equivalent volcanic rocks the Shayban formation (777-771 Ma). It is inferred that the same M2A event resulted in the emplacement of the Arba'at pluton, dated at 779 ± 3 Ma by Stern and Abdelsalam (1998), south of the Nakasib suture in Sudan.

Deformation, uplift and denudation of the plutonic

and stratigraphic units south of the suture occurred during the apparent 15 Ma break in igneous activity following M2A and was responsible for the development of widespread unconformities, most notably between the Samran and Amudan formations and between the Mahd and Ghamr groups (Fig. 4B). Magmatism resumed during M2B with intrusion of the Hadabah gneiss (751-748 Ma) of the Qudayd suite and deposition of the time-equivalent Amudan formation (753-746 Ma) in the Tharwah segment. To the east in the Bi'r Umq segment, renewed activity in the Ramram volcano emplaced the younger part of the Ramram ring-dike (749 Ma), and eruptions there may have been responsible for the Ghamr group (748 Ma). Undated plutons of the Kamil suite that intrude the Amudan formation represent the last pulse of M2 magmatism south of the suture, but plutonic activity may have continued north of the suture until ca. 715 Ma with intrusion of the Shufayyah complex (C. Hedge, cited as pers. comm. in Camp, 1986a). Magmatism in Sudan concurrent with M2A is recorded by conventional U-Pb zircon ages of 754 ± 3 Ma and 740 ± 3 Ma for plutons south of the Nakasib suture and 748 ± 3 Ma for a pluton north of the suture (Stern and Abdelsalam, 1998).

Suture-related deformation along the BUSZ after, and perhaps during, M2 involved folding of the Samran and Mahd group rocks and subhorizontal dextral shearing along the Labunah thrust zone, as recorded by the Hadabah gneiss (751-748 Ma), and along associated fault systems farther south, such as the Rima shear zone. Deformation in Sudan appears to have ended in the eastern part of the Nakasib suture by the time an undeformed pluton intruded at 754 Ma (Stern and Abdelsalam, 1998), but continued farther west until after emplacement of a foliated pluton at 740 ± 3 Ma (Stern and Abdelsalam, 1998). The minimum age limit for deformation in Arabia comes from the undeformed Nukhu and Missir megadikes that intruded the Amudan formation at 700 Ma.

A third magmatic episode, M3 (700-633 Ma) followed the end of deformation and a nearly 50 Ma hiatus in magmatism along the BUSZ. Episode M3 is first recorded along the BUSZ by the intrusion of the Nukhu and Missir megadikes (700 Ma) south of the BUSZ and by evidence for thermal resetting of Rb-Sr ages at 700 Ma in Sudan (Abdelsalam, 1993). Episode M3 may have begun slightly earlier in Sudan, as suggested by the 710 ± 3 Ma age (Stern and Abdelsalam, 1998) for the posttectonic Hantouly pluton that intruded across the axis of the Nakasib suture. That age is similar to the unverified 715 Ma age for the Shufayyah complex north of the BUSZ, an intrusion that could also be posttectonic. The BUSZ lies at the margin of igneous activity concentrated at ca. 710 Ma to the north (e.g., Bailo and others, 2003), and thus related activity along the suture was weak. Subsequent M3 magmatism along the BUSZ was sporadic and resulted in emplacement of posttectonic plutons of the 696-687 Ma Subh suite (Clark and Duyverman, 1983; Aleinikoff and Stoeser, 1988) and the deposition of the 663-633 Ma Furayh group (C. Hedge, cited as pers. comm. in Camp, 1986a) north of the suture. Episode M3 was apparently very minor, as suggested by the limited extent of these units compared with those from earlier episodes, and was probably associated with local extension, as suggested by the morphology of the megadikes, the compositions of the Subh suite intrusions, megadikes, and Furayh volcanic rocks, and opening of basins into which the Furayh group was deposited. Continuing extension following M3 was responsible for development of unconformities on the Furayh group and opening the basins into which the Shayma Nasir group rocks were deposited.

The final magmatic episode, M4, is well defined by the 598-566 Ma ages (Brown and others, 1978; Calvez and Kemp, 1982; Fleck, 1985) for numerous granitoids of the Raghiyah intrusive suite and related units. More than sixty similar intrusions occur throughout the northern ANS and are part of a supersuite of hundreds of postorogenic A-type granites and related volcanic rocks (Murdamah and Shammar groups) spread out over >15 x 106 km^2 of the ANS and North and Saharan Africa (Bentor, 1985; Stoeser, 1985, and references therein) and extending into southern Ethiopia (Yibas and others, 2002; Miller and others, 2003). In the northern ANS, this supersuite was emplaced over the period 690-510 Ma, which suggests that Episodes M3 and M4 may be part of a single, more protracted episode. The U-Pb zircon age of ca. 510 Ma (Aleinikoff and Stoeser, 1988) for the youngest rock in the supersuite supports the 520 ± 15 Ma Rb-Sr mineral age (Brown and others, 1978) for part of the Raghiyah suite, which suggests that M4 lasted until ca. 520 Ma. The origin of alkalic rocks of this type is thought to be, at least in part, formed through anatexis of the lower continental crust as a result of crustal thickening (e.g., Radain and others, 1981), possibly associated with continental collision along the East African Orogen. The fact that most of the rocks representing M4 (and part of M3?) were intruded at such a late stage is common for postorogenic alkalic igneous provinces, which may appear as late as 70 Ma after collision (Stoeser, 1985, and references therein).

Older Basement in the Western Arabian Shield

A long-standing controversy centers on the extent to which pre-Neoproterozoic continental crust exists in the ANS. It is generally agreed that most of the shield was constructed by the accretion of intraoceanic arc terranes or oceanic plateaux. However, it is now well documented from geological (Agar, 1985; White, 1985), geochronological (Calvez and others, 1983), and Pb, Nd, and Sr isotopic data (Baubron and others, 1976; Kröner and others, 1979; Stacey and others, 1980; Fleck and Hadley, 1982; Stacey and Stoeser, 1983; Stacey and Hedge, 1984; Stacey and Agar, 1985; Windley and others, 1996) that the central parts of the Afif terrane (Khida terrane) in the eastern Arabian shield in Saudi Arabia and parts of the shield in Yemen were influenced by, or are immediately underlain by, Mesoproterozoic to

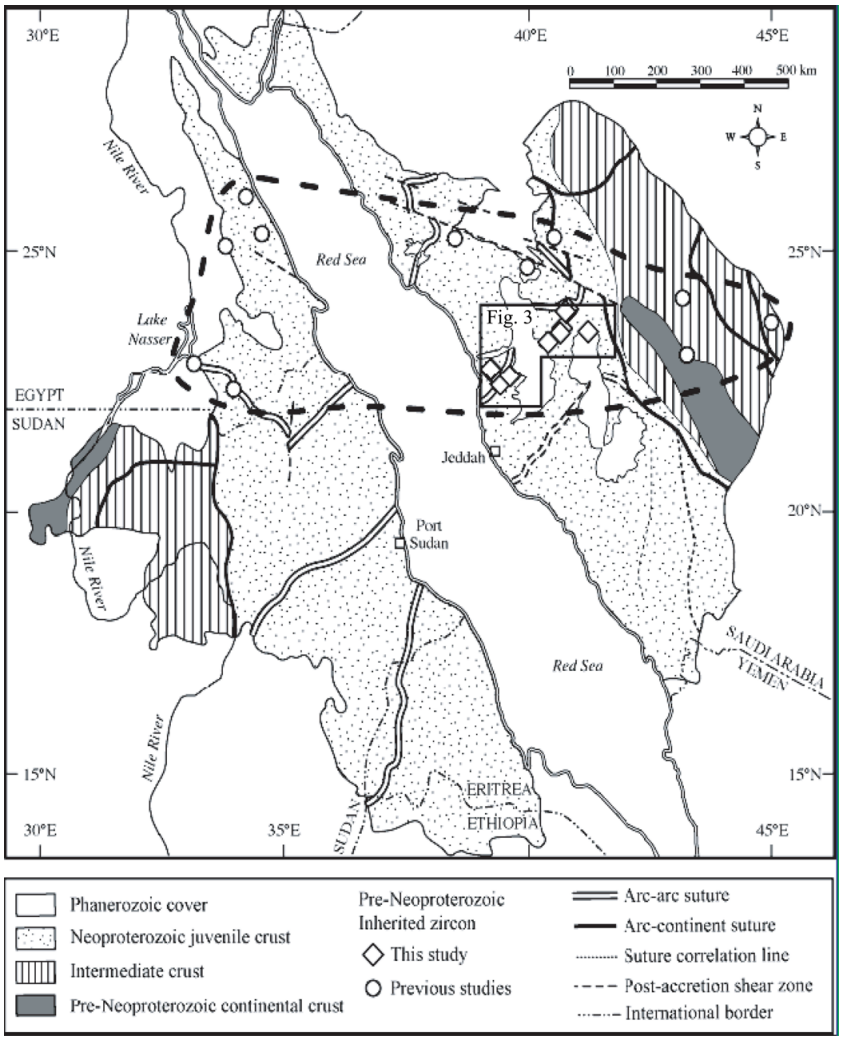

Figure 31. Map of the Arabian-Nubian Shield, modified from Johnson and Woldehaimanot (2003), showing the location of samples containing zircon inherited from pre-Neoproterozoic sources (Stacey and Agar, 1985; Pallister and others, 1988b; Sultan and others, 1990; Kröner and others, 1992; Kennedy and others, 2004; Hargrove, 2006), the region affected by such inheritance (heavy dashed line), and the distribution of Neoproterozoic juvenile (ensimatic) crust, intermediate, and pre-Neoproterozoic (ensialic) continental crust, based on whole-rock initial εNd and TDM values and initial $^{208}Pb/^{204}Pb$, $^{207}Pb/^{204}Pb$, $^{206}Pb/^{204}Pb$ isotopic data from feldspar, galena, and whole-rock samples. Data sources for isotopic divisions of the shield are listed in Johnson and Woldehaimanot (2003). The location of Figure 3 is outlined.

Archean crust (Figs. 1, 31). The known extents of pre-Neoproterozoic continental crust in those areas exhibit continental $^{207}Pb/^{206}Pb$ isotopic signatures (Type III of Stoeser and Stacey, 1988), low or commonly negative initial εNd values, and old TDM ages. The juvenile core of the ANS, comprising the Gerf-Midyan, Gebeit-Hijaz, Haya-Jeddah, Asir-Tokar, and Hulayfah terranes as well as the westernmost parts of the Afif and Ha'il terranes, is characterized by oceanic initial $^{207}Pb/^{206}Pb$ isotopic signatures (Type I), highly positive initial εNd, and young TDM ages (Figs. 1, 31). Remaining parts of the shield exhibit isotopic signatures that are transitional between oceanic and continental (Figs. 1, 31).

Some of the earliest evidence for old crust in the juvenile Neoproterozoic core of the ANS was reported by Sultan and others (1990) for deformed (pre-tectonic) granite in the Central Desert of Egypt (Figs. 1, 31). The granite yielded a $^{207}Pb/^{206}Pb$ age of 578±15 Ma, based on one nearly concordant analysis, but contained an older component at least 829 Ma old. Linear regression through the youngest and oldest points produced an upper intercept age of ca. 1650 Ma, which Sultan and others (1990) interpreted as the maximum age of the inherited material. Such an interpretation was supported by the higher initial $^{87}Sr/^{86}Sr$ and $^{207}Pb/^{204}Pb$ of the granite compared to more primitive rocks of the same age from the shield, despite an initial εNd value (+5.7) typical of juvenile crust.

Kennedy and others (2004) reported minor Mesoproterozoic to Archean inherited zircon grains from volcanic rocks in late Neoproterozoic post-amalgamation basins in the northern Arabian Shield. That they found Paleoproterozoic aged zircons in 600-665 Ma rhyolite tuff in the central Afif terrane is not surprising, considering that that part of the shield exhibits initial Pb isotopic ratios transitional between juvenile and continental type (Fig. 31) and contains well-documented exposures of pre-Neoproterozoic continental crust. It is surprising that they found such old zircon grains, up to 2750 Ma, in parts of the shield that are generally accepted as being underlain by strictly juvenile Neoproterozoic crust, such as the northern Hijaz terrane.

Evidence from the present study

The extent of the Arabian Shield affected by pre-Neoproterozoic crust, which is referred to herein as the "contaminated shield," is poorly known. Some of the units discussed herein contain the highest concentration of inherited zircon grains yet discovered anywhere in the apparently juvenile western part of the Arabian shield; Neoproterozoic arc-related plutons in the Khida terrane contain abundant zircon grains inherited from pre-Neoproterozoic sources (Stacey and Hedge, 1984). The $^{207}Pb/^{206}Pb$ ages for those zircons extend the known limits of the contaminated shield. They also provide evidence that pre-Neoproterozoic continental crust was not confined to the Afif terrane, but was important in the "juvenile" terranes at the core of the shield as well.

During this study, a total of 422 analyses were conducted, all but 32 of which were concordant in terms of their two-sigma error ellipses. Ages younger than 500 Ma, although shown in Table 3, are not included in the following discussion, because magmatic events younger than that are not known in the shield and such ages are likely the result of severe lead loss. Omitting those analyses left 403 that are considered geologically

meaningful. Analyses of zircons suspected to have experienced mild lead loss due to recent weathering are included because in most cases the change in apparent age is only significant in terms of calculating a concordia age for the whole sample. In the following discussion, $^{238}U/^{206}Pb$ ages are used for zircons younger than 1000 Ma and $^{207}Pb/^{206}Pb$ ages are used for zircons older than 1000 Ma, based on the relative magnitude of the errors shown by each.

Of the 403 analyses, 356 (~88%) yielded Neoproterozoic ages (1000-540 Ma), and 347 (~86%) yielded ages in the range of 900-500 Ma (Fig. 32A), which is the range expected from previous dating campaigns for crust along the BUSZ and currently accepted models for ANS formation. Consequently, 56 (~14%) of the net analyses yielded ages older than expected for juvenile ANS crust. The reader is reminded that no crust older than 870 Ma is exposed within the Jeddah or Hijaz terranes in Arabia or their equivalents in Sudan and Egypt, although pre-Neoproterozoic crust is documented to the south and east.

Of the 56 "older than expected" zircons, 12 (~22%) yielded early Neoproterozoic ages, 31 (~55%) yielded Mesoproterozoic ages, 9 (~16%) yielded Paleoproterozoic ages, and 4 (~7%) yielded Archean ages (Fig. 32B). The older (inherited) zircon ages from this study can be assigned to four groups: 900-1050 Ma, 1075-1250 Ma, 1300-2000 Ma, and 2700-2850 Ma. The oldest SHRIMP-RG age from this study (a discordant age of 2839 Ma; SA04-366-12.1) is the oldest yet reported from the Arabian Shield. The two youngest groups overlap the Kibaran tectonothermal event of southern and central Africa, also recorded in the detrital zircon study of Avigad and others (2003).

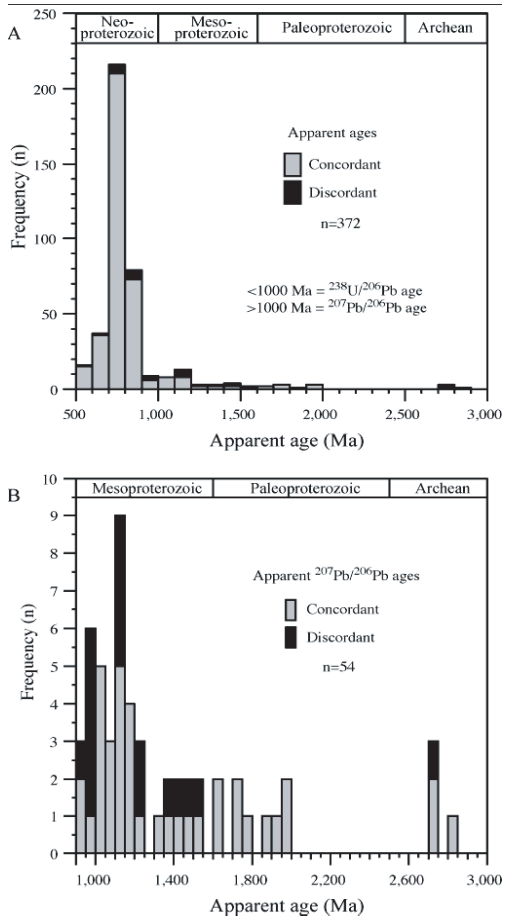

Figure 32. Histograms of single-grain SHRIMP-RG ages of zircon analyzed during this study: (A) all ages older than 500 Ma; (B) subset of ages 900-3000 Ma. Ages <1000 Ma are 238U/206Pb ages and those >1000 Ma are 207Pb/206Pb ages.

Source of the inheritance

The extent to which the construction of the ANS involved preexisting continental crust is an important problem, but equally important is determining the origin of the inherited zircons. There are two main possibilities: (1) inadvertent contamination in the laboratory; and (2) natural contamination associated with magmatic processes. The possibility of contamination in the lab is a serious concern, but can be eliminated for the following reasons. First, some of the material and facilities at UTD used to process whole-rock samples for zircon, such as separatory funnels for heavy liquid separation, sample containers, filters, etc., were newly purchased and could not be a source of the contamination. Second, the facilities were not in use by any other workers at the time and previous studies using the equipment did not process samples of the age encountered among the suspected inherited zircons. Third, great care was taken to ensure that all equipment and labware was thoroughly cleaned between samples. Finally, the recognition of inheritance elsewhere in the ANS by several other workers indicates that it is a natural phenomenon and not due to human error, especially since the age of the inherited component observed by Pallister and others (1988b) in the Tharwah ophiolite was essentially replicated during this study. Noting that, the possible natural sources of inheritance in juvenile Neoproterozoic rocks along the BUSZ are now discussed.

Avigad and others (2003) reported the results of U-Pb SHRIMP II dating of detrital zircons from Cambrian sandstones at the northern edge of the Arabian Shield in Israel. They attributed the source of 550-650 Ma detrital zircons to the Arabian-Nubian Shield south of Israel and attributed the source of 1650-1850 Ma and 2450-2700 Ma zircons to the more distant Afif terrane to the southeast and the Saharan metacraton to the southwest, each ca. 1000 km distant. They postulated that the source of 900-1100 Ma zircon grains was Kibaran crust exposed more than 3000 km to the south in central and eastern Africa. Such long-travelled zircon grains may have been fluvially transported, but the zircon morphologies are more characteristic of grains that were either locally derived or were transported intact by other processes, such as within clasts carried by glaciers (Avigad and others, 2003).

Support for glacially transported zircon is growing with the increasing recognition of major glacial episodes during the Neoproterozoic. The polymict breccia that separates the Dhukhr batholith and the overlying Mahd group may represent one of those glacial episodes and could be a source of inherited zircons, which occur in the volcanic rocks of the Bi'rak, Samran, and Mahd

groups and related hypabyssal intrusions, in posttectonic granites of the Raghiyah intrusive suite, and in gabbro of the Tharwah ophiolite. Inherited zircon is most abundant within the volcanic units. One explanation for this circumstance could be that the magmas from which the volcanic rocks were derived interacted and assimilated material from sheets of tillite. The tillite must have contained abundant zircon in order to account for the variety in ages and number of inherited grains in some of the samples. This argument is not preferred, simply because the Mahd basal diamictite is at most a few meters thick, is discontinuously exposed, and correlative units are not anywhere preserved in the nearly continuous Samran stratigraphic section nor within the Bi'rak group.

Alternatively, it could be argued that a thick blanket of terrigenous clastic sediment covered the Mozambique seafloor upon which the Jeddah and Hijaz arc terranes were later constructed. In this case, only the shallow magma chambers that fed the volcanic centers associated with the Bi'rak, Samran, and Mahd groups would have interacted with the detrital sediments, and the source of the anatectic melts that produced the posttectonic Raghiyah suite may have included the same terrigenous sediments, as inferred from the chemistry of the intrusions. Those sediments may have been shed into marine basins developed along passive margins, which could account for the breadth of ages represented by the inherited zircon. Most, but not all, of the inherited zircons analyzed during this study are discrete rounded grains or rounded cores surrounded by more euhedral overgrowths. The rounded morphologies are consistent with a detrital history and lend support to both of the above arguments. However, the same morphologies could also arise through partial resorption in magma at depth. This possibility and the fact that some inherited zircons exhibit euhedral morphologies and no apparent cores, characteristics that are more consistent with juvenile grains, suggests that many of the inherited zircon grains were assimilated in situ from their original host igneous rocks. This opens up yet another possibility, which is that a tract of previously unrecognized continental crust exists beneath the northern and central parts of the ANS, the extent of which may be approximated by the region shown in Figure 31 from which inheritance of pre-Neoproterozoic zircon has been documented. This interpretation is not supported by numerous regional Nd, Sr, and Pb isotopic studies, which show that the igneous rocks on both sides of the Bi'r Umq-Nakasib suture zone (in Sudan and Saudi Arabia) have largely ensimatic signatures. However, the influence of older crustal material, either crystalline basement or terrigenous sediments underlying the arc, is clearly indicated by the pervasive zircon inheritance. That influence is also supported by a more recent study (Hargrove and others, 2006), which reveals a subtle correlation between zircon inheritance and reduced initial Nd isotopic ratios of the rocks studied here.

Suggestions for Future Work

A number of important contributions can be made towards further understanding the tectonic evolution of the crust along the BUSZ. Foremost among these is the determination of accurate U-Pb zircon crystallization ages for the Tharwah and Bi'r Umq ophiolites, which should be obtained from units (e.g., cumulate or isotropic gabbro, sheeted dikes, etc.) that can be unambiguously shown to belong to the ophiolite section. As mentioned previously, the relative ages of the ophiolites and flanking plutonic terranes are pivotal to the tectonic model (Wilson cycle or simple arc accretion) applied to the BUSZ. Second, it is recommended that zircon ages be obtained for major plutons in the Makkah and Hafnah batholiths, which can be compared to the ca. 870 Ma age of the potentially coeval Erkowit pluton in Sudan and with the ages of the ophiolites. Third, Dating detrital zircon grains and zircon grains from clasts within the breccia at the base of the Mahd group is necessary to test the hypothesis that the possibly glacial deposit is a source of pre-Neoproterozoic inherited zircon. Fourth, based on the results of the geochronology reported herein, it is recommended that the stratigraphy of the region be revised to include the new ages. In this respect, the Nida, Shayban, and Amudan formations within the Samran group probably each represent individual groups rather than formations based on their age differences. Likewise, many of the plutonic assemblages (e.g., the Kamil intrusive suite) should be divided into smaller suites based on geographical location and their respective ages. Lastly, zircon ages are needed for the Milhah, Furayh, and Ghamr groups in order to more firmly establish stratigraphic correlations in the region.

ACKNOWLEDGMENTS

Field activities and logistical su port for this project in Saudi Arabia were done as part of the SGS Technical Work Program for 2004, Subproject 4.1.1.5.1 *Research and Special Studies* and the work was funded by a grant (EAR0309799) from the National Science Foundation to Stern, a Graduate Research Fellowship from NSF (0412278) and the Japan Society for the Promotion of Science to Hargrove, and a grant (7151-02) from the Geological Society of America to Hargrove. Thorough reviews and insightful comments were provided by Alfred Kröner and Douglas Stoeser. We thank HE Dr. Mohammed A. Tqwfiq, former President of SGS of his support of this work in Saudi Arabia. We thank Ammar Abdulshakoor, Sa'ad Al-Gharny, Zabin Al-Harbi, Mohammed Ali, Bander Shaikan, Ghazi Kattu, Wadee Kashkari, and Yahiya Mufarhah of SGS for their assistance in the field, Alim Saddiqi for excellent thin-section preparation, and Adam Franklin for assistance with sample preparation. We are grateful to Joe Wooden and Frank Mazdab at the USGS/Stanford micro-analytical lab for their assistance and helpful discussions. U. Hargrove wishes to acknowledge Shimane University for its contributions to his fellowship in Japan and to thank Bob Rutford for his support and insight during

the first trip to Saudi Arabia. This is UTD Geosciences contributions 1109.

DATABASE

A digital record of this report is available in the SGS Geoscience Database and may be retrieved by the report number, title, authors, or the following keywords: *Arabian-Nubian shield, Neoproterozoic, geochronology, crustal history*

REFERENCES

Abdel-Rahman, M., 1993, Geochemical and geotectonic controls of the metallogenic evolution of selected ophiolite complexes from the Sudan. Berliner geowissenschafliche Abhandlungen, 145: 175p.

Abdelsalam, M.G., 1993, Tectonic evolution of the late Precambrian Nakasib suture and Oko shear zone, Red Sea Hills, Sudan. Ph.D. dissertation, The University of Texas at Dallas, Richardson.

Abdelsalam, M.G., 1994, The Oko Shear Zone, Sudan: post-accretionary deformation in the Arabian-Nubian Shield. Journal of the Geological Society of London, v. 151: p. 767-776.

Abdelsalam, M.G. and Stern, R.J., 1993a, Structure of the late Proterozoic Nakasib suture, Sudan. Journal of the Geological Society of London, v. 150: p. 1065-1074.

Abdelsalam, M.G. and Stern, R.J., 1993b, Tectonic evolution of the Nakasib suture, Red Sea Hills, Sudan: evidence for a late Precambrian Wilson cycle. Journal of the Geological Society of London, 150: 393-404.

Abdelsalam, M.G. and Stern, R.J., 1993c, Timing of events along the Nakasib suture and the Oko shear zone, Sudan. In: U. Thorweihe and H. Schandelmeier (Editors), Geoscientific Research in northeast Africa. Balkema, Rotterdam, p. 99-103.

Abu Rashid, A.R., 1973. Geology and mineralization of Rabigh quadrangle, Hijaz area. Saudi Arabian Deputy Ministry for Mineral Resources Open-File Report 476, 37 p.

Afifi, A.M., 1983. Environments of late Precambrian volcanism in the Mahd adh Dhahab District, Saudi Arabia. Geological Society of America Abstracts with Programs, v. 15(6): p. 512.

Afifi, A.M., 1989, Geology of the Mahd adh Dhahab district, Kingdom of Saudi Arabia: Saudi Arabian Directorate General of Mineral Resources Open-File Report USGS-OF-09-2, 32 p.

Agar, R.A., 1985, Stratigraphy and palaeogeography of the Siham Group; direct evidence for a late Proterozoic continental microplate and active continental margin in the Saudi Arabian Shield. Journal of the Geological Society of London, 142, Part 6: p. 1205-1220.

Al-Damegh, K., Sandvol, E. and Barazangi, M., 2005, Crustal structure of the Arabian plate: new constraints from the analysis of teleseismic receiver functions. Earth and Planetary Science Letters, v. 231(3-4): p. 177.

Al-Muallem, M.S., 1983, Geology and mineralization of the Wadi Hawarah-Wadi Hamluck area, western Saudi ArabiaKing Abdulaziz University, Jeddah.

Al-Rehaili, M.H., 1980, Geology of the mafic-ultramafic complex of Bi'r Umq area. M.Sc., King Abdulaziz University, Jiddah, 160 p.

Al-Rehaili, M.H. and Warden, A.J., 1980, Comparison of the Bir Umq and Hamdah ultrabasic complexes, Saudi Arabia. Institute of A plied Geology Bulletin, v. 3(4): p. 143-156.

Al-Shanti, A.M.S., 1970, Rabigh barite deposits. Mineral Resources Research: Saudi Arabian Deputy Ministry for Mineral Resources, p. 51-57.

Al-Shanti, A.M.S. and Abdel-Monem, A.A., 1982, Rb-Sr dating and petrochemistry of Um Gerad granitic rocks, western Saudi Arabia (abstract). Precambrian Research, v. 16: p. A6.

Al-Shanti, A.M.S., Abdel-Monem, A.A. and Radain, A.A.M., 1983, Rb-Sr dating and petrochemistry of Um Gerad granitic rocks (Rabigh area), western Saudi Arabia. Bulletin of the Faculty of Earth Sciences, King Abdulaziz University, 6: p. 221-232.

Alabouvette, B., Bournat, G., Maillard, J. and Daesslé, M., 1972. Summary review of the Jabal Sayid copper prospect: bureau de Recherches Géologiques et Minières Technical Record 72-JED-5, 50 p.

Aldrich, L.T., Brown, G.F., Hedge, C.E. and Marvin, R., 1978, Radiometric age determinations of some rocks from the Arabian Shield: U.S. Geological Survey Saudi Arabian Project Report 240, Section 1, p. 9.

Aleinikoff, J.N. and Stoeser, D.B., 1988. Zircon morphology and U-Pb geochronology of seven metaluminous and peralkaline post-orogenic granite complexes of the Arabian Shield, Kingdom of Saudi Arabia: Saudi Arabina Deputy Ministry for Mineral Resources Open File Report USGS-OF-06-5, 32 p.

Alsac, C., Lacomme, A., Delfour, J., Sabir, H., Le Metour, J., Turkistani, A.R., Kemp, J., Al-Shanti, A.M.S. and Fauvelet, E., 1982. Guidebook for excursion "B" in the Jabal Sayid region, 1st Symposium IGCP 164, Pan-African crustal evolution in the Arabian Nubian Shield. King Abdulaziz University Faculty of Earth Science Research Series, p. 58.

Ashwal, L.D., Tucker, R.D. and Zinner, E.K., 1999, Slow cooling of deep crustal granulites and Pb-loss in zircon. Geochimica et Cosmochimica Acta, v. 63:

p. 2839-2851.

Avigad, D., Kolodner, K., McWilliams, M., Persing, H. and Weissbrod, T., 2003, Origin of northern Gondwana Cambrian sandstone revealed by detrital zircon SHRIMP dating. Geology, v. 31(3): p. 227-230.

Badri, M., 1991, Crustal structure of central Saudi Arabia, from seismic refraction profiling. Tectonophysics, 136: 357-374.

Bailo, T., Schandelmeier, H., Franz, G., Sun, C.-H. and Stern, R.J., 2003, Plutonic and metamorphic rocks from the Keraf Suture (NE Sudan); a glimpse of Neoproterozoic tectonic evolution on the NE margin of W. Gondwana. Precambrian Research, 123(1): 67-80.

Baubron, J.C., Delfour, J. and Vialette, Y., 1976. Geochronological measurements (Rb/Sr; K/Ar) on rocks of the Arabian Shield, Kingdom of Saudi Arabia: Bureau de Recherches Géologique et Miniè res Technical Record 76-JED-22, p. 151.

Bentor, Y.K., 1985, The crustal evolution of the Arabo-Nubian Massif with special reference to the Sinai Peninsula. Precambrian Research, 28(1): 1-74.

Black, L.P., Kamo, S.L., Allen, C.M., Davis, D.W., Aleinikoff, J.N., Valley, J.W., Mundil, R., Campbell, I.H., Korsch, R.J., Williams, I.S. and Foudoulis, C., 2004. Improved $^{206}Pb/^{238}U$ microprobe geochronology by the monitoring of a trace-element-related matrix effect; SHRIMP, ID-TIMS, ELA-ICP-MS and oxygen isotope documentation for a series of zircon standards. Chemical Geology, 205(1-2): 115.

Bokhari, F.Y. and Kramers, J.D., 1981, Island arc character and late Precambrian age of volcanics at Wadi Shwas, Hijaz, Saudi Arabia; geochemical and Sr and Nd isotopic evidence. Earth and Planetary Science Letters, 54(3): 409-422.

Bonatti, F., Ligi, M., Borsetti, A.M., Gasperini, L., Negri, A. and Sartori, R., 1996. Lower Cretaceous deposits trapped near the equatorial Mid-Atlantic Ridge. Nature London, 380(6574): 518-520.

Brown, G.F., Hedge, C.E. and Marvin, R., 1978. Tabulation of Rb-Sr and K-Ar ages given by rocks of the Arabian Shield: U.S. Geological Survey Saudi Arabian Project Report 240, Section 2, p. 20.

Brown, G.F., Schmidt, D.L. and Huffman, A.C., 1989. Geology of the Arabian peninsula, Shield area of western Saudi Arabia: U.S. Geological Survey Professional Paper 560-A.

Calvez, J.Y., Alsac, C., Delfour, J., Kemp, J. and Pelaton, C., 1983. Geological evolution of western, central, and eastern parts of the northern Precambrian shield, Kingdom of Saudi Arabia: Saudi Arabian Deputy Ministry for MIneral Resources Open-File Report BRGM-OF-03-17, 57 p.

Calvez, J.Y. and Kemp, J., 1982, Geochronological investigations in the Mahd adh Dhahab quadrangle, central Arabian Shield: Saudi Arabian Deputy Ministry for Mineral Resources Technical Record BRGM-TR-02-5, p. 41.

Camp, V.E., 1984, Island arcs and their role in the evolution of the western Arabian Shield. Geological Society of America Bulletin, 95(8): 913-921.

Camp, V.E., 1986a, Explanatory notes to accompany the geologic map of the Umm al Birak quadrangle, Sheet 23D, Kingdom of Saudi Arabia. Ministry of Petroleum and Mineral Resources, p. 40.

Camp, V.E., 1986b, Geologic map of the Umm al Birak quadrangle, sheet 23D, Kingdom of Saudi Arabia. Saudi Arabian Directorate General of Mineral Resources Geologic Map GM 87, 40 p.

Clark, M.D. and Duyverman, H.J., 1983, Preliminary isotopic age determination and stratigraphic correlation in the Al Hamra-Badr-Hunayn region: Saudi Arabian Directorate General for Mineral Resources Open File Report DGMR-OF-03-09, p. 10.

Collins, A.S., Ranzakamanana, T. and Windley, B.F., 2000, Neoproterozoic extensional detachment in central Madagascar; implications for the collapse of the East African Orogen. Geological Magazine, 137: 39-51.

Conraux, J., 1966, Report on the mineral resources and geology of the Umm ad Dammar-Jabal Rokkam area :(sheet 112, Zone I South): Bureau de Recherches Géologique et Minières Technical Record SG-JED-66-A9, 93 p.

Cooper, J.A., Stacey, J.S., Stoeser, D. and Fleck, R.J., 1979, An evaluation of the zircon method of isotopic dating in the Southern Arabian Craton. Contributions to Mineralogy and Petrology, 68(4): 429-439.

Dalziel, I.W.D., 1991, Pacific margins of Laurentia and East Antarctica-Australia as a conjugate rift pair: Evidence and implications for an Eocambrian supercontinent. Geology, 19(598-601).

Darbyshire, D.P.F., Jackson, N.J., Ramsay, C.R. and Roobol, M.J., 1983, Rb-Sr isotope study of latest Proterozoic volcano-sedimentary belts in the central Arabian shield. Journal of the Geological Society of London, 140(2): 203-213.

Delfour, J., 1981, Geologic map of the Al Hissu quadrangle, Sheet 24E, Kingdom of Saudi Arabia. Saudi Arabian Deputy Ministry for Mineral Resources Geoscience Map GM 58, p. 47.

Deschamps, Y., Lescuyer, J.L. and Guerrot, C., Osman, A.A., 2004, Lower Neoproterozoic age of the Ariab volcanogenic massive sulphide mineralization, Red

Sea Hills, NE Sudan. 20th Colloquium of African Geology (Orléans, France) Abstracts: 133.

Dick, H.J.B. and Bullen, T., 1984, Chromian spinels as a petrogenetic indicator in abyssal and alpine-type peridotites and spatially associated lavas. Contributions to Mineralogy and Petrology, 86: 54-76.

Dilek, Y. and Ahmed, Z., 2003, Proterozoic ophiolites of the Arabian Shield and their significance in Precambrian tectonics, Ophiolites in Earth History, Geological Society of London Special Publication, p. 685-700.

Dixon, T.H. and Golombek, M.P., 1988, Late Precambrian crustal accretion rates in Northeast Africa and Arabia. Geology, 16: 991-994.

Dixon, T.H., Stern, R.J. and Hussein, I.M., 1987, Control of Red Sea rift geometry by Precambrian structures. Tectonics, 6(5): 551-571.

Dottin, O., 1975, Revised geology of the Sufaynah quadrangle, 23/40D : Bureau de Recherches Géologiques et Minières Technical Record 75-JED-29, 30 p.

Dunlop, H.M., Kemp, J. and Calvez, J.Y., 1986, Geochronology and isotope geochemistry of the Bi'r Umq mafic-ultramafic complex and Arj-group volcanic rocks, Mahd adh Dhahab quadrangle, central Arabian Shield: Saudi Arabian Deputy Ministry for Mineral Resources BRGM-OF-07-7, 38 p.

Durrheim, R.J. and Mooney, W.D., 1991, Archean and Proterozoic crustal evolution: Evidence from crustal seismology. Geology, 19: 606-609.

Fleck, R.J., 1985, Age of diorite-granodiorite gneisses of the Jiddah-Makkah region, Kingdom of Saudi Arabia: Saudi Arabian Deputy Ministry for Mineral Resources Professional Paper, P-2: 19-27.

Fleck, R.J., Greenwood, W.R., Hadley, D.G., Anderson, R.E. and Schmidt, D.L., 1979, Rubidium-strontium geochronology and plate tectonic evolution of the southern part of the Arabian Shield. USGS Saudi Arabian Project Report SA (IR) 245, 105 p.

Fleck, R.J. and Hadley, D.G., 1982, Ages and strontium initial ratios of plutonic rocks in a transect of the Arabian Shield: Saudi Arabian Deputy Ministry for Mineral Resources Open-File Report USGS-OF-03-38, p. 43.

Fujii, K. and Okumi, S., 1978, Geology of the Wadi Hawarah-Wadi Sitarah area, north Samran disrtict: Saudi Arabian Deputy Ministry for Mineral Resources Technical Record TR-1978-8, 7 p.

Fujii, K., Ozawa, A. and Kato, K., 1978, Geology and geochemistry of Wadi Hawarah district: Saudi Arabian Deputy Ministry for Mineral Resources Technical Record TR-1978-13, 12 p.

Gettings, M.E., Blank, H.R., Mooney, W.D. and Healey, J.H., 1986, Crustal structure of southwestern Saudi Arabia. Journal of Geophysical Research, 91: 6491-6512.

Gettings, M.E. and Stoeser, D.B., 1981, A tabulation of radiometric age determinations for the Kingdom of Saudi Arabia: U.S. Geological Survey Saudi Arabian Mission Miscellaneous Document SA (IR)-353, 52 p.

Gilboy, C.F. and Skiba, W., 1978a, Geology of the Rabigh Quadrangle, Sheet 22/39 A, Kingdom of Saudi Arabia: Ministry of Petroleum and Mineral Resources, Deputy Ministry for Mineral Resources, Jeddah.

Gilboy, C.F. and Skiba, W., 1978b, Geology of the Rabigh Quadrangle, Sheet 22/39 B, Kingdom of Saudi Arabia: Ministry of Petroleum and Mineral Resources, Deputy Ministry for Mineral Resources, Jeddah.

Gilboy, C.F. and Skiba, W., 1978c, Geology of the Rabigh Quadrangle, Sheet 22/39 C, Kingdom of Saudi Arabia.:Ministry of Petroleum and Mineral Resources, Deputy Ministry for Mineral Resources, Jeddah.

Gilboy, C.F. and Skiba, W., 1978d, Geology of the Rabigh Quadrangle, Sheet 22/39 D, Kingdom of Saudi Arabia: Ministry of Petroleum and Mineral Resources, Deputy Ministry for Mineral Resources, Jeddah.

Goldsmith, R. and Kouther, J.H., 1971, Geology of the Mahd adh Dhahab-Umm ad Damar area, Kingdom of Saudi Arabia: Saudi Arabian Directorate General of Mineral Resources Bulletin 6, p. 20.

Golynsky, A. and Jacobs, J., 2001, Grenville-Age versus Pan-African Magnetic Anomaly Imprints in Western Dronning Maud Land, East Antarctica. Journal of Geology, 109: 136-142.

Gradstein, F.M., Ogg, J.G., Smith, A.G., Bleeker, W. and Lourens, L.J., 2004, A new geologic time scale, with special reference to Precambrian and Neogene. Episodes, 27(2): 83-100.

Hargrove, U.S., 2006, Crustal evolution of the Neoproterozoic Bi'r Umq suture zone, Kingdom of Saudi Arabia: Geochronological, isotopic, and geochemical constraints. Unpublished Ph.D. dissertationThe University of Texas, Richardson, 359 p.

Hargrove, U.S., Stern, R.J., Kimura, J.-I., Manton, W.I. and Johnson, P.R., in review. How juvenile is the Arabian-Nubian Shield? Evidence from Nd isotopes and pre-Neoproterozoic inherited zircon. Earth and Planetary Science Letters.

Henjes-Kunst, F., Altherr, R. and Baumann, A., 1990.

Evolution and composition of the lithospheric mantle underneath the western Arabian Peninsula; constraints from Sr-Nd isotope systematics of mantle xenoliths. Contributions to Mineralogy and Petrology, 105: 460-472.

Hopwood, T., 1979, An exploration study of metal deposits in the Jabal Sayid region: Saudi Arabian Deputy Ministry for Mineral Resources Open-File Report RFO-1979-9, 169 p.

Huckerby, J.A., 1984, Structural setting and mineralisation at the Mahd adh Dhahab gold mine, western Saudi Arabia. Unpublished Ph.D. Thesis, University of London.

Ireland, T.R. and Williams, I.S., 2003, Considerations in zircon geochronology by SIMS. Reviews in Mineralogy and Geochemistry, 53: 215-241.

Johnson, P.R., 1998, The structural geology of the Samran-Shayban area, Kingdom of Saudi Arabia: Saudi Arabian Deputy Ministry for Mineral Resources Technical Report USGS-TR-98-2, Jiddah, 57 p.

Johnson, P.R., Abdelsalam, M. and Stern, R.J., 2002, The Bi'r Umq-Nakasib shear zone: Geology and structure of a Neoproterozoic suture in the northern East African Orogen, Saudi Arabia and Sudan: Saudi Geological Survey Technical Report SGS-TR-2002-1, 33 p.

Johnson, P.R., Abdelsalam, M.G. and Stern, R.J., 2003, The Bi'r Umq-Nakasib suture zone in the Arabian-Nubian Shield; a key to understanding crustal growth in the East African Orogen. Gondwana Research, 6(3): 523-530.

Johnson, P.R. and Kattan, F., 2001, Oblique sinistral transpression in the Arabian Shield; the timing and kinematics of a Neoproterozoic suture zone. Precambrian Research, 107: 117-138.

Johnson, P.R., Kattan, F.H. and Al-Saleh, A.M., 2004, Neoproterozoic ophiolites in the Arabian Shield: Field relations and structure. In: K.C. Condie (Editor), Developments in Precambrian Geology. Elsevier, p. 129-162.

Johnson, P.R. and Woldehaimanot, B., 2003., Development of the Arabian-Nubian shield: Perspectives on accretion and deformation in the northern East African Orogen and the assembly of Gondwana. In: M.Yoshida, S. Dasgupta and B. Windley (Editors), Proterozoic East Gondwana: Supercontinent assembly and breakup. Geological Society of London, Special Publication 206, London, p. 289-325.

Jourde, G., 1976, Jabal Sayid copper deposit (Kingdom of Saudi Arabia): Progress Report No. 4 (February 1, 1976-July 31, 1976). Joint Venture SEREM/U.S. Steel Corporation Open File Report.

Kana'an, F.M., 1970, Report on geology of As Suleim quadrangle, a portion of Arabian Shield: Saudi Arabian Deputy Ministry for Mineral Resources Open-File Report DGMR-361, 46 p.

Kana'an, F.M., 1977, Geology of As Suleim quadrangle, part of the Arabian Precambrian Shield, Kingdom of Saudi Arabia. Saudi Arabian Deputy Ministry for Mineral Resources Technical Record TR-1977-3, 23 p.

Kana'an, F.M. and Liddicoat, W.K., 1979, Geology and mineralization of the Jabal Shayban prospect. Saudi Arabian Deputy Ministry for Mineral Resources Technical Record TR-1979-9, 23 p.

Kemp, J., 1980, Geology of the Wadi Al 'Ays quadrangle, sheet 25 C, Kingdom of Saudi Arabia. 135.

Kemp, J., Gros, Y. and Prian, J.-P., 1982a, Explanatory notes to the geologic map of the Mahd adh Dhahab quadrangle, Sheet 23E, Kingdom of Saudi Arabia.: Saudi Arabian Deputy Ministry for Mineral Resources Geologic Map GM-64, p. 39.

Kemp, J., Gros, Y. and Prian, J.P., 1982b, Geologic map of the Mahd adh Dhahab quadrangle, Sheet 23E. Kingdom of Saudi Arabia: Saudi Arabian Deputy Ministry for Mineral Resources Geologic Map GM-64, scale 1:250,000, .

Kemp, J., Pellaton, C. and Calvez, J.Y., 1980, Geochronological investigations and geological history in the Precambrian of northwestern: Saudi Arabian Deputy Ministry for Mineral Resources Open-File Report BRGM-OF-01-1, 120 p.

Kennedy, A., Johnson, P.R. and Kattan, F.H., 2004, SHRIMP geochronology in the northern Arabian Shield, Part 1: Data acquisition. Saudi Geological Survey Open-File Report SGS-OF-2004-11, p. 28.

Kobayashi, K., Kasuga, S. and Okin, K., 1995, Backarc basins: Tectonics and magmatism. In: B. Taylor (Editor). Plenum Press, New York, p. 381-405.

Kröner, A., Linnebacher, P., Stern, R.J., Reischmann, T., Manton, W. and Hussein, I.M., 1991, Evolution of Pan-African island arc assemblages in the southern Red Sea Hills, Sudan, and in southwestern Arabia as exemplified by geochemistry and geochronology. Precambrian Research, 53(1-2): 99-118.

Kröner, A., Roobol, M.J., Ramsay, C.R. and Jackson, N.J., 1979, Pan African ages of some gneissic rocks in the Saudi Arabian Shield. Journal of the Geological Society of London, 136(4): 455-461.

Kröner, A., Todt, W., Hussein, I.M., Mansour, M. and Rashwan, A.A., 1992. Dating of late Proterozoic ophiolites in Egypt and the Sudan using the single grain zircon evaporation technique. Precambrian Research, 59(1-2): 15-32.

Le Metour, J., Johan, V. and Tegyey, M., 1982,

Relationships between mafic-ultramafic complexes and volcanosedimentary rocks in the Precambrian Arabian Shield: Saudi Arabian Deputy Ministry for Mineral Resources Open-File Report BRGM-OF-02-15, 108 p.

Lee, J., Stern, R.J. and Bloomer, S.H., 1995 Forty million years of magmatic evolution in the Mariana arc: The tephra glass record. Journal of Geophysical Research, 100: 17671-17687.

Lefevre, J.C., 1969, Mineral resources and geology of the Sufaynah quadrangle : Bureau de Recherches Géologique et Minières Technical Record 69-JED-8, 16 p.

Liddicoat, W.K., 1971, The North Samran exploration area: Saudi Arabian Deputy Ministry for Mineral Resources Technical Record TR-1971-1, 74 p.

Ludwig, K.R., 1998, On the Treatment of Concordant Uranium-Lead ages. Geochimica et Cosmochimica Acta, 62(4): 665.

Ludwig, K.R., 2000, Isoplot/Ex 3.0: A geological toolkit for Microsoft Excel. Berkeley Geochronology Center Special Publication, 1.

Ludwig, K.R., 2001, 2001 SQUID 1.02 Add-In for Excel™. Berkeley Geochronology Center Special Publication, 2.

McGuire, A.V. and Stern, R.J., 1993, Granulite xenoliths from western Saudi Arabia: the lower crust of the late Precambrian Arabian-Nubian Shield. Contributions to Mineralogy and Petrology, 114: 395-408.

Miller, N., Alene, M., Sacci, R., Stern, R.J., Kröner, A., Conti and Zu pi, G., 2003, Significance of the Tambien Group (Tigrai, N. Ethiopia) for Snowball Earth Events in the Arabian-Nubian Shield. Precambrian Research, 121(3-4): 263-283.

Moore, T.A. and Al-Rehaili, M.H., 1989a, Explanatory notes to the geologic map of the Makkah quadrangle, Sheet 21D, Kingdom of Saudi Arabia: Saudi Arabian Directorate General of Mineral Resources Geiscience Map GM- 62 p.

Moore, T.A. and Al-Rehaili, M.H., 1989b. Geologic map of the Makkah quadrangle, Sheet 21 D, Kingdom of Saudi Arabia: Saudi Arabian Directorate General of Mineral Resources Geoscience Map GM-107, scale 1:250,000, 62 p.

Muhongo, S., Kröner, A. and Nemchin, A.A., 2001. Single zircon evaporation and SHRIMP ages for granulite-facies rocks in the Mozambique Belt of Tanzania. Journal of Geology, 109: 171-189.

Nassief, M.O., 1981. Geology and petrology of the Jabal Thurwah area, Western Province, Saudi ArabiaUniversity of Lancaster, England, 180 p.

Nassief, M.O., MacDonald, R. and Gass, I.G., 1984. The Jebel Thurwah U per Proterozoic ophiolite complex, western Saudi Arabia. Journal of the Geological Society of London, 141: 537-546.

Nebert, K., 1969, Geology of the Jabal Samran and Jabal Farasan region, Kingdom of Saudi Arabia: Saudi Arabian Directorate General of Mineral Resources Bulletin 4, 32 p.

Ono, T., 1976a, Geology and Mineral Deposits of Jabal Samran and Abu Umm Shut: Saudi Arabian Deputy Ministry for Mineral Resources Technical Record TR-1976-16, 20 p.

Ono, T., 1976b, Mineralization in the Wadi Hawarah district: Saudi Arabian Deputy Ministry for Mineral Resources Technical Record TR-1976-4, 17 p.

Ozawa, A., 1978, Geology of the Wadi Hawarah and Wadi Shagiah areas: Saudi Arabian Deputy Ministry for Mineral Resources Technical Record TR-1978-6, 10 p.

Pallister, J.S., Stacey, J.S., Fischer, L.B. and Premo, W.R., 1988a, Precambrian ophiolites of Arabia; a summary of geologic settings, U-Pb geochronology, lead isotope characteristics, and implications for microplate accretion, Kingdom of Saudi Arabia: U. S. Geological Survey OF 88-0606, Reston, 81 p.

Pallister, J.S., Stacey, J.S., Fischer, L.B. and Premo, W.R., 1988b, Precambrian ophiolites of Arabia; geologic settings, U-Pb geochronology, Pb-isotope characteristics, and implications for continental accretion. Precambrian Research, 38(1): 1-54.

Patchett, P.J. and Chase, C.G., 2002, Role of transform continental margins in major crustal growth episodes. Geology, 30(1): 39-42.

Paterson, S.R., Vernon, R.H. and Tobisch, O.T., 1989. A review of criteria for the identification of magmatic and tectonic foliations in granitoids. Journal of Structural Geology, 11(3): 349-363.

Pellaton, C., 1981, Geologic map of the Al Madinah quadrangle, sheet 24D, Kingdom of Saudi Arabia: Saudi Arabian Deputy Ministry for Mineral Resources Geoscience Map GM-52 1:250,000 scale

Pilot, J., Werner, C.-D., Haubrich, F. and Baumann, N., 1998. Palaeozoic and Proterozoic zircons from the Mid-Atlantic Ridge. Nature, 393(6686): 676-679.

Radain, A.A.M., 1978, Petrogenesis of some peralkaline and non-peralkaline posttectonic granites in the Arabian Shield, Kingdom of Saudi Arabia. Unpublished Ph.D. thesis, University of Western Ontario, London, Ontario, Canada.

Radain, A.A.M., Fyfe, W.S. and Kerrich, R., 1981. Origin of peralkaline granites of Saudi Arabia. Contributions to Mineralogy and Petrology, 78(3): 358-366.

Ramsay, C.R., 1986a, Explanatory notes to the geologic

map of the Rabigh quadrangle, Sheet 22D, Kingdom of Saudi Arabia. Ministry of Petroleum and Mineral Resources, Deputy Ministry for Mineral Resources, 49 p.

Ramsay, C.R., 1986b, Geologic map of the Rabigh quadrangle, Sheet 22D, Kingdom of Saudi Arabia: Saudi Arabian Deputy Ministry for Mineral Resources Geoscience Map GM-84 C 1:250,000 scale.

Rexworthy, S.R., 1972, Geology and mineralisation of the Precambrian metavolcanics and intrusives of the Jabal Samran-Wadi Hawarah region of the southern Hijaz. Ph.D., University of London.

Reymer, A. and Schubert, G., 1984, Phanerozoic addition rates to the continental crust and crustal growth. Tectonics, 3(1): 63-77.

Roobol, M.J., 1989, Stratigraphic control of exhalative mineralization in the Shayban paleovolcanoes (22/39A): Saudi Arabian Directorate General of Mineral Resources Open-File Report DGMR-OF-10-7, 29 p.

Roobol, M.J., Ramsay, C.R. and Jackson, N.J., 1983.,Late Proterozoic lavas of the central Arabian Shield-evolution of an ancient volcanic arc system. Journal of the Geological Society of London, 140: 185-202.

Roobol, M.J., Ramsay, C.R., Jackson, N.J., Darbyshire, D.P.F. and Al Shanti, A.M.S., 1982, Petrochemistry of lavas from the central Arabian Shield, Precambrian Research, p. A36-A37.

Roobol, M.J. and White, D.L., 1985, Cauldron-subsidence structures and calderas above Arabian felsic plutons; a preliminary survey. Journal of African Earth Sciences, 4: 123-134.

Schandelmeier, H., Abdel Rahman, E.M., Wipfler, E., Küster, D., Utke, A. and Matheis, G., 1994, Late Proterozoic magmatism in the Nakasib suture, Red Sea Hills, Sudan. Journal of the Geological Society of London, 151: 485-497.

Shimron, A.E., 1990. The Red Sea line; a late Proterozoic transcurrent fault. Journal of African Earth Sciences, 11(1-2): 95-112.

Skiba, W. and Gilboy, C.F., 1975, Geology of the Rabigh-Khulays quadrangle, 22/39, Kingdom of Saudi Arabia. Unpublished manuscript in DGMR Technical Library Jeddah, 597 p.

Stacey, J.S. and Agar, R.A., 1985, U-Pb isotopic evidence for the accretion of a continental micro-plate in the Zalm region of the Saudi Arabian Shield. Journal of the Geological Society of London, 142(6): 1189-1203.

Stacey, J.S., Delevaux, M.H., Gramlich, J.W., Doe, B.R. and Roberts, R.J., 1980, A lead isotopic study of mineralization in the Arabian Shield. Contributions to Mineralogy and Petrology, 74: 175-188.

Stacey, J.S. and Hedge, C.E., 1984. Geochronologic and isotopic evidence for early Proterozoic crust in the eastern Arabian Shield. Geology, 12(5): 310-313.

Stacey, J.S. and Kramers, J.D., 1975, A proximation of terrestrial lead isotope evolution by a two-stage model. Earth and Planetary Science Letters, 26(2): 207-221.

Stacey, J.S. and Stoeser, D.B., 1983, Distribution of oceanic and continental leads in the Arabian-Nubian Shield. Contributions to Mineralogy and Petrology, 84: 91-105.

Stern, R.J., 1994, Arc assembly and continental collision in the Neoproterozoic East African Orogen: Implications for the consolidation of Gondwanaland. Annual Review of Earth and Planetary Sciences, 22: 319-351.

Stern, R.J., 2002. Crustal Evolution in the East African Orogen: a Neodymium Isotopic perspective. Journal of African Earth Sciences, 34(3-4): 109-117.

Stern, R.J. and Abdelsalam, M.G., 1998, Formation of juvenile continental crust in the Arabian-Nubian Shield; evidence from granitic rocks of the Nakasib Suture, NE Sudan. Geologische Rundschau, 87(1): 150-160.

Stern, R.J., Fouch, M.J. and Klemperer, S.L., 2003, An overview of the Izu-Bonin-Mariana subduction factory, Inside the Subduction Factory. American Geophysical Union Geophysical Monograph 138, p. 175-221.

Stern, R.J., Johnson, P.R., Kröner, A. and Yibas, B., 2004, Neoproterozoic Ophiolites of the Arabian-Nubian Shield. In: T. Kusky (Editor), Precambrian Ophiolites.

Stoeser, D.B., 1985, Distribution and tectonic setting of plutonic rocks of the Arabian Shield. Journal of African Earth Sciences, 4: 21-46.

Stoeser, D.B. and Camp, V.E., 1985, Pan-African microplate accretion of the Arabian shield. Geological Society of America Bulletin, 96: 817-826.

Stoeser, D.B. and Stacey, J.S., 1988, Evolution, U-Pb geochronology, and isotope geology of the Pan-African Nabitah orogenic belt of the Saudi Arabian Shield. In: S. El Gaby, R.O. Greiling and A. Vogel (Editors), The Pan-African Belts of Northeast Africa and Adjacent Areas. Friedr Vieweg und Sohn, Braunschweig, p. 227-288.

Sultan, M., Becker, R., Arvidson, R.E., Shore, P., Stern, R.J., El Alfy, Z. and Attia, R.I., 1993, New constraints on Red Sea rifting from correlations of Arabian and Nubian Neoproterozoic outcrops. Tectonics, 12: 1303-1319.

Sultan, M., Chamberlain, K.R., Bowring, S.A.,

Arvidson, R.E., Abuzied, H. and El Kaliouby, B., 1990, Geochronologic and isotopic evidence for involvement of pre-Pan-African crust in the Nubian Shield, Egypt. Geology, 18(8): 761-764.

Taylor, B., 1992, Rifting and the volcanic-tectonic evolution of the Izu-Bonin-Mariana Arc. Ocean Drilling Program College Station, .

Tera, F. and Wasserburg, G.J., 1972, U-Th-Pb systematics in three Apollo 14 basalts and the problem of initial Pb in lunar rocks. Earth and Planetary Science Letters, 14(3): 281-304.

Vervoort, J.D. and Blichert-Toft, J., 1999, Evolution of the depleted mantle; Hf isotope evidence from juvenile rocks through time. Geochimica et Cosmochimica Acta, 63(3-4): 533-556.

Wetherill, G.W., 1956, Discordant uraium-lead ages I. Transactions of the American Geophysial Union, 37: 320-326.

White, D.L., 1985, The significance of continental derivation of the Proterozoic Mahanid Formation, southeastern Arabian Shield. Journal of the Geological Society of London, 142, Part 6: 1235-1238.

White, R. and McKenzie, D., 1989, Magmatism at rift zones; the generation of volcanic continental margins and flood basalts. Journal of Geophysical Research, 94(B6): 7685-7729.

Wiles, J.W., 1972, The geology of the country around Sipolilo, 76 p.

Williams, I.S., 1997, U-Th-Pb geochronology by ion microprobe: not just ages but histories. Society of Economic Geologists Reviews of Economic Geology, 7: 1-35.

Williams, I.S., 1998, U-Th-Pb geochronology by ion microprobe. Reviews in Economic Geology, 7: 1-35.

Williams, I.S., Compston, W., Black, L.P., Ireland, T.R. and Foster, J.J., 1984, Unsupported radiogenic Pb in zircon; a case of anomalously high Pb-Pb, U-Pb and Th-Pb ages. Contributions to Mineralogy and Petrology, 88(4): 322-327.

Windley, B.F., Whitehouse, M.J. and Ba-Bttat, M.A.O., 1996, Early Precambrian gneiss terranes and Pan-African island arcs in Yemen; crustal accretion of the eastern Arabian Shield. Geology, 24(2): 131-134.

Wipfler, E., 1996, Transpressive structures in the Neoproterozoic Ariab-Nakasib Belt, Northeast Sudan: Evidence for suturing by oblique collision. Journal of African Earth Sciences, 23: 347-362.

Worl, R., 1978, Mineral exploration; Mahd adh Dhahab district, Kingdom of Saudi Arabia: U.S. Geological Survey Saudi Arabian Project Report 233, 85 p..

Yibas, B., Reimold, W.U., Armstrong, R., Koeberl, C., Anhaeusser, C.R. and Phillips, D., 2002. The tectonostratigraphy, granitoid geochronology and geological evolution of the Precambrian of southern Ethiopia. Journal of African Earth Sciences, 34(1-2): 57-84.

Ziab, M.A., 1982, Geology and mineralisation of the ancient mining area of Hamar, Al-Marasia, Wutailah, Abu-Shiaab, and Thufar, north of Samran. M.Sc., King Abdulaziz University, Jeddah.